Republic of Iraq

Ministry of Higher Education & Scientific Research

University of Kerbala

College of Engineering

Civil Engineering Department

Structural Behavior of Composite Castellated Beams Under Monotonic and Repeated Loads

A Thesis Submitted to the Council of the Faculty of the College of the Engineering/University of Kerbala in Partial Fulfillment of the Requirements for the Master Degree in Civil Engineering

By

Noorulhuda Kadhim Hussein

Supervisors

Assist Prof. Dr. Bahaa Hussain Al-Abbas

Assist Prof. Dr. Ali Ghanim Abbas Al-Khafaji

April 2024 Ramadan 1445

بِسْمِ اللَّهِ الرَّحْمَٰنِ الرَّحِيمِ

وَإِذَا سَأَلَكَ عِبَادِي عَنِّي فَإِنِّي قَرِيبٌ ۖ

أُجِيبُ دَعْوَةَ الدَّاعِ إِذَا دَعَانِ ۖ فَلْيَسْتَجِيبُوا لِي

وَلْيُؤْمِنُوا بِي لَعَلَّهُمْ يَرْشُدُونَ

صدق الله العلي العظيم

(البقرة: من الآية 186)

Examination committee certification

We certify that we have read the thesis entitled " **Structural Behavior of Composite Castellated Beams Under Monotonic and Repeated Loads**" and as an examining committee, we examined the student " **Noorulhuda Kadhim Hussein**" in its content and what is connected with it and that, in our opinion, it is adequate as a thesis for the degree of Master of Science in Civil Engineering.

Supervisor

Signature:
Name: Assist Prof. Dr. Bahaa H. Al-Abbas
Date: 22 / 4 / 2024

Supervisor

Signature:
Name: Assist Prof. Dr. Ali Ghanim Abbas Al-Khafaji
Date: 22 / 4 / 2024

Member

Signature:
Name: Assist Prof. Dr. Shereen Qasim Abdulridha
Date: / / 2024

Member

Signature:
Name: Dr. Mustafa M. Raheem
Date: 22 / 4 / 2024

Chairman

Signature:
Name: Prof. Dr. Sadjad A. Hemzah
Date: / / 2024

Signature:
Name: Dr. Awad Ali Sagheer
Head of the Department of Civil Engineering
Date: / / 2024

Signature:
Name: Assist. Prof. Dr. Haider Nadhom Azziz
Dean of the Engineering College
Date: 28 / 4 / 2024

Supervisor certificate

We certify that the thesis entitled " **Structural Behavior of Composite Castellated Beams Under Monotonic and Repeated Loads** " was prepared by **Noorulhuda Kadhim Hussein** under our supervision at the Department of Civil Engineering, College of Engineering, University of Kerbala as a partial fulfillment of the requirements for the Degree of Master of Science in Civil Engineering.

Signature:

Assist Prof. Dr. Bahaa H. Al-Abbas

Date: / /2024

Signature:

Assist Prof. Dr. Ali Ghanim Abbas Al-Khafaji

Date: / /2024

Linguistic certificate

I certify that the thesis entitled " **Structural Behavior of Composite Castellated Beams Under Monotonic and Repeated Loads,**" which has been submitted by **Noorulhuda Kadhim Hussein,** has been proofread, and its language has been amended to meet the English style.

Signature:

Assist Prof. Dr. Anmar falih Diekan

Date: / /2024

Undertaking

I certify that the research work titled " **Structural Behavior of Composite Castellated Beams Under Monotonic and Repeated Loads** " is my own work. The work has not been presented elsewhere for assessment. Where material has been used from other sources, it has been properly acknowledged/referred.

Signature:

Noorulhuda Kadhim Hussein

Date: 28 / 4 / 2024

Dedication

To the one who conveyed the message, fulfilled the trust, and advised the nation... To the Prophet of Mercy and Light of the Worlds, ***the Holy Prophet Mohammad*** *(peace be upon him and his household),*

*To the one hidden from sight—****the Imam Mahdi*** *(may God hasten his reappearance).*

To the one who taught me that life is a struggle and its weapon is knowledge and science... To the one who strived for my comfort and success, to the greatest and most beloved man in the universe, ***my dear father****.*

To that beloved one whom the Most Gracious has commanded me to be kind and good to... To the one whose prayers were the secret of my success: ***my dear mother.***

To those with whom I share my moments... To those who rejoice in my success as if it were their success, I dedicate this humble effort to you.

Acknowledgments

In the name of Allah, the most gracious, the most merciful, praise be to Allah, who has granted me the syncretizing and enabled me to achieve this thesis. I want to take this opportunity to express my sincere thanks to my supervisors, ***Prof. Dr. Bahaa Hussain Al-Abbas*** *and* ***Prof. Dr. Ali Ghanim Abbas Al-Khafaji****, for reviewing my thesis and providing guidance throughout the project. I had the honor of being under their guidance and supervision. Their precious advice and constructive suggestions were highly distinct throughout this work. I would also like to thank my parents, to whom I owe gratitude and appreciation that could never be repaid. Thank you for all the sacrifices you have made and for the support you have constantly given. Finally, special thanks be to my friends from the bottom of my heart for assisting me in the experimental tests. Great, thanks to all.*

Abstract

The present study focuses on conducting experimental and numerical analyses to examine the performance of composite castellated beams subjected to repeated loading. This study investigates multiple parameters, such as shaped openings (hexagonal, circular, and square) and shear stud spacings of 150 mm and 300 mm, in both the presence and absence of stiffeners. The experimental work involved conducting experiments on materials' mechanical and chemical properties. The beams underwent repeated (25%Pu-50%Pu-75%Pu-100%Pu, etc.) and monotonic loading. In addition, the extension ratio resulted in a 50% increase in the height of the web. In the experimental phase, fifteen composite sections were fabricated, with three of them serving as control samples. The connection between the concrete deck slab and the steel I-beam was established using headed steel studs welded onto the top flanges. The deck slab has dimensions of 1500 mm in length, 350 mm in breadth, and 70 mm in thickness. The structural element utilized was an I-beam, namely an IPE 140, with a length of 1500 mm. The composite beams were categorized into five groups based on variable factors. Each group is comprised of three beams. The study found that certain factors significantly impact the structural integrity of composite castellated beams. Decreased spacing increased load-carrying capabilities and decreased deflections. The design of the opening significantly affects the performance, with hexagonal configurations regularly surpassing circular and square forms in all groups, which varies from 28.26% to 100.43%, emphasizing the structural superiority of hexagonal apertures. Furthermore, the distance between shear connections significantly impacts the maximum load capacities, resulting in variations ranging from 7.91% to 58.09%. It is crucial

to thoroughly evaluate the spacing of shear connectors in the design of castellated steel beams. Finally, reinforcement methods demonstrate efficacy, resulting in percentage increments in maximum load ranging from 17.89% to 66.53%. The study also compares numerical simulations and experimental findings using ABAQUS/Explicit software. The analysis includes parameters like opening configuration, shear connector distribution, and strengthening. Finite element analysis confirms these findings, demonstrating a high level of accuracy of around 94% in predicting ultimate load and load-deflection correlations. The study provides valuable insights into the design of composite castellated beams, emphasizing the need to optimize design parameters to enhance structural efficiency.

Table of Contents

Undertaking.....**Error! Bookmark not defined.**
Dedication ii
Acknowledgments..... iii
Abstract iv
Table of Contents..... vi
List of Tables ix
List of Figures x
List of Abbreviations xv
List of Symbols..... xvi
Chapter One: Introduction 1
1.1 General View..... 1
1.1.1 Castellated Steel Beam (CSB) 1
1.1.2 Shear Connectors 3
1.1.3 Reinforced Concrete Slab (RCS) 5
1.2 Terminology 5
1.3 Geometry Properties..... 6
1.4 Failure Modes of Castellated Beam 6
1.4.1 Compression Buckling of the Web-Post..... 7
1.4.2 Vierendeel Bending Mechanism..... 7
1.4.3 Shear Buckling of the Web-Post..... 8
1.4.4 Lateral Torsional Buckling 9
1.4.5 Significant Web Distortion 9
1.5 Repeated Loading..... 11
1.6 Applications of Castellated Beams 12
1.7 Advantages of Castellated Beams..... 12
1.8 Aim and Objectives of Study 13
1.9 Outline of Thesis 14
Chapter Two: Literature Review 16
2.1 Introduction 16
2.2 Castellated Steel Beams (CSB)..... 16
2.3 Composite Castellated Beams (CCB) 22
2.4 Strengthening Composite Castellated Beams 32
2.5 Summary 38
Chapter Three: Experimental Work 40
3.1 Introduction 40
3.2 Description of Specimens..... 44
3.2.1 Geometry..... 44
3.2.2 Test Specimens 44
3.2.3 Steel Section Cutting and Welding..... 45
3.3 Stiffeners in Composite Castellated Beams: 52
3.3.1 Design, Analysis, and Applications..... 52
3.4 Material 56
3.4.1 Cement..... 56

3.4.2 Fine Aggregate 58
3.4.3 Coarse Aggregate 59
3.4.4 Silica Fume 61
3.4.5 Superplasticizer 62
3.4.6 Water 62
3.5 Supports 63
3.6 Steel Section 64
3.7 Stud Shear Connectors 66
3.8 Welding Processes 68
3.8.1 Molds 69
3.9 Preparation of the Specimens 70
3.9.1 Concrete Mix Design 70
3.10 Mechanical Properties 71
3.10.1 Compressive Strength Test 71
3.10.2 Splitting Tensile Strength Test 72
3.10.3 Flexural Strength Test 73
3.10.4 Modulus of Elasticity 74
3.11 Steel Reinforcement 75
3.11.1 Steel Reinforcement Mesh 75
3.12 Curing 77
3.13 Beams Testing 80
3.14 Strain Measurement 82
Chapter Four: Experimental Results and Discussion 86
4.1 Introduction 86
4.2 Test Setup and Instrumentation 87
4.3 Load-Deflection Behavior 87
4.3.1 Load-Deflection Relationship 88
4.4 Parameters Influence 127
4.4.1 First Parameter - Shape of Opening 127
4.4.2 Second Parameter - Space Between Shear Connector 128
4.4.3 Third Parameter - Used Strengthening 130
4.5 Load-Slip Relationship 132
4.6 Distribution of Normal Strain 134
4.7 Summary of Experimental Results 136
Chapter Five: Finite Elements Analysis 138
5.1 Introduction 138
5.2 Finite Element Modeling 138
5.2.1 Geometry 138
5.2.2 Convergence Study 140
5.2.3 Material Properties 1
5.2.4 Interaction 143
5.2.5 Loading and Boundary Conditions 144
5.3 Numerical Results 145
5.4 Comparison Between Experimental and Finite Element Results 146
5.4.1 Group one 146
5.4.2 Group Two 148

5.4.3 Group Three 151
5.4.4 Group Four 153
5.4.5 Group Five 157
5.5 Load-Slip Relationship 162
5.6 Validation of Numerical Analysis 167
5.7 Parametric Study 172
5.7.1 Number of rows for stud connectors 172
5.7.2 The stiffeners in the I-steel section. 174
5.8 Summary 176
Chapter Six: Conclusion and Recommendation 178
6.1 Summary 178
6.2 Conclusions from Experimental Work 178
6.3 Conclusions from Finite Element Analysis 180
6.4 Recommendations for Further Research 180
References 181
APPENDIX-A 1
Design Examples of The Tested Beams 1
APPENDIX-B 1
B.1 Datasheet of silica fume provided by the manufacturer 1
B.2 Datasheet of superplasticizer provided by the manufacturer 3
APPINDEX-C 1
C. 1 Ingredients used in ABAQUS Program 1
C.2 3D Solid Elements 3
C.3 Truss Element 4
C.4 Rigid elements 4
الخلاصة 1

List of Tables

Table 3-1 :Details of all the test beams in the present study. 43
Table 3-2 : Chemical Composition of Cement 57
Table 3-3: Physical Properties of The Cement. 57
Table 3-4:Grading of The Fine Sand Compared with The Requirements of Iraqi Specification No.45/1984. 58
Table 3-5:Chemical Properties of Fine Aggregate. 58
Table 3-6:Sieve analysis of coarse aggregate No. 45/1984. 59
Table 3-7:Chemical Property of Coarse Aggregate Chemical Property. 59
Table 3-8:Properties of MasterRoc MS610[52]. 61
Table 3-9:Properties of Steel Section. 65
Table 3-10:Mechanical Properties of Shear Connectors. 67
Table 3-11:The Mix Material Proportion of High Strength Concrete. 70
Table 3-12:Compression and Tension Strength of Concrete. 74
Table 3-13:Average Modulus of Elasticity. 74
Table 3-14 Steel reinforcement test results 75
Table 4-1: Experimental Results of the Tested Beams 88
Table 4-2: Ultimate load and deflection in the middle of each 89
Table 4-3:Ultimate load and deflection in the middle of each 93
Table 4-4: Ultimate Load and Deflection in The Middle of Each Three. 102
Table 4-5:Ultimate load and deflection in the middle of each span. 109
Table 4-6:Ultimate load and Deflection in The Middle of Each Span 118
Table 4-7:Influence of Shear Connector Spacing on Ultimate Load of CCB. ... 129
Table 4-8:Impact of Different Strengthening. 130
Table 4-9:Experimental Slip at Ultimate Load. 132
Table 5-1: Finite Element Types for Composite Castellated Beam Model 139
Table 5-2: Effect of Mesh Size on Ultimate Load And Deflection. 141
Table 5-3: Finite Element Interactions for Composite Castellated Beam Model. 143
Table 5-4: Comparison of the Ultimate Load and Ultimate Deflection. 145
Table 5-5:Comparison between experimental and numerical slip 163
Table 5-6:The Effect of number rows on the Ultimate load 172
Table 5-7:The Effect of stiffeners on the Ultimate load 174
Table 6-1: Material Model Behavior for Steel Section and Stiffeners. 1

List of Figures

Figure 1-1: Castellated Steel Beam (Hexagonal, Circular, and Square)..... 2
Figure 1-2: Types of Shear Connectors (Garcia 2002)[5] 4
Figure 1-3: Components of the Castellated Beams..... 5
Figure 1-4:Compression Buckling of the Web Post.[7]..... 7
Figure 1-5:Vierendeel Action or Parallelogram Mechanism [8] 7
Figure 1-6: Vierendeel Truss Analogy [9]..... 8
Figure 1-7: Phases of Beam Failure, Subsequent Deformation Schemes[11]..... 10
Figure 1-8: Failure Modes of Perforated Steel Beams [12]..... 10
Figure 1-9:Types of Cyclic Loading [10]. 11
Figure 2-1: Profile of I-Beam is Halved Along its Body[20]. 17
Figure 2-2: Geometry of Castellated Beam Cut Point[20]. 17
Figure 2-3: Beam rest for the (a) Normal Beam [NB],..... 18
Figure 2-4: Strut in the Web-Post. (a) Inclined Compression Strut..... 19
Figure 2-5:Free Body in the CSB with Polygonal Web Openings[23]. 19
Figure 2-6:The Parameter of Hexagonal Hole in Castellated Steel Beam[24]..... 20
Figure 2-7:Castellated I-beak Produced from Original Profile..... 21
Figure 2-8:Web Buckling Due to Shear[25]..... 21
Figure 2-9: Composite Concrete-Castellated Steel Beam Details[33]. 24
Figure 2-10: Geometry And Installation of Composite Beam Sample[34]. 25
Figure 2-11:Typical Simply Supported Beam Layout (All dimensions in mm). . 26
Figure 2-12:Plan of Composite Castellated Beam (λ=0, 25, 33.8 ,50%). 27
Figure 2-13:Asymmetrical Castellated Steel Beam..... 30
Figure 2-14: Cellular Beam Details 31
Figure 2-15:Manufacturing Steps of Hexagonal and Octagonal 33
Figure 2-16: A-Castellated Beam with Stiffeners in The Transverse Direction... 34
Figure 2-17:Terminology for Stiffener Along the Edge of The Opening..... 34
Figure 2-18:Rejoined Castellated Steel Beam With Increment Plate..... 35
Figure 2-19:A-Stiffener in Two Adjacent Web Holes at Each End 36
Figure 2-20:Fabrication of TCBs by Placing Variable Expansion Plates..... 36
Figure 2-21:Dimensions and notations of all tested specimens..... 37
Figure 3-1:Flowchart of Testing Matrix. 41
Figure 3-2: The Details of Coding the Composite Castellated Beam Models..... 42
Figure 3-3:Composite Castellated Steel-Concrete Sample CB-H4R2..... 44
Figure 3-4: (a) Roller and (b) Hinge Support 46
Figure 3-5:Design of Castellated Beams with Hexagonal Opening. 47
Figure 3-6:Manufacturing Process of a Castellated Beam. 47
Figure 3-7:Dimensions and Details of Tested Specimens 47
Figure 3-8:Design of Castellated Beams with a Circular Opening..... 48
Figure 3-9:Manufacturing Process of a Castellated Beam. 48
Figure 3-10:Design of Castellated Beams with Square Opening 49
Figure 3-11:Manufacturing Process of a Castellated Beam. 49
Figure 3-12:Dimensions and Details of Tested Specimens 50
Figure 3-13 :Dimensions and Details of Tested Specimens (Control Beam)..... 51
Figure 3-14:Dimensions and Details of Tested Specimens 53

Figure 3-15:Dimensions and Details of Tested Specimens 54
Figure 3-31:Analysis Step Used in the Program .Uy= Ux=0 63
Figure 3-32:Analysis Step Used in the Program .Uy= Ux=0 63
Figure 3-33:Analysis Step Used in the Program .Uy= Ux=0 63
Figure 3-19:The Load-Deflection Curves of Steel Samples. 67
Figure 3-20 Steel reinforcement mesh 76
Figure 3-21:Details of Testing Machine Used in This Study. 80
Figure 3-22: History of the repeated load. 82
Figure 3-23:GOM software icon 82
Figure 3-24:The interface of the software. 82
Figure 3-25:The second interface of the software. 83
Figure 4-1:Load-Deflection Curve of Monotonic Load beam (CB-9S). 90
Figure 4-2: Load-Deflection Curve of Monotonic Load Beam (CB-H4S). 91
Figure 4-3: Load-Deflection Curve of Monotonic Load Beam (CB-S9S). 92
Figure 4-4: Load-Deflection Curve of Repeated Load Beam (CB-H9R1). 94
Figure 4-5: Loading Setup of The Beam Under Repeated Load (CB-H9R1). 94
Figure 4-6: Load-Deflection Curve of Repeated Load Beam (CB-C9R1). 97
Figure 4-7: Loading Setup of The Beam Under Repeated Load (CB-C9R1)..... 97
Figure 4-8: Load-Deflection Curve of Repeated Load Beam (CB-S9R1). 99
Figure 4-9: Loading Setup of The Beam Under Repeated Load (CB-S9R1). 99
Figure 4-10: Load-deflection curve of repeated load beam (H4R1)..... 103
Figure 4-11: Loading setup of the beam under repeated load(H4R1). 103
Figure 4-12: Load-Deflection Curve of Repeated Load Beam (C4R1)..... 105
Figure 4-13: Loading Setup of The Beam Under Repeated Load (CB-C4R1)... 105
Figure 4-14: Load-Deflection Curve of Repeated Load Beam (CB-S4R1) 107
Figure 4-15: Loading Setup of The Beam Under Repeated Load (CB-S4R1)... 107
Figure 4-16: Load-Deflection Curve of Repeated Load Beam (CB-H9R2)..... 110
Figure 4-17: Loading Setup of The Beam Under Repeated Load (CB-H9R2). . 110
Figure 4-18: Load-deflection curve of repeated load beam (C9R2)..... 113
Figure 4-19: Loading setup of the beam under repeated load (CB-C9R2)..... 113
Figure 4-20: Load-Deflection Curve of Repeated Load Beam (S9R2). 115
Figure 4-21: Loading Setup of The Beam Under Repeated Load (S9R2)..... 115
Figure 4-22: Load-deflection curve of repeated load beam (H4R2)..... 119
Figure 4-23: Loading setup of the beam under repeated load (H4R2). 119
Figure 4-24: Load-Deflection Curve of Repeated Load Beam (CB-C4R2)..... 121
Figure 4-25: Loading Setup of The Beam Under Repeated Load (CB-C4R2)... 121
Figure 4-26: Load-deflection curve of repeated load beam (CB-S4R2)..... 124
Figure 4-27: Loading setup of the beam under repeated load (CB-S4R2) 124
Figure 4-28:Compare The Results For The Shape of The Openings..... 128
Figure 4-29:Compare results for distance between stud shears. 130
Figure 4-30:Compare results after strengthening. 131
Figure 4-31: Horizontal Slip Between the Concrete and Steel Constituents. 133
Figure 4-32: Strain Distribution at Mid-Span of Beam. 134
Figure 4-33: Strain Distribution at Mid-Span of Beam. 135
Figure 5-1: Geometry of the Numerical Model. 139
Figure 5-2: Mesh Size Effect on Mid-Span Load-Deflection Curve. 140

Figure 5-3: Effect of Mesh Size on Ultimate Load and Deflection. 141
Figure 5-4: Finite Element Mesh Density. 142
Figure 5-5: Interactions for Composite Castellated Beam Model. 144
Figure 5-7:Analysis Step Used in the Program .Uy= Ux=0 144
Figure 5-8:Analysis Step Used in the Program .Uy= Ux=0 146
Figure 5-9:Analysis Step Used in the Program .Uy= Ux=0 146
Figure 5-10:Analysis Step Used in the Program .Uy= Ux=0 146
Figure 5-11: Distribution of von Mises Stresses for Group Two. 148
Figure 5-12: Deflection Shape of model CB-H9R1. 149
Figure 5-13: Comparison between Exp. and Num.Load-Deflection Curve 149
Figure 5-14: Comparison between Exp. and Num. Load-Deflection Curve 150
Figure 5-15: Distribution of von Mises Stresses for (CB-H4R1) Specimen 151
Figure 5-20: Comparison between Exp. and Num. Load-Deflection Curve 152
Figure 5-21: Distribution of von Mises Stresses for (CB-H9R2) Specimen 153
Figure 5-22: Distribution of von Mises Stresses for (CB-C9R2) Specimen. 154
Figure 5-23: Distribution of von Mises Stresses for (CB-S9R2) Specimen. 155
Figure 5-27: Comparison between Exp. and Num. Load-Deflection Curve 156
Figure 5-28: Distribution of von Mises Stresses for (CB-H4R2) Specimen 157
Figure 5-29: Distribution of von Mises Stresses for (CB-C4R2) Specimen. 158
Figure 5-30: Distribution of von Mises Stresses for (CB-S4R2) Specimen. 159
Figure 5-31:Deflection Shape of model CB-S4R2. 160
Figure 5-32: Comparison between Exp. and Num. Load-Deflection Curve 160
Figure 5-33: Comparison between Exp. and Num. Load-Deflection Curve 161
Figure 5-34: Comparison between Exp. and Num. Load-Deflection Curve 161
Figure 5-35: Slip Shape of The Finite Element Beam at Ultimate Load. 162
Figure 5-41:Comparison between Exp. and Num. Slip at Ultimate Load 164
Figure 5-45:Comparison between Exp. and Num. Slip at Ultimate Load 166
Figure 5-46:Comparison of the Exp. and FEA Failure modes (CB-9S). 167
Figure 5-47:Comparison of the Exp. and FEA Failure modes. (CB-H9R1) 168
Figure 5-48:Comparison of the Exp. and FEA Failure modes. (CB-C4R1)..... 168
Figure 5-49:Comparison of the Exp. and FEA Failure modes. (CB-S4R2) 169
Figure 5-50:Comparison of the Exp. and FEA Failure modes. (CB-S9R2) 170
Figure 5-51:Comparison of the Exp. and FEA Failure modes. (CB-S9R1) 171
Figure 5-52:Comparison of the Exp. and FEA Failure modes. (CB-C9R1)..... 171
Figure 5-53: Compare the Results for The Number of Rows Between Stud Shears. 173
Figure 5-54:Compare the Results for The Stiffeners in The I-Steel Section. 175
Figure 6-2:Elements types in ABAQUS. 2

List of Plates

Plate 1-1:Some Uses of Castellated Steel Beams (Alkafeel Garage). 3
Plate 1-2: Shear Buckling in the Web Post of Castellated Beam[3]. 9
Plate 3-1: Photograph for a Zigzag Pattern by CNC. 45
Plate 3-2: Assembling Technique of the Tee Sections. 46
Plate 3-3: Distribution of Shear Connectors of CB-9S 51
Plate 3-4 :Dimensions and Details of Stiffeners to Reinforce Castellated Beam. 52
Plate 3-5:Cement Used in This Study. 56
Plate 3-6:Sieving and washing coarse aggregate before used. 60
Plate 3-7:Silica fume used in this study. 61
Plate 3-8:Type of Superplasticizer Used in This Study. 62
Plate 3-9: The form of support used in the test. 63
Plate 3-10:Photos of Tensile Test Specimens. 64
Plate 3-11:Tensile Steel Testing Machine. 65
Plate 3-12:The Studs Used in This Study, (A)Before Cutting; (B)After Cutting. 66
Plate 3-13: Illustration depicting stud shear connectors. 68
Plate 3-14:The Plywood Molds Used in Casting HSC Concrete Slab. 69
Plate 3-15:The Compression Strength Test Machine 71
Plate 3-16:Splitting Tensile Strength Test Machine. 72
Plate 3-17: Flexural Strength (Modulus of Rupture) Test. 73
Plate 3-18:Tensile Testing Machine for Steel Reinforcement. 76
Plate 3-19: Photographs for the Curing Process. 77
Plate 3-20:Stages of Casting. 78
Plate 3-21 : Instruments Used Throughout the Tests. 79
Plate 3-22:View of the Controlling Program. 79
Plate 3-23: Loading arm used in the test. 81
Plate 4-1: Shape of Beam CB-9S Before and After Testing. 90
Plate 4-2: Shape of Beam CB-H4S Before Testing. 91
Plate 4-3: Shape of Beam CB-S9S Before Testing. 92
Plate 4-4:Failure of Beam CB-S9S after Testing. 92
Plate 4-5: Shape of Beam CB-H9R1 Before Testing. 95

Plate 4-6: Failure of Beam CB-H9R1 After Testing. 95
Plate 4-7: Failure of Beam CB-H9R1 After Testing (Web Post Buckling)..... 96
Plate 4-8: Shape of Beam CB-C9R1 before Testing. 98
Plate 4-9: Failure of Beam CB-C9R1 after Testing. 98
Plate 4-10: Effect of First Crack Load on Stud Shear Connectors. 98
Plate 4-11: Shape of Beam CB-S9R1 Before Testing. 100
Plate 4-12: Failure of Beam CB-S9R1 After Testing. 100
Plate 4-13: Failure of Beam CB-S9R1 After Testing (Buckling and yielding).. 101
Plate 4-14 : Shape of Beam CB-H4R1 Before Testing..... 104
Plate 4-15: Failure of Beam CB-H4R1 After Testing. 104
Plate 4-16: Failure of Beam CB-C4R1 after Testing. 106
Plate 4-17 : Shape of Beam CB-C4R1 Before Testing. 106
Plate 4-18: Shape of Beam CB-S4R1 before Testing. 108
Plate 4-19: Failure of Beam CB-S4R1 after Testing. 108
Plate 4-20: Shape of Beam CB-H9R2 Before Testing..... 111
Plate 4-21: Failure of Beam CB-H9R2 After Testing. 111
Plate 4-22 :Tearing and Inelastic Local Buckling for Beam CB-H9R2. 111
Plate 4-23: Failure of Beam CB-H9R2 after Testing..... 112
Plate 4-24: Shape of Beam CB-C9R2 before Testing. 114
Plate 4-25: Failure of Beam CB-C9R2 after Testing. 114
Plate 4-26: Shape of Beam CB-S9R2 Before Testing. 116
Plate 4-27: Failure of Beam CB-S9R2 After Testing. 116
Plate 4-28: Failure of Beam CB-S9R2 After Testing. 117
Plate 4-29: Shape of Beam CB-H4R2 Before Testing..... 120
Plate 4-30: Failure of Beam CB-H4R2 After Testing. 120
Plate 4-31: Shape of Beam CB-C4R2 Before Testing. 122
Plate 4-32: Failure of Beam CB-C4R2 After Testing. 122
Plate 4-33: Failure of Beam CB-C4R2 After Testing. 123
Plate 4-34: Shape of Beam CB-S4R2 before Testing. 125
Plate 4-35: Failure of Beam CB-S4R2 after Testing. 125
Plate 4-36: Failure of Beam CB-S4R2 After Testing. 126

List of Abbreviations

Symbol	Description
1D	One-dimensional
3D	Three-dimensional
AASHTO	American Association of State Highway and Transportation Officials
ABAQUS	Finite Element Computer Program
ACI	American Concrete Institute
AISC	American Institute of Steel Construction
ASTM	American Society for Testing and Materials
BS	British Standard
CCSB	Composite Castellated Steel Beam
C3D8R	8-Node Linear Brick Element with 3 Degrees of Freedom
CDP	Concrete Damaged Plasticity
CED	Civil Engineering Department
CNC	Computer Numerical Control
Eq.	Equation
Exp.	Experimental
FEA	Finite Element Analysis
FEM	Finite Element Model
HSC	High-strength concrete
I.S.S.	Iraqi Standards Specifications
IQS.	Iraqi Specification
kN	Kilo-Newton
LVDT	Linear Variable Displacement Transducer
Max.	Maximum
Min.	Minimum
MPa	Megapascals
MS	Micro Silica
mm	Millimeter
No.	Number
RC	Reinforced Concrete
R.C. S	Reinforced Concrete Structures
T3D2	2 Nodes with 3 Degrees of Freedom

List of Symbols

Symbol	Description
h	Height (Gross depth of the castellated beam.)
d	Depth of the original rolled section before the castellation process.
h_o	Height of Perforation (Opening height)
L	Total Span of a Beam
WT	Width of The Throat
S	Spacing Between Two Perforations
θ	Angle of Cut
DT	Depth of Throat
e	Distance Between Two Perforations
ø	Diameter of Perforation
Fy	Tensile Stress (Yielding Stress)
Fu	Ultimate Tensile Strength
bf	Flange Width
tf	Flange Thickness
tw	Web Thickness
Es	Modulus of Elasticity
As	Sectional Area at Opening
Ix	Moment of Inertia at Opening
$\boldsymbol{\psi}$	Expansion Ratio

Chapter One: Introduction

Chapter One: Introduction

1.1 General View

In current structural engineering, pursuing innovation and efficiency is a continuous endeavor. Engineers consistently strive to enhance the utilization of materials while retaining structural integrity and performance. One innovation that has attracted much notice is the application of castellated steel beams (CSB). This introductory chapter provides an overview of the broader context of CSB and establishes the foundation for the remaining discussions presented in this thesis.

The present study investigates the structural efficacy of composite castellated beams, which are widely utilized in construction due to their remarkable strength-to-weight ratios. An analysis of the experimental performance of shear connectors, shape openings, and stiffeners under repeated loading is conducted.

1.1.1 Castellated Steel Beam (CSB)

Castellated steel beams (CSBs) are a significant structural design and construction innovation. The beams exhibit a distinct cellular or "castellated" cross-sectional profile, setting them apart from conventional steel beams. The term "castellated" is derived from its resemblance to the battlements or crenellations found in medieval castles. The unique arrangement, defined by evenly distributed gaps or apertures along the central section of the beam, offers considerable benefits in many structural contexts [1]. (CSBs) are gaining popularity in construction due to their weight reduction, load-bearing capacity, and visual appeal. They are ideal for construction projects like commercial towers, bridges, and industrial structures. However, their integration requires a thorough understanding of their advantages,

potential obstacles, and performance attributes [2]. Engineers must study CSB behavior under various loading conditions to ensure safety and effectiveness. Since World War II, castellated beams have been used in steel construction, but their widespread use has been limited due to high material costs and reduced labor costs. [3]. In the present-day environment, the progress made in automated cutting and welding technology has significantly reduced the production expenses associated with castellated beams. The castellated beam operates flexibly, exhibiting performance comparable to that of a Vierendeel truss. As depicted in Figure 1-1, castellated beams are produced by enlarging the diameters of rolled structural beams, augmenting their ability to bear loads without a concurrent increase in their total weight.

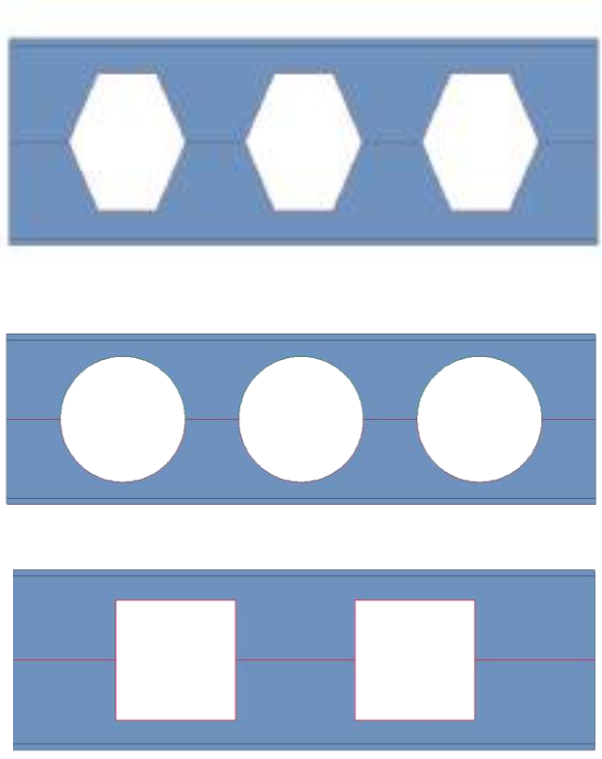

Figure 1-1: Castellated Steel Beam (Hexagonal, Circular, and Square).

Plate 1-1:Some Uses of Castellated Steel Beams (Alkafeel Garage).

1.1.2 Shear Connectors

Shear connectors are important for transmitting shear forces between steel and concrete parts, ensuring that composite structures are strong and can hold loads. These connectors are crucial in avoiding vertical separation or slippage between the steel and concrete elements. In general practice, shear connections are commonly welded onto the upper flange of steel beams before the pouring of concrete slabs. The careful and thorough installation procedure ensures that the composite component, which consists of two different materials, operates as a single and integrated unit [4].

As illustrated in Figure (1-2), several varieties of shear connectors are available, with the stud connector being the most commonly used, as

shown in the same figure. The stud connector comprises a head and a plain shank that are precisely joined to steel components via a welded collar. Headed stud connectors are commonly preferred in composite buildings due to their notable characteristics, including their convenient design, rapid installation, and ability to endure shear forces from various directions effectively.

Some of the most common ways that shear connectors fail are when the concrete around the connector breaks because of compression, which happens more often when larger studs are used. Additionally, the detachment of connectors at their base is a common failure mode, particularly when slender studs are involved. The influence of concrete strength on the failure load and mechanism of failure displayed by shear connections is a notable aspect to consider [5].

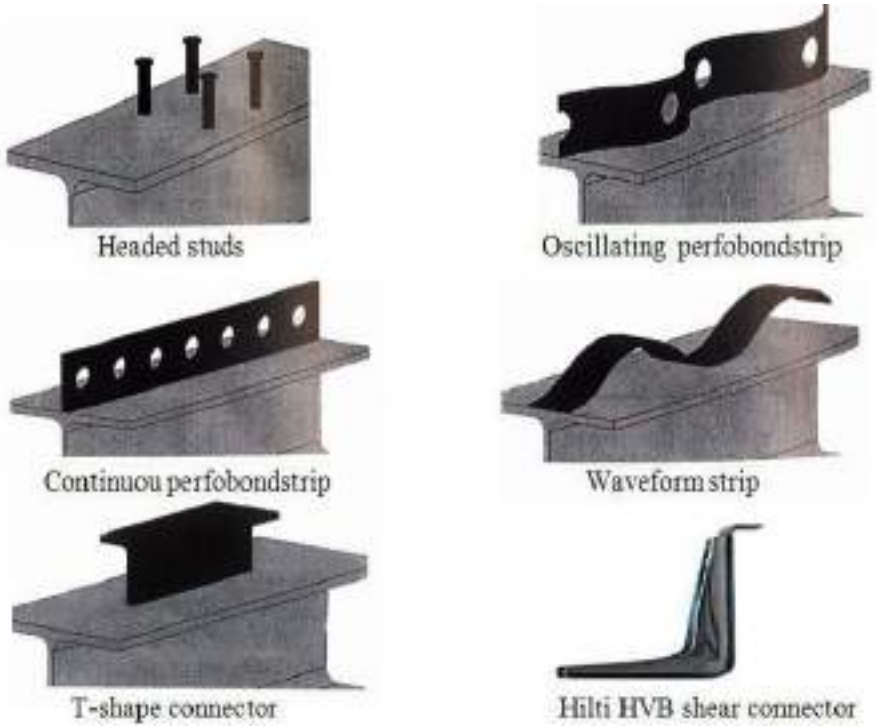

Figure 1-2: Types of Shear Connectors (Garcia 2002)[5]

1.1.3 Reinforced Concrete Slab (RCS)

High-strength concrete, often known as H.S.C., is typically used for concrete structures with a compressive strength above 55 MPa [6]. High-strength concrete is well-suited for applications involving significant expected loads, such as those encountered in constructing bridges, buildings, and columns. Steel reinforcement, commonly in the shape of rebar, enhances the tensile strength of concrete components. This study examines the structural characteristics of reinforced high-strength concrete slabs, specifically engineered to achieve a desired strength of 60 MPa within a 28-day timeframe. 8-mm rebars are used in high-strength concrete slabs on slabs that have a thickness of 70 mm.

1.2 Terminology

This section introduces various terms shown in **Figure (1-3)**, which will be used to define the castellated beam's components and analyze the test results.

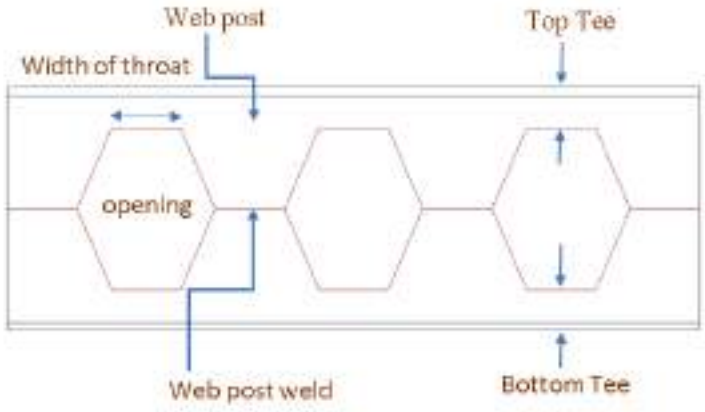

Figure 1-3: Components of the Castellated Beams.

- **Web Post:** The portion that is located between two openings.
- **Throat Width:** The horizontal cutting length on the original beam or the portion length of the web, which is associated with the flanges.

- **Throat Depth:** The total depth of the tee section that connects the web to the flanges.
- **Expansion Ratio (ψ):** it is a ratio between fabricated or castellated beam depth to the original (root) beam depth.

1.3 Geometry Properties

The cutting pattern of the web in the CSB leads to multiple failure modes because of variations in its geometrical qualities caused by different opening size. The characteristics above will have a significant impact on the beam's behavior. For instance, enlarging the opening size to accommodate ductwork will reduce the moment of inertia and increase the bending stress within the tee section due to the secondary moment of the applied shear. Therefore, there exist relevant equations concluded by referring to **Figure (1-3)** as follows [3]:

$$\psi = D/d \quad \textbf{(1-1)}$$

$$D = 2\times DT + h_o \quad \textbf{(1-2)}$$

$$d = 2\times DT + h_\%2 \quad \textbf{(1-3)}$$

1.4 Failure Modes of Castellated Beam

The failure mechanism of castellated beams is influenced by several factors, including beam slenderness, castellation parameters (such as expansion ratio, height, angle of cut, width, spacing of the openings, and weld length), and the kind of stress. Including hexagonal, square, and circular apertures in the web of castellated beams will result in additional failure modes. This is due to the different geometries of the web and the passage of shear forces via the perforated sections. There are six potential failure scenarios associated with castellated steel beams: **[7]**

1.4.1 Compression Buckling of the Web-Post

The mode of failure in castellated steel beams shares similarities with web crippling in solid webbed beams. It is typically observed in areas near reaction forces or under concentrated loads, as illustrated in Figure (1-4).

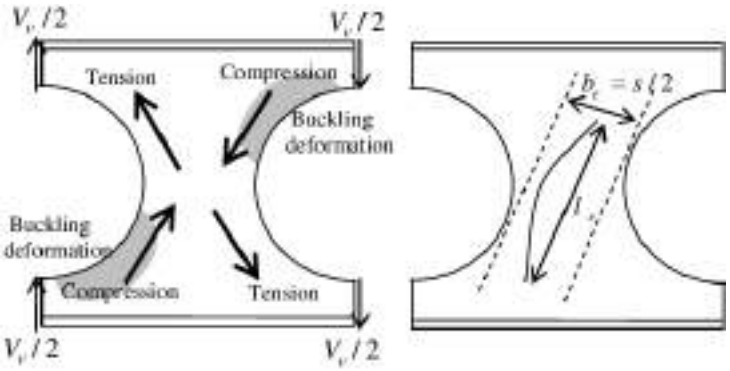

Figure 1-4:Compression Buckling of the Web Post.[7]

1.4.2 Vierendeel Bending Mechanism

The "Vierendeel mechanism" or "parallelogram action" (Figure 1-5) is observed in regions of high shear forces within structural members. This mode of failure results in the formation of plastic hinges at the four corners of an opening, leading to a deformation pattern resembling a parallelogram.

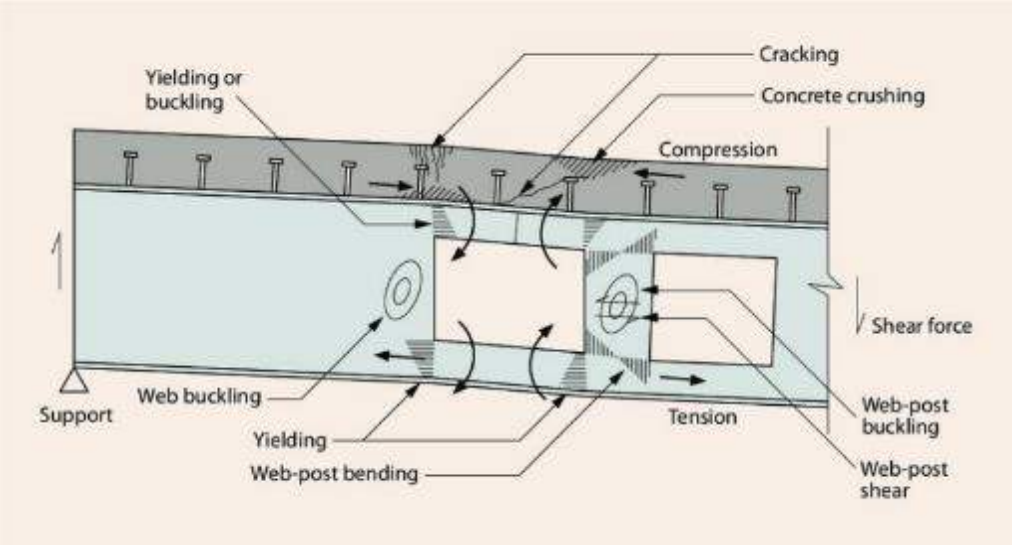

Figure 1-5:Vierendeel Action or Parallelogram Mechanism [8]

1.4.2.1 Vierendeel Truss Analogy

The Vierendeel truss analogy for castellated beams draws parallels between castellated beam behavior and Vierendeel truss structures. It highlights that in regions of high shear forces, the beam behaves as if composed of rigid rectangular panels, resulting in a deformation pattern similar to a parallelogram. This concept aids in analyzing and designing castellated beams, particularly in areas with high shear forces, contributing to their efficient use in construction and engineering applications [9]**.**

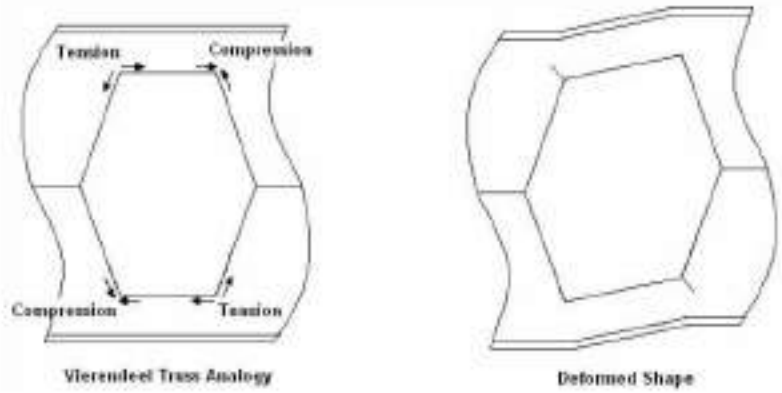

Figure 1-6: Vierendeel Truss Analogy [9]**.**

1.4.3 Shear Buckling of the Web-Post

This occurs when the horizontal shear force within the web post is associated with double curvature bending along the height of the post. In castellated beams, one inclined edge of the opening experiences compressive stress, while the opposite edge experiences tensile stress. This imbalance in stress distribution can lead to buckling, causing a twisting effect along the height of the web post. The result is a deformation of the post as it tries to accommodate the varying forces acting upon it, creating a twisting or torsional effect. This phenomenon is visualized in Plate (1-2).

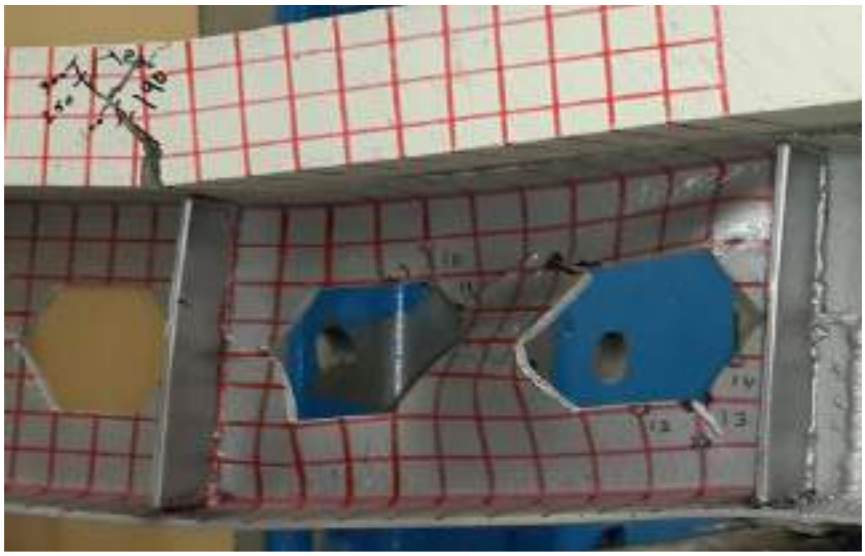

Plate 1-2: Shear Buckling in the Web Post of Castellated Beam[3]**.**

1.4.4 Lateral Torsional Buckling

Lateral torsional buckling is a structural instability in beams and other slender structures resulting from lateral deflection and torsional rotation. This occurs when a beam experiences axial compression and bending moments. It is crucial in structural engineering and design as it can lead to structural failure if not properly addressed [10].

1.4.5 Significant Web Distortion

Web crippling in structural engineering refers to the significant distortion or displacement experienced by the vertical or diagonal web element of a beam, which is crucial in resisting shear stresses. This distortion can be caused by high loads, buckling, or structural deficiencies, posing a significant risk to a building's integrity and safety. Mitigating web distortion requires a thorough structural examination and appropriate measures.

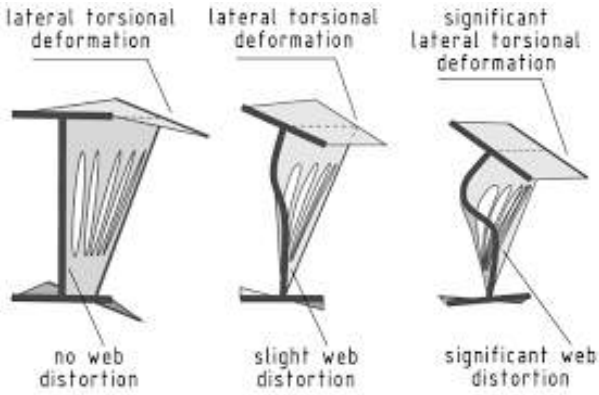

Figure 1-7: Phases of Beam Failure, Subsequent Deformation Schemes[11]

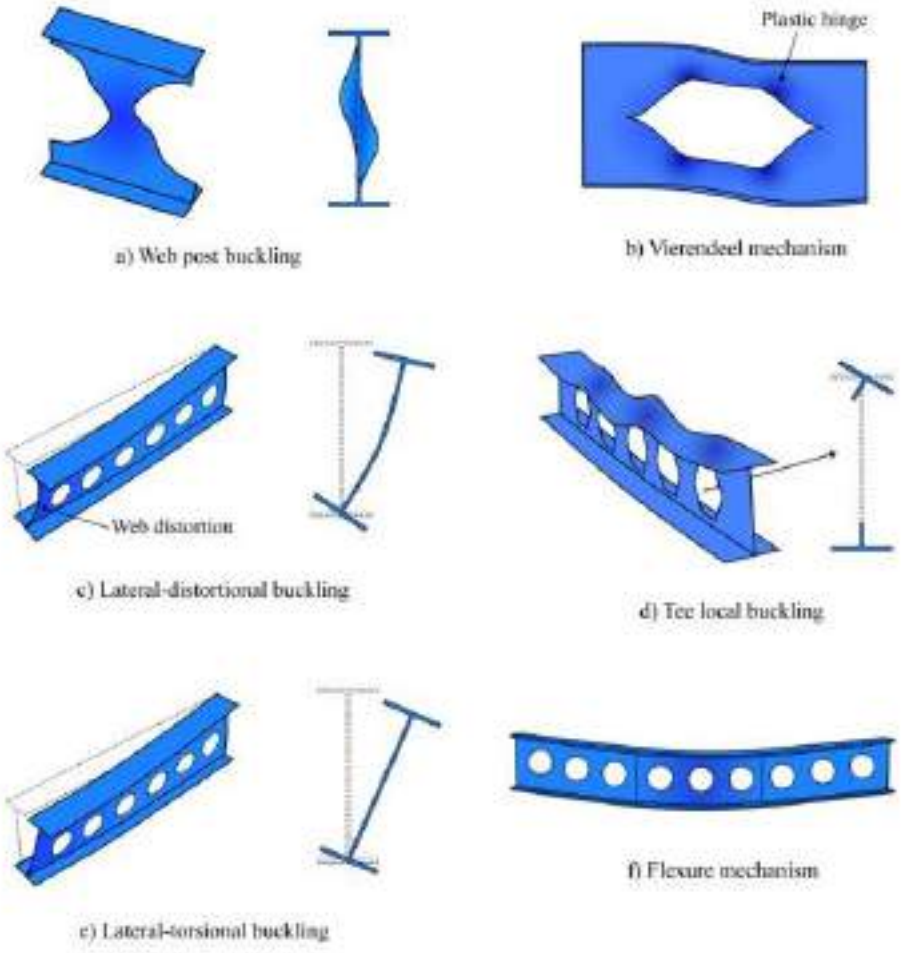

Figure 1-8: Failure Modes of Perforated Steel Beams [12]**.**

1.5 Repeated Loading

Various definitions exist for cyclic loading, including constant or varying intensity. However, there are two primary categories of cyclic loading:

1- Unidirectional Cyclic Loading: All the cycles follow the same direction (either positive or negative) and are referred to as repeated loads, such as the load caused by the movement of vehicles or the impact of water, as seen in Figure (1-9a) [13].

2- Reversed Cyclic Loading: This phenomenon is characterized by alternating positive and negative half cycles within each cycle, as seen in Figure (1-9b). Instances of cyclic loads include those caused by wind, explosions, and earthquakes. The seismic stresses manifest abruptly, intensely, and without prior notice and are regarded as one of the most hazardous cyclic loads [13].

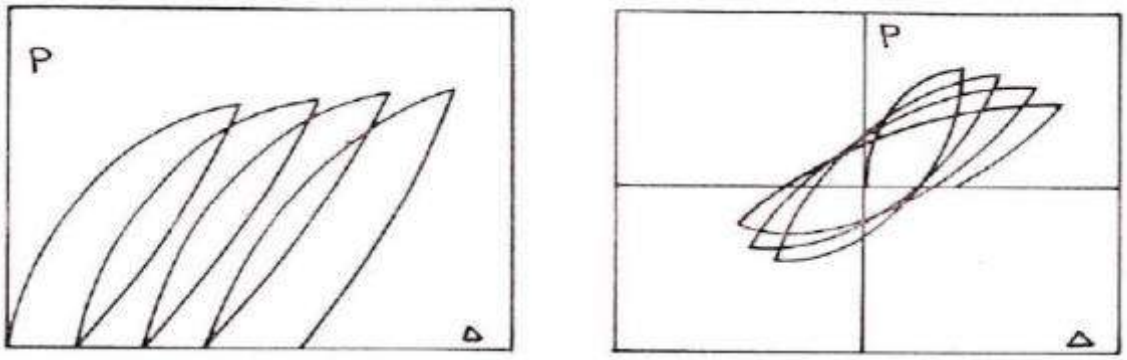

a: Repeated loads b: Reversed loads

Figure 1-9:Types of Cyclic Loading [10].

1.6 Applications of Castellated Beams

Castellated beams have a wide range of uses:[14]

1. Bridge construction: due to its interlocking design, which enhances stability and strength.
2. Residential construction: offering a cost-efficient and streamlined approach to constructing residential properties.
3. Commercial construction encompasses structures designed for commercial use, such as office buildings and retail centers.
4. Industrial construction encompasses structures specifically designed for industrial use, such as warehouses and manufacturing facilities.

1.7 Advantages of Castellated Beams

The benefits of castellated beams encompass the following: [15]

1. The assembly process is quick, efficient, and uncomplicated, eliminating the need for extra fasteners.
2. Enhanced strength and stability: the crenelated structure of castellated beams provides increased resistance against bending and deformation.
3. Enhanced load-bearing capacity: the interlocking design allows for optimal performance in demanding tasks.
4. Substantial cost savings: The simplicity of installation and the decreased need for extra fasteners frequently make castellated beams more cost-effective compared to other beam types.

1.8 Aim and Objectives of Study

The study aims to advance the understanding of the structural performance of composite castellated beams, with a particular emphasis on investigating their experimental behavior when subjected to repeated loads. The study aims to contribute valuable insights into the following key aspects:

1- The primary objective is to analyze and comprehend the structural performance of composite castellated beams. This involves assessing how these beams behave under monotonic and repeated loading conditions.

2- The study explores various variable parameters that can influence the structural behavior of composite castellated beams. These parameters include the shape of the aperture, the type of loading, the spacing of shear connectors, and the presence of stiffeners.

3- Evaluate the load-deformation characteristics of composite CSBs subjected to cyclic loading conditions.

4- Identify and analyze probable failure modes and processes during repetitive loading.

5- Investigate the impact of stiffeners on the performance of composite CSBs under cyclic loading.

6- Evaluating the validity and accuracy of carrying out a finite element analysis to simulate the nonlinear behavior of the composite castellated steel beam failure by using the ABAQUS (version 2021) computer program.

1.9 Outline of Thesis

- Chapter One: The comprehensive overview of CSB (composite castellated beams), shear connectors, RCS (reinforced concrete slabs), and their respective applications A short reference was made to castellated steel beams' manufacturing process and failure mechanisms. Next, the study's goals were introduced.
- Chapter Two: This chapter focuses on the prior investigations conducted on composite and non-composite castellated steel beams, including experimental and analytical studies.
- Chapter Three encompasses the empirical investigation, which encompasses the characteristics of concrete and steel, the procedure of welding, and the quantity and categories of samples examined in this research.
- Chapter Four presents the results and discussion of the experimental work.
- Chapter Five presents implementing finite element (FE) analysis to examine composite castellated steel beams. The numerical analysis results are then shown and compared with the experimental findings.
- Chapter Six: This chapter includes a comprehensive analysis, findings, and suggestions to enhance this study further.

Chapter Two: Literature Review

Chapter Two: Literature Review

2.1 Introduction

This literature analysis provides an excellent basis for comprehending the experimental behavior of composite castellated beams subjected to repeated loads. The review synthesizes and analyzes previous research, offering valuable insights into the fundamental aspects affecting the performance of structural elements. The study examines load-carrying capability, deflection behavior, and other relevant parameters while highlighting existing knowledge deficiencies that drive the ongoing research.

This chapter provides a comprehensive review of the current body of research on experimental and analytical studies on non-composite and composite castellated steel beams and detailed accounts of specimens used in previous research investigations.

2.2 Castellated Steel Beams (CSB)

Engineers are continually improving the materials and practices of construction and design. Structural engineers have made numerous attempts to find innovative ways to lower the cost of steel structures. One of these attempts was castellated steel beams, or expanded beams, in the mid-1930s. The first use of castellated steel beams was made by Horton, who used them to build the Chicago steel bridge in the 1940s [16],[17]. The concept of castellated beams was first developed in 1935 by Boyd in Argentina while he was working for a steel fabricator. Boyd's idea came when a large depth of steel beam was required. At that time, beams with minimal depths were only available in the fabricator. Initially, he considered the option of vertically aligning two beams with small depths to achieve greater depth. However, he ultimately chose to enlarge the steel beam [17], initially known as the "Boyd beam," and then changed this name later to castellated beam. This name is

derived from the pattern of web openings because castellated means “built like a castle, having battlements, or regular openings in the walls, like a castle” [18] [19].

Sandy and Limbong in 2014 [20] A study on castellated steel beams with hexagonal variation was conducted using monotonic loading and static loading. The results showed that beams with a cutting angle of 60° and a web opening distance of 90 mm could withstand maximum loads. However, buckling and lateral torsion buckling damaged all test specimens. The study also aimed to determine optimal dimensions and load capacity. A numerical modeling approach was used to determine the opening angle and spacing between openings on the hexagonal castellated beam. The finite element model was developed using ABAQUS/CAE software, and the Von Mises failure criteria were used to determine the failure load. The results showed that opening spacing of 6 mm and an opening angle of 60° provided better results for load at yield, deflection at yield, and Von-Mises stress.

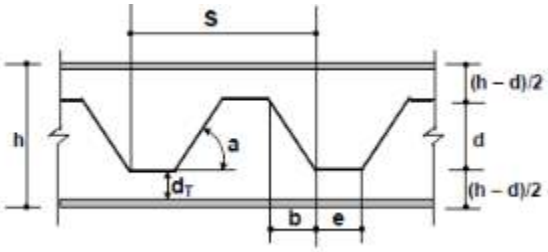

Figure 2-1: Profile of I-Beam is Halved Along its Body[20].

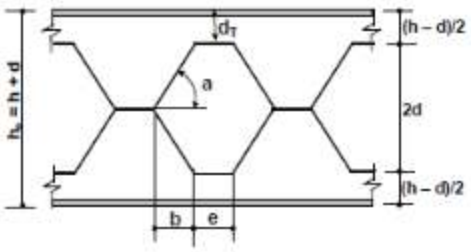

Figure 2-2: Geometry of Castellated Beam Cut Point[20].

Junus et al. in 2015 [21] The study examined the behavior of castellated beams reinforced with concrete under cyclic loading and their potential use as

structural elements for seismic load resistance. The test beams included normal beams (CB), castellated beams with concrete filler between the flanges (CCB), and normal beams (NB). Results showed that CB had advantages in increased flexural capacity and energy absorption but disadvantages in decreased ductility, resistance ratio, and accelerated stiffness degradation rate. CCB showed further improvements in these aspects, making it a potential choice for seismic load resistance. The flexural strength of CB with concrete filler increased by 184.78%, while energy absorption increased by 217.1%.

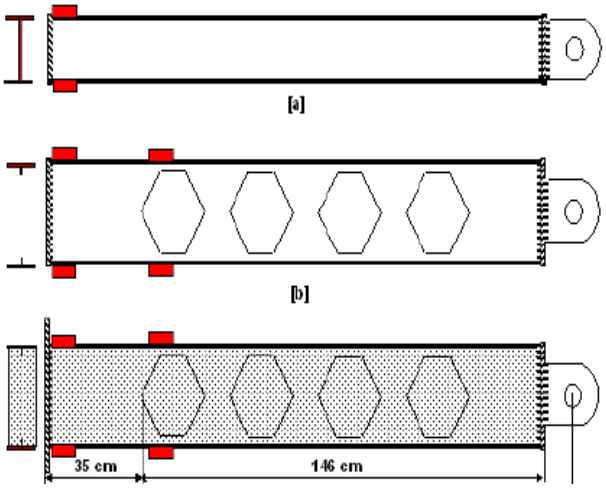

Figure 2-3: Beam rest for the (a) Normal Beam [NB], (b)Castellan Beam [CB], (c)Castellan Composite Beam [CCB] [21].

Shaikh and Autade's study in 2016 [22] significantly contributes to castellated beam analysis and design, particularly in cantilevered configurations. The study presents a new analytical method for determining critical buckling load and reveals the correlation between web shear deformation and load. It compares web posts like fillet corner hexagonal web apertures and cellular beams, focusing on structural failure mechanisms and offering solutions. The study emphasizes the importance of using web reinforcing stiffeners, moment of inertia, and section properties in castellated beam design, as these factors directly impact vertical bending stiffness, serviceability requirements, and aesthetic aspects of the beams.

.The study by Wang et al. in 2016 [23] aimed to determine the shear buckling strengths of web posts in Castellated Steel Beams (CSBs) with hexagonal web openings using the finite element method. Design equations for the vertical shear buckling strength are proposed using thin-plate shear buckling theory. The shear buckling coefficient (k) is obtained through inverse analysis and found to decrease non-linearly with the increase in web-post width to web thickness ratio and web height of the Tee section above the opening to the web thickness and increase linearly with the increase in incline angle of the opening edge and opening height to web thickness ratio. The proposed method for calculating the vertical shear buckling strength aligns well with finite element simulation results but may overestimate the shear buckling strength in the elastic-plastic state. A safety factor of 1.2 was implemented to mitigate this, reducing the average disparity between computed and experimental outcomes.

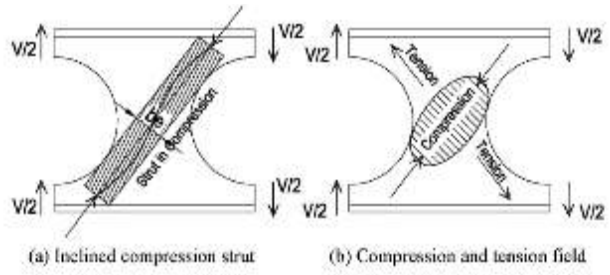

Figure 2-4: Strut in the Web-Post. (a) Inclined Compression Strut. (b)Compression and Tension Field

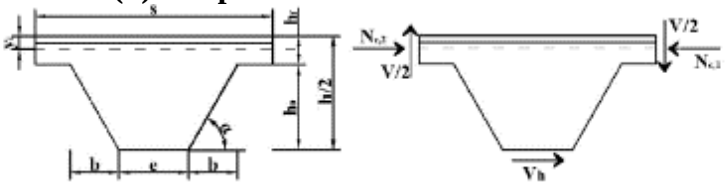

Figure 2-5:Free Body in the CSB with Polygonal Web Openings[23]**.**

The study by Budi et al. in 2017 [24] focuses on optimizing the size and spacing of hexagonal holes in castellated steel beams (CSBs). This research

employs a combination of finite element method (FEM) analysis and laboratory testing to achieve its objectives. Researchers used FEM analysis to optimize CSBs with hexagonal holes from modified 150-mm-high IWF section profiles. The results showed a significant increase in strength compared to the original IWF profile. The optimal configuration was identified as having a 60° opening angle and hole distances ranging from 0.186h° to 0.266h°. The study also found that hole spacing affects stress concentration in CSBs, with wider spacing causing stress at corner areas and shorter spacing shifting it to the weld joint area. This research contributes to understanding and designing CSBs for various engineering applications, potentially leading to cost savings and more efficient designs. The optimization analysis of castellated steel beams with hexagonal holes showed an increase in strength compared to the original IWF profile with a factor of 1.938 to 2.041.

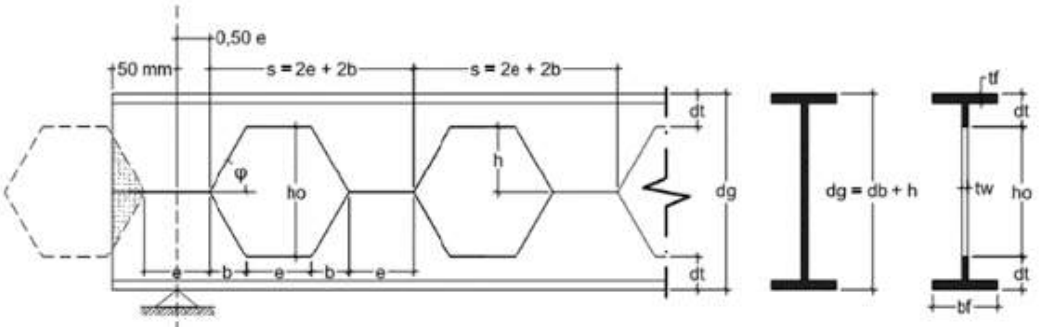

Figure 2-6:The Parameter of Hexagonal Hole in Castellated Steel Beam[24].

A study by Mazin A. Al-Mazini in 2017 [25] focuses on the structural performance of castellated beams, examining the influence of geometric hole shapes and span lengths. It evaluates the precision of two equations, Biodgett and Halleux, in forecasting these beams' ultimate and limit loads. The ultimate load of castellated beams decreases by about 25% with an increase in the cutting angle. The Biodgett equation provides accurate estimations for

maximum load under conditions when the cutting angle does not exceed 50°, but the Halleux equation's accuracy is compromised when the cutting angle approaches 50°. The research used ANSYS-12 software for finite element analysis, achieving a convergence rate of around 78%. The study presented parameters such as cutting angle (ϕ), welding length (n), and expansion parameter (α) to describe the geometric properties of holes in castellated beams. The study emphasizes the dependability of the Biodgett equation [26] and the importance of finite element analysis in substantiating conclusions. The study also found that the cutting angle significantly affects the number of castellations per unit length of the beam. n=hc/4 [27].

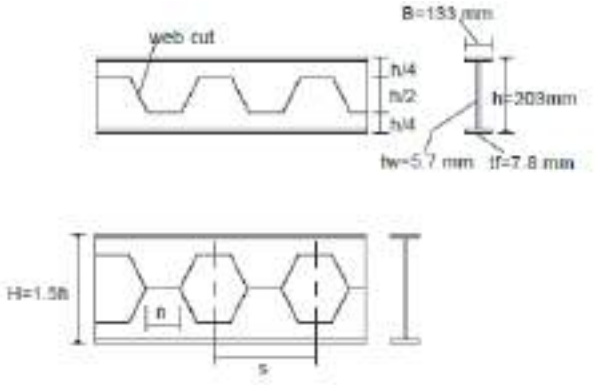

Figure 2-7:Castellated I-beak Produced from Original Profile

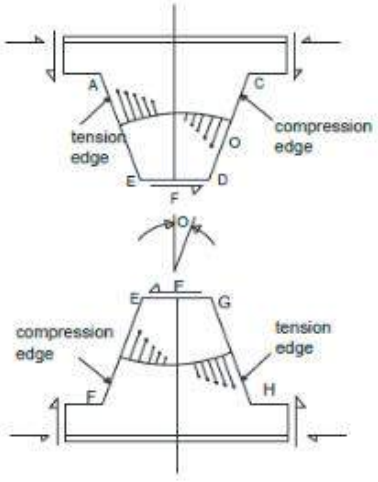

Figure 2-8:Web Buckling Due to Shear[25]**.**

The paper by Mehetre and Talikoti et al. (2020) [28] investigated the torsional moment capacity of CSBs with hexagonal, honeycomb, and sinusoidal openings. The authors found that the torsional moment capacity of CSBs is higher than solid I-beams. The hexagonal section with a 60° opening angle showed the highest torsional capacity, followed by the sinusoidal section with a 30° opening angle.

Cashell et al. in 2021 [29] A study on stainless steel cellular beams revealed that they experience web-post buckling around 28 minutes after firing, even without fire safety measures. A finite element model was developed to study the thermo-mechanical behavior of these beams, and it was found that loading arrangement doesn't significantly impact the beam's lifespan, but fire resistance decreases with increasing load ratios, regardless of steel grade. Stainless steel beams show superior survival time and deflections compared to carbon steel beams, with austenitic grades showing commendable performance. Composite Sandwich Cores (CSCs) are a viable alternative for lightweight and rigid I-beams.

2.3 Composite Castellated Beams (CCB)

The literature on composite castellated beams provides valuable insights into their structural behavior, performance, and optimization strategies, aiding researchers and engineers in designing, implementing, and contributing to the advancement of structural engineering methods. However, several factors can affect the performance of composite castellated beams under repeated loads, such as the type of opening, the number of openings, the spacing of the openings, the size and type of the shear connectors, and the concrete strength.

In the comprehensive investigation carried out by E.S. Ismail and his research team in 2014 [30] , a study by E.S. Ismail aimed to understand the behavior of continuous, partially composite castellated beams under vertical loads using a nonlinear 3D finite element model created using ABAQUS software. The model considered initial geometric imperfections and material nonlinearities, ensuring a robust analysis. The research found that strategic application of techniques like vertical stiffeners, stiffeners around openings, and initiating web openings after the negative moment region significantly increased the ultimate load of composite castellated beams. Additionally, these techniques significantly altered the ductility ratio, reducing it by 50%, 61.2%, and 68.6%. Steel strength variations significantly influenced the ultimate load and ductility. Concrete strength had a limited impact on initial stiffness but increased strength and ductility by 4% and 23%, respectively. Slab thickness also played a role, with reduced slab slenderness leading to increased ultimate load and ductility. The study provides practical insights for structural engineering and design optimization.

The research conducted by Al-Zuhairi and colleagues in 2017 [31], This study aimed to investigate the structural behavior of composite concrete castellated steel beams under flexural loading conditions using the Finite Element Method (FEM). The researchers used three-dimensional brick elements to represent the concrete flange and shell elements to model the castellated steel section. The ANSYS11 program was used as a computational tool for the investigation. A parametric analysis focused on the variation of castellation ratios at 25%, 35%, and 45%. The study found that the resistive moment of the composite beam increased as the castellation ratio was raised, particularly when the beam reached the maximum allowable deflection at its midpoint. A negative correlation was found between mid-span deflection and the

castellation ratio, indicating that an increase in the castellation ratio led to a decrease in mid-span deflection. The load required to cause the maximum allowable deflection at the midpoint of the structure increased with an increase in the castellation ratio.

The study conducted by Oukaili and Abdullah (2017) [33] examined the behavior of composite concrete-castellated steel beams under flexure and torsion. They used two strengthening techniques: one involving intermediate stiffeners and the other combining external prestress. The study tested nine specimens, each supported over a 2900 mm span. The results showed that the first technique improved load-carrying capacity by 26%, while the second technique, which combined intermediate stiffeners with external prestress, led to even greater improvements. The study also found that the first technique reduced mid-span deflection under service loads by 56%. The study concluded that using intermediate stiffeners improved strength and ductility while combining intermediate stiffeners and external prestress increased flexural and torsional capacities. The study also demonstrated the potential for longer spans for composite concrete-castellated steel beams, potentially leading to substantial materials economy in structural design and construction practices.

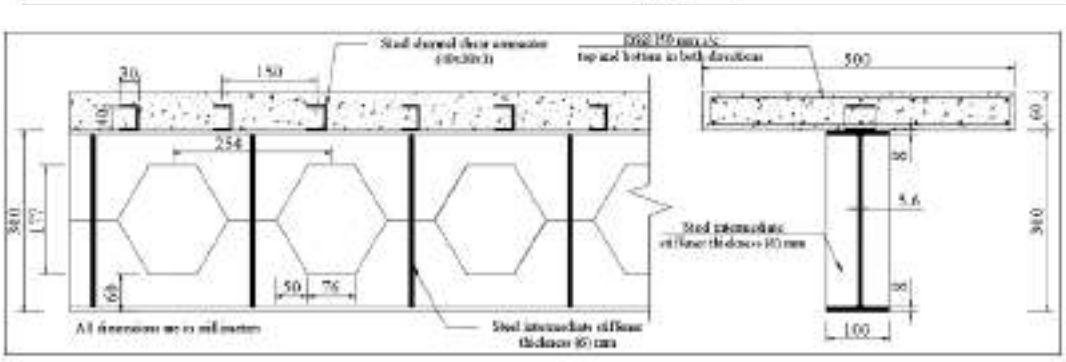

Figure 2-9: Composite Concrete-Castellated Steel Beam Details[33].

Yahya Al-Darzi in 2017 [34] conducted a study on the performance of steel-concrete composite beams under both monotonic and repeated loading conditions. The study involved sixteen beams with compressive strengths ranging from 25 to 43.9 MPa. The results showed that High Strength Concrete (HSC) significantly improved load-carrying capacity, increasing it by approximately 18.82% under monotonic loading and 52.91% under repeated loading scenarios. However, beam resistance decreased when subjected to repeated loading, ranging from 5% to 28.53%. Introducing steel fibers into the concrete mixture led to improvements in ultimate strength, with increases of 10% to 28.65%. This was accompanied by reduced deflection and slipping. However, the ultimate strengths determined through experimental testing were lower than those projected by the AISC-LRFD specifications. The study provides valuable insights into the influence of HSC on composite steel-concrete beam performance, highlighting discrepancies between experimental results and AISC formula predictions for ultimate strength.

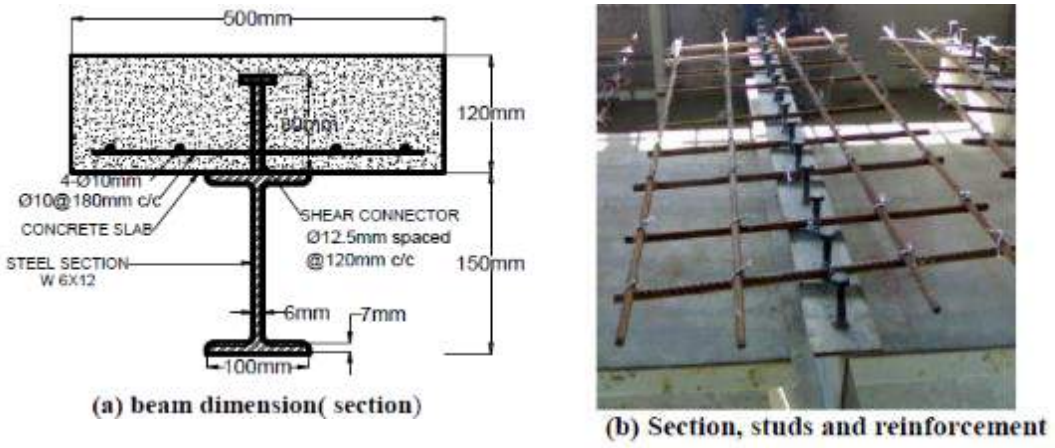

Figure 2-10: Geometry And Installation of Composite Beam Sample[34]**.**

In the study conducted by Al-Hadithy and Jaafar in 2017 [35], A study analyzed the behavior of composite beams with headed stud shear connectors under monotonous and displacement-controlled non-reversible repeated

loadings. Factors such as cross-sectional proportioning, partial interaction, ductile deformability, and loading type were examined. The results, validated against authoritative investigations, provided valuable insights for structural designers. The study involved eleven one-third scaled composite beams with push-out segments and tested in five pairs. The results showed that adding a bottom steel plate to the neutral axis increased flexural resistance by 24.7%. Reducing the number of headed studs to half resulted in a 160.58% increase in flexural resistance. Lengthening medium-length headed studs by 72% also increased flexural stiffness by 41.1% and decreased the residual cyclic slippage index by 54.3%. These findings can enhance the design and performance of composite systems featuring headed stud shear connectors.

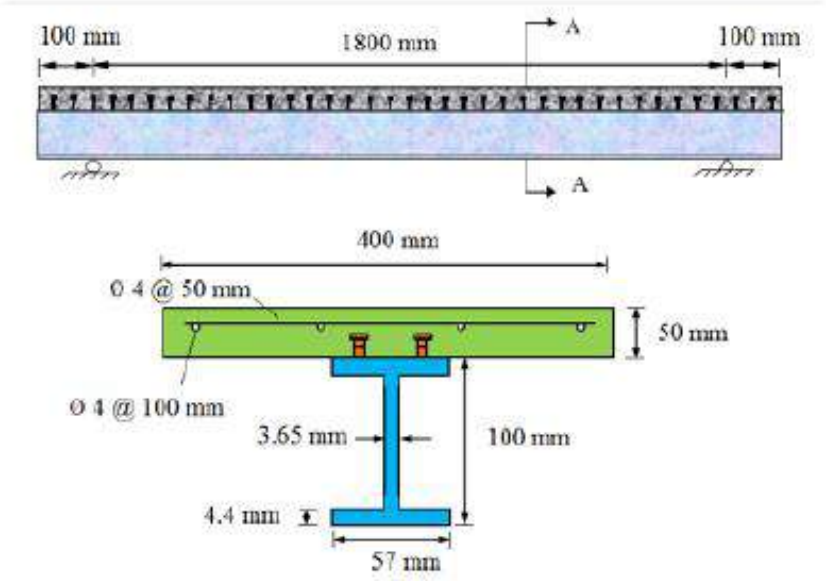

Figure 2-11:Typical Simply Supported Beam Layout (All dimensions in mm).

Abdulridha et al. [36] investigate the structural behavior of composite castellated steel-concrete beams when subjected to an impact load. These composite beams, consisting of self-compacting concrete and connected to self-compacting concrete using stud shear connectors, were tested with

varying degrees of castellation, ranging from 0% to 50%. Free-falling steel balls generated impact loads, and specialized test rigs equipped with sensors and Lab VIEW 2016 programming were used to record crucial parameters during the experiments.

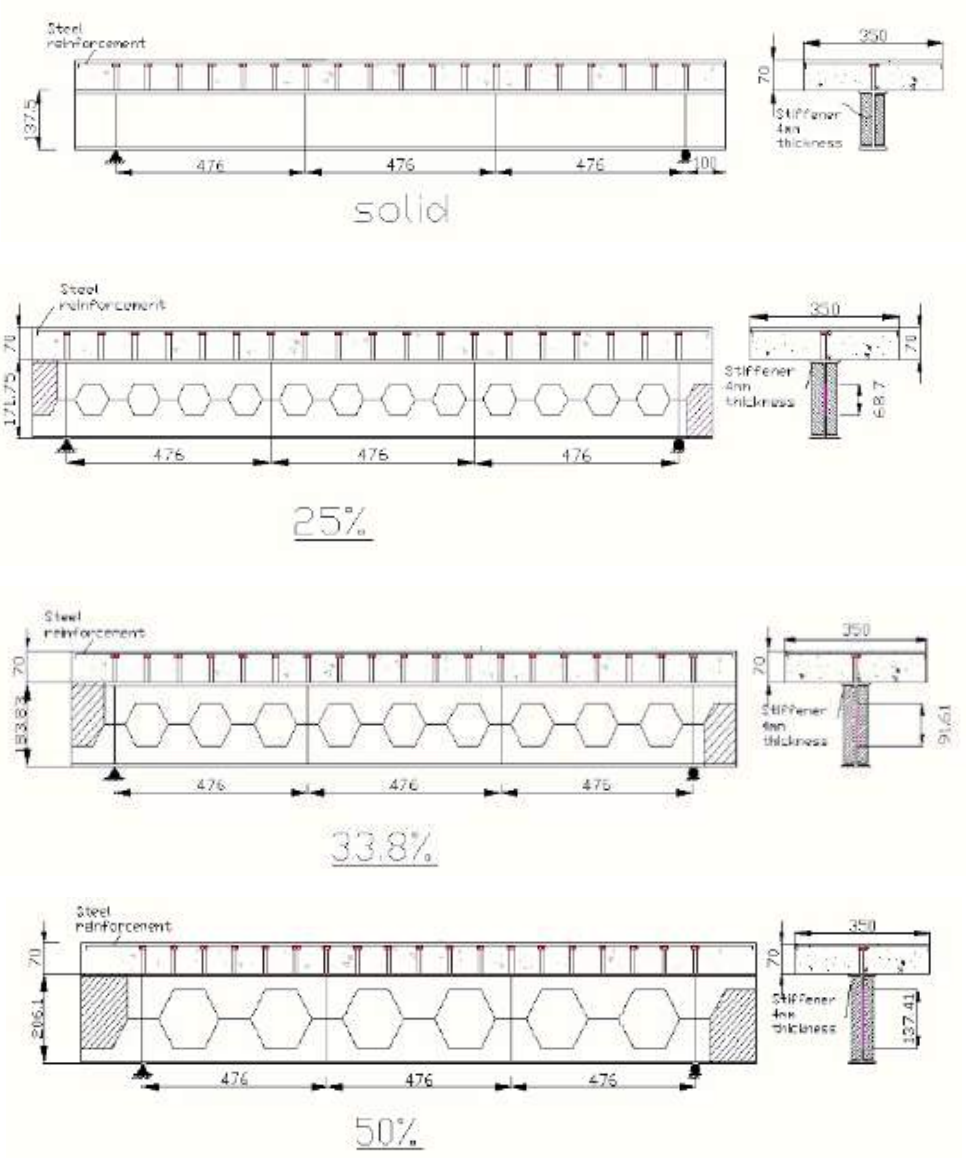

Figure 2-12:Plan of Composite Castellated Beam (λ=0, 25, 33.8 ,50%).

The study reveals that the force response of composite castellated steel-concrete beams under impact loads increases significantly during the first vibration cycle, reaching the peak impact force. The force dampens, and vibrations subside over multiple cycles. The maximum impact load increases

slightly with increasing castellation, indicating the kinetic energy of the falling mass. The maximum displacement amplitude increases, particularly after the third strike, by around 23%. Greater degrees of castellation lead to quicker damping of displacement fluctuations and reduced vibration amplitudes. Crack widths do not exceed 0.025 mm after the first strike. Still, those with castellated steel I-sections have narrower cracks, suggesting that the castellation process enhances beam performance and reduces crack widths.

This study, conducted by Sukanya et al. in 2019 [37], focuses on the performance of profiled deck slabs in composite floor systems, specifically when combined with steel castellated beams. The research uses ANSYS software to model and analyze composite deck slabs with castellated beams. The composite deck slab with the castellated beam section has an increased load-carrying capacity compared to other systems. The ultimate load-carrying capacity of the composite deck slab was 216 kN, compared to 183 kN for a theoretical capacity of 183 kN. The castellated beam exhibits less deflection than an ordinary ISMB 200 section, increasing load-carrying capacity, stiffness, and energy absorption. The wider bearing width of the slab reduces deflection of the profiled deck sheet.

Rossi et al. in 2020 [38] investigated the behavior of steel-concrete composite beams subjected to negative moments. They found that the most influential parameters affecting lateral distortional buckling (LDB) strength are the cross-sectional shape of the steel profile and the presence of web stiffeners. Conventional approaches, such as lateral-torsional buckling theories for partially restrained beams and the U-frame model, yielded conservative results, suggesting an overestimation of the risk of LDB failure. The study

highlights the need for further investigations to enhance our understanding of how steel-concrete composite beams behave under negative moments.

The paper authored by Ferreira et al. in 2021 [39] delves into the buckling and post-buckling analyses of composite cellular beams. The study investigates the strength of composite cellular beams through post-buckling analysis, focusing on six cross-sectional configurations with variations in opening diameter and web post length. Key findings include that the end post plays a crucial role in determining the strength of composite cellular beams, with smaller opening diameters leading to greater critical global shear. Variations in the height of the cellular beam have minimal influence, especially for larger diameters and web post widths. In asymmetric sections, web post-buckling is not observed in the first buckling mode, and altering the beam's height increases global shear. The study also introduces a numerical model capable of representing experimental composite cellular beam models, comparing elastic and inelastic analyses and analytical procedures. The findings highlight potential overestimations in certain cases and suggest the need for potential revisions.

The research conducted by Ferreira et al. in 2021 [40] investigates the sensitivity of composite cellular beams to variations in constitutive material models and parameters related to concrete fracture. This study examines the sensitivity of composite cellular beams to variations in steel and concrete constitutive models and parameters related to concrete damage plasticity. The research uses geometrically nonlinear analyses and experimental tests. Key findings show that dilation angles do not significantly influence flexural behavior, post-peak behavior improves with a dilation angle equal to 40º, and viscosity parameter variation doesn't significantly impact load-displacement relationship behavior. The study emphasizes the importance of considering

these factors when designing structural elements and proposes a control mechanism for instability-related problems.

The study conducted by Hayder Wafi in 2022 [41] focused on an in-depth investigation of the structural behavior of composite concrete slabs when acting in conjunction with symmetrical and asymmetrical castellated steel beams interconnected through the utilization of stud connectors.

During experimentation, five supported composite beams were subjected to two-point loading conditions. Two of these specimens were constructed using conventional standard steel beams as control specimens, while the remaining three were meticulously assembled using castellated steel beams. The ultimate load capacity of a composite castellated beam fabricated from an IPE120 section was 46% greater than that of a composite beam built up using the parent beam. The ultimate load capacity of a composite castellated beam fabricated from a wide-flanged HEA120 section increased by 21% over the parent beam control specimen. The ultimate load capacity of the composite specimen built up using the asymmetrical castellated beam (IPE120/HEA120) achieved increases of 69% and 12%, respectively, compared to the control specimens built up from standard sections.

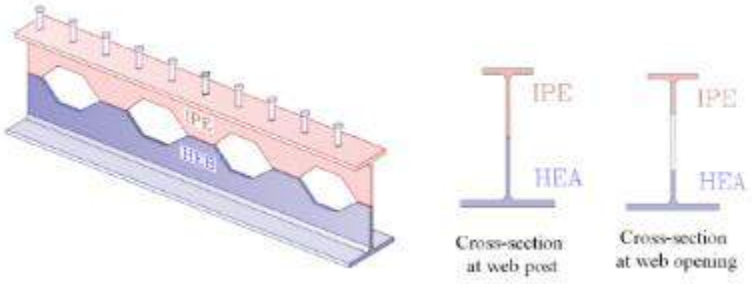

Figure 2-13:Asymmetrical Castellated Steel Beam

In their study, Dakhela and Mohammed, 2022 [42], conducted a comprehensive investigation into the feasibility of employing composite

cellular beams featuring lightweight reinforced concrete deck slabs as integral structural elements for buildings subjected to harmonic loads. The experimental program encompassed the examination of beams supported by three fixed ends, spanning 2140 mm, and incorporated three distinct concrete deck types: Normal Weight Concrete (NWC), Lightweight Aggregate Concrete (LWAC), and Lightweight Fiber Reinforced Aggregate Concrete (LWACF). Various operating frequencies were systematically evaluated, specifically 5, 10, 15, 20, 25, and 30 Hz.

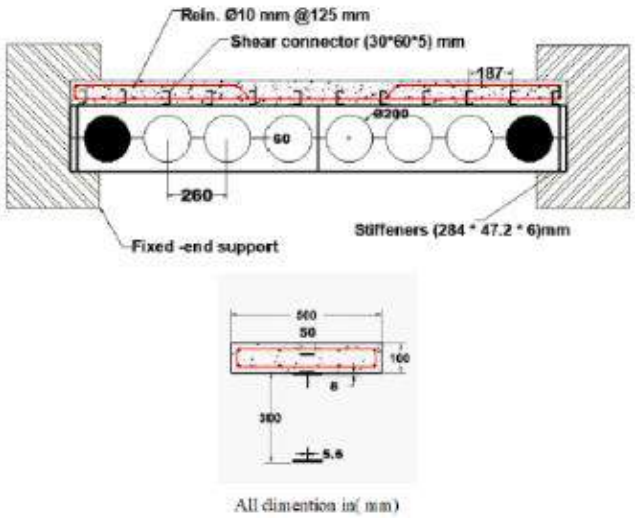

Figure 2-14: Cellular Beam Details

The study reveals that the type of concrete deck slab significantly affects the response and structural behavior of composite cellular beams under harmonic loading conditions. Fiber reinforcement in lightweight concrete (LWACF) is crucial, yielding responses similar to normal weight concrete (NWC). LWACF is more suitable for cellular composite beams due to its negligible response variations and 27% reduction in density.

In this study performed by Alharthi et al. in 2023 [43], a study was conducted to examine the flexural behavior and capacity of composite concrete-steel beams (CRCSB), focusing on the influence of shear

connections and bearing stiffeners. Five comprehensive CRCSB samples were fabricated and subjected to four-point bending experiments using four different forms of shear connections. The results showed that the geometry of the shear connector significantly impacts the concrete component's behavior, particularly crack propagation and widening. Shear connectors, such as angles and channels, help impede the transmission of compressive forces within the slab. Bearing stiffeners significantly influence the behavior of cold-formed steel channel sections with web openings. The inclusion of bearing stiffeners resulted in a significant increase in load capacity (55% increase) and displacement (229%). The study provides insight into the significant influence of shear connections and bearing stiffeners on the structural performance and load-carrying capacity of CRCSBs, offering significant contributions to understanding flexural stress situations.

2.4 Strengthening Composite Castellated Beams

Strengthening composite castellated beams is essential for optimizing their performance and safety in real-world applications. These strengthening methods enhance their load-bearing capacity, resistance to deflection, and overall durability. Properly reinforced castellated beams contribute to more efficient and sustainable construction practices, ultimately advancing the field of structural engineering.

The study undertaken by Afefy et al. in 2012 [44] focuses on the behavior of composite castellated beams when subjected to various strengthening configurations and external pre-stressing. The study analyzed ten specimens of composite castellated beams, divided into three groups: reference castellated beams without a specific strengthening configuration, three specimens with additional vertical stiffeners, and three partially encased

composite castellated beams. The connection between the concrete slab and the beam was considered perfect, with slip prevention achieved through designed shear connectors. Key parameters like ultimate strength, vertical mid-span deflection, strain measurements on concrete and steel components, and strain applied to the pre-stressed bars were recorded and analyzed. The findings highlighted the impact of external pre-stressing on the behavior of composite castellated beams, emphasizing the need to address issues related to the beam's end zone. The study also highlighted the positive effects of pre-stressing, particularly on the concrete section of composite beams compared to steel beams.

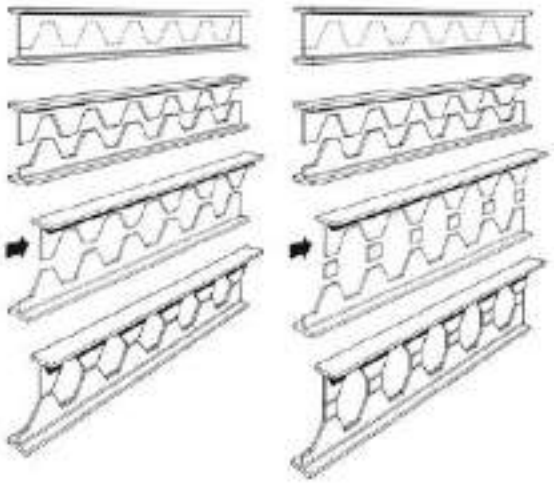

Figure 2-15:Manufacturing Steps of Hexagonal and Octagonal Castellated Beams.

This study conducted by Patil and Kumbhar in 2016 [45] focuses on castellated beams, which are engineered by cutting I-sections in a zigzag manner and subsequently rejoining them to increase the depth of the parent I-section. This research examines using transverse and edge stiffeners in castellated beams to improve structural performance. The study uses ABAQUS software to compare the two types of stiffeners. Transverse stiffeners require less steel than edge stiffeners but do not improve load-

carrying capacity. The study suggests that transverse stiffeners are more suitable for enhancing structural performance, as they consume less volume and function as a single short column. Edge stiffeners reduce stress concentration along the opening edge but do not contribute to increased load-carrying capacity. The study concludes that transverse stiffeners are a more effective choice for enhancing structural performance in castellated beams. The findings suggest that transverse stiffeners are more suitable and effective for enhancing structural performance.

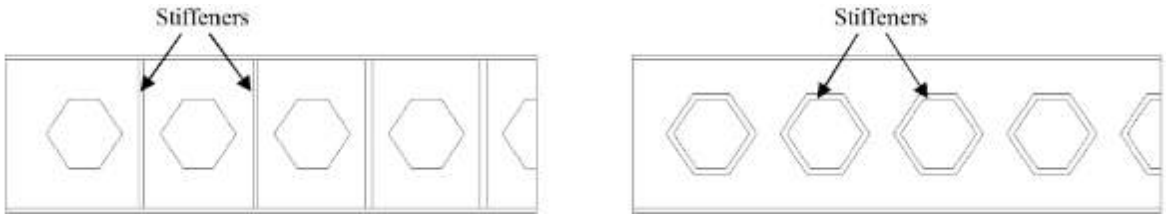

Figure 2-16: A-Castellated Beam with Stiffeners in The Transverse Direction. B-Castellated Beam Provided with Stiffeners Along Edge of Openings

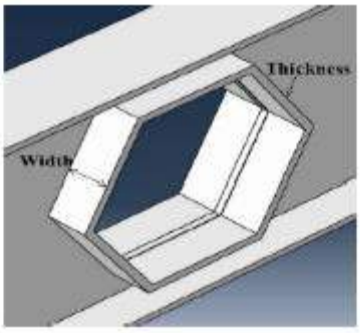

Figure 2-17:Terminology for Stiffener Along the Edge of The Opening.

The study by H. W. A. Al-Thabhawee and Al-Kannoon in 2018 [46] focuses on enhancing the performance of castellated steel beams. This research aims to improve the behavior of both hexagonal and octagonal castellated beams by adding spacer plates. The ultimate strength of an original I-section beam increases with the depth of the castellated beam. By adding ring stiffeners to the edges of holes, the finite element model (FEM) analysis reveals that the web of castellated beams becomes stronger. This reduces stress concentration around hole edges and improves beam behavior by increasing ultimate

strength and minimizing deflection. Octagonal castellated steel beams can increase their ultimate strength by up to 53% compared to parent beams. The nonlinear model also shows higher failure loads for castellated beams with eight hexagonal openings.

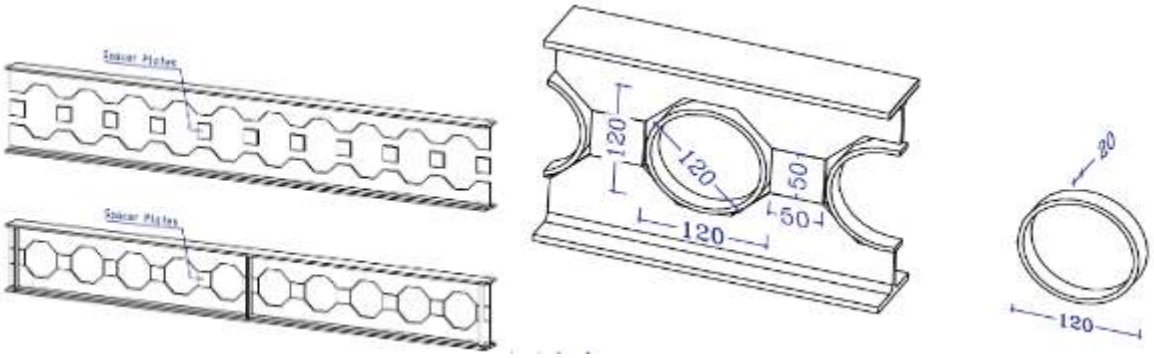

Figure 2-18:Rejoined Castellated Steel Beam With Increment Plate (Octagonal Opening) [46]**.**

Kumaragurubaran et al.'s 2021 [47] study investigates the impact of stiffeners on the shear strength of castellated beam chassis under cyclic loading. The researchers tested three different configurations of castellated beam chassis: no stiffeners, vertical stiffeners at two end holes, and diagonal stiffeners at the two end holes. The results showed that the castellated beam chassis with diagonal stiffeners at the two end holes had the highest shear strength and minimal deflection. Forward cyclic loading induced more deflection than reverse cyclic loading. The study concluded that adding stiffeners to castellated beam chassis significantly enhanced shear strength and deflection performance. The findings have implications for design and engineering of castellated beam chassis, as diagonal stiffeners at the two end holes can enhance shear strength and mitigate deflection, making them valuable in applications requiring stringent load-bearing capacity, structural stiffness, and deflection control.

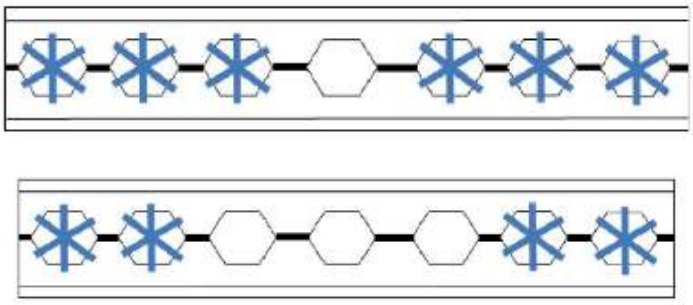

Figure 2-19:A-Stiffener in Two Adjacent Web Holes at Each End of The Beam Chassis Specimen, B- Stiffener in Three Consecutive Web Holes at Each End of The Beam Chassis Specimen

The research conducted by H. W. Al-Thabhawee and Al-Kannoon in 2022 [48] The study examines the use of tapered castellated beams (TCBs) in mid-span concentrated loads. TCBs, engineered by cutting I-section webs in a specific pattern and rejoining them using variable expansion plates, can significantly increase the ultimate load capacity compared to the parent section. They meet the International Building Code's deflection limits and can withstand up to 83% deflection. However, failure modes like web-post buckling and joint-weld rupture are found. TCBs with higher expansion depth ratios show superior stiffness and strength than prismatic castellated beams. These findings have significant implications for long-span structural member design and engineering.

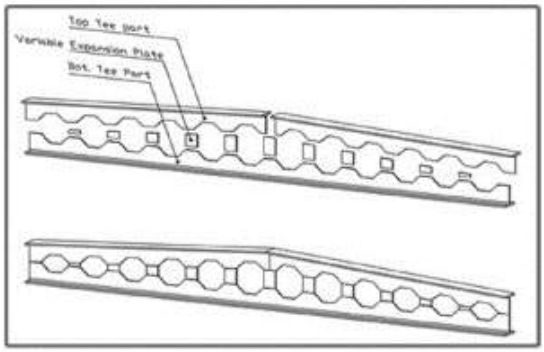

Figure 2-20:Fabrication of TCBs by Placing Variable Expansion Plates.

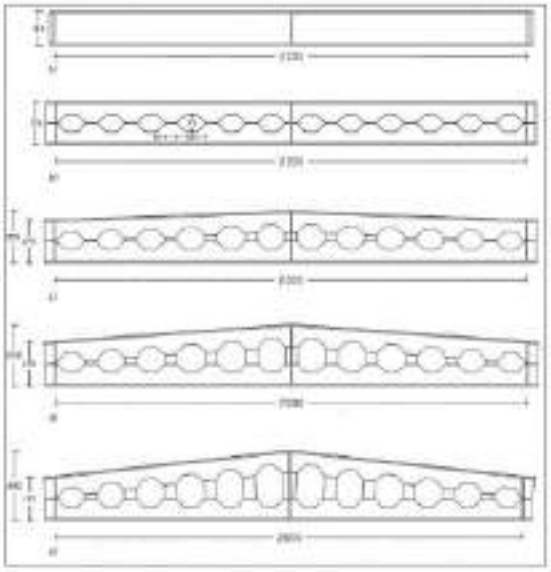

Figure 2-21:Dimensions and notations of all tested specimens. (a) Parent beam: specimen (Control), (b) castellated beam without expansion plate: specimen (CBN-0) [H /h = 1.0], (c) tapered castellated beam with variable expansion plate: specimen (CBN-1) [H/h = 1.2], [48].

The study by Abbas and Al-Thabhawee in 2022 [49] A study on composite steel-concrete beams, specifically cellular beams, was conducted using an IPE140 hot-rolled I-section steel beam. Four specimens were created: a control beam, a non-composite beam, a composite steel-concrete beam (CLB1), and a composite steel-concrete beam (CLB4-R). The results showed that the non-composite beam had a 29% lower ultimate load capacity than the composite beam. The CLB4-R beam could carry a load 77.3% higher than the original beam. Transforming the solid beam into a cellular beam increased the ultimate load by 5.3% without additional material. The study also found that web-post buckling was the dominant failure mode for cellular beams with substantial web openings.

2.5 Summary

The study aims to address gaps in research on composite castellated beams. By examining their behavior and optimization, the study focuses on factors such as shaped openings, shear stud spacings, and stiffeners to improve load-carrying capabilities and structural performance.

In conclusion, research on Castellated Steel Beams (CSBs) provides valuable insights into their structural behavior and optimization. Specific geometric configurations, such as cutting angles and web opening distances, significantly influence CSBs' load capacity and overall performance. Incorporating concrete filler between flanges and exploring reinforcement techniques enhances flexural ability and energy absorption.

Investigations into shear buckling strengths offer practical design equations, with recommended safety factors, addressing elastic-plastic state discrepancies. Optimization studies on hexagonal hole configurations emphasize spacing and opening angles, guiding engineers to achieve increased strength.

Torsional moment capacity studies show CSBs' superiority over solid I-beams, with some configurations exhibiting enhanced strength. Stainless-steel cellular beams display commendable fire resistance, positioning them as reliable structural choices. Insights into load capacity, seismic resistance, and fire performance contribute to efficient and resilient structural solutions. Stiffeners significantly impact ultimate load capacity, deflection performance, and buckling resistance of castellated beams. Initiating web apertures after the negative moment region enhances load capacity and flexibility. Enhanced material strength, thicker slabs, spacer plates, and steel rings augment CSBs' performance. Incorporating diagonal stiffeners at terminal apertures effectively enhances shear strength and deflection characteristics.

Chapter Three: Experimental Work

Chapter Three: Experimental Work

3.1 Introduction

The principal objective of conducting this research is to study the experimental behavior of composite castellated beams subjected to repeated load tests. This research has examined and analyzed many main parameters, such as shear connectors, shaped openings, and strengthening. The chapter describes the materials, specimens, formwork, casting, instruments, and testing setup. On the other hand, the mechanical and chemical properties of the specimens' materials (cement and fine and coarse aggregate) were tested according to the Iraqi specifications (IQ.S.) and the American Society for Testing and Materials (ASTM). Besides that, different destructive tests were done to determine the mechanical properties of the steel coupons' yield stress and ultimate strength and the concrete's compressive strength, flexural strength, and splitting tensile strength after 28 days of curing in water.

This chapter describes fifteen composite beams with different variables, which were of overall length (1.5m) consisting of the concrete slab (0.07 m) thickness and (0.35 m) width and steel section (IPE140), connected by shear connectors. This chapter also presents a general description of testing machines, the preparation of the specimens for tests, and the testing methods. All experiments were executed at the University of Kerbala’s College of Engineering labs.

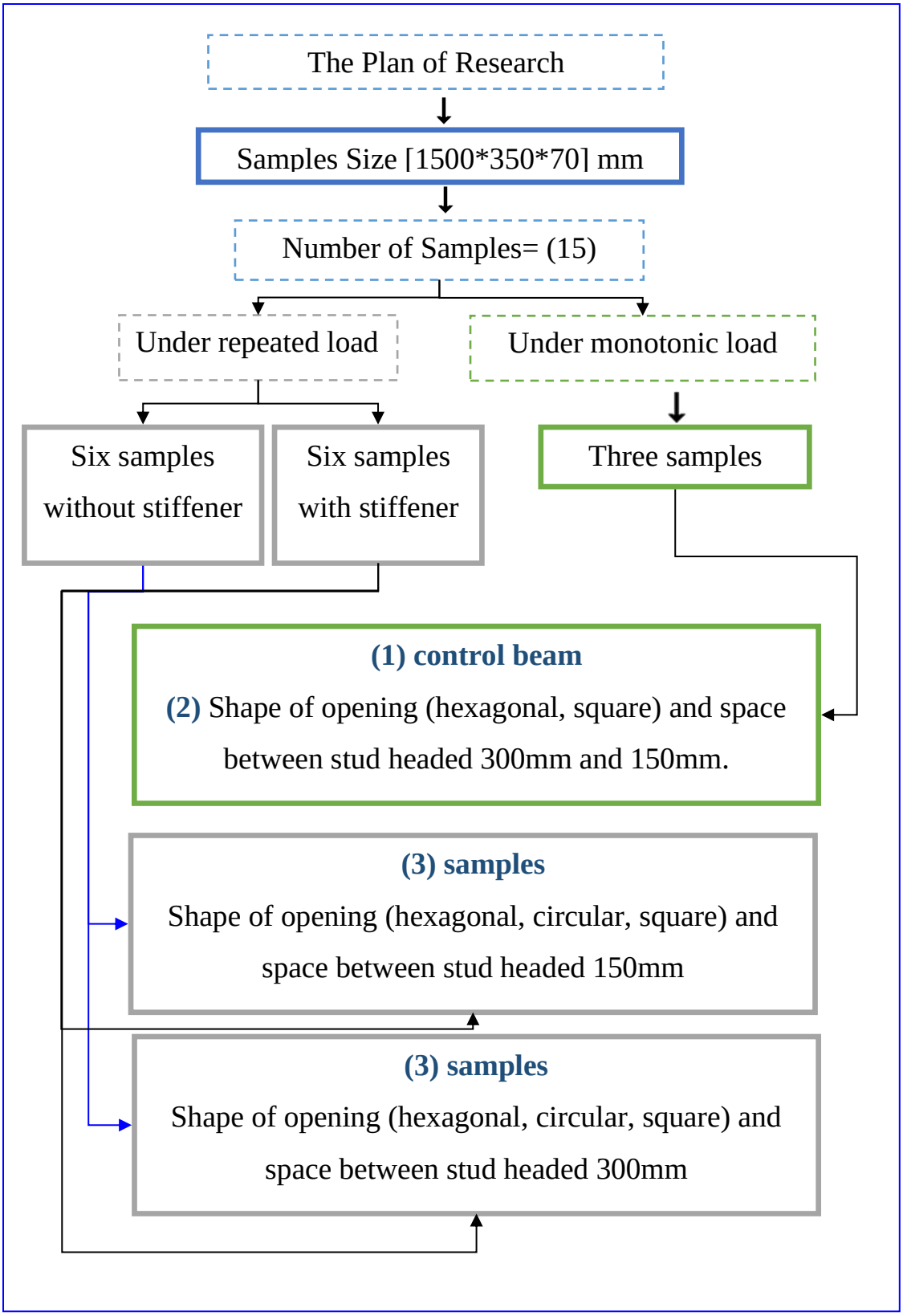

Figure 3-1:Flowchart of Testing Matrix.

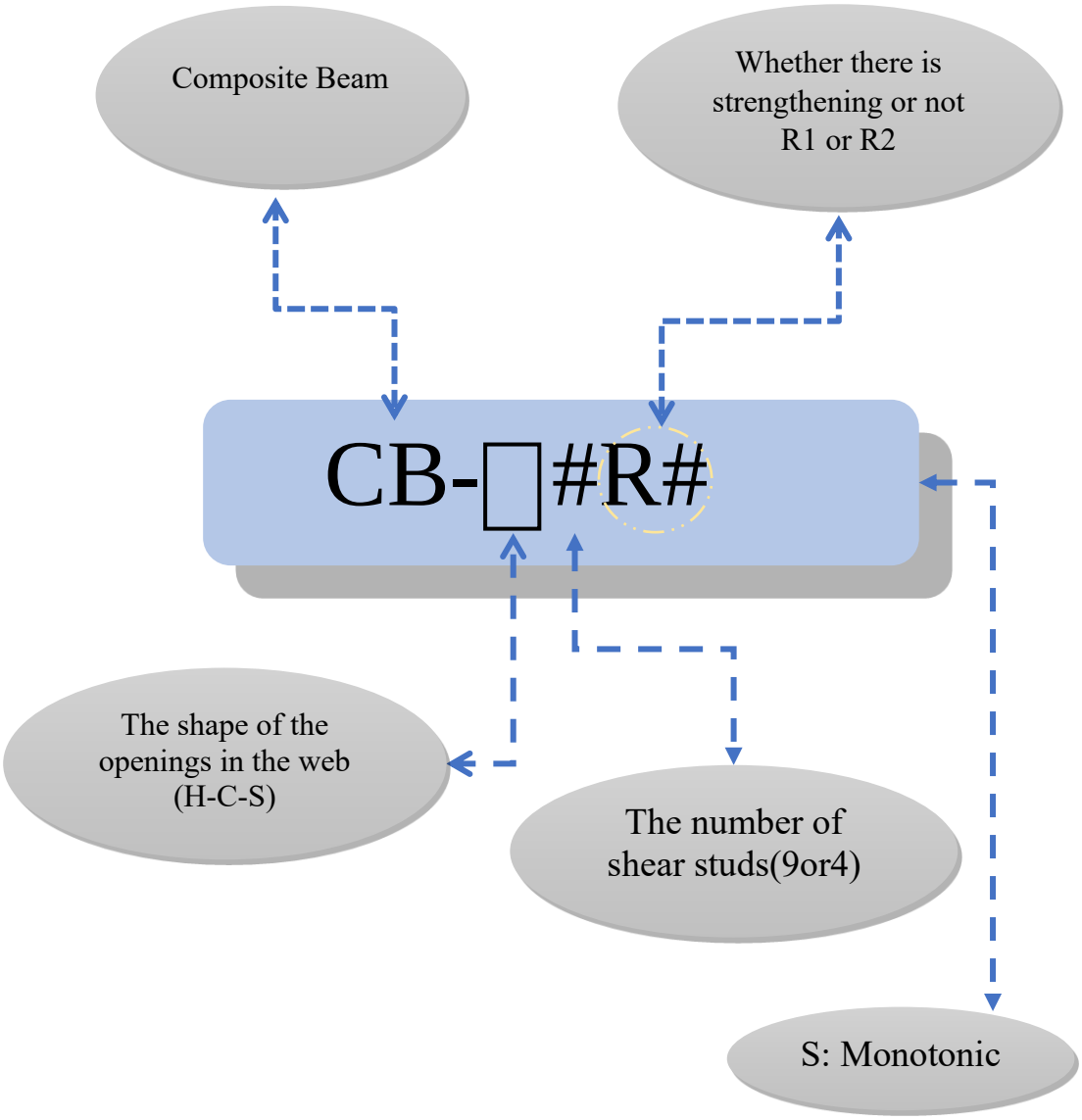

Figure 3-2: The Details of Coding the Composite Castellated Beam Models.

Table 3-1 :Details of all the test beams in the present study.

Group	Name of sample	Shape of opening	Shear connectors		Long of span (mm)	Type of strengthening	Type of loading
			Number	Spacing (mm) c/c			
One	CB-9S	None	9	150	1500	-----	monotonic
	CB-S9S	Square	9	150	1500	-----	monotonic
	CB-H9S	Hexagonal	4	300	1500	-----	monotonic
Two	CB-H9R1	Hexagonal	9	150	1500	-----	Repeated 25%Pu
	CB-C9R1	Circular	9	150	1460	-----	Repeated 25%Pu
	CB-S9R1	Square	9	150	1500	-----	Repeated 25%Pu
Three	CB-H4R1	Hexagonal	4	300	1500	-----	Repeated 25%Pu
	CB-C4R1	Circular	4	300	1460	-----	Repeated 25%Pu
	CB-S4R1	Square	4	300	1500	-----	Repeated 25%Pu
Four	CB-H9R2	Hexagonal	9	150	1500	Stiffeners	Repeated 25%Pu
	CB-S9R2	Square	9	150	1500	Stiffeners	Repeated 25%Pu
	CB-C9R2	Circular	9	150	1460	Stiffeners	Repeated 25%Pu
Five	CB-H4R2	Hexagonal	4	300	1500	Stiffeners	Repeated 25%Pu
	CB-C4R2	Circular	4	300	1460	Stiffeners	Repeated 25%Pu
	CB-S4R2	Square	4	300	1500	Stiffeners	Repeated 25%Pu

3.2 Description of Specimens

3.2.1 Geometry

The experimental program involved testing fifteen simply supported composite castellated steel beams with the same span and different geometry properties. The study has focused on the overall shear behavior mechanism because the castellated beam is more susceptible to shear stresses.

3.2.2 Test Specimens

Fifteen composite beams were fabricated for the experiments, each with different variables. The beams had an overall length of 1.5 meters. Six beams were tested without stiffeners, and the open section shape varied among circular, hexagonal, and square. The spacing of shear studs in these beams was either 150mm c/c or 300mm c/c in one row. Additionally, six beams were tested with stiffeners, following the same open section shapes and shear stud spacing variations. In addition to the beams with variable parameters, three monotonic load tests were conducted. These included one non-castellated beam, one beam with a square opening, and one beam with a hexagonal opening. The loads applied to these beams were two-point loads.

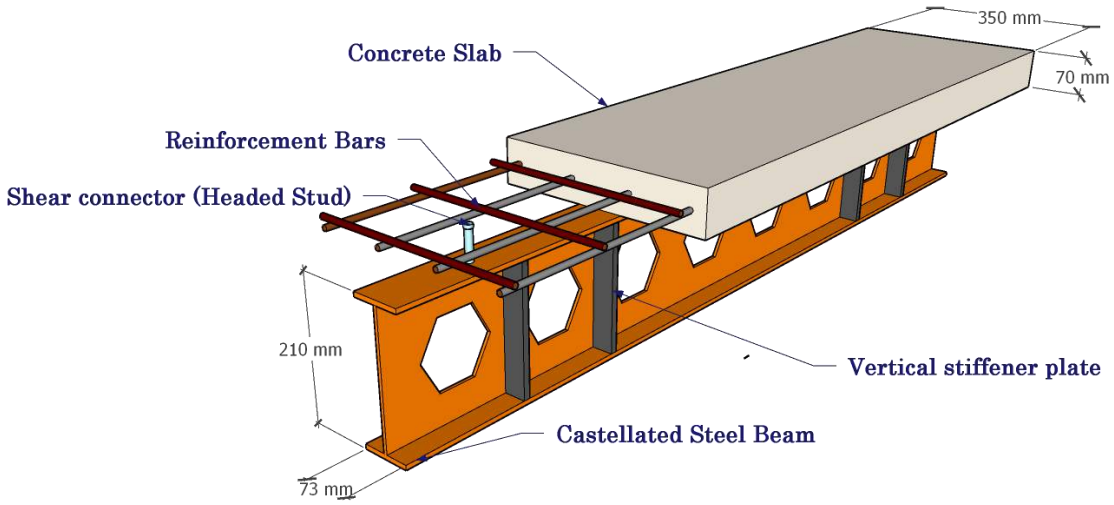

Figure 3-3:Composite Castellated Steel-Concrete Sample CB-H4R2.

3.2.3 Steel Section Cutting and Welding

The researcher uses a computer numerical control (CNC) plasma technique to cut the web beam, ensuring the openings are seamlessly and accurately aligned. This process yielded a smooth and precise outcome, as Plate (3–1) depicts.

b- After manufacturing

a- During manufacturing

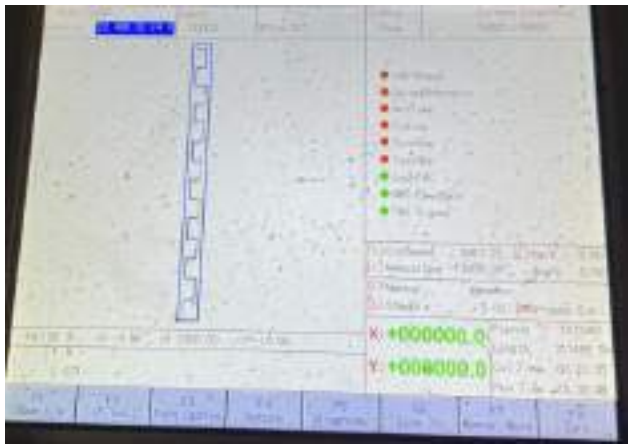

c- The machine interface used

Plate 3-1: Photograph for a Zigzag Pattern by CNC. (Al-Rasool blacksmith)

After cutting, the top and bottom tee sections were separated, shifted, and welded back together. Plate (3-2) shows the upper and lower portions attached.

Plate 3-2: Assembling Technique of the Tee Sections.

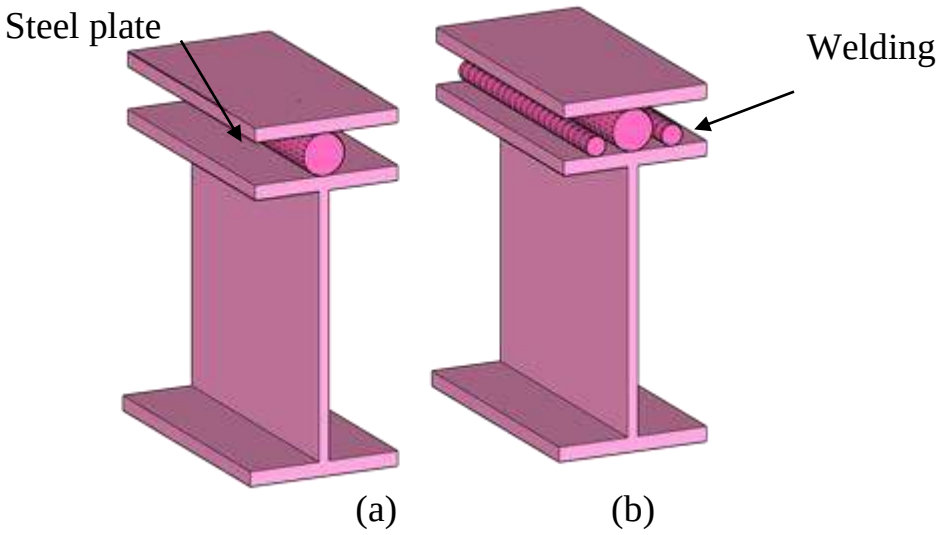

Figure 3-4: (a) Roller and (b) Hinge Support

1- Hexagonal opening

Figure (3-5) shows a castellated beam with a hexagonal opening. The following are the parameters considered for this beam in the present study.

1. Overall, Height (*h*) - 210mm
2. Height of perforation (h_o) -140mm
3. Total span of a beam (*L*) - 1500mm
4. Width of the throat (*W*T) - 60mm
5. Spacing between two perforations (*S*) - 183mm
6. Angle of cut (θ) - 67°
7. Depth of throat (*D*T) - 35mm
8. Distance between two perforations (*e*) - 60mm

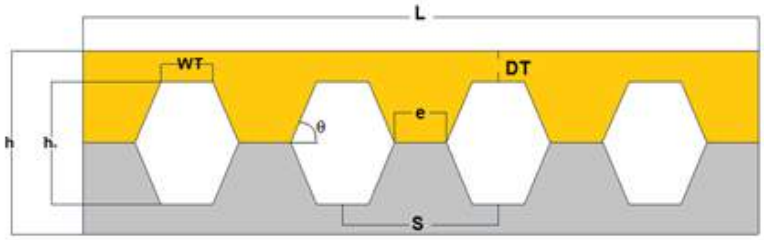

Figure 3-5:Design of Castellated Beams with Hexagonal Opening.

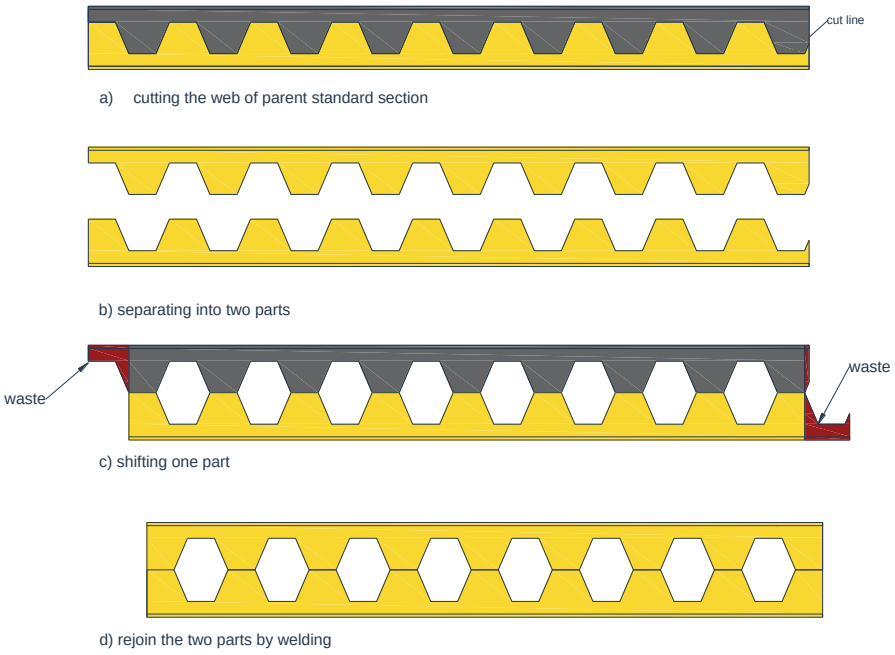

Figure 3-6:Manufacturing Process of a Castellated Beam.

2- Circular opening

Figure (3-8) shows a castellated beam with a circular opening. The following are the parameters considered for this beam in the present study.

1. Overall Height (*h*) - 190mm
2. Height of perforation (h_o) - 140mm
3. Total span of the beam (*L*) - 1460mm
4. Width of the throat (*W*T) - 140mm
5. Spacing Between two perforations (*S*) - 200mm
6. Depth of throat (*D*T) - 35mm.
7. Diameter of perforation (ø) - 140mm
8. Distance between two perforations (*e*) - 60mm

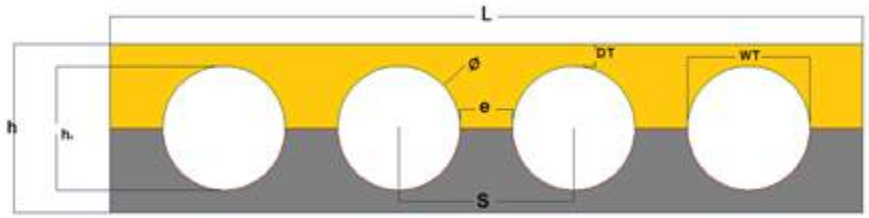

Figure 3-8:Design of Castellated Beams with a Circular Opening.

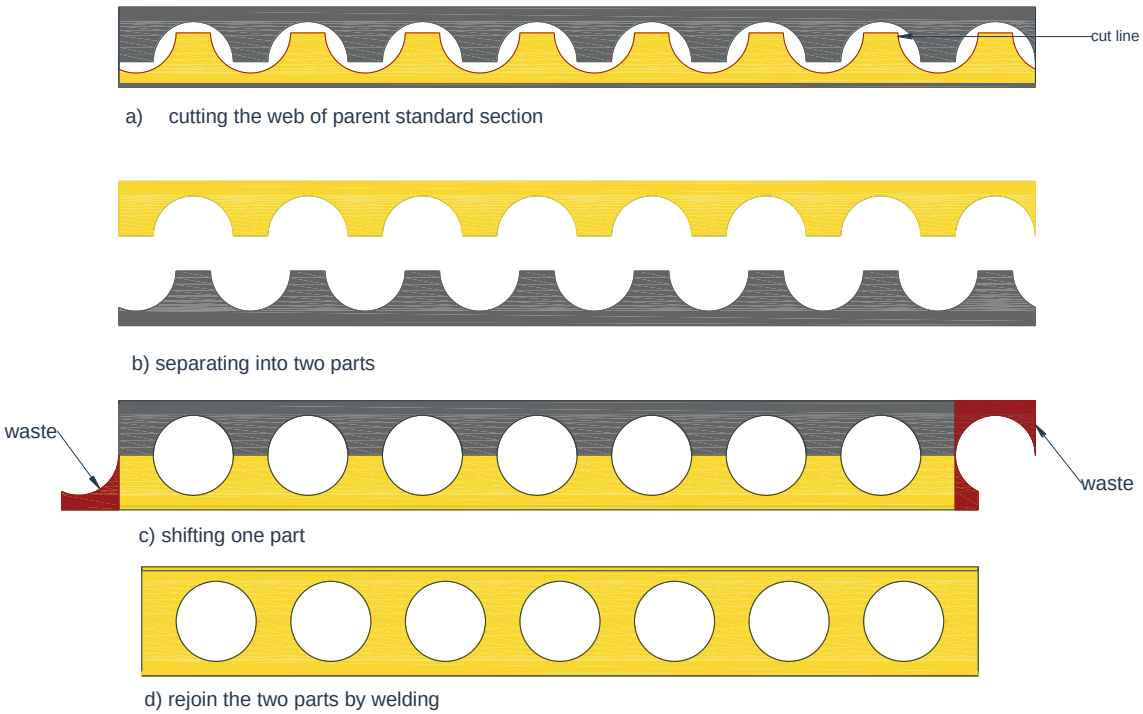

Figure 3-9:Manufacturing Process of a Castellated Beam.

3- Square opening

Figure (3-10) shows a castellated beam with a square opening. The following are the parameters considered for this beam in the present study.

1. Overall Height (h) - 210mm
2. Height of perforation (h_o) - 140mm
3. Total span of the beam (L) - 1500mm
4. Width of the throat (WT) - 140mm
5. Spacing between two perforations (S) - 280mm
6. Depth of throat (DT) - 35mm
7. Distance between two perforations (e) - 140mm

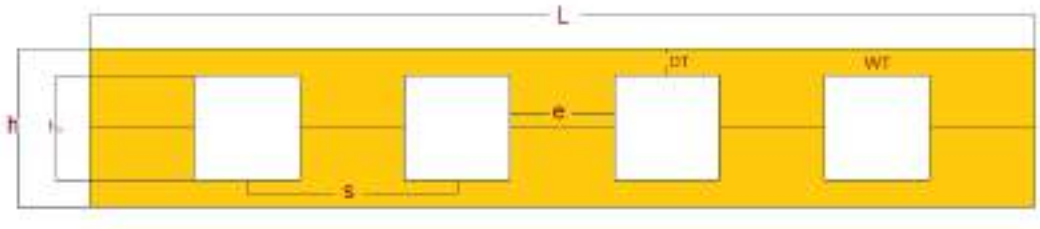

Figure 3-10:Design of Castellated Beams with Square Opening

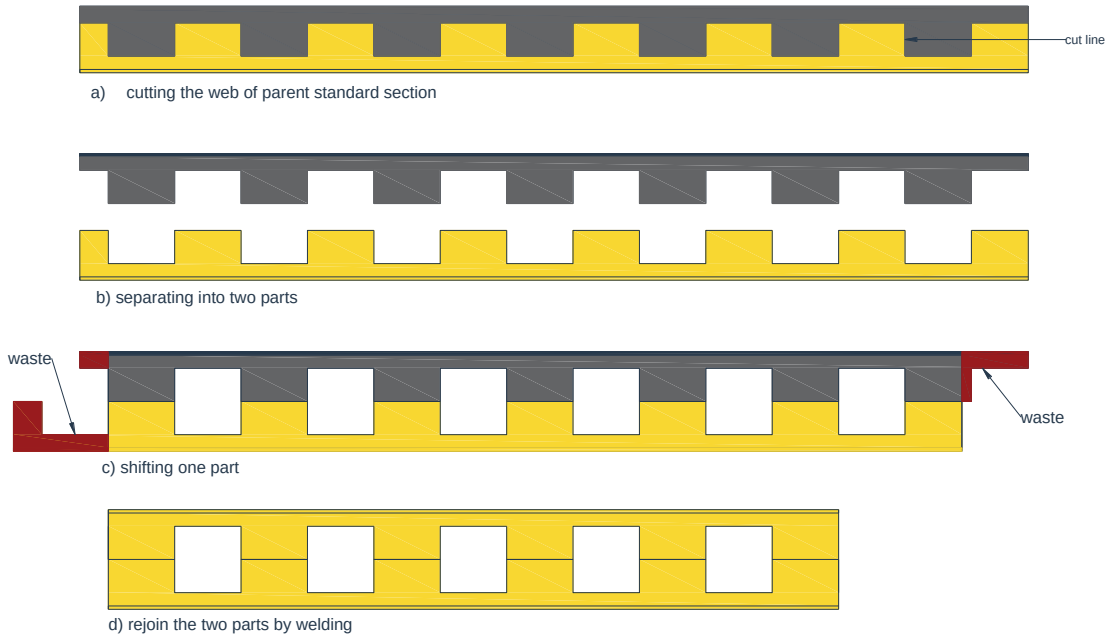

Figure 3-11:Manufacturing Process of a Castellated Beam.

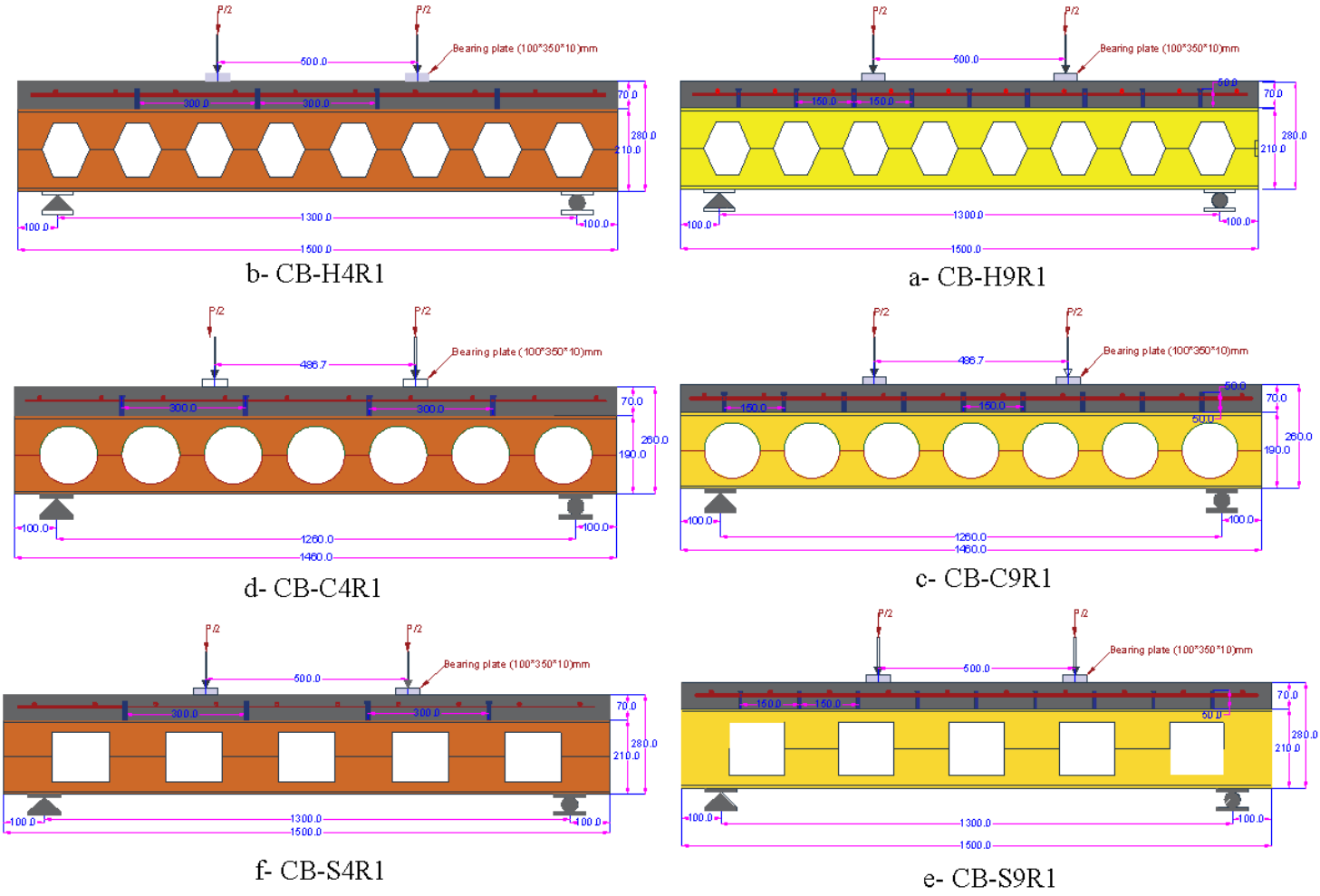

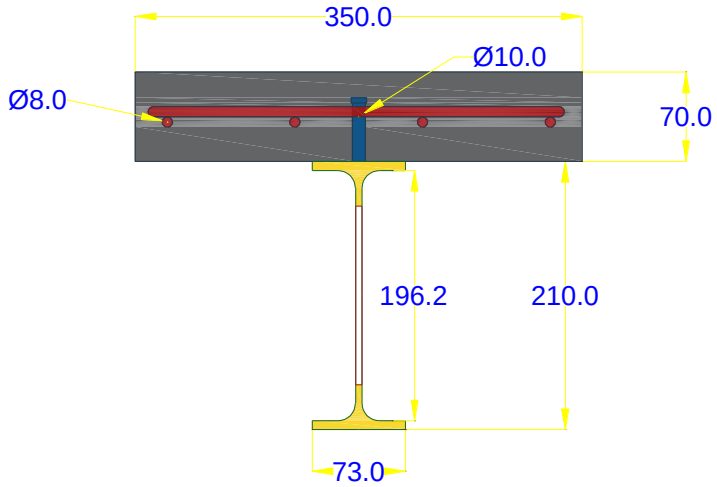

Figure 3-12:Dimensions and Details of Tested Specimens .

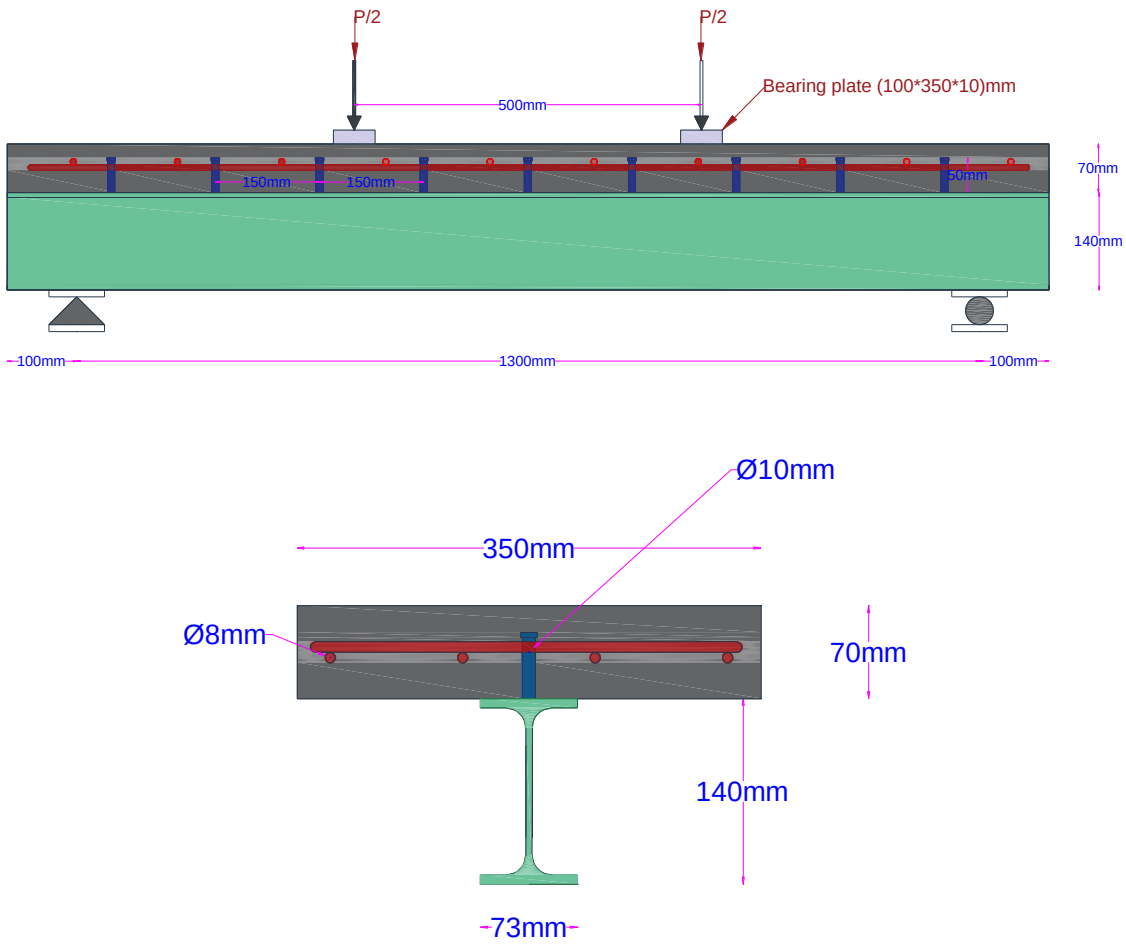

Figure 3-13 :Dimensions and Details of Tested Specimens (Control Beam)

Plate 3-3: Distribution of Shear Connectors of CB-9S

3.3 Stiffeners in Composite Castellated Beams:

3.3.1 Design, Analysis, and Applications

The composite castellated beam has four vertical stiffener plates positioned at each end, with a 200 mm separation between them. These plates are strategically placed at the second opening in the web to enhance the beam's structural integrity and bearing load capacity. The distance between the plates is determined based on engineering factors and loading conditions. The spacing is chosen to maximize support, considering web aperture dimensions and configuration. The stiffener plates are typically made from steel and attached to the beam using welding or bolting methods. This ensures a robust and inflexible linkage between the stiffeners and the beam. and designed according to AISC specifications [50] using the LRFD method.

Plate 3-4 :Dimensions and Details of Stiffeners to Reinforce Castellated Beam.

Transverse full depth bearing stiffeners were provided and attached to the web at reactions and compressive concentrated loads to prevent the local yielding, crippling, sidesway buckling and compression buckling of the web. Steel plates with cross-section dimensions of (34.2 ×10) mm were used as shown before in **plate (3-4)**.

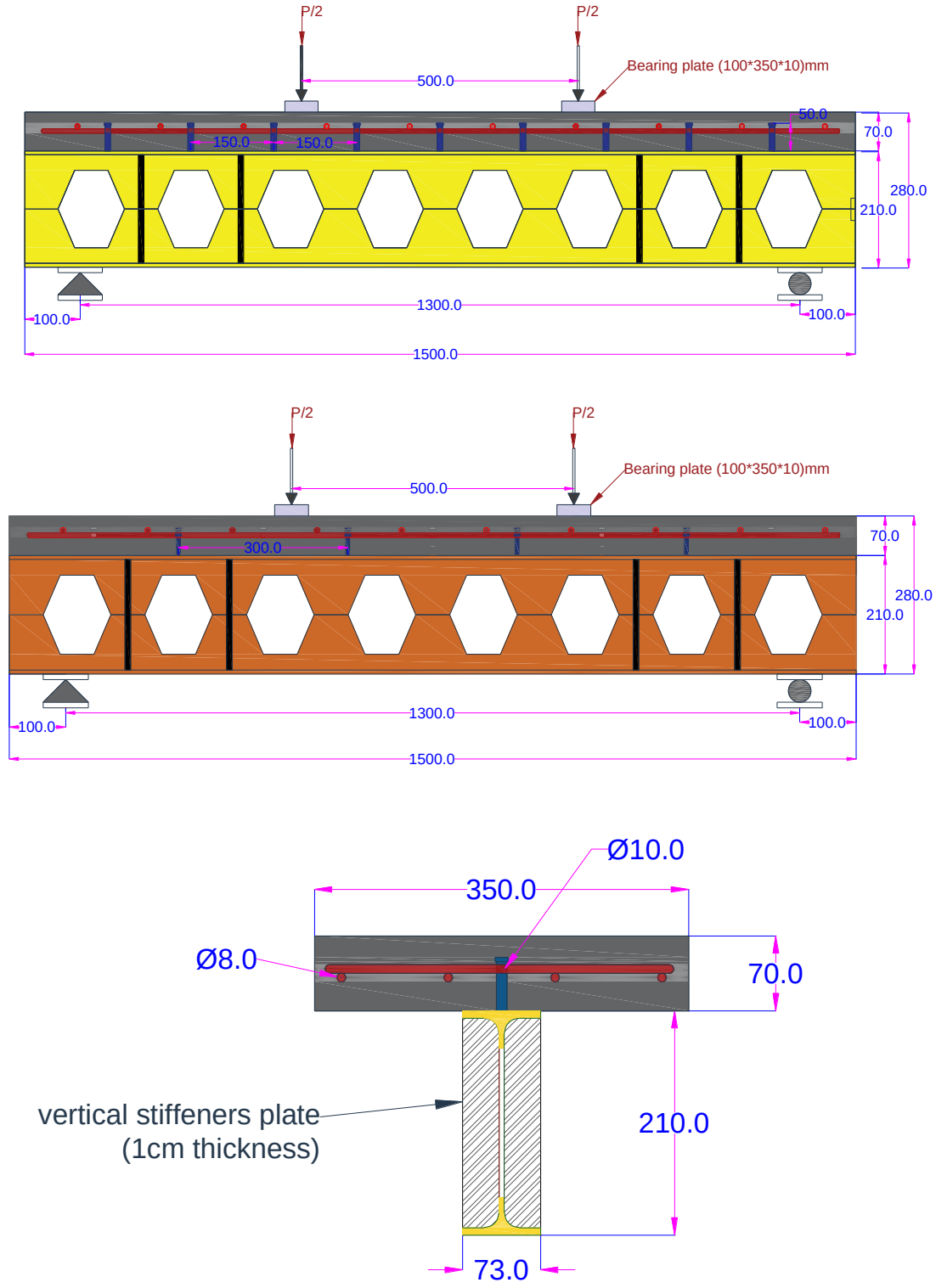

Figure 3-14:Dimensions and Details of Tested Specimens

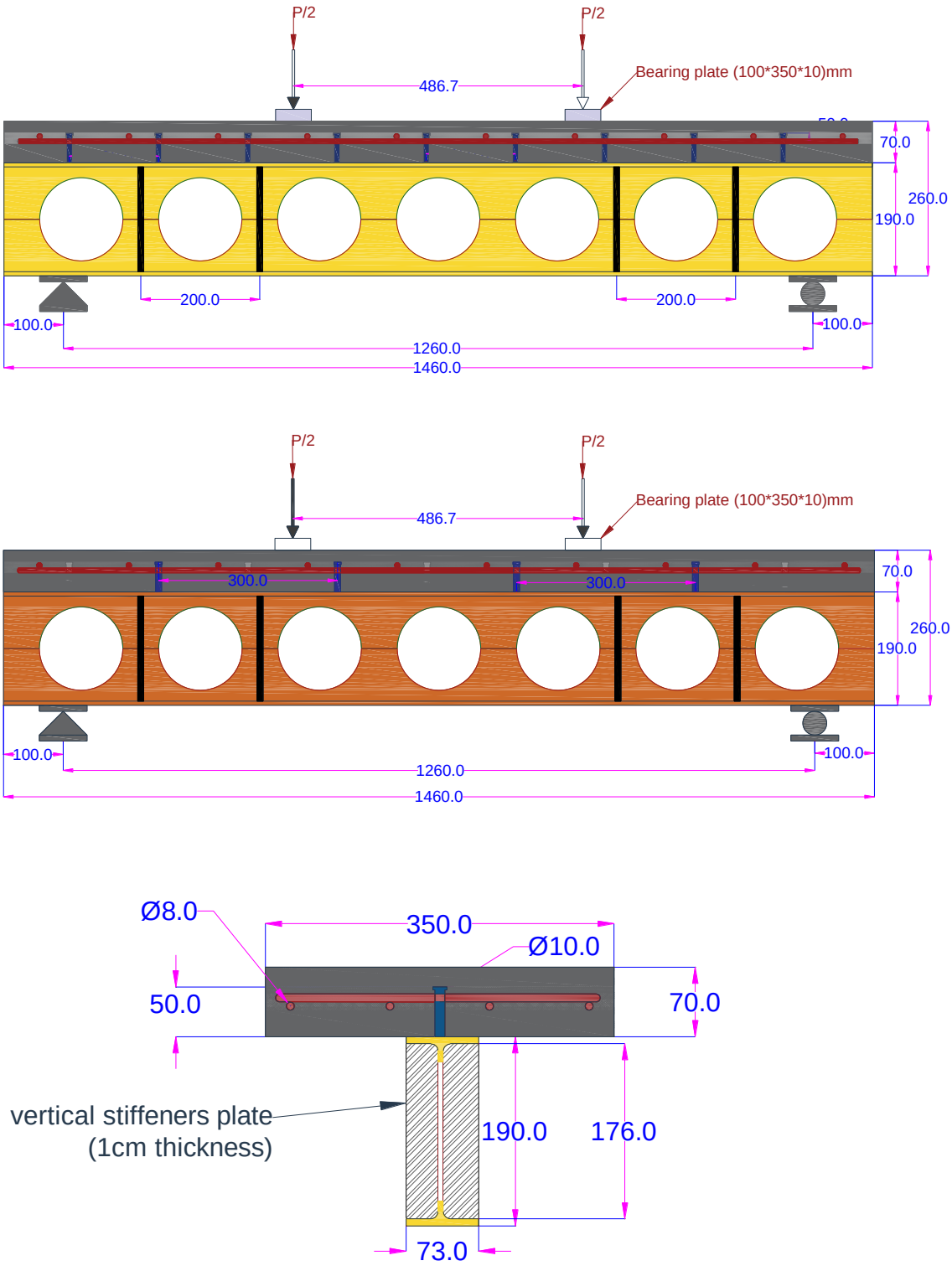

Figure 3-15:Dimensions and Details of Tested Specimens

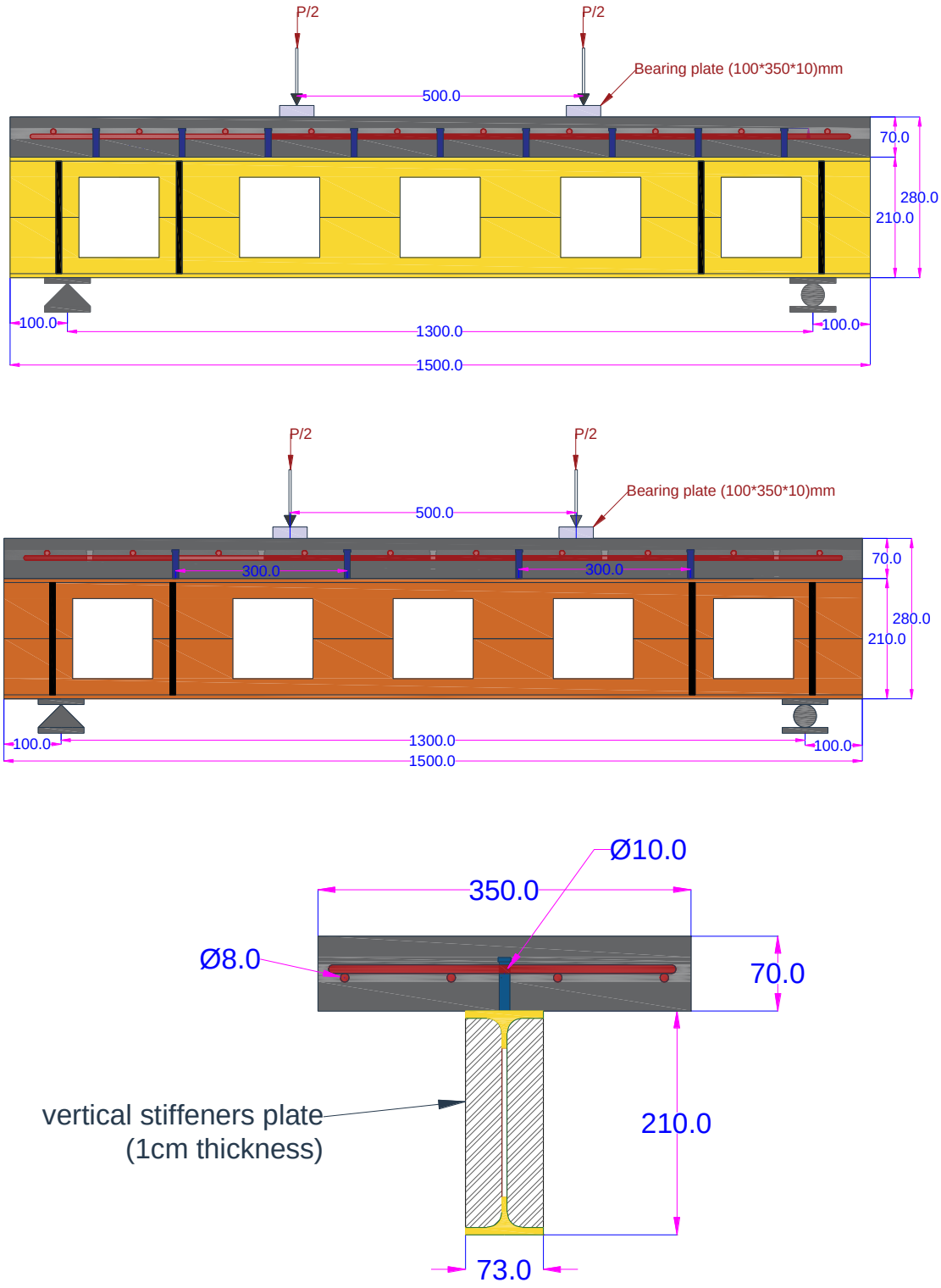

Figure 3-16: Dimensions and Details of Tested Specimens.

3.4 Material

Several construction materials will be examined for the research to meet the following conditions:

3.4.1 Cement

The research uses KARASTA cement, as seen in Plate (3-5). a cement produced by Kerbala Cement Manufacturing Limited (KCML), for various applications like high-strength concrete, ready-mix concrete, precast concrete, and general construction projects.

It is pertinent to note that Lafarge cement conforms to Iraqi specifications No. (5) at 1984 [51] , and its characteristics have been examined in the laboratory of the University of Kerbala. The results of the tests, comprising the physical and chemical properties of KARASTA cement, are presented in Tables 3-2 and 3-3.

Plate 3-5:Cement Used in This Study.

Table 3-2 : Chemical Composition of Cement *

Oxide	Chemical formula	Percentage by weight %	I.Q.S No. 5/1984
Lime	Cao	55	/
Silica	SiO_2	20.7	/
Alumina	Al_2O_3	5.17	/
Iron oxide	Fe_2O_3	5.92	/
Sulfate	SO_3	2.01	≤ 2. 5
Magnesia	MgO	2.49	≤ 5
Sodium oxide	Na_2O	0.25	/
Potassium oxide	K_2O	0.65	/
Insoluble residue	I.R	0.8	≤ 1.5
Loss on ignition	L.O. I	3.98	≤ 4%
Lime saturation factor	L. S. F	0.93	0.660 – 1.020
Bogue potential compound composition		% By weight	
Tri-calcium silicate (C3S)		25.06	/
Di-calcium silicate (C2S)		31	/
Tri-calcium aluminate (C3A)		4.34	≤ 3. 5
Tetra calcium aluminoferrite (C4AF)		14.99	/

* This test was carried out by lab staff in University of

Table 3-3: Physical Properties of The Cement.

No.	Physical properties	Units	Value	I.Q.S No. 5/1984
1	**Specific surface area (Blaine method)**	**m^2/kg**	**313**	**≥ 230**
2	**Setting time**			
	Initial	Min.	195	≥ 45
	Final	Hrs.	5.5	≤ 10
3	**Compressive strength**			
	3 Days	MPa	17.5	≥ 15
	7 Days	MPa	26.36	≥ 23

3.4.2 Fine Aggregate

The present study employed clean sand from a local region known as AL-Akhaidir during the experimental phase. The sand's grading, specific gravity, sulfate content, and absorption were examined, and the results indicated that they conformed to the Iraqi standard specification No. 45 / 1984. Moreover, the tests revealed that the sand's sulfate content and grading satisfied the limitations of the Iraqi specification No.45/1984 Zone 2. The Materials Laboratory at the College of Engineering/University of Kerbala conducted these tests. Detailed information regarding the properties of the sand is presented in Table 3-4 and Table 3-5.

Table 3-4:Grading of The Fine Sand Compared with The Requirements of Iraqi Specification No.45/1984.

Size of Sieve (mm)	Passing Percentage %	I.Q.S No.45/1984 Zone No. 2
10	100.00	100
4.75	91.87	90 - 100
2.36	76.93	75 - 100
1.18	62.80	55 - 90
0.6	42.87	35 - 59
0.3	11.73	8 - 30
0.15	1.47	0 - 10
pan	0.00	0.0

Table 3-5:Chemical Properties of Fine Aggregate.

Property	Test result	Specification limits % I.Q.S No.45/1984
Material Passing 75 µm Sieve	3.1 %	< 5 %
Sulfate content (SO3)	0.097 %	≤ 0.5 %

3.4.3 Coarse Aggregate

The use of black-crushed gravel from the Al-Niba'ai region in a concrete mixture was employed in this study. The coarse aggregate was thoroughly cleaned and sourced from the Al-Nebai region. Particles exceeding 9.5mm in size were separated using a sieve and underwent a meticulous washing process to ensure the removal of all dust and fine material before being stored. The aggregate's properties and grading were assessed to conform with the requirements outlined by the Iraqi specification No.45 / 1984[52].Table (3-6) and Table (3-7) provides pertinent information regarding the physical and chemical properties of the coarse aggregate.

Table 3-6:Sieve analysis of coarse aggregate No. 45/1984.

Sieve size (mm)	Passing %	Specification limits % Iraqi specification No.45/1984[52]
12.5	100.00	100
9.5	98.73	85-100
4.75	1.67	0-25
2.36	0.20	0-10
pan	0	0

Table 3-7:Chemical Property of Coarse Aggregate Chemical Property.

Property	Test result	Specification limits % Iraqi specification No.45/1984[52]
Material Passing 75 µm Sieve	0.43 %	≤ 3 %
Sulfate content (SO3)	0.077 %	≤ 0.1 %

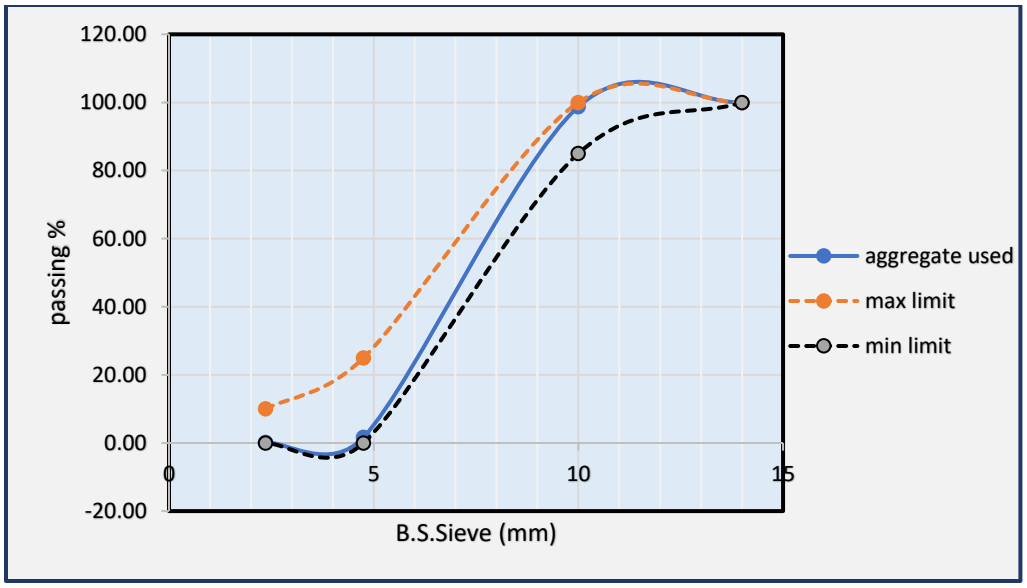

Figure 3-17: Grading Curve for Separated Sand Compared with Requirements of Iraqi Specification No.45/1984

Plate 3-6:The coarse aggregate used in this study.

3.4.4 Silica Fume

The type of silica fume used as an additional percentage of the weight of cement is MasterRoc MS610 [53] and its from CDP company According to the specification (ASTM C1240-15) [54]. These are very fine grains changed the superstructure of concrete to denser concrete and increased the strength of concrete for any change of environment. The properties of silica fume are shown in table (3-8).

Table 3-8:Properties of MasterRoc MS610[52].

Property	Test result
Color	grey
Density (Kg/lt)	0.55-0.7
Chloride content	<0.1%
Dosage %	5-15

Plate 3-7:Silica fume used in this study.

3.4.5 Superplasticizer

A high-range water-reducing admixture was used in this research work for the HSC mixture only, as explained in Appendix (A). It was a third-generation superplasticizer for concrete and mortar. MasterGlenium® 54[55] was high-water, reducing water use by up to 30%, as shown in Plate (3-8). It has several advantages besides reducing water content in the mixture, such as improved shrinkage and creep behavior and increased early strength and density, it meets the superplasticizer standards set by ASTM C-494 and BS EN 934-2 types G and F [83].

Plate 3-8:Type of Superplasticizer Used in This Study.

3.4.6 Water

It is advised that clean water be utilized for the purpose of mixing concrete. The study in question implemented tap water for the mixing and curing of the concrete, adhering to the guidelines outlined in Iraqi Specification No.1703/1992 [56]concerning the water quality.

3.5 Supports

Lateral supports are implemented to stabilize the web area of the beam, thereby preventing any lateral or sideways movement that could lead to distortion or displacement during the inspection process.

The lateral supports are crucial for maintaining the structural integrity of a beam by providing stability and reinforcement to its web area. They are constructed using two 2-cm boards, chosen for their strength and rigidity. The boards are attached to the support base using screws, ensuring a secure connection and minimizing the risk of detachment or failure. The supports are designed to be placed at both ends of the beam to effectively stabilize the web area and provide a stable foundation for the entire setup.

Plate 3-9: a-The form of support used in the test.
b-Using Two Boards Strengthens the Support System

3.6 Steel Section

The Ukrainian, was used to represent the structural steel I-section. This section has 140 mm height, 73 mm flange width and **13.1** kg/m weight. The flange and web thickness are 6.9 and 4.7 mm, respectively. To determine the mechanical properties of the steel material, a total number of three tensile samples were taken from the webs of all the specimens. The samples fabricated according to ASTM-A370 [54], were tested by using a tensile testing machine available in the Strength of Materials laboratory at Al Sebtayn company for specialized structural and chemical surveys and soil investigation. as shown in Plate (3-11) and the load-deflection curves results are shown in Figure (3-18). The average values of yield stress, ultimate strength and elongation are given in Table (3-9).

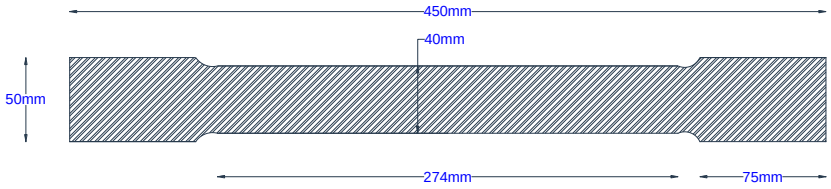

(a)Specimens before Testing (b)Specimens after Testing

Plate 3-10:Photos of Tensile Test Specimens.

a- Mechanical Parts b- Digital Parts

Plate 3-11:Tensile Steel Testing Machine.

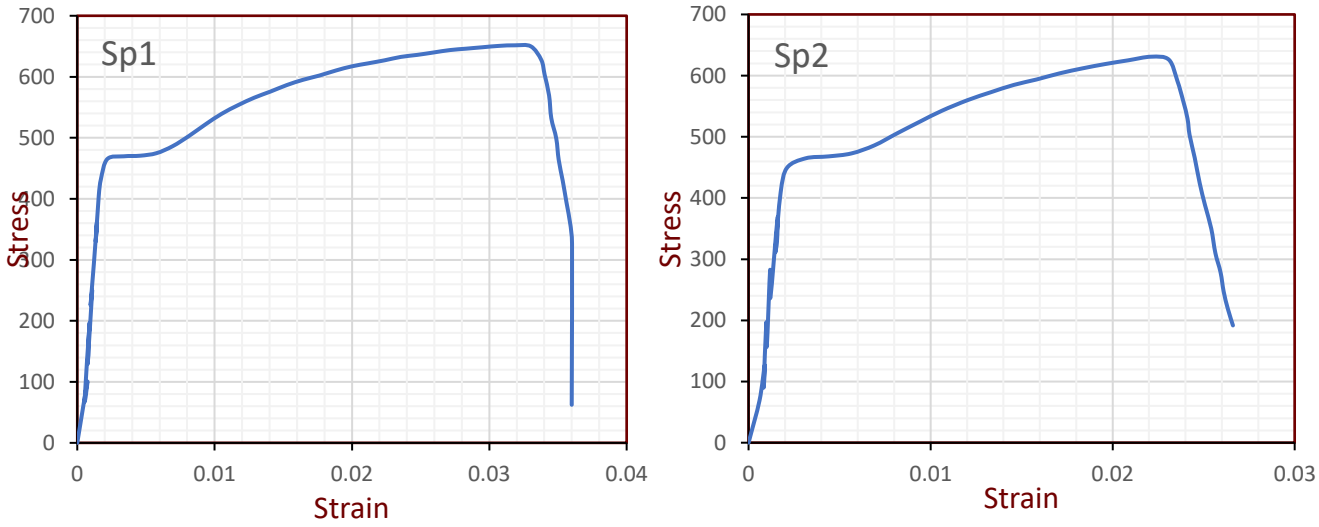

Figure 3-18: The Load-Deflection Curves of Steel Samples.

Table 3-9:Properties of Steel Section.

Steel Specimens	Specimen No.	Tensile Stress (Fy) (MPa)	Ultimate Tensile Strength (Fu) (MPa)	Elongation %	Thickness (mm)
Steel beam	Sp1	490	652.15	14.38	4.7
	Sp2	490	632.13	10.01	4.6
	Sp3	480	609.79	10.57	4.7
Average		486.67	631.36	11.65	4.67

3.7 Stud Shear Connectors

Stud shear connectors are commonly used in composite steel-concrete construction to provide a strong bond between the steel beam and the concrete slab. These connectors typically consist of short steel studs that are welded to the top flange of the steel beam, and then extend into the concrete slab. The primary function of these connectors is to transfer the load from the concrete slab to the steel beam, allowing the two materials to act together as a single unit. Without the connectors, the concrete slab would tend to separate from the steel beam, reducing the overall strength and stiffness of the composite member. To ensure effective composite action, the stud shear connectors must be designed to resist both shear and pull-out forces. The shear forces arise from the horizontal loads applied to the composite member, while the pull-out forces arise from the vertical loads applied to the concrete slab.

In the particular case described, the stud shear connectors used have a height of 50 mm and a diameter of 10 mm. They are distributed along the entire span of the beam, with a spacing of 150 mm and 300 mm center-to-center, as shown in Plates (3-12).

(a) **(b)**

Plate 3-12:The Studs Used in This Study, (a)Before Cutting; (b)After Cutting.

Table 3-10:Mechanical Properties of Shear Connectors.

Steel Specimens	Specimen No.	Measured Diameter (mm)	Tensile Stress (Fy) (MPa)	Ultimate tensile strength (Fu) (MPa)	Elongation %
Steel Bolt (stud)	Sp1	10	543.4	747.60	13.5
	Sp2		515.8	717.9	16.5
	Sp3		525	761.68	20
Average			528.07	742.39	16.67

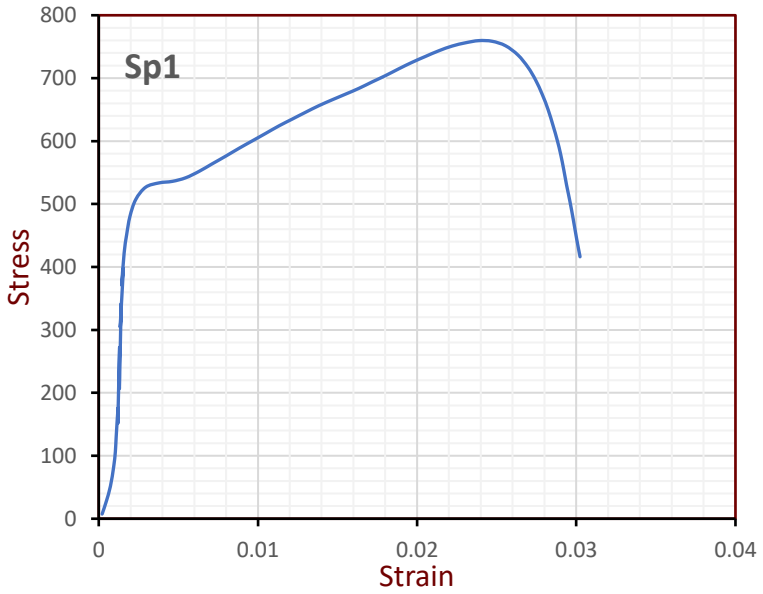

Figure 3-19:The Load-Deflection Curves of Steel Samples.

3.8 Welding Processes

This research used two welding processes. The first process includes welding nine stud connectors in one of the specimens and four studs in one specimen in a single row at a uniform spacing. The second process is welding four stiffeners with a thickness of 10 mm at a distance of 20 mm from center to center along the web of the beam. Plate (3-13) shows the steel girders with the welded stud. The studs were cut and fabricated from the bottom end to provide welding in the steel girder. The choice of butt joint welding with a thickness of 3 cm depends on the specific requirements of the experiment or structural application. Factors like material properties, anticipated loads, and design considerations can influence the choice. However, this welding technique offers strength, stability, and weld quality for joining heavy-duty structural components effectively, making it suitable for applications requiring robust and reliable connections.

Plate 3-13: Illustration depicting stud shear connectors.

3.8.1 Molds

Plywood mold was used for manufacturing the concrete slab (HSC) specimens in this study as shown in Plate (3-14). The mold was cleaned well and the internal faces were lubricated before casting. molds were prepared to enable casting concrete. Each mold consists of a bed and four movable sides. The sides were fixed to the bed by screws. The clear dimensions of the molds are (1500 × 350×70) mm.

Plate 3-14:The Plywood Molds Used in Casting HSC Concrete Slab.

3.9 Preparation of the Specimens

3.9.1 Concrete Mix Design

The high-strength concrete (HSC) was designed according to the American method of mix proportions selection. The target concrete strength (fc′) for all test specimens was (60) MPa at 28 days.

High-strength concrete (HSC) mix was performed in a rotary mixer. For HSC concrete, the coarse aggregate and fine sand were mixed in a dry state for about 2 minutes to disperse the fine sand particles throughout the coarse aggregate. Then, the silica fume and cement were added, and the mixture was mixed for 2 minutes. The superplasticizer was dissolved in water, and the solution of water and superplasticizer was gradually added during the mixing process. The entire mixture was then mixed for 4 minutes. In total, the mixing of one batch required approximately 10 minutes from adding water to the mix.

In this study, the HSC mix was taken by designing several experimental mixes to obtain 28 days of compressive strength equal to nearly 70 MPa following the ACI (211-15**) (ACI- Committee 211 R- 2015)**, Table (3.11) provides the quantities of the components required to have one cubic meter of HSC.

Table 3-11:The Mix Material Proportion of High Strength Concrete.

Material	Units	HSC
Cement	**Kg/m^3**	**550**
Silica fume	**Kg/m^3**	**70**
Fine sand	**Kg/m^3**	**720**
Coarse aggregate	**Kg/m^3**	**1060**
water	**L**	**155**
superplasticizer	**L**	**16.5**

3.10 Mechanical Properties

Mechanical properties include three tests to know the behavior of mixtures mechanically, provided that these tests are conducted for each type of mixture that has been made.

3.10.1 Compressive Strength Test

The compressive strength test was determined according to (BS.1881: Part 116:1989) [57] and (ASTM C39-C39M)[58]. The average of all specimens at the time of testing for cubes and cylinders was 72.72 MPa and 60.57 MPa, respectively as shown in **Table (3-12)**., with each cube having dimensions of 100 mm x 100 mm x 100 mm. A digital pressure machine with a capacity of 2000 kN was used for the test, as shown in the plate. The testing was conducted 28 days after the curing process. The average of the results from the three cubes was taken to represent the compressive strength.

Plate 3-15:The Compression Strength Test Machine - Compressive Strength Test.

3.10.2 Splitting Tensile Strength Test

In this study, three concrete cylinders were prepared and the average splitting tensile strength was determined. The cylinders had dimensions of (100×200) mm as specified in the ASTM C 496-496M standard [59]. The digital pressure machine with a strength capacity of up to (2000) kN was utilized to perform the test, which was conducted after 28 days of curing, as illustrated in Figure (3-16). The average of all specimens at the time of testing for cylinders was 4.73 MPa. The formula employed to compute the splitting tensile strength was as follows.

$$\mathbf{fst} = \frac{\mathbf{2P}}{\boldsymbol{\pi}\mathbf{DL}} \qquad (3\text{-}1)$$

fst: Splitting tensile strength (MPa).

L: Cylinder length (mm).

P: Peak load at failure (N) and

D: $Cylinder\ diameter\ (mm)$.

Plate 3-16:Splitting Tensile Strength Test Machine.

3.10.3 Flexural Strength Test

According to the provided information, a test was conducted to determine the flexural strength of three concrete prisms, each measuring $(100 \times 100 \times 500)$ mm, as per the ASTM C293-02 standard[60]. The procedure involved applying a central force to the prisms using a hydraulic device, while the prisms were affixed as simple supports and subjected to a span length of 400 mm. By measuring the maximum load applied to the prisms at the point of failure, as well as considering their dimensions and the span length, the flexural strength (modulus of rupture) of the concrete was computed the average flexural strength of the three prisms was 5.66MPa. was calculated using the following equation.

$$fr = \frac{3PL}{2bh^2} \qquad (3\text{-}2)$$

fr: Flexural strength in (MPa), P: Maximum applied load in (N)

L: Average span length in (mm), b: Width of prism in (mm), and

h: Depth of prism in (mm)

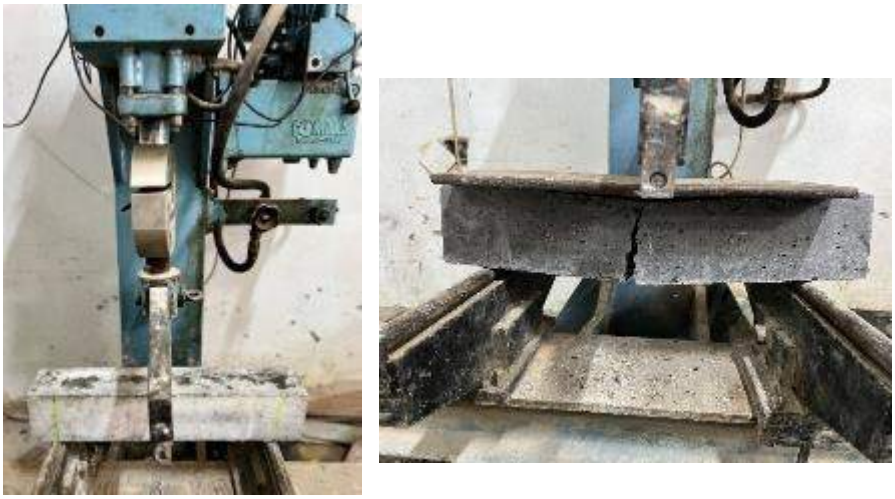

Plate 3-17: Flexural Strength (Modulus of Rupture) Test.

Table 3-12:Compression and Tension Strength of Concrete.

Group Specimen Symbol	Concrete Compressive Strength, *fcu* MPa		Splitting Tensile Strength, *fct* MPa	Rupture Modulus, *fr* MPa
	cube	cylinder		
1	77.76	62.21	4.9	5.7
2	70.5	59.4	4.5	5.31
3	69.9	60.1	4.8	5.97
average	72.72	60.57	4.73	5.66

3.10.4 Modulus of Elasticity

The modulus of elasticity samples or each mix of HSC using the average value of three samples of cylinders with dimensions (100 × 200) mm. the vertical displacement was measured when the load was applied by the compressive state.

Equation (3-3) represented the formula of modules of elasticity for high strength of concrete was compared with the ACI 363R-23 [61].

$$Ec = 3320\sqrt{fc} + 6900 \quad (3\text{-}3)$$

The value of modulus of elasticity for each mixture calculated by the previous equations represented in Table 3-13.

Table 3-13:Average Modulus of Elasticity.

No. of specimens	Modulus of elasticity (Ec) for High strength concrete (MPa)
1	33085.9
2	32487.7
3	32638.03
Average	32737.21

3.11 Steel Reinforcement

The study utilized steel bars with a diameter of 8 mm and a grade of 40. These bars were utilized to reinforce all of the tested slabs and were produced in accordance with the guidelines set forth in the ASTM-A615/A615M − 15a [62]specification (refer to Table 3-14 for more details).

Table 3-14 Steel reinforcement test results *

Property	Unit	Value	ASTM-A615/2020
Nominal diameter	mm	8	-
Actual diameter	mm	7.91	-
Cross-section area	mm^2	49.0	-
Yield stress	MPa	460.0	≥ 280
Ultimate stress	MPa	608.2	≥ 420
Elongation	%	25.9	-
Nominal weight	Kg/m	0.39	-

* This test was carried out by lab staff.

3.11.1 Steel Reinforcement Mesh

All the slabs were reinforced with Ø 8mm steel reinforcement. The ratio of reinforcement was taken identical for both directions of slabs. The mesh of reinforcement is shown in (Figure 3-20).

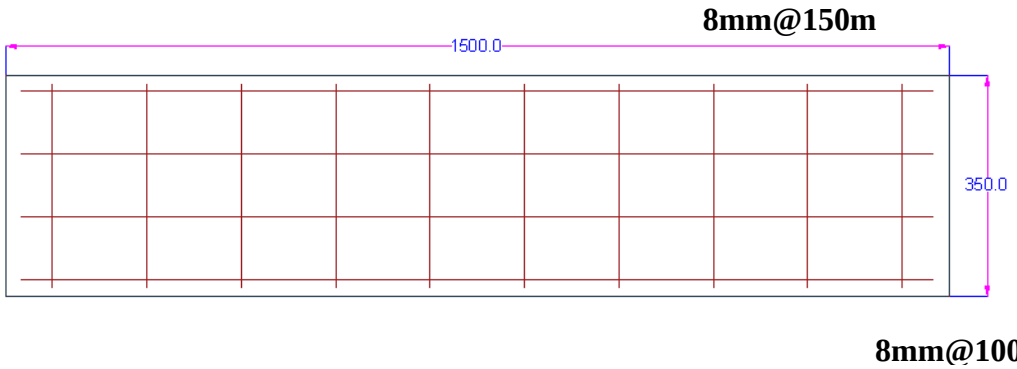

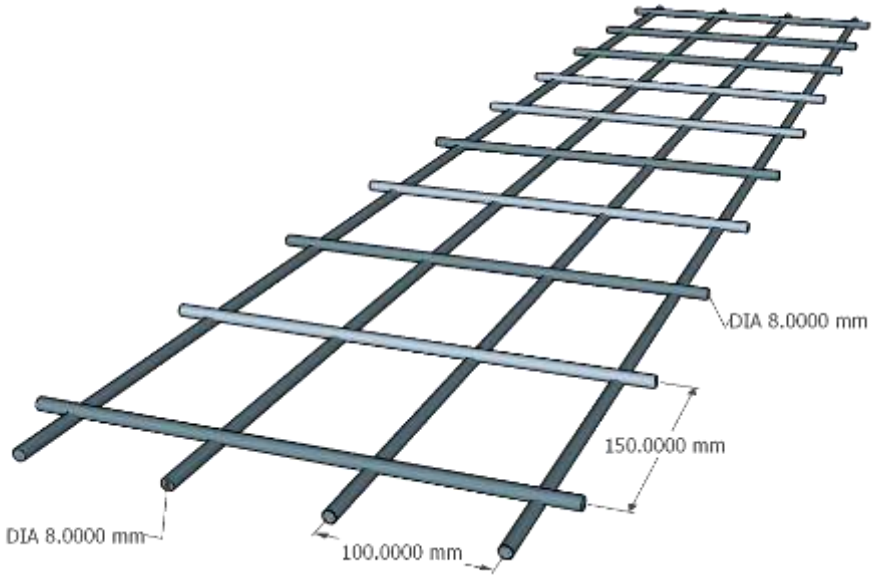

Figure 3-20 Steel reinforcement mesh

Plate 3-18:Tensile Testing Machine for Steel Reinforcement.

3.12 Curing

Process Following the casting process, the formwork was left in place for three days before being removed. It was crucial to understand that the formwork needed to remain in place for more than one or two days to allow the concrete to harden fully. This extended duration was due to the high dosage of superplasticizer used in the mix design.

To assess the concrete's strength, three cubes measuring 100mm each and six cylinders of (100×200) mm were cast. The compressive strength was calculated based on these specimens. Additionally, three prisms of (500×100×100) mm were cast to determine the flexural strength (modulus of rupture) of the high strength concrete (HSC). All composite specimens, including cubes, cylinders, and prisms, were cured for 28 days. They were kept together underwater at a constant temperature ranging from 24 to 30 °C [63], as shown in Plate (3-19).

Plate 3-19: Photographs for the Curing Process.

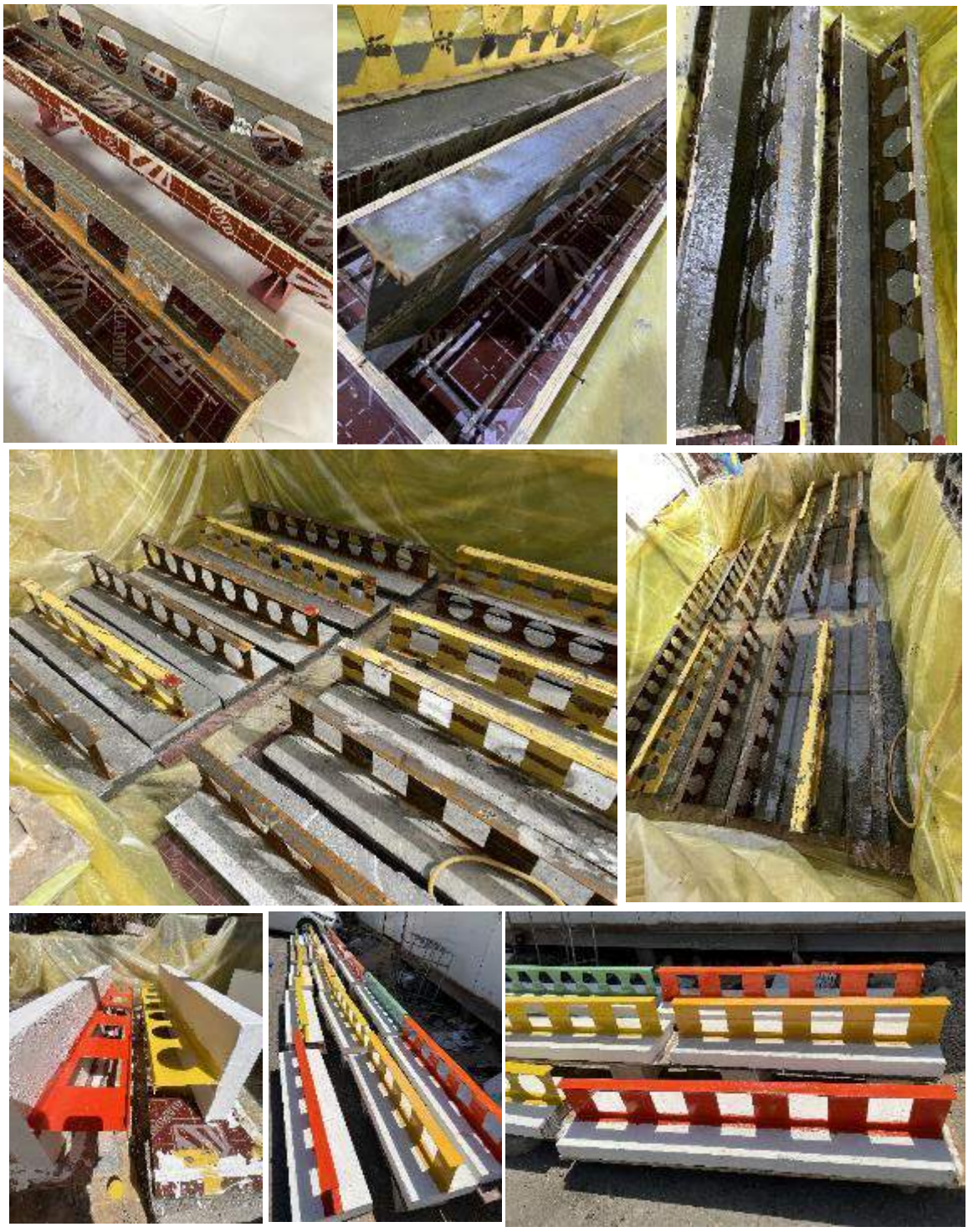

Plate 3-20:Stages of Casting.

3.6 Instruments

The instruments used consisted of a linear variable displacement transducer (LVDT) with displacement capacities of 12mm and 50mm and load cells for measurement of beam deflections and slips between concrete slabs and steel.

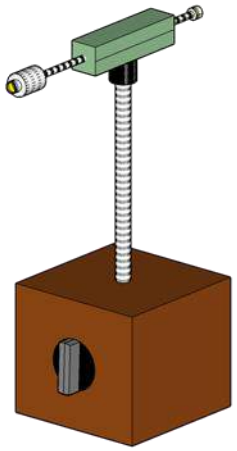

Plate 3-21 : Instruments Used Throughout the Tests.

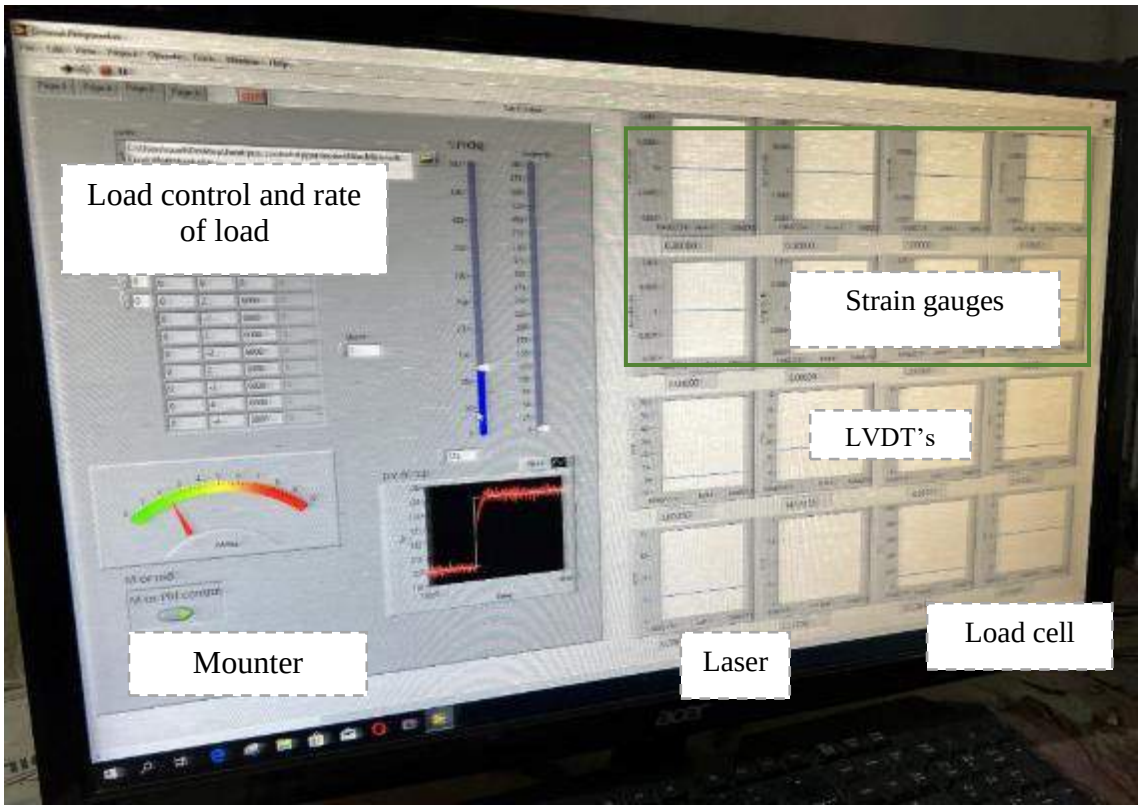

Plate 3-22:View of the Controlling Program.

3.13 Beams Testing

At the end of the curing duration, all beams and control specimens were removed from the water tank, left to dry, and then cleaned and painted white for the concrete slab to detect cracks easily. Each beam was placed on simple supports, with a distance of 10 cm from each end of the machine, providing a clear span of 130 cm between the two supports. The machine used for testing the beams had a capacity of 2000 kN. It was one of the hydraulic types available in the Material Laboratory of the Civil Engineering Department at the College of Engineering, Kerbala University, as shown in Figure (3-21).

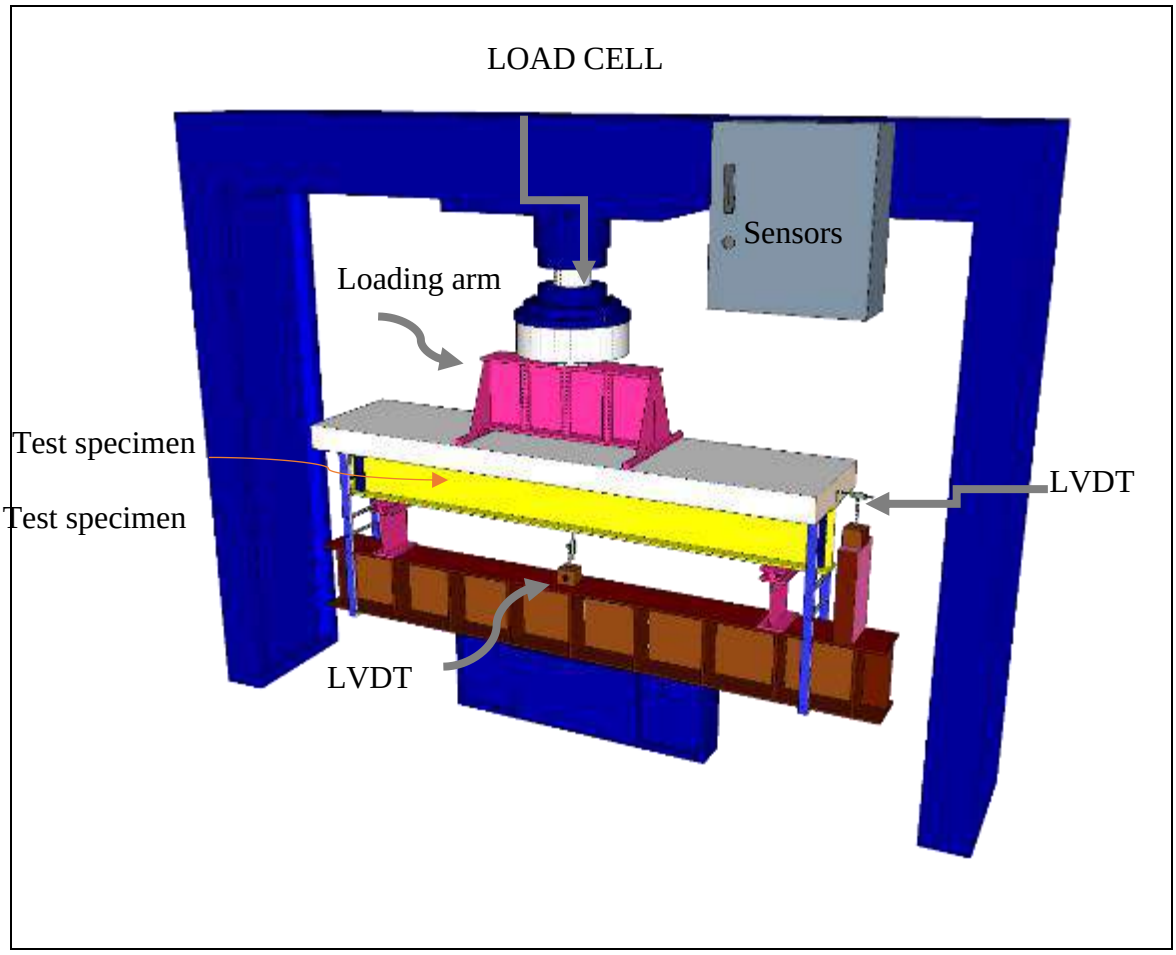

Figure 3-21:Details of Testing Machine Used in This Study.

All beams were tested under two-point loads, using a steel beam over the beam with a clear span of 500 mm. This arrangement allowed for the

division of the total applied load onto two steel rods with a cross-section of 25 mm, applied on steel plates to avoid stress concentration on the slab flange, as shown in Plate (3-23).

Plate 3-23: Loading arm used in the test.

The load was applied in successive increments of approximately 5 kN at each step. The deflection and slip values were recorded at each load increment, and any cracks observed were marked. The load at which each crack occurred was also noted. The test was terminated when a drop in loading was observed, and the beam exhibited significant deflection. When the beam reached the failure point, the load was removed, the load at failure was recorded, and the cracks were marked. For repeated load testing, the load was applied cyclically until failure occurred. Each cycle consisted of two steps: in the first step, the load was increased to a selected level from the ultimate load of the control model (slab under concentrated load), and in the second step, the load was unloaded to zero. The selected load levels were 0.25Pu, 0.5Pu, 0.75Pu, and so on, up to the point of failure, where Pu represented the estimated ultimate load of the control model. The first cracking load and its location were recorded. At each load increment, observations of crack development on the concrete slab were made.

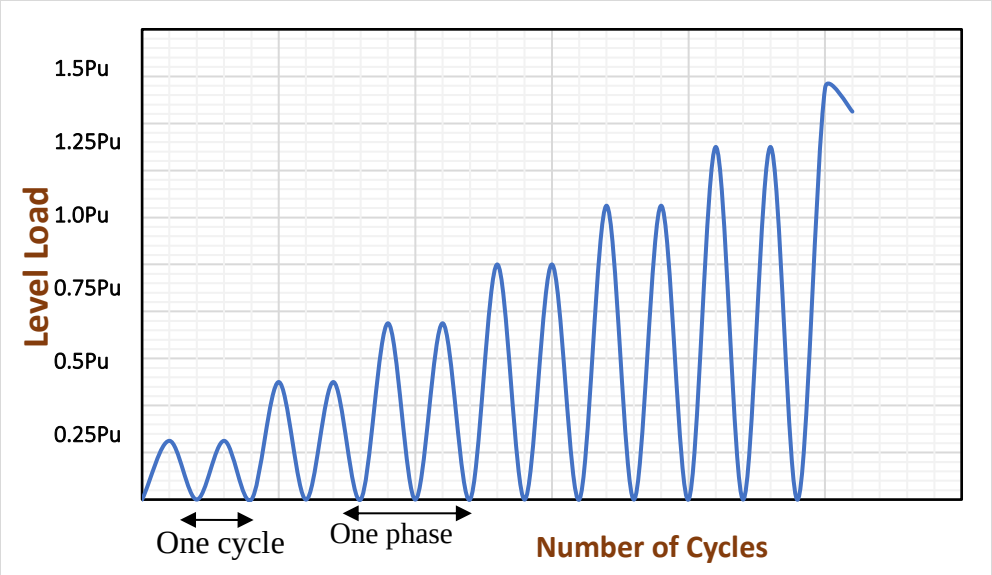

Figure 3-22: History of the repeated load.

3.14 Strain Measurement

The strain was measured using GOM software [64], and the area was coated with black spray paint, as depicted in the image. Shown in Figure (3-24).

Figure 3-23:GOM software icon

Figure 3-24:The interface of the software.

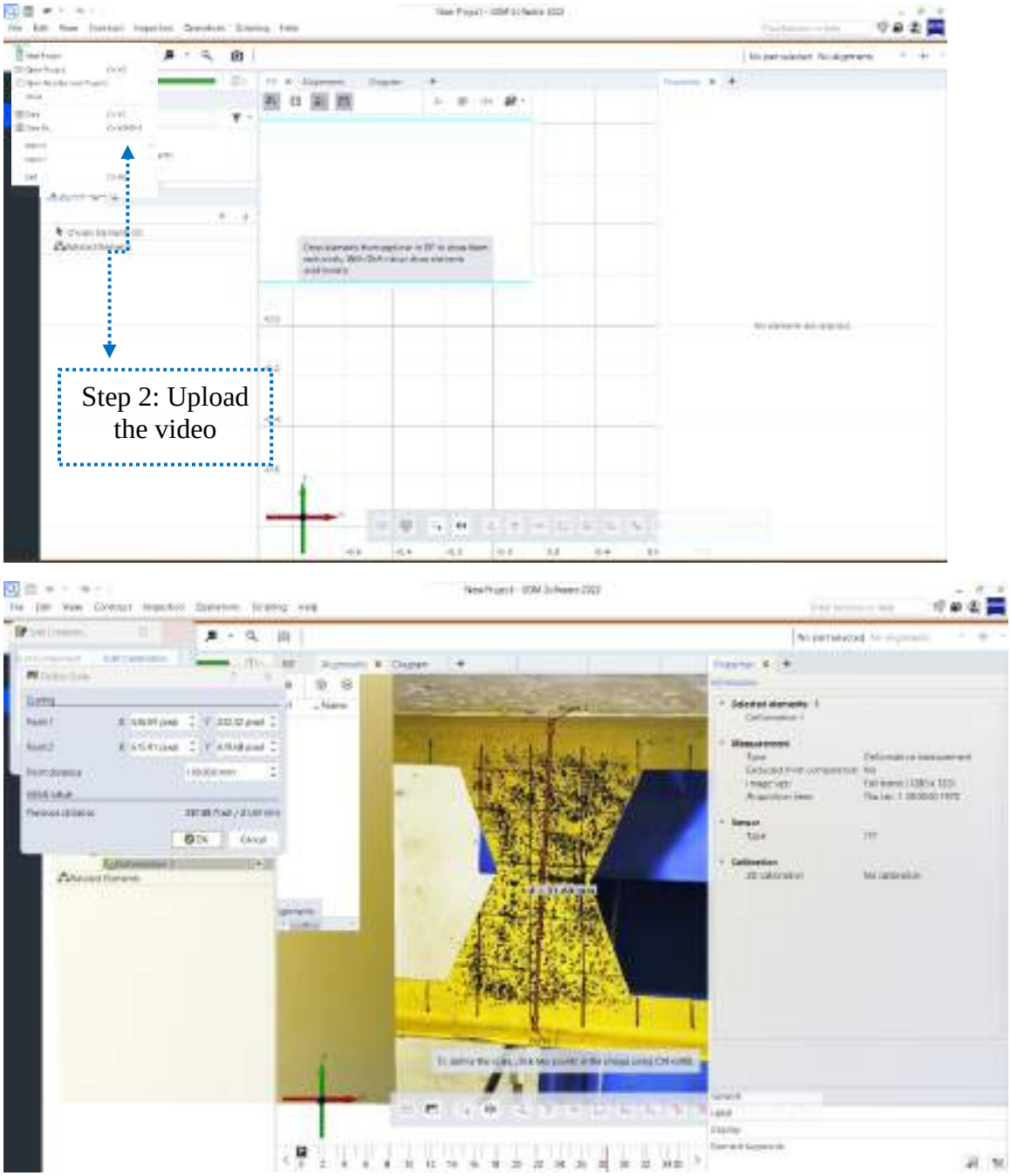

Figure 3-25:The second interface of the software.

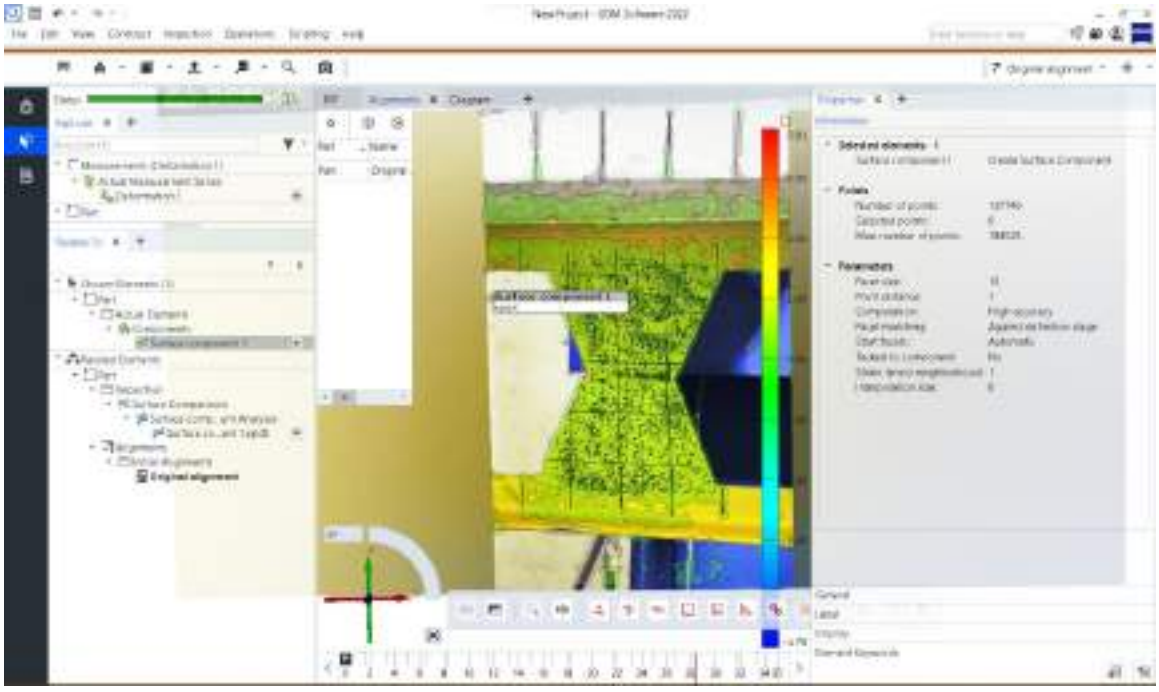

Figure 3-26:The Final Interface of the Software.

Specify the region in which the strain is computed. Next, select the specific point for which you desire to determine the strain, and repeat this process for all other places.

The strain was measured at six levels across the depth of the composite beam at one side at mid-span for all beams.

GOM Correlate is free software that enables digital image correlation (DIC) and evaluation. Digital image correlation is an optical technique that allows measuring 2D or 3D coordinates without physical contact. Coordinates can be utilized to infer displacements and strains of specimens for a diverse array of applications in materials and component testing. GOM Correlate offers 2D digital image correlation, enabling the assessment and documentation of digital image sequences or video files. Hence, it is ideal for in-plane testing applications using pre-existing cameras.

Chapter Four: Experimental Results and Discussion

Chapter Four: Experimental Results and Discussion

4.1 Introduction

The present chapter discussed the experimental findings about evaluating composite castellated beams subjected to monotonic and repeated loading conditions. The characteristics can be categorized into four distinct areas: the shape of the opening, the type of loading, the spacing of the shear connectors, and the presence of stiffeners. Fifteen composite castellated beams were tested, with each group including three beams. The first group directed their attention toward the beam group subjected to monotonic loading. Distinct shear connection spacings and opening forms characterized these beams. Specifically, one composite beam had a shear connector spacing of 150mm from c/c.

In contrast, the other two composite castellated beams had hexagonal and square openings with shear connector spacings of 300mm and 150mm from c/c, respectively. The second group consisted of individuals possessing identical shear connector spacing (150mm c/c) yet exhibiting distinct opening shapes (hexagonal, circular, and square). However, the subsequent cohort investigated beams comparable to those studied by the previous group, with a distinct shear connection spacing of 300mm from c/c. This modification aimed to ascertain the impact of varying the quantity of shear connectors on the ultimate load capacity. The fourth group consisted of composite castellated beams with identical shear connector spacing, measured at 150mm c/c, and similar opening forms: hexagonal, circular, and square. The beams were equipped with supplementary panels and longitudinal strengthening within the web. The models in the fifth group exhibited similarities to those in the fourth group, albeit with a distinct variation in shear connector spacing,

namely at a c/c distance of 300mm. This chapter looks at how changing certain parameters affects the behavior of a composite castellated beam. It does this by visually showing types of failure and explaining how they behave under different loads.

4.2 Test Setup and Instrumentation

Before delving into the findings, it is imperative to provide a comprehensive overview of the experimental test configuration and instruments employed. The composite castellated beams were manufactured according to the standards outlined in Chapter Three. GOM software was used along each beam to measure strain fluctuations during loading—furthermore, displacement and measuring the extent of deflection by LVDT.

4.3 Load-Deflection Behavior

The load-deflection behavior of the composite castellated beams was evaluated under repeated loading conditions. The cyclic loading was applied using a hydraulic actuator capable of generating the desired load amplitudes and frequencies.

The results showed that the composite castellated beams exhibited a linear elastic response during the initial loading cycles. However, the beams exhibited signs of stiffness degradation as the number of cycles increased. This was evident from the increase in deflections observed at similar load amplitudes as the loading cycles progressed. The stiffness degradation was attributed to various factors, including material fatigue, local damage accumulation.

4.3.1 Load-Deflection Relationship

The vertical deflection of the test beams was recorded at each load increment.

Table 4-1: Experimental Results of the Tested Beams

No	Beam designation	Total applied load(kN)			Maximum Deflection (mm)	Type of Failure
		Pcr	Pu	Pcr/Pu	Δcr	
1	CB-9S	100	130.40	0.50	33.13	Lateral Torsional Buckling
	CB-H4S	50	101.30	0.54	32.90	Web Post Buckling
	CB-S9S	72	92.50	0.54	14.60	Buckling and Yielding
2	CB-H9R1	70	98.60	0.76	24.90	Web Post Buckling Vierendeel Mechanism
	CB-C9R1	50	74.89	0.83	24.09	Web Post Buckling
	CB-S9R1	60	67.34	0.70	16.90	Buckling and Yielding
3	CB-H4R1	75	89.00	0.84	26.80	Web Post Buckling Vierendeel Mechanism
	CB-C4R1	50	69.40	0.72	29.20	Web Post Buckling
	CB-S4R1	25	58.70	0.43	16.10	Buckling and Yielding
4	CB-H9R2	90	164.20	0.55	47.44	Vierendeel Truss Analogy
	CB-C9R2	50	121.30	0.62	38.60	Location of The Relevant Plastic Hinges
	CB-S9R2	75	109.40	0.69	25.30	Buckling and Yielding Tee Local Buckling
5	CB-H4R2	75	138.60	0.54	28.20	Vierendeel Truss Analogy
	CB-C4R2	50	102.40	0.49	49.10	The Four-Hinged Failure Mechanism
	CB-S4R2	50	69.20	0.72	14.60	Buckling and Yielding Tee Local Buckling

4.3.1.1 Group One

This group consisted of three specimens' controls (CB-9S, CB-H4S, and CB-S9S).

Table 4-2: Ultimate load and deflection in the middle of each span for group one

Beams (controls)	Ultimate Load (kN)	Crack Load (kN)	Mid-span deflection at the first crack (mm)	Mid-span deflection at ultimate load(mm)
CB-9S	130.4	100	8.99	33.1
CB-H4S	101.3	72	4.78	32.9
CB-S9S	92.5	50	4.21	14.6

The study examines the performance of group one (CB-9S, CB-S9S, and CB-H4S) beams under monotonic load conditions. The CB-9S, a control beam without castellation, has a high strength level and increased adaptability. The study compares the ultimate load capacities of three Castellated Steel Beams (CSBs) as control specimens. The CB-S9S beam, with square openings and a stud spacing of 150 c/c, demonstrated an ultimate load of 92.5 kN. In contrast, the CB-H4S beam, featuring hexagonal openings and a wider stud spacing of 300 c/c, exhibited a slightly lower ultimate load of 101.3 kN. The results show that the spacing between the shear connectors and the shapes of the openings affect the final load capacity. In this case, the CB-H4S configuration performed better than the CB-S9S variant. The CB-9S structure experienced significant lateral torsional deformation, web distortion, and lateral torsional buckling due to structural modifications during loading. The failure of CB-H4S was due to web post-buckling, while CB-S9S experienced buckling and yielding.

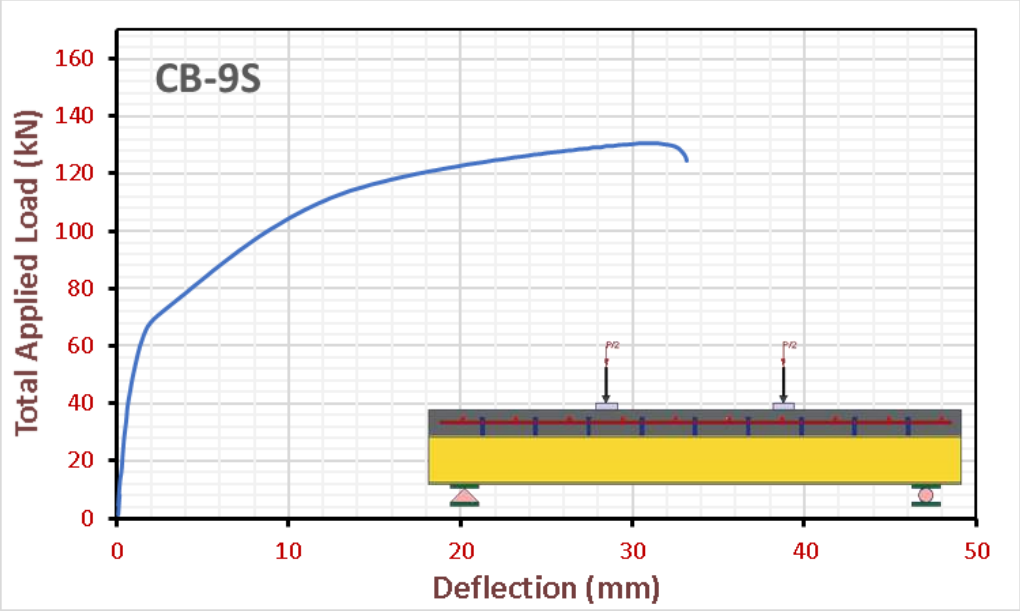

Figure 4-1:Load-Deflection Curve of Monotonic Load beam (CB-9S).

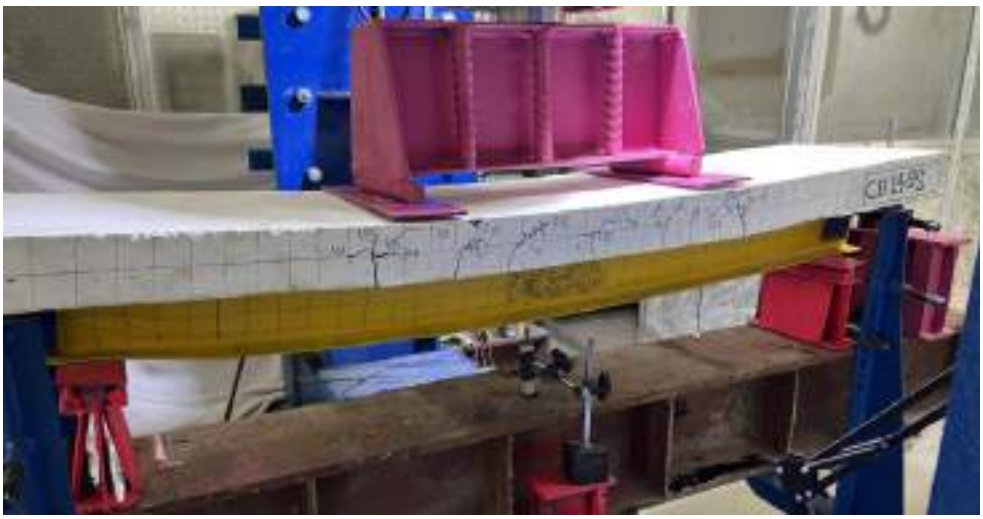

Plate 4-1: Shape of Beam CB-9S Before and After Testing.

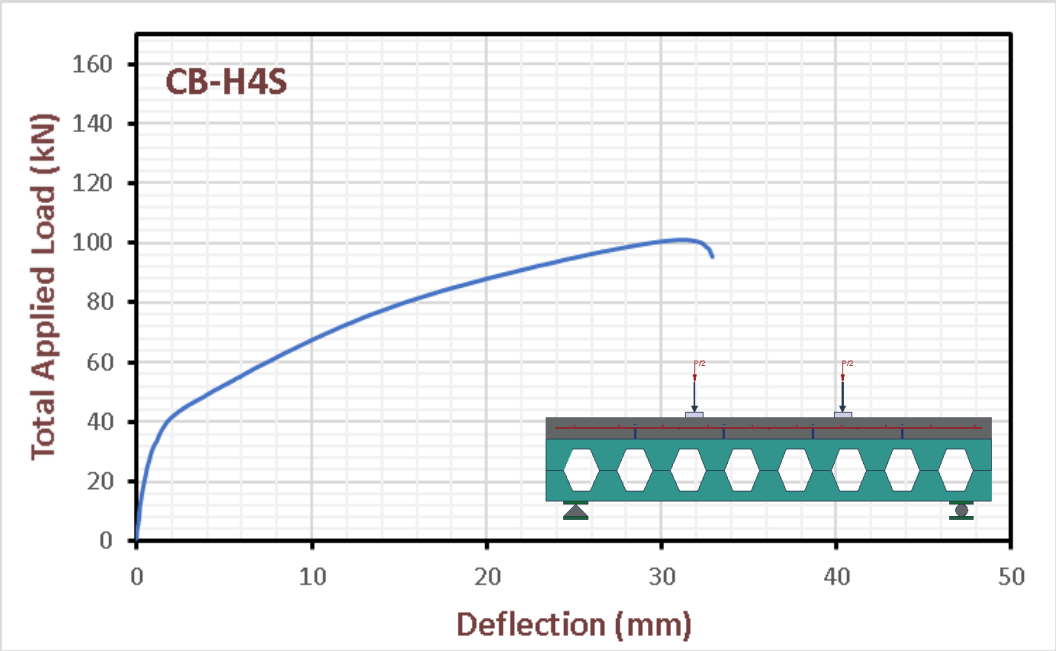

Figure 4-2: Load-Deflection Curve of Monotonic Load Beam (CB-H4S).

Plate 4-2: Shape of Beam CB-H4S Before Testing.

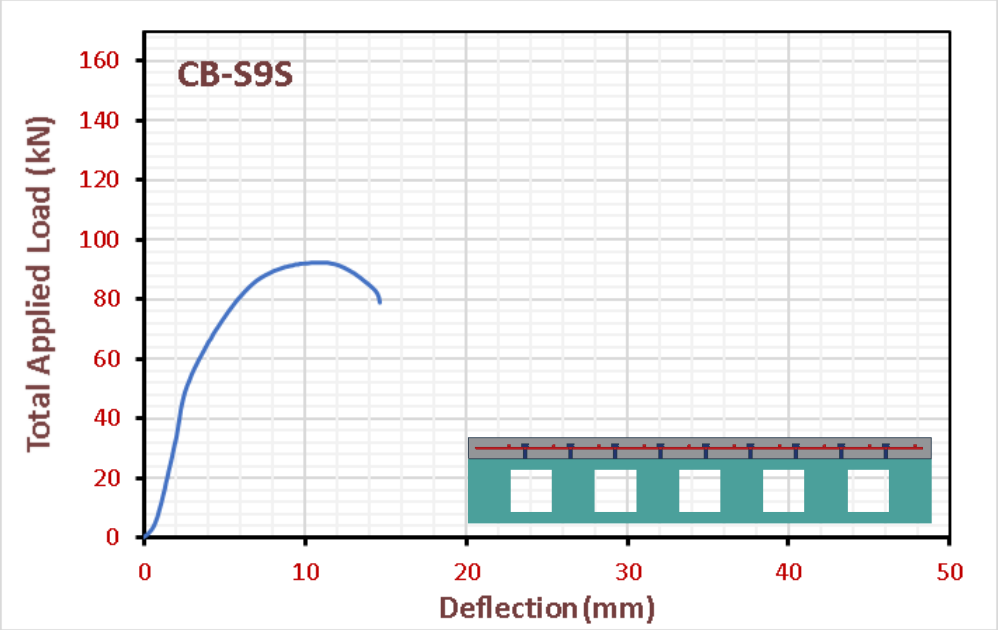

Figure 4-3: Load-Deflection Curve of Monotonic Load Beam (CB-S9S).

Plate 4-3: Shape of Beam CB-S9S Before Testing.

4.3.1.2 Group Two

Group two comprised three specimens, namely CB-H9R1, CB-C9R1, and CB-S9R1. Each is characterized by a unique opening shape (hexagonal, circular, and square). The space between the studs is 150 mm. The specimens underwent a repetitive load testing technique., with two cycles occurring within a single phase. The cyclic loading approach involves a gradual increase in applied loads, first at 25% of the ultimate capacity (Pu) and subsequently progressing in 50% to 75% increments until finally reaching 100% Pu.

Table 4-3:Ultimate load and deflection in the middle of each span for group two

Beams	Ultimate Load (kN)	Crack Load (kN)	Mid-span deflection at the first crack (mm)	Mid-span deflection at ultimate load(mm)
CB-H9R1	98.6	70	12.55	24.9
CB-C9R1	74.89	50	2.55	24.09
CB-S9R1	67.34	60	6.24	16.90

The performance of three different models of composite castellated beams under repeated loads. The hexagonal opening model had the highest maximum load deflection of 98.6 kN.

In contrast, the circular opening model performed well with a slightly lower maximum load deflection but outperformed the square opening model. The square opening model displayed the least resistance to deformation, indicating lower structural efficiency. The CB-H9R1 beam displayed a combination of failure modes, including web post-buckling and the Vierendeel mechanism, suggesting a complex pattern of load redistribution before ultimate failure. The CB-C9R1 primarily experienced web post-buckling, indicating the beam's web failed under applied loads due to compressive stress. The CB-

S9R1 also experienced buckling and yielding, indicating plastic deformation due to the material exceeding its yield strength.

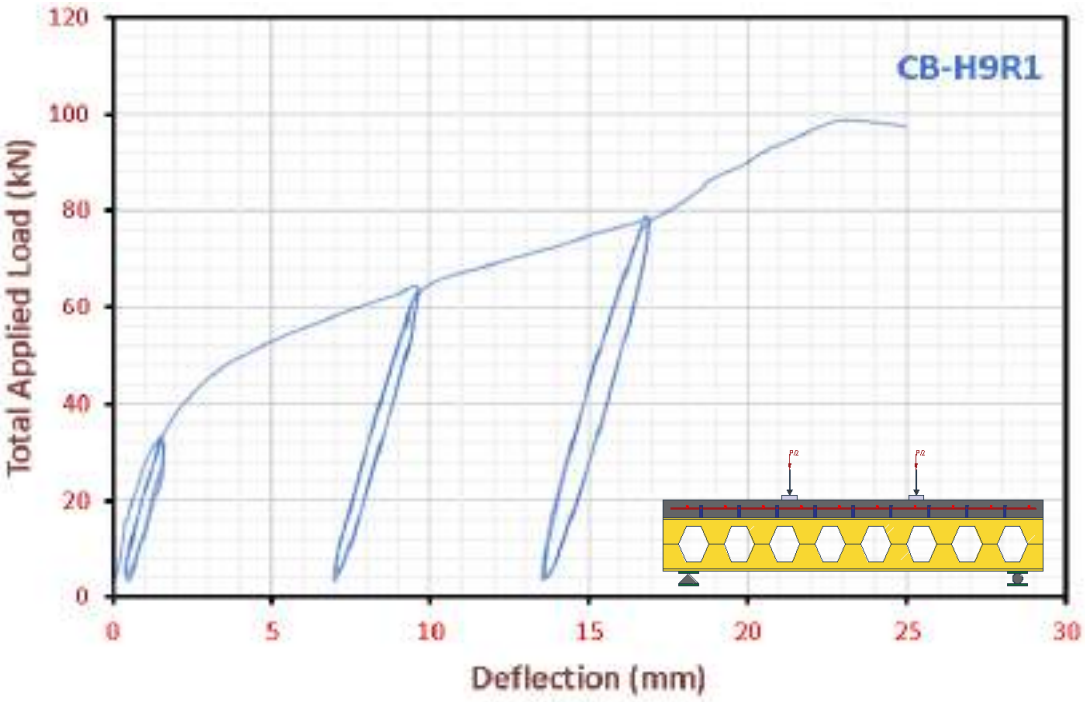

Figure 4-4: Load-Deflection Curve of Repeated Load Beam (CB-H9R1).

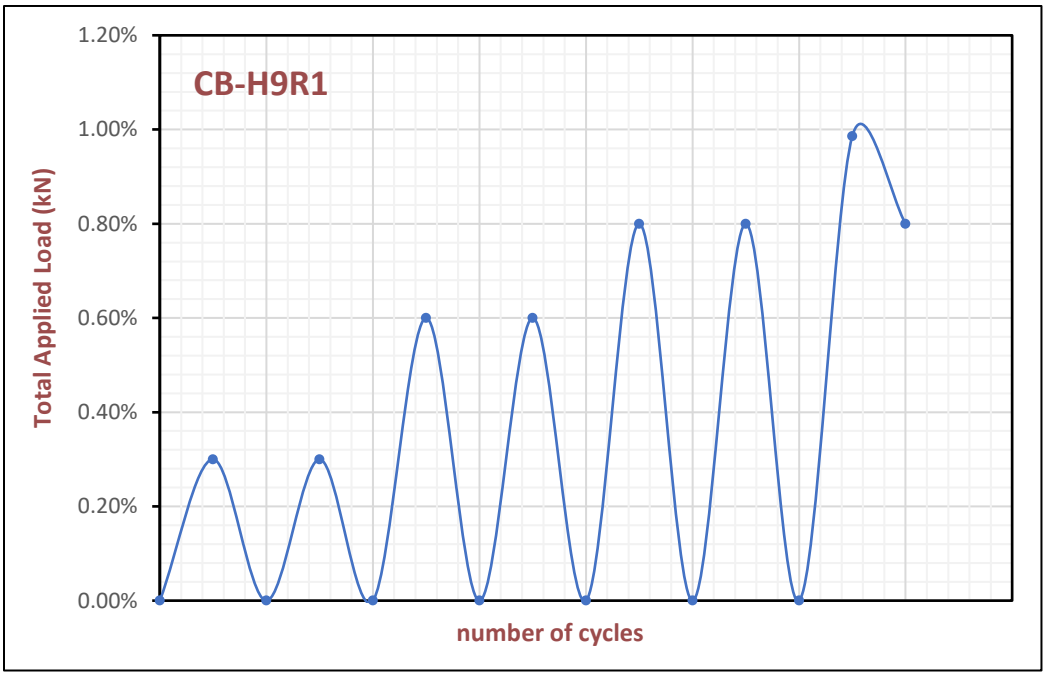

Figure 4-5: Loading Setup of The Beam Under Repeated Load (CB-H9R1).

Plate 4-5: Shape of Beam CB-H9R1 Before Testing.

Plate 4-6: Beam CB-H9R1 at Failure.

Plate 4-7: Failure of Beam CB-H9R1 After Testing (Web Post Buckling)

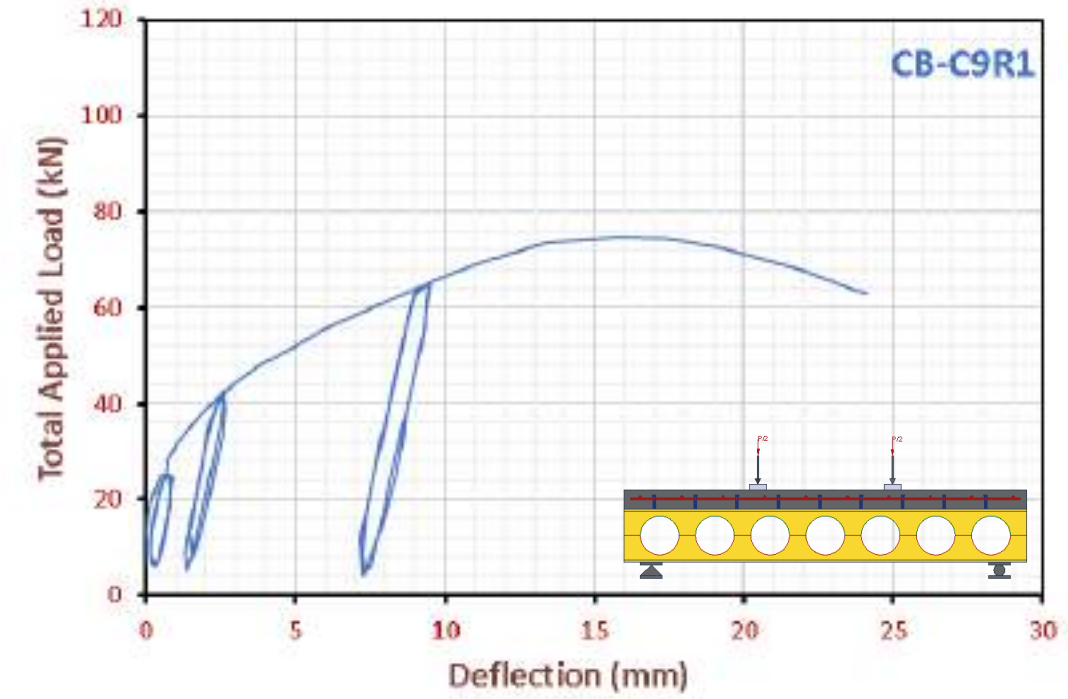

Figure 4-6: Load-Deflection Curve of Repeated Load Beam (CB-C9R1).

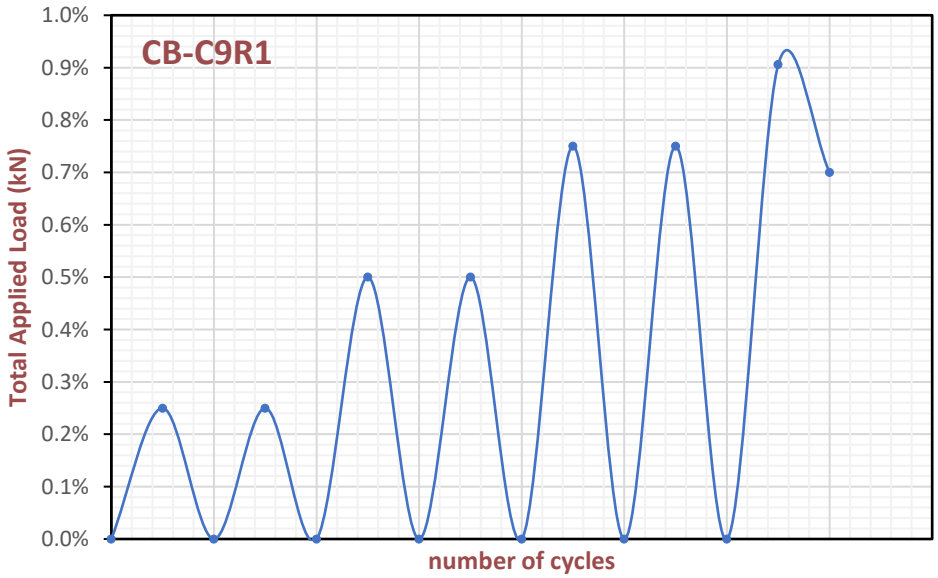

Figure 4-7: Loading Setup of The Beam Under Repeated Load (CB-C9R1).

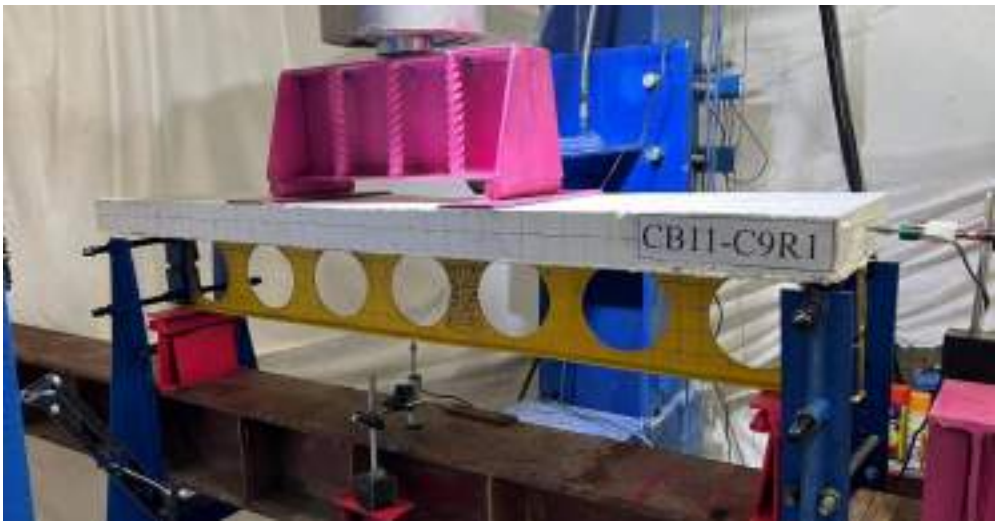

Plate 4-8: Shape of Beam CB-C9R1 before Testing.

Plate 4-9: Beam CB-C9R1 at Failure.

Plate 4-10: Effect of First Crack Load on Stud Shear Connectors.

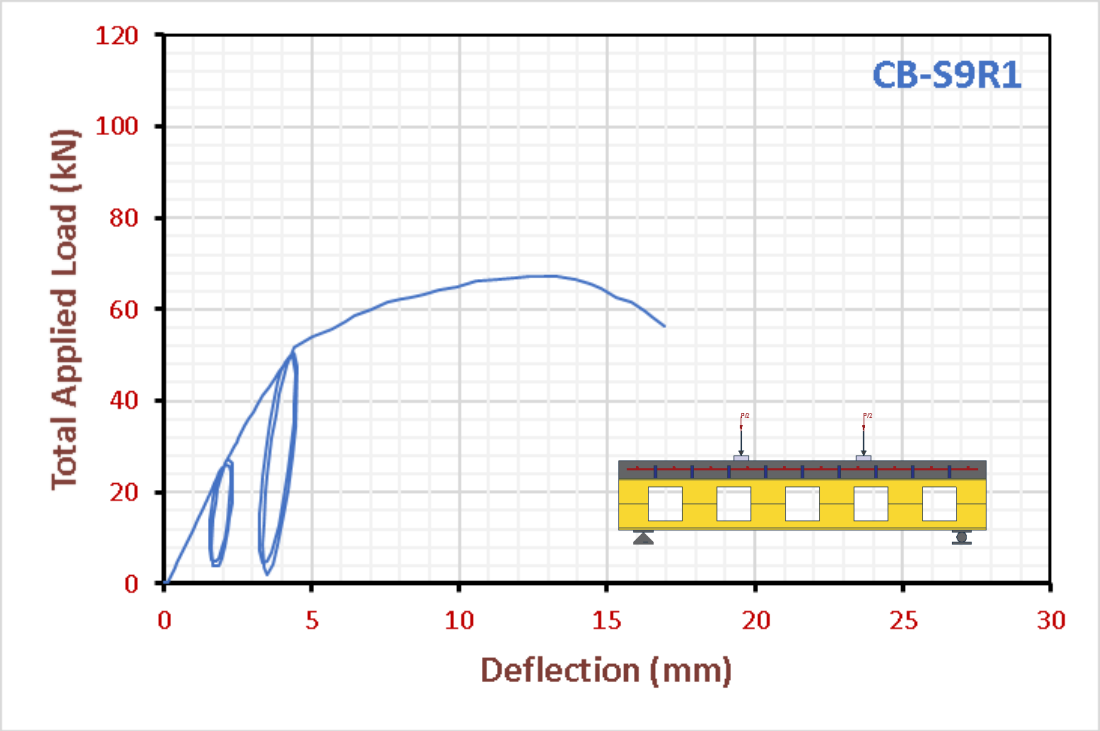

Figure 4-8: Load-Deflection Curve of Repeated Load Beam (CB-S9R1).

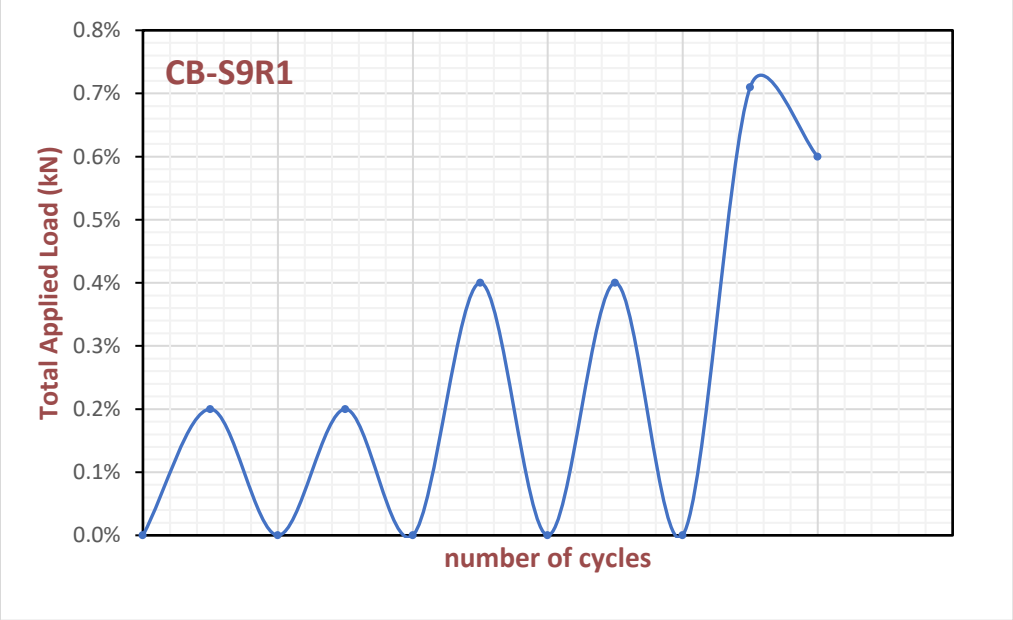

Figure 4-9: Loading Setup of The Beam Under Repeated Load (CB-S9R1).

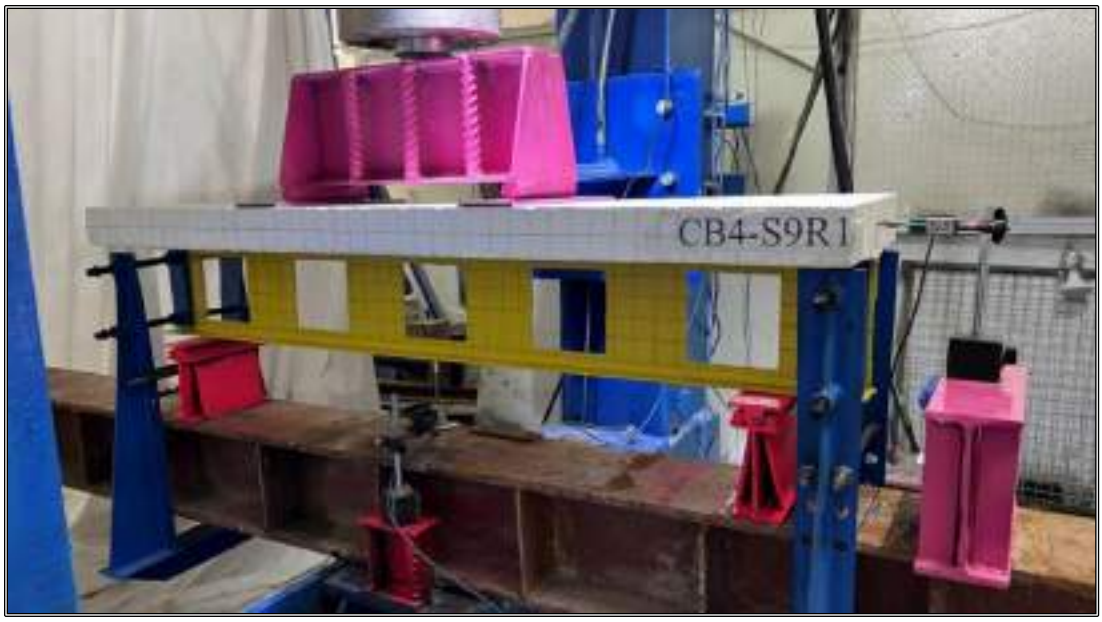

Plate 4-11: Shape of Beam CB-S9R1 Before Testing.

Plate 4-12: Beam CB-S9R1 at Failure.

Plate 4-13: Failure of Beam CB-S9R1 After Testing (Buckling and yielding).

4.3.1.3 Group Three

The group comprised three specimens, namely CB-H4R1, CB-C4R1, and CB-S4R1, each exhibiting distinct shapes of openings, specifically hexagonal, circular, and square. Additionally, the specimens were characterized by a stud spacing of 300mm. First, the repeated load is gradually applied up to (25% Pu) for the control beam.

Table 4-4: Ultimate Load and Deflection in The Middle of Each Span for Group Three.

Beams	Ultimate Load (kN)	Crack Load (kN)	Mid-span deflection at the first crack (mm)	Mid-span deflection at ultimate load(mm)
CB-H4R1	89.0	75	15.46	26.8
CB-C4R1	69.4	50	4.54	29.2
CB-S4R1	58.7	25	1.36	16.1

The hexagonal opening model had a maximum load deflection of 89.0 kN, while the circular opening model had a maximum deflection of 69.4 kN. The square opening model had a maximum deflection of 58.7 kN. Comparing these results with previous models with nine shear connectors revealed significant changes in load deflection. The hexagonal opening model experienced a decrease from 98.6 kN to 89.0 kN, the circular opening model from 90.6 kN to 69.4 kN, and the square opening model from 71.0 kN to 58.7 kN. The study reveals that using more shear connectors in composite castellated beams enhances their structural performance under repeated load conditions, with models with nine connectors consistently showing higher maximum load deflection values. The CB-H4R1 beam experienced various failure modes, including web post-buckling and the Vierendeel mechanism. Web post-buckling was the primary failure mode for CB-C4R1, indicating web failure due to compressive stress. Buckling and yielding occurred in CB-S4R1.

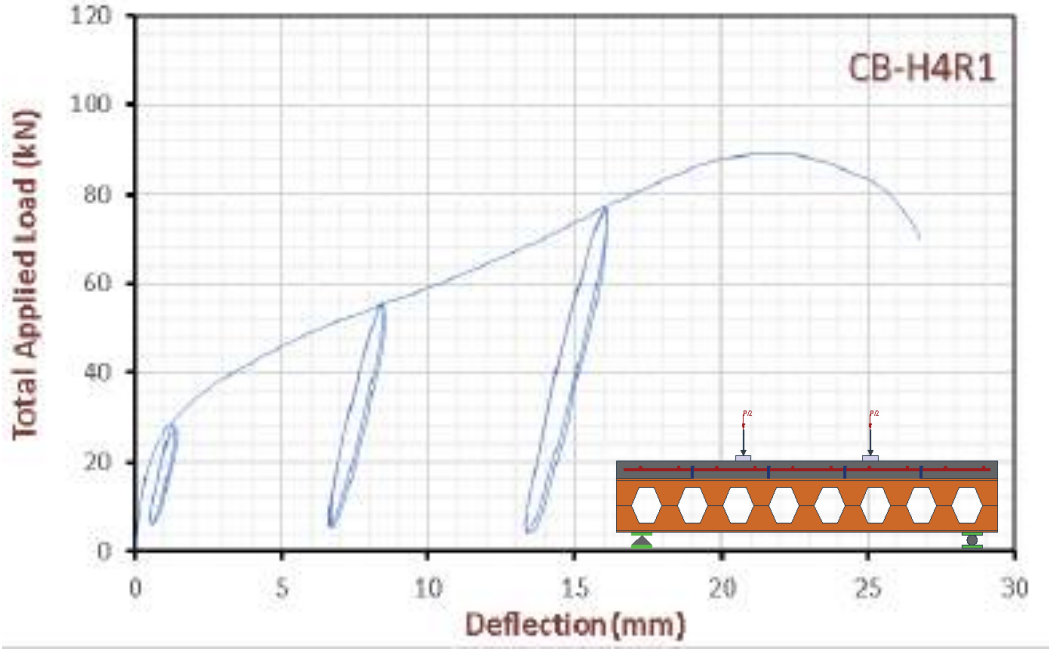

Figure 4-10: Load-deflection curve of repeated load beam (H4R1).

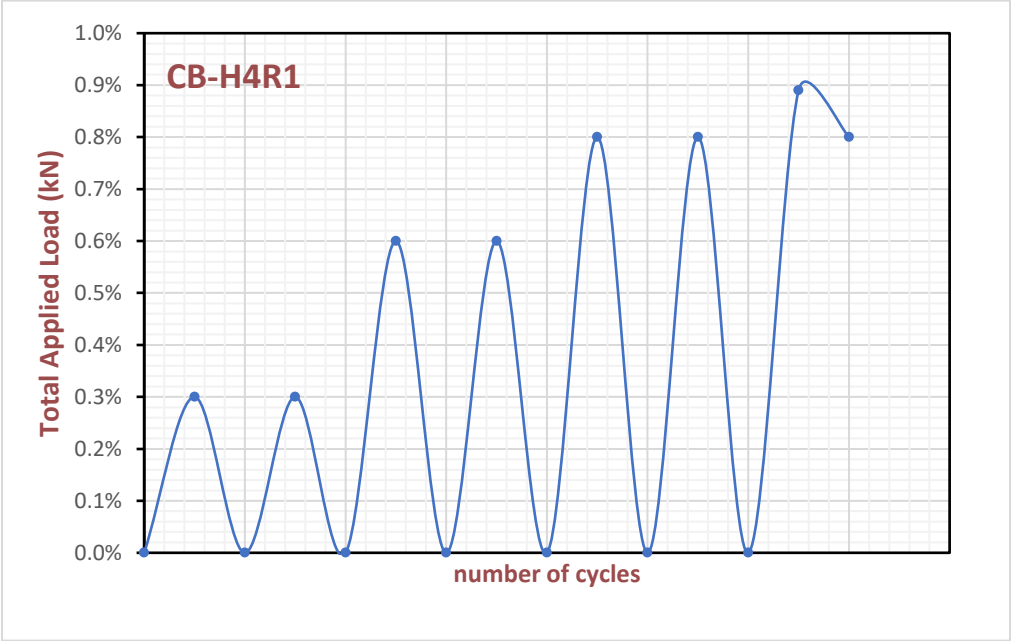

Figure 4-11: Loading setup of the beam under repeated load(H4R1).

Plate 4-14 : Shape of Beam CB-H4R1 Before Testing.

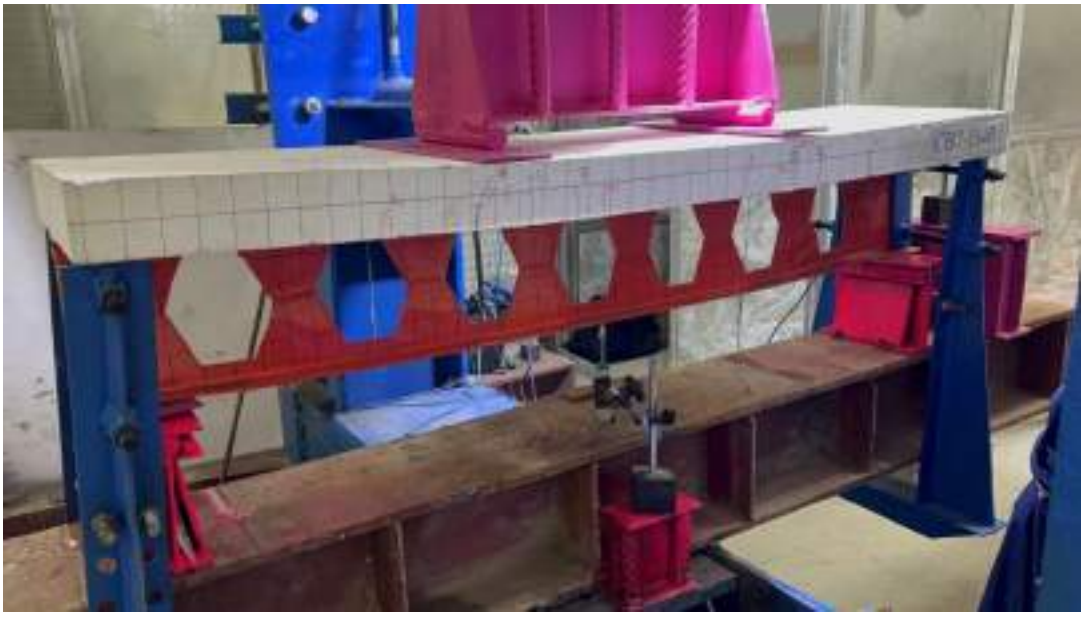

Plate 4-15: Beam CB-H4R1 at Failure.

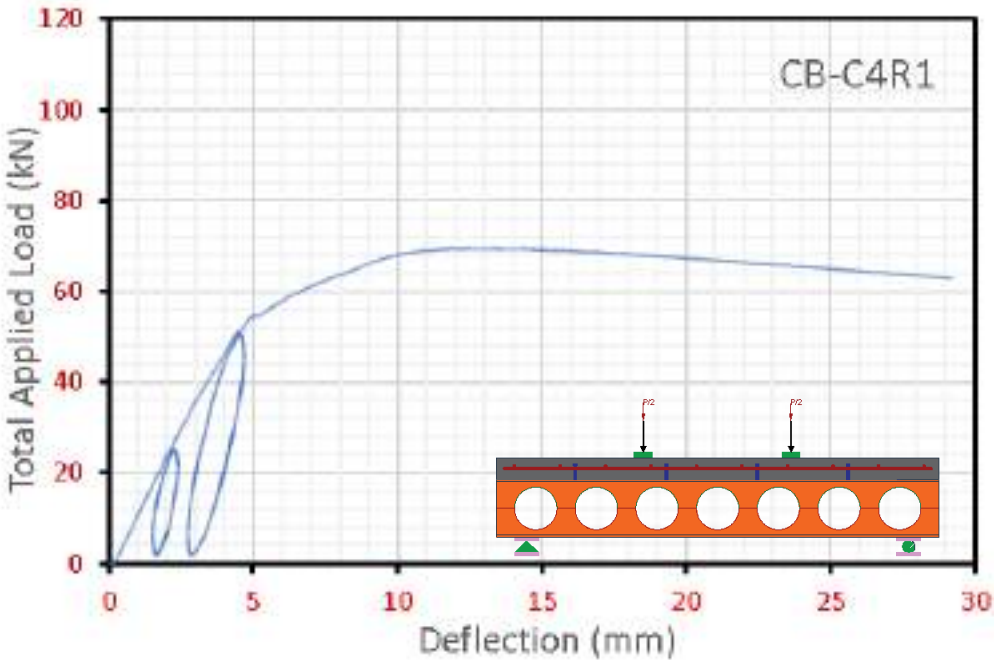

Figure 4-12: Load-Deflection Curve of Repeated Load Beam (C4R1).

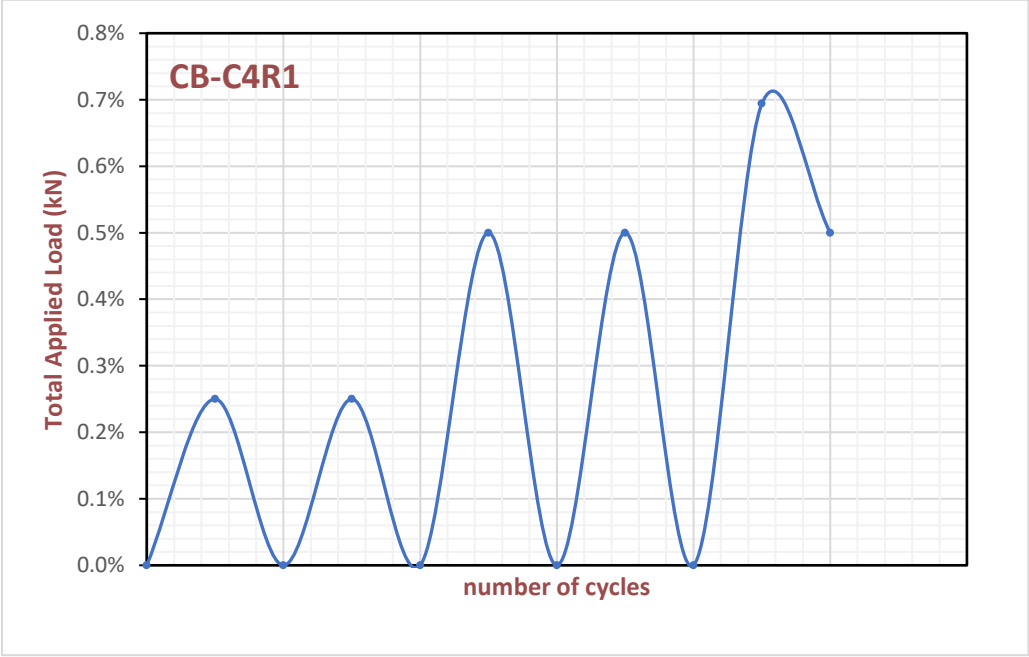

Figure 4-13: Loading Setup of The Beam Under Repeated Load (CB-C4R1).

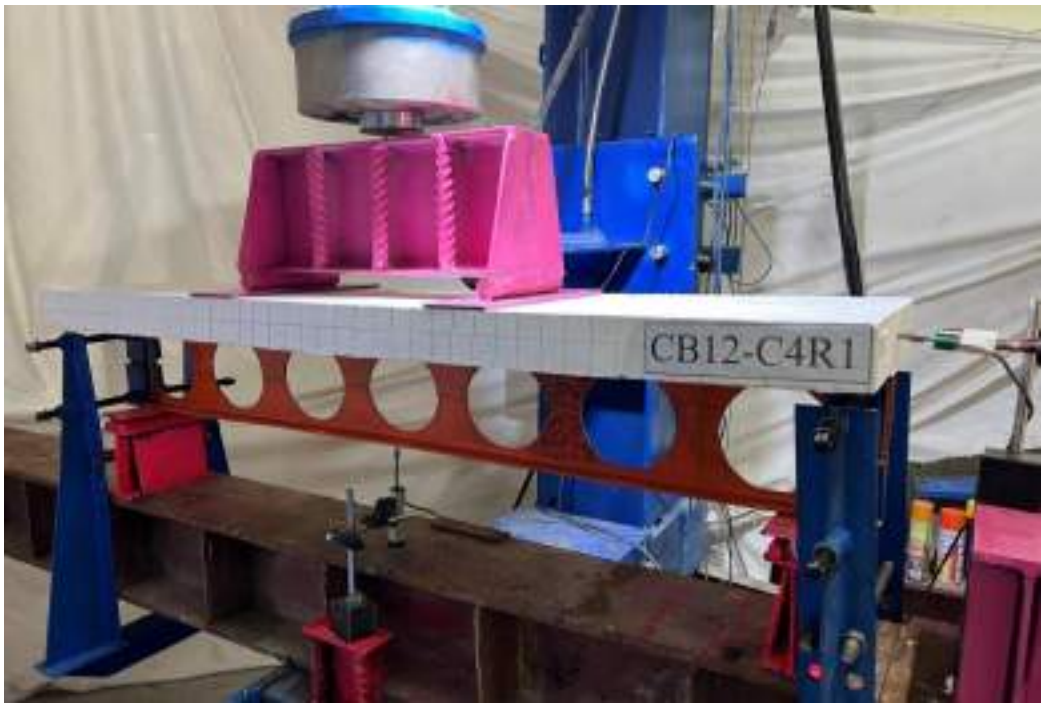

Plate 4-17 : Shape of Beam CB-C4R1 Before Testing.

Plate 4-16: Beam CB-C4R1 at Failure.

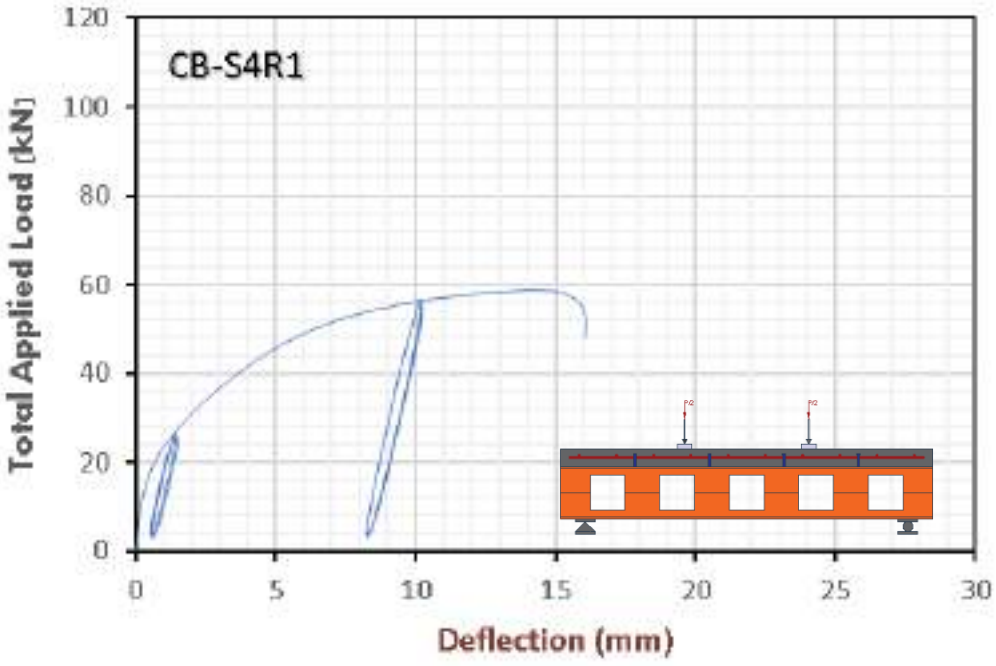

Figure 4-14: Load-Deflection Curve of Repeated Load Beam (CB-S4R1)

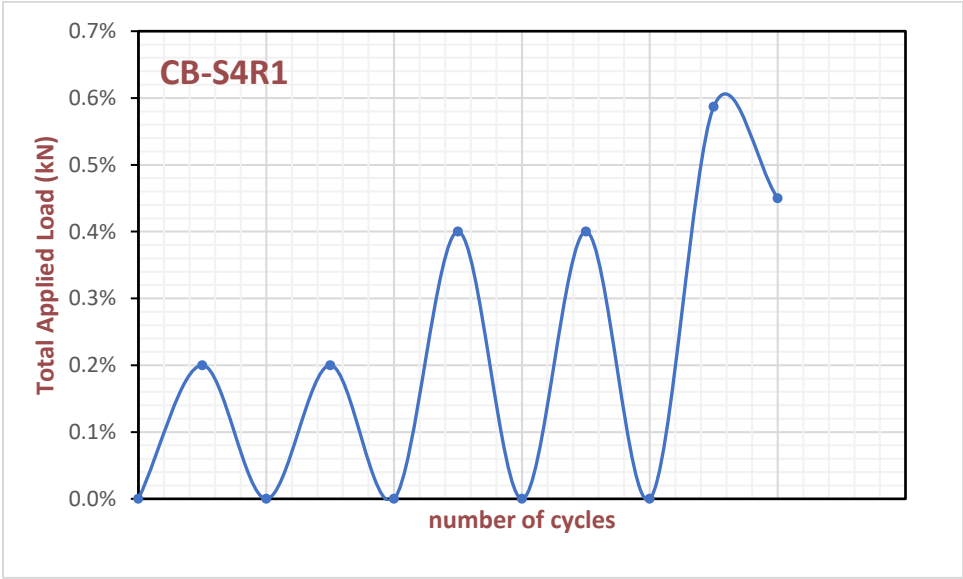

Figure 4-15: Loading Setup of The Beam Under Repeated Load (CB-S4R1)

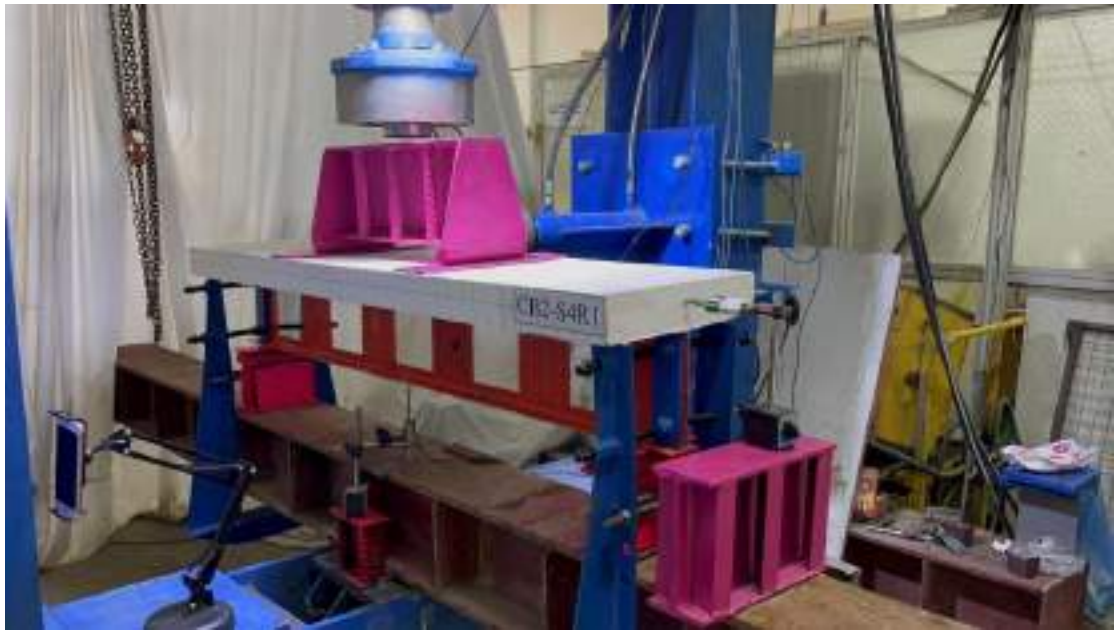

Plate 4-18: Shape of Beam CB-S4R1 before Testing.

Plate 4-19: Beam CB-S4R1 at Failure.

4.3.1.4 Group Four

However, the fourth group differs from the second by including strengthening within the web region.

Table 4-5:Ultimate load and deflection in the middle of each span for group Four.

Beams	Ultimate Load (kN)	Crack Load (kN)	Mid-span deflection at the first crack (mm)	Mid-span deflection at ultimate load(mm)
CB-H9R2	164.2	90	12.99	47.4
CB-C9R2	121.3	75	8.32	38.6
CB-S9R2	109.4	50	3.55	25.3

The initial model, consisting of a hexagonal beam with stiffeners and a hexagonal opening, demonstrated the highest load deflection of 164.2 kN after six cyclic tests. The second model, consisting of a circular beam with a circular opening, had a maximum load deflection of 121.3 kN. The third model, consisting of a square hole, had a maximum load deflection of 109.4 kN. The hexagonal opening configuration exhibited a substantial 35.3% increase in ultimate load compared to the circular opening, emphasizing the favorable structural characteristics of hexagonal designs. Moreover, the hexagonal configuration displayed a 49.8% higher ultimate load when comparing hexagonal and square openings. These results underscore the importance of the shape of openings, with hexagonal configurations showcasing superior structural performance in terms of ultimate load. Results showed that CB-H9R2 had load distribution and deformation characteristics similar to the Vierendeel truss, with plastic hinges playing a significant role in structural behavior and ultimate failure. The study recommends using hexagonal apertures for castellated beam design, avoiding square openings due to diminished capacity, and considering fatigue failure potential when designing for repeated loading scenarios.

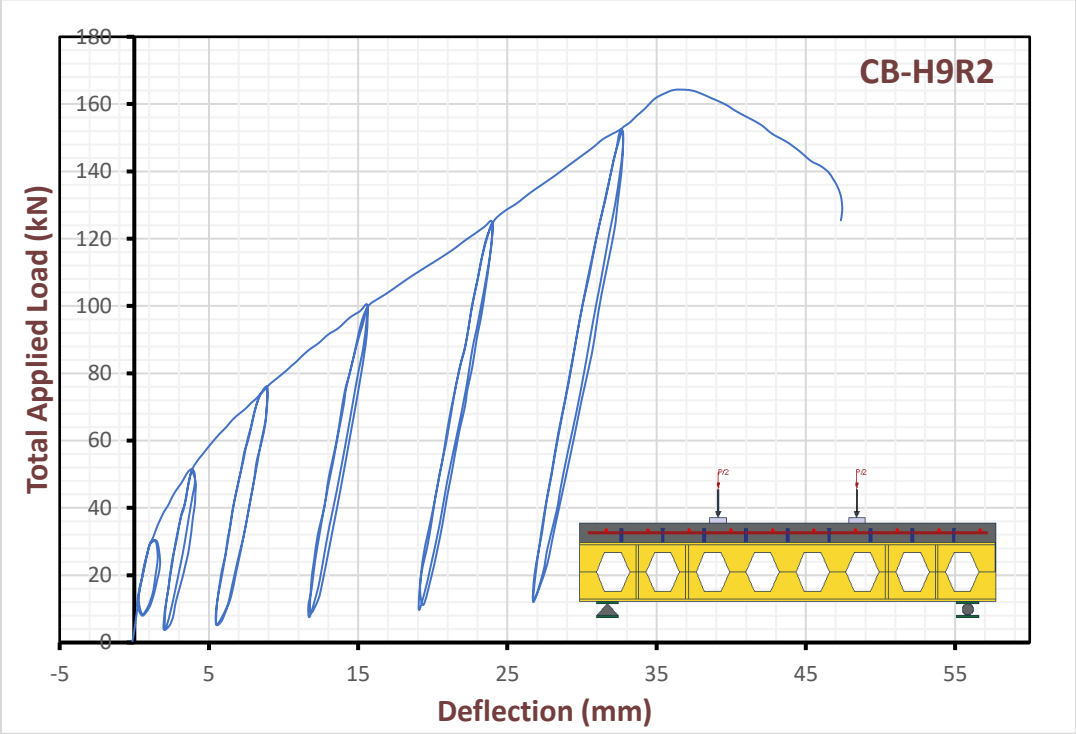

Figure 4-16: Load-Deflection Curve of Repeated Load Beam (CB-H9R2).

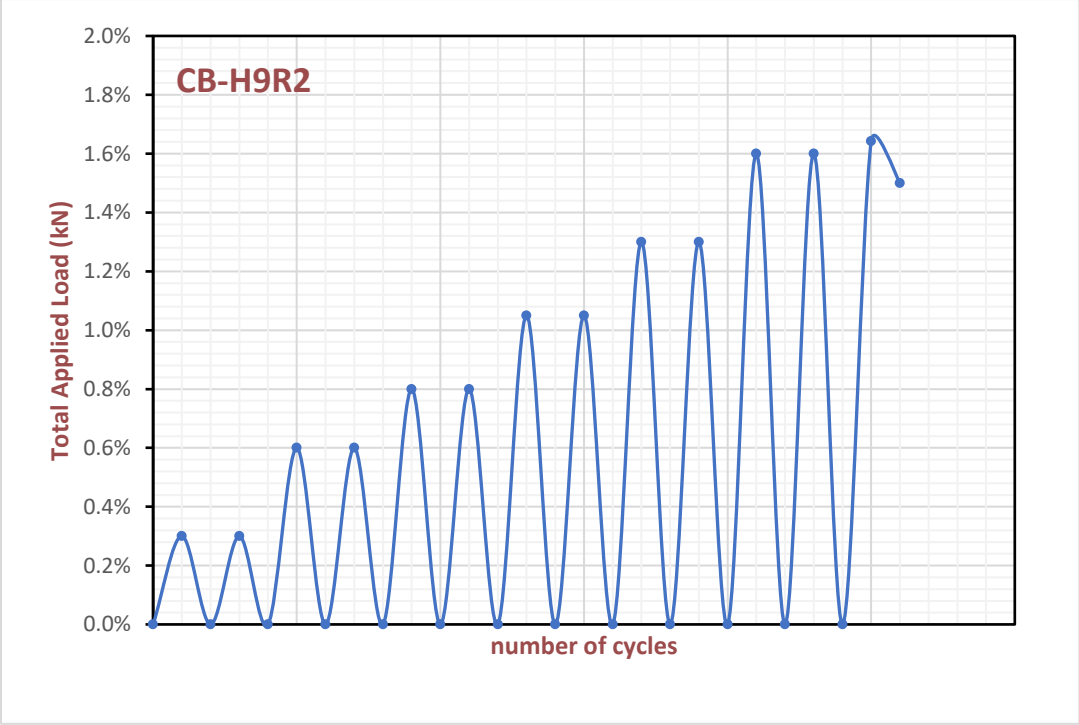

Figure 4-17: Loading Setup of The Beam Under Repeated Load (CB-H9R2).

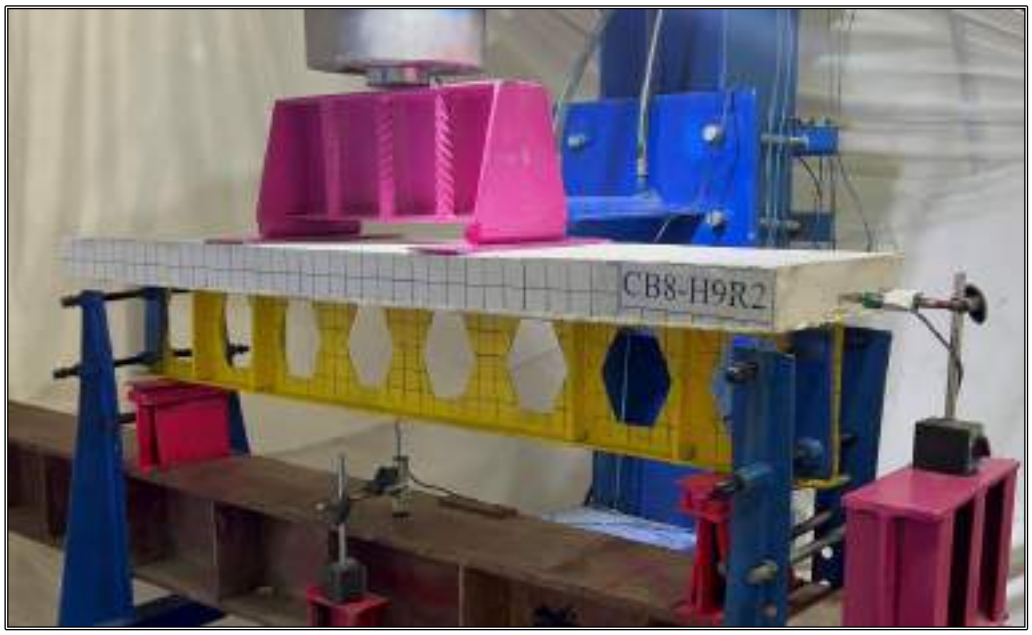

Plate 4-20: Shape of Beam CB-H9R2 Before Testing.

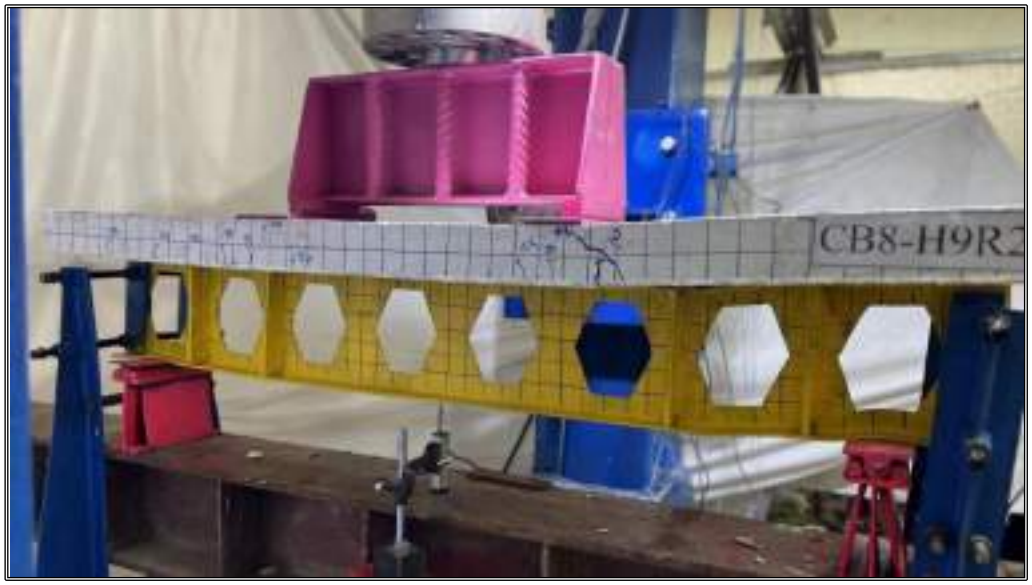

Plate 4-21: Beam CB-H9R2 at Failure.

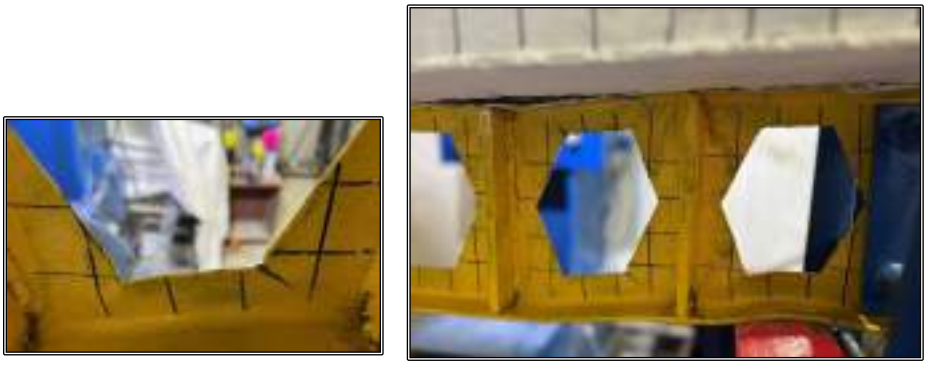

Plate 4-22 :Tearing and Inelastic Local Buckling for Beam CB-H9R2.

Plate 4-23: Beam CB-H9R2 at Failure.

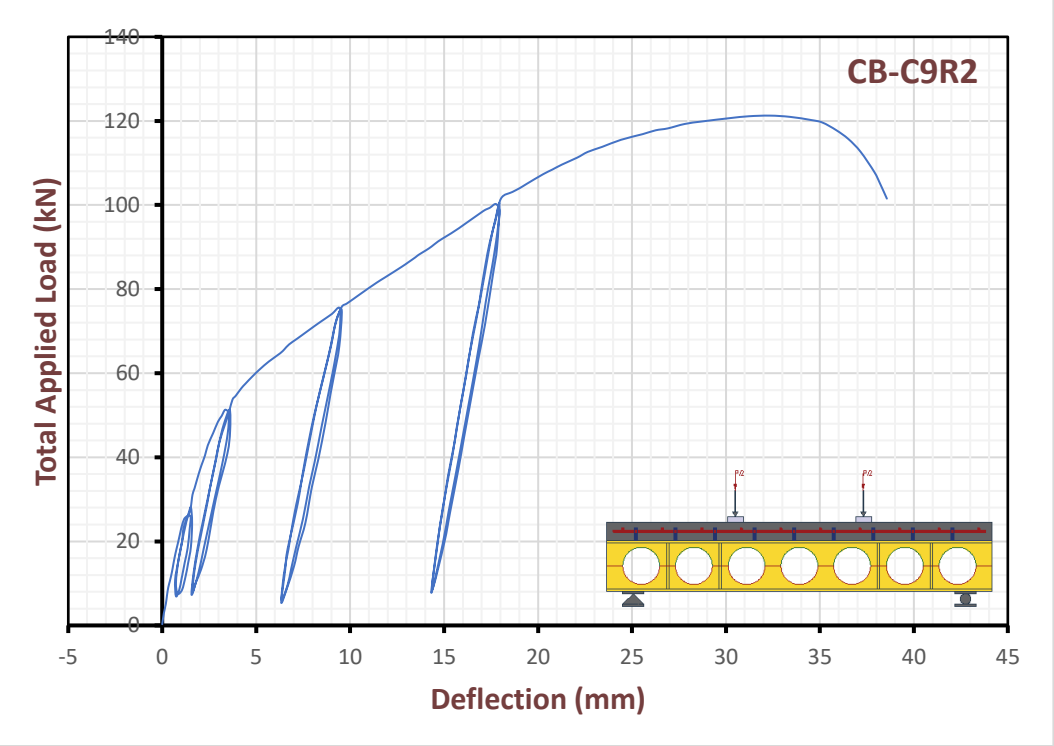

Figure 4-18: Load-deflection curve of repeated load beam (C9R2).

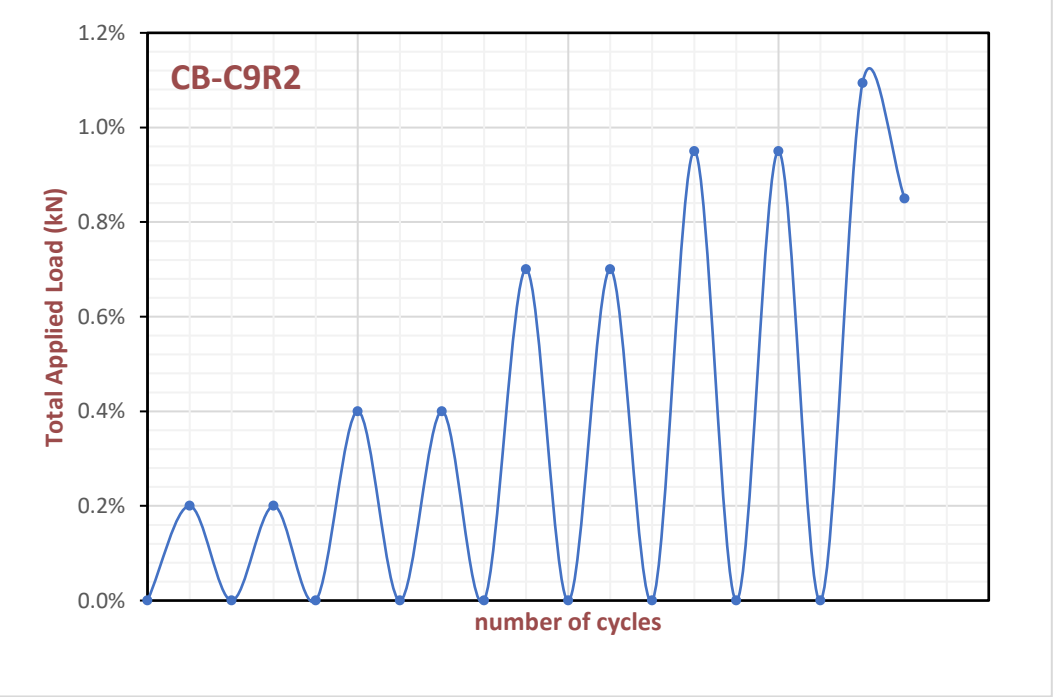

Figure 4-19: Loading setup of the beam under repeated load (CB-C9R2).

Plate 4-24: Shape of Beam CB-C9R2 before Testing.

Plate 4-25: Beam CB-C9R2 at Failure.

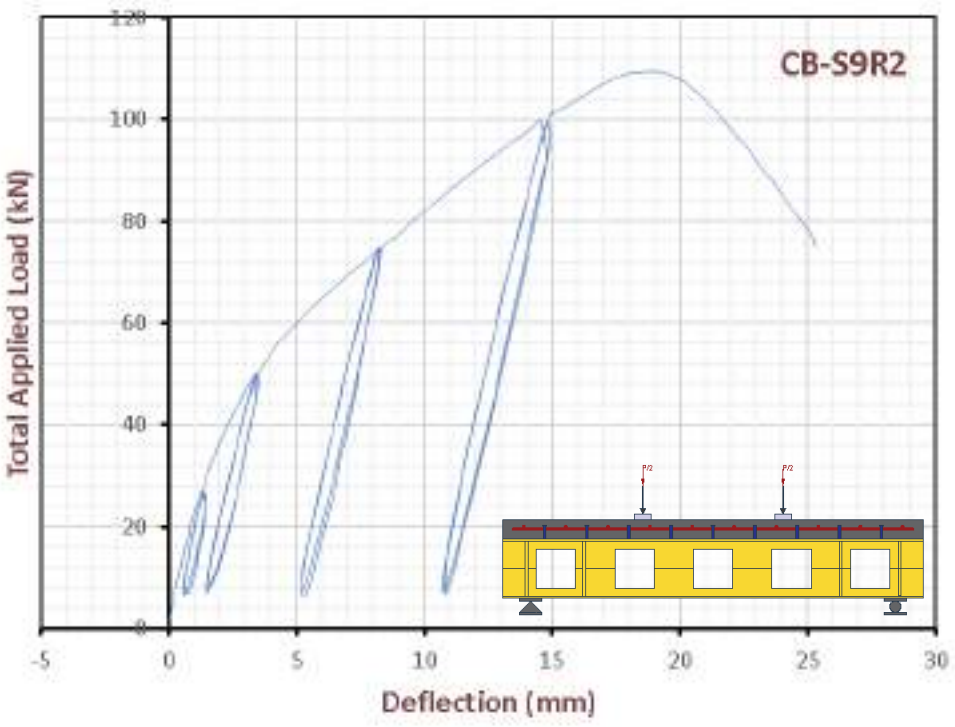

Figure 4-20: Load-Deflection Curve of Repeated Load Beam (S9R2).

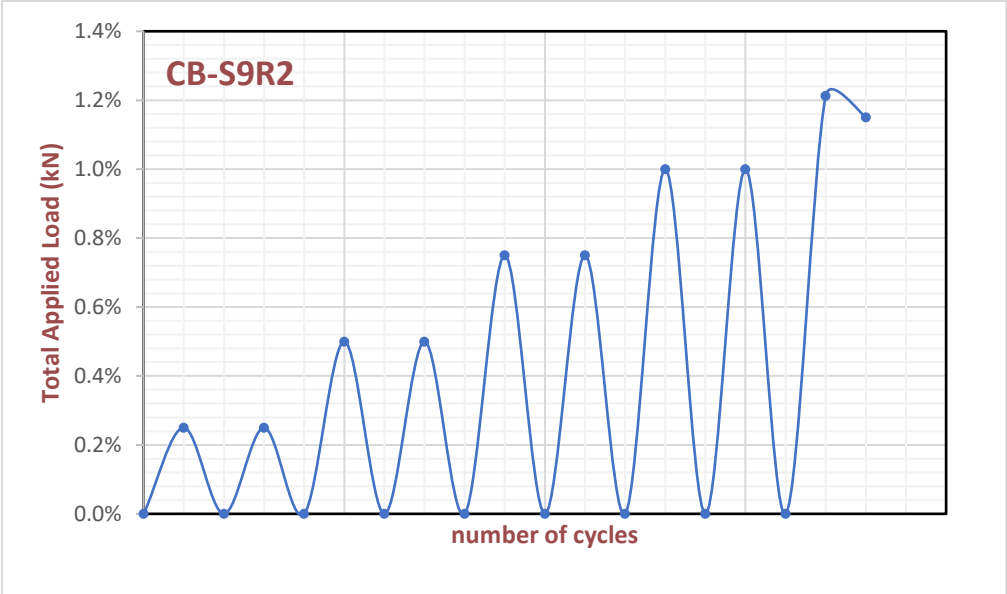

Figure 4-21: Loading Setup of The Beam Under Repeated Load (S9R2).

Plate 4-26: Shape of Beam CB-S9R2 Before Testing.

Plate 4-27: Beam CB-S9R2 at Failure.

Plate 4-28: Beam CB-S9R2 at Failure.

4.3.1.5 Group Five

The fifth group resembles the third group, however, and is distinguished by the inclusion of strengthening within the web region.

Table 4-6:Ultimate load and Deflection in The Middle of Each Span for Group Five.

Beams	Ultimate Load (kN)	Crack Load (kN)	Mid-span deflection at the first crack (mm)	Mid-span deflection at ultimate load(mm)
CB-H4R2	138.6	75	8.86	28.2
CB-C4R2	102.4	50	6.02	49.1
CB-S4R2	69.2	50	4.55	14.6

The study found that models with four-shear connectors showed improved load-deflection performance, suggesting that existing stiffeners can improve structural efficiency. The composite castellated beams, CB-H4R2, CB-C4R2, and CB-S4R2, exhibited different failure types, showcasing their unique characteristics. The study also found that hexagonal apertures were more effective in optimizing load-bearing capacity and deflection performance, especially under static loading conditions. However, square apertures reduced ultimate load and deflection capabilities. The study suggests that vertical plates within the web of castellated beams could enhance their structural integrity, especially under significant load conditions. The failure of the three specimens in Group Four was attributed to a combination of the Vierendeel truss analogy, the four-hinged failure mechanism, and local buckling.

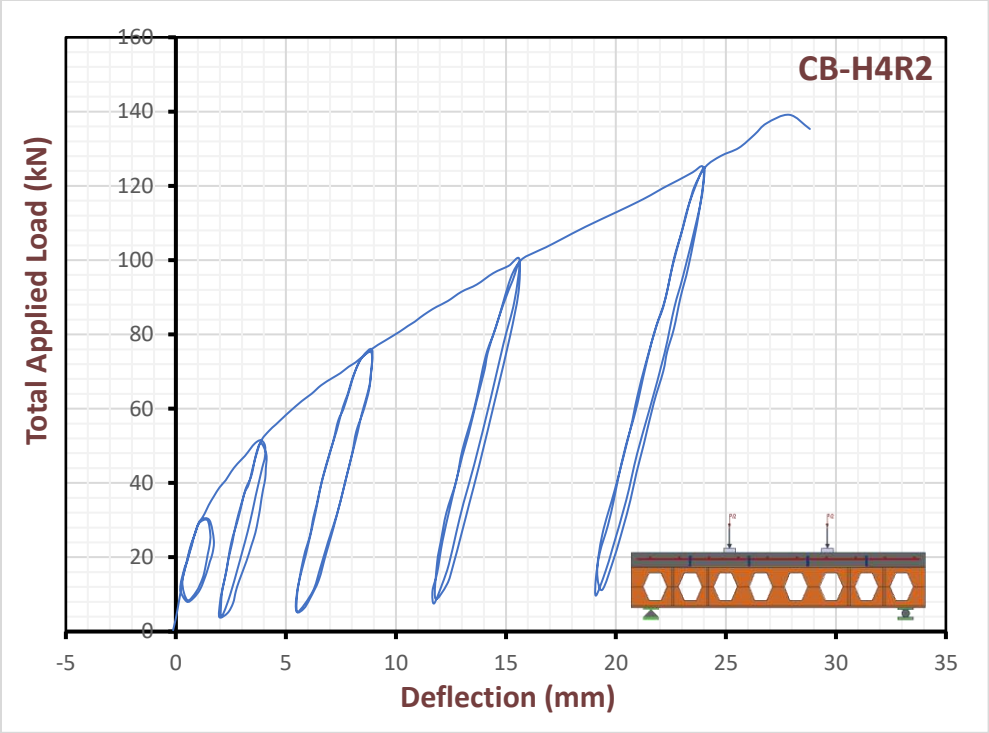

Figure 4-22: Load-deflection curve of repeated load beam (H4R2).

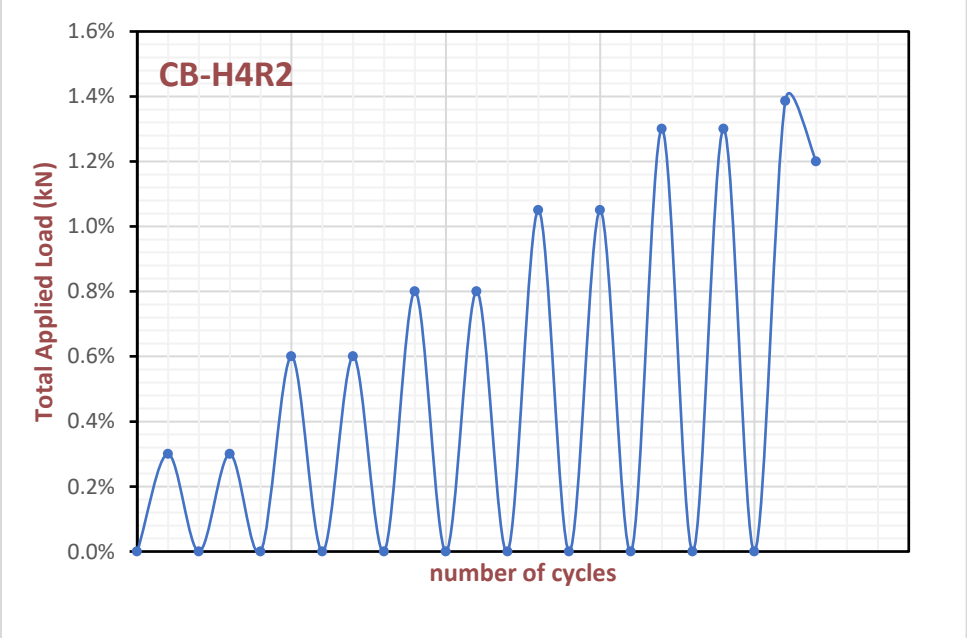

Figure 4-23: Loading setup of the beam under repeated load (H4R2).

Plate 4-29: Shape of Beam CB-H4R2 Before Testing.

Plate 4-30: Beam CB-H4R2 at Failure.

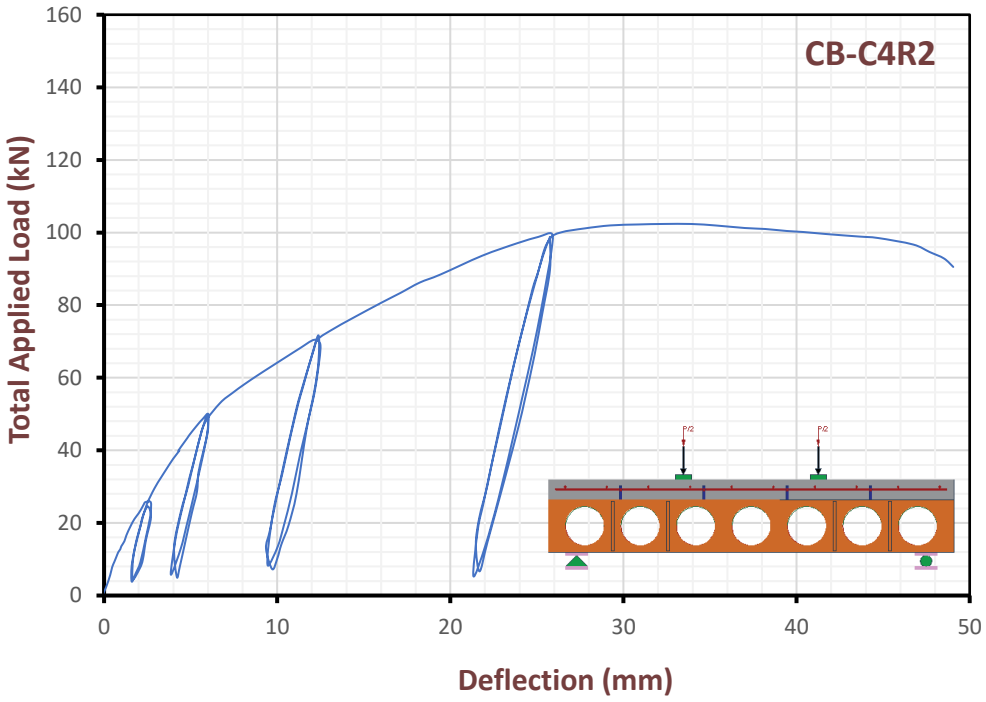

Figure 4-24: Load-Deflection Curve of Repeated Load Beam (CB-C4R2).

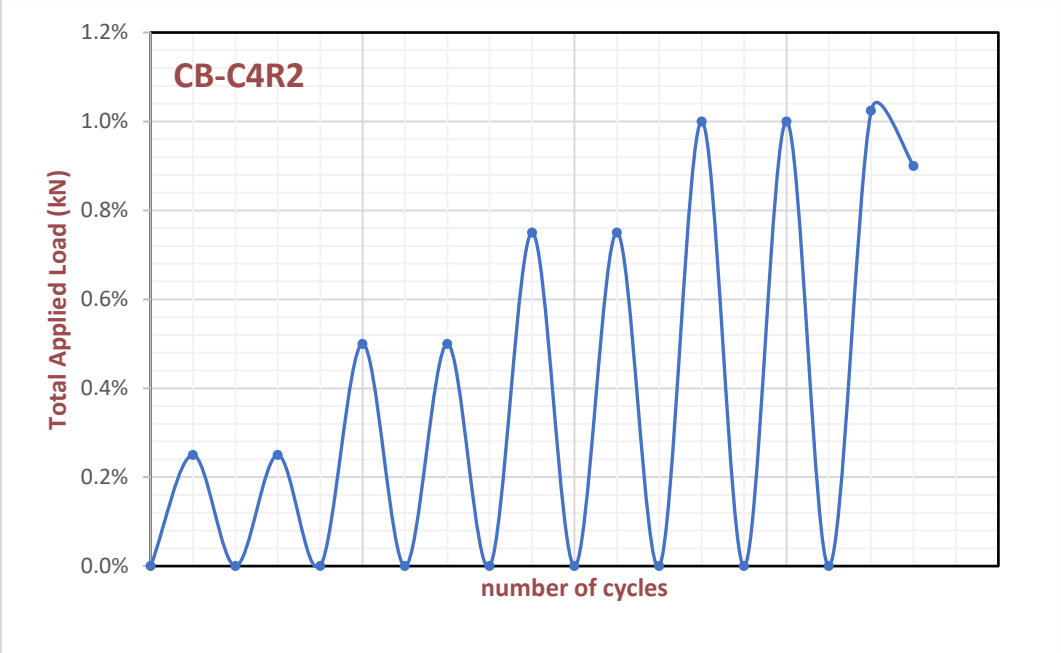

Figure 4-25: Loading Setup of The Beam Under Repeated Load (CB-C4R2).

Plate 4-31: Shape of Beam CB-C4R2 Before Testing.

Plate 4-32: Beam CB-C4R2 at Failure.

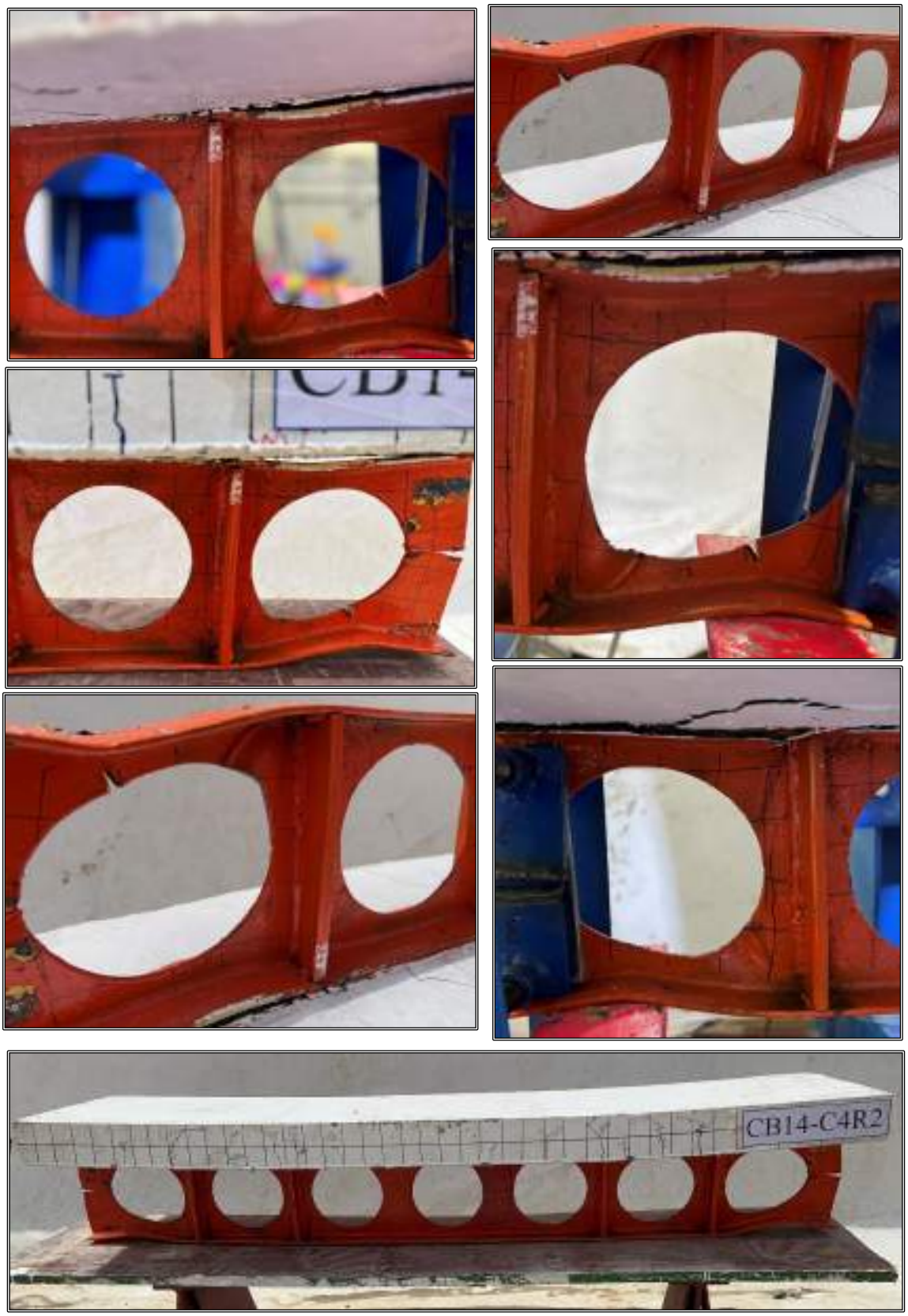

Plate 4-33: Failure of Beam CB-C4R2 After Testing.

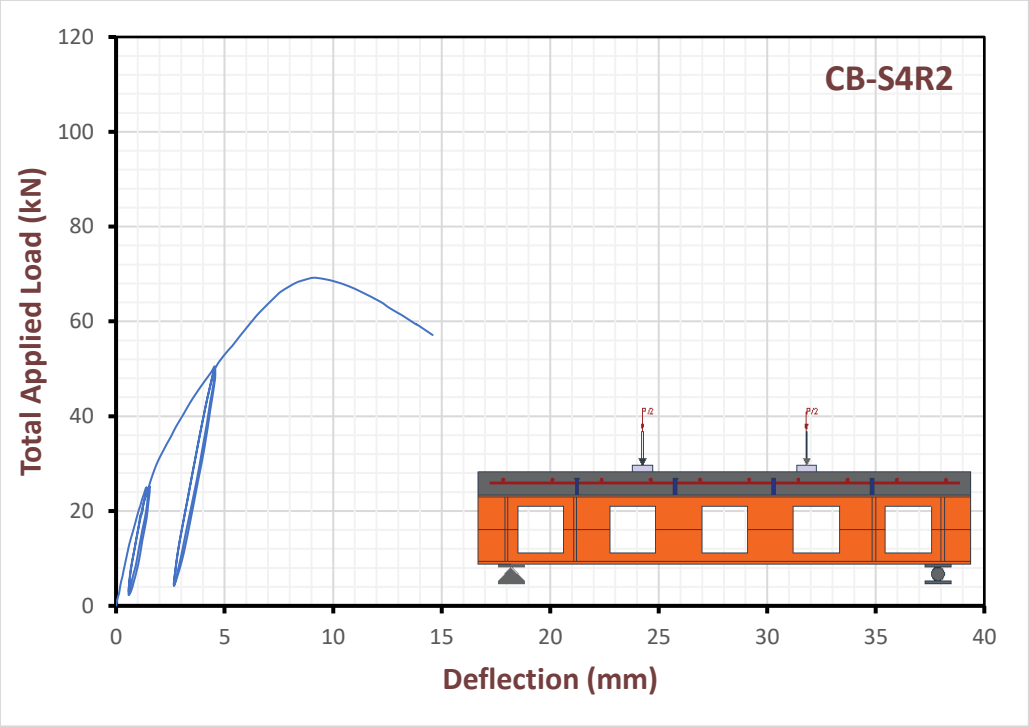

Figure 4-26: Load-deflection curve of repeated load beam (CB-S4R2)

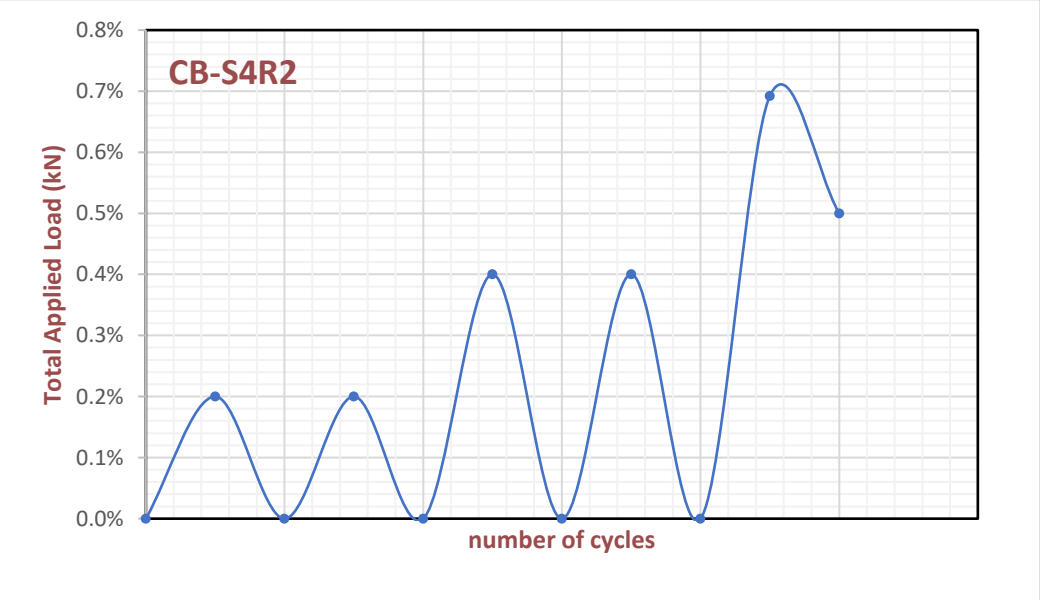

Figure 4-27: Loading setup of the beam under repeated load (CB-S4R2) .

Plate 4-34: Shape of Beam CB-S4R2 before Testing.

Plate 4-35: Beam CB-S4R2 at Failure.

Plate 4-36: Beam CB-S4R2 at Failure.

4.4 Parameters Influence

4.4.1 First Parameter - Shape of Opening

Percentage Differences in Ultimate Load Between Opening Shapes Within Each Group:

Group	Comparison	Percentage Difference
2	Hexagonal vs. Circular	31.63%
	Hexagonal vs. Square	46.30%
	Circular vs. Square	11.20%
3	Hexagonal vs. Circular	28.26%
	Hexagonal vs. Square	51.61%
	Circular vs. Square	18.26%
4	Hexagonal vs. Circular	35.36%
	Hexagonal vs. Square	49.96%
	Circular vs. Square	9.83%
5	Hexagonal vs. Circular	35.28%
	Hexagonal vs. Square	100.43%
	Circular vs. Square	47.93%

The table shows that hexagonal openings have a superior load-bearing capacity compared to circular and square shapes. In Group 2, hexagonal openings increase ultimate load by 31.63% and 46.30%, respectively. In Group 3, hexagonal openings surpass both circular and square shapes by 28.26% and 51.61%, respectively. In Group 4, hexagonal openings show superiority by 35.36% and 49.96%, with a slight increase of 9.83% compared to square shapes. In Group 5, hexagonal openings maintain their advantage, nearly double the ultimate load of square openings.

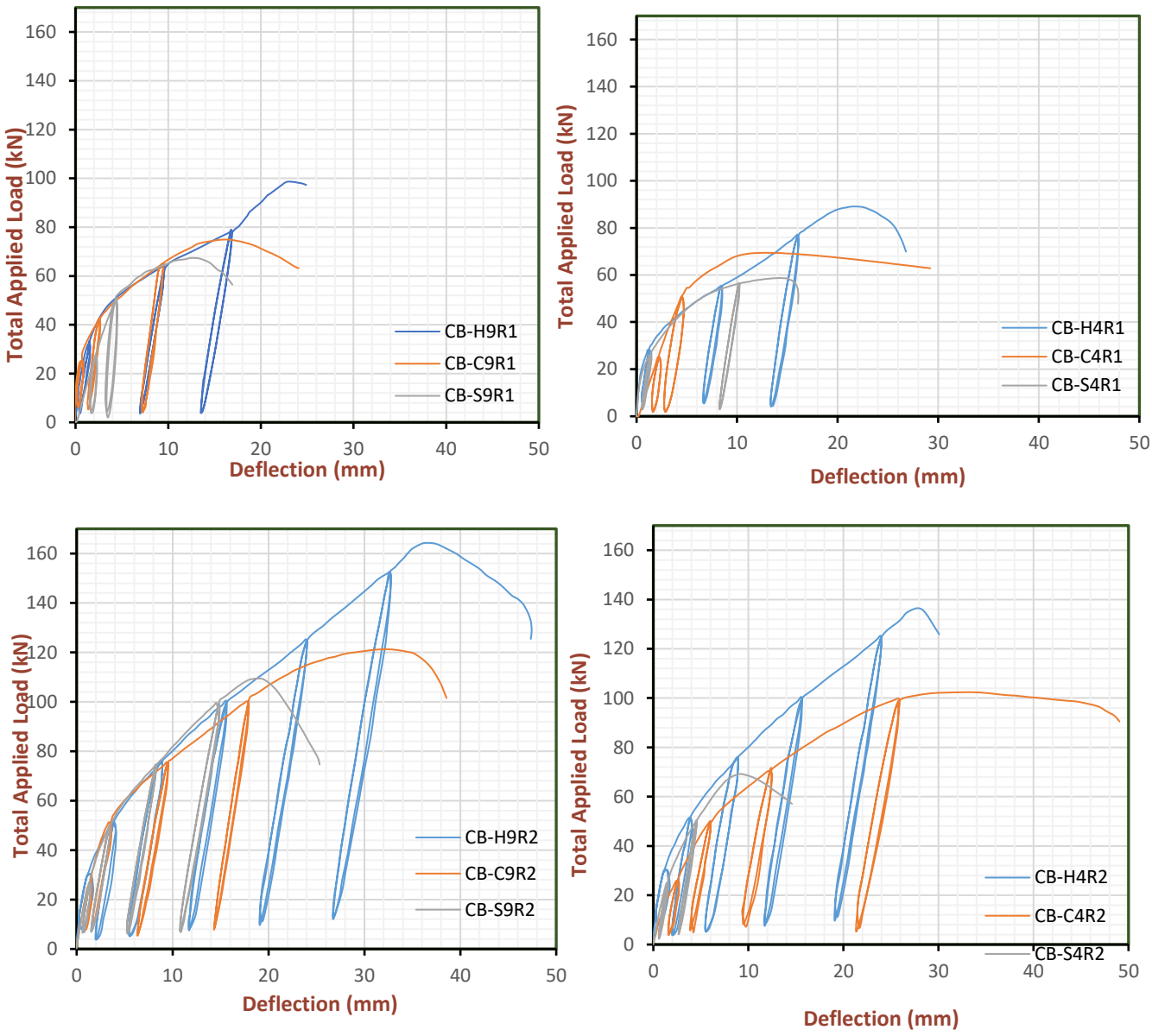

Figure 4-28:Compare the Results for The Shape of The Openings.

4.4.2 Second Parameter - Space Between Shear Connector

The second parameter of the study focuses on the spacing between shear connectors and its influence on the ultimate load of castellated steel beams.

Table 4-7:Influence of Shear Connector Spacing on Ultimate Load of CCB.

No.	Beams		shear connectors effect %
1	CB-H9R1	CB-H4R1	10.79%
2	CB-C9R1	CB-C4R1	7.91%
3	CB-S9R1	CB-S4R1	14.72%
4	CB-H9R2	CB-H4R2	18.47%
5	CB-C9R2	CB-C4R2	18.46%
6	CB-S9R2	CB-S4R2	58.09%

Shear connector spacing significantly impacts ultimate load in beams, with a 10.79% difference between hexagonal and circular configurations. Square openings show a higher sensitivity to spacing, with a 14.72% difference. The impact is more pronounced for hexagonal openings, with an 18.47% difference. Circular openings have a smaller effect, but square openings show a significant 58.09% difference, highlighting their critical role in performance.

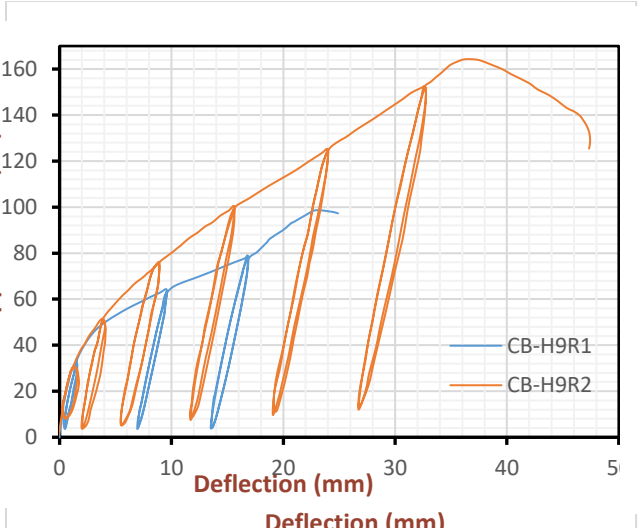

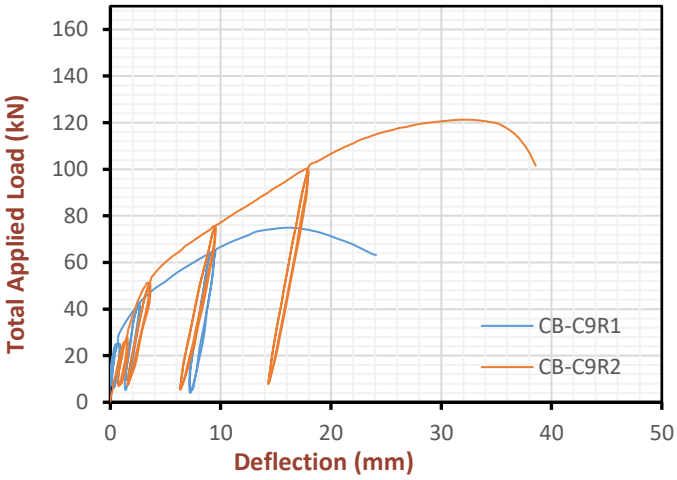

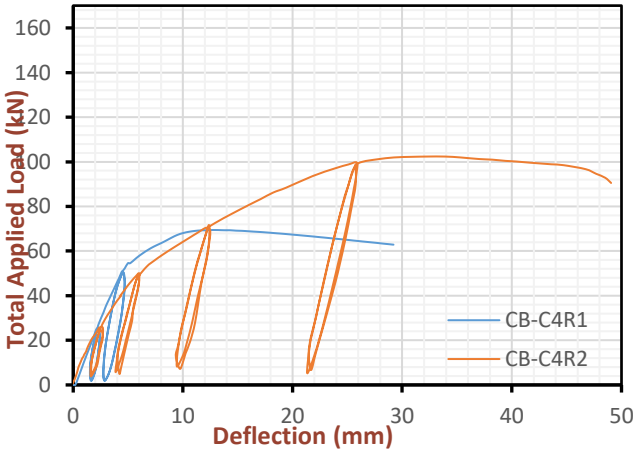

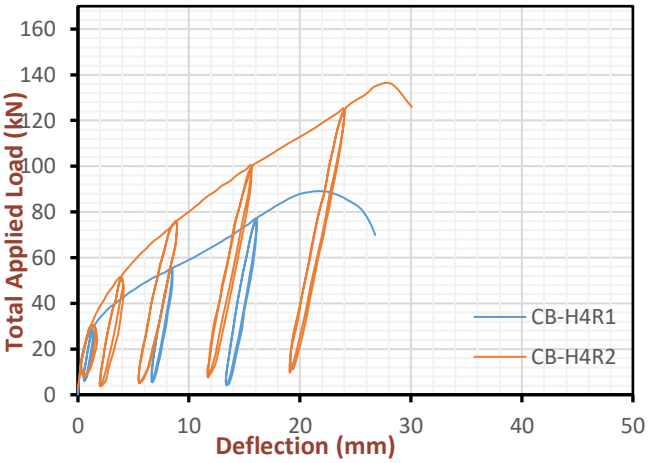

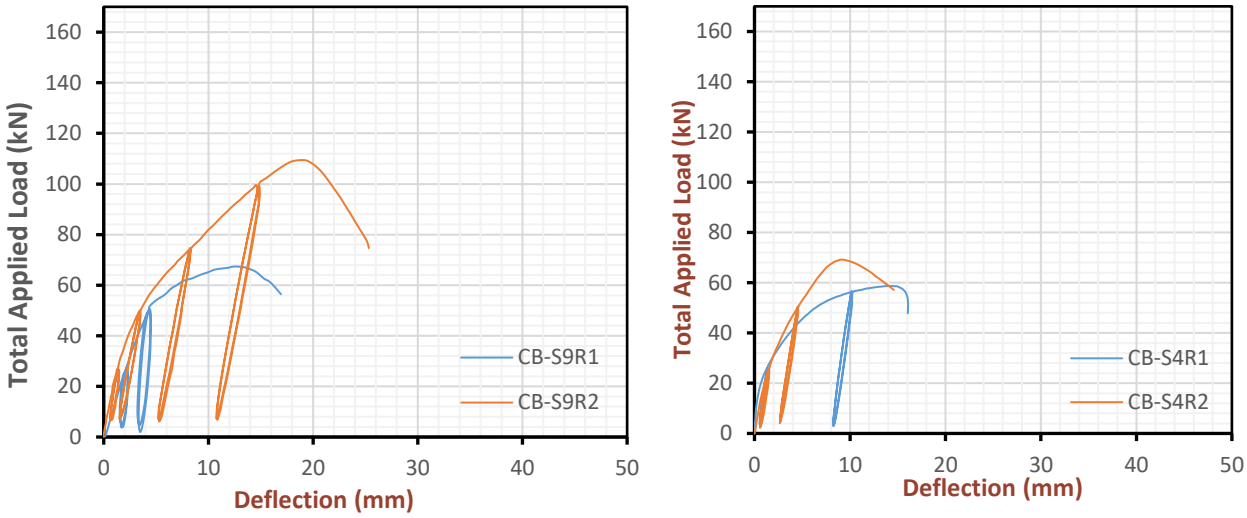

Figure 4-29:Compare results for distance between stud shears.

4.4.3 Third Parameter - Used Strengthening

The third parameter of the study focuses on the impact of different strengthening techniques on the performance of castellated steel beams.

Table 4-8:Impact of Different Strengthening Techniques on Beam Performance.

Beams		Strengthening%
CB-H9R1	CB-H9R2	66.53%
CB-C9R1	CB-C9R2	61.97%
CB-S9R1	CB-S9R2	62.46%
CB-H4R1	CB-H4R2	55.73%
CB-C4R1	CB-C4R2	47.55%
CB-S4R1	CB-S4R2	17.89%

Strengthening hexagonal, circular, square, and hexagonal beams significantly increases ultimate load, with hexagonal openings enhancing by 66.53%, circular openings by 61.97%, square openings by 62.46%, and square openings by 17.89%.

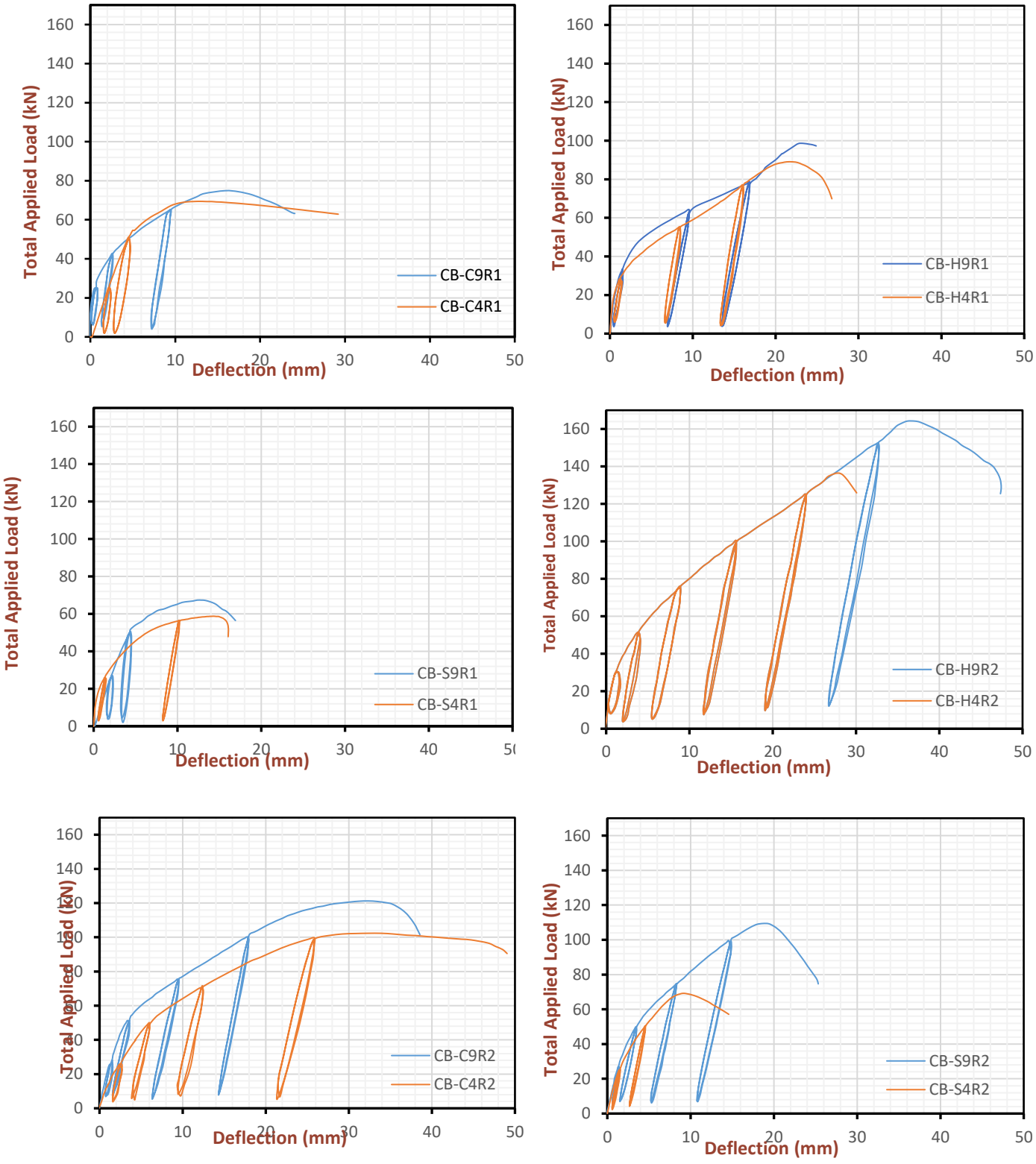

Figure 4-30:Compare results after strengthening.

4.5 Load-Slip Relationship

A study on slip in composite beams showed Figure 4-31 depicting slip-induced beam shapes under vertical loads. Ten composite beams were made by connecting steel beams and concrete slabs with shear connectors for material interaction.

Table 4-9:Experimental Slip at Ultimate Load.

Specimens	(mm)	(kN)
CB-C9R1	7.3	89.3
CB-S9R1	3.4	71.7
CB-C4R1	5.4	69.2
CB-S4R1	2.8	58.4
CB-C9R2	9.6	121.2
CB-S9R2	5.5	109.2
CB-C4R2	2.2	76.3
CB-S4R2	1.5	69.2
CB-9S	3.3	130.4
CB-S9S	1.5	92.5

When a load is applied to a composite beam, it results in horizontal slip or relative displacement between the concrete and steel constituents. This lateral displacement decreases the flexural rigidity of the composite cross-section. The study provides insights into the behavior of composite beams and the impact of characteristics like shear connectors and opening shapes on slip occurrence and structural reaction. The results show that specimens with square openings (CB-S9S) have the highest degree of slip at the point of ultimate load, while those subjected to repeated loading have a greater degree of slip. Those with more shear connectors (CB-C9R1 and CB-C9R2) show reduced slip at the point of ultimate stress. The study concludes that reducing the slip of composite beams can be achieved by using hexagonal apertures

instead of square openings, minimizing repetitive loading, and increasing the use of shear connectors.

Figure 4-31: Horizontal Slip Between the Concrete and Steel Constituents.

4.6 Distribution of Normal Strain

Figures (4-41) to (4-43) show the relationship between the longitudinal strain and load through the depth of the composite beam at mid-span for different load levels, including failure load. The strain was measured at six levels across the depth of the composite castellated beam.

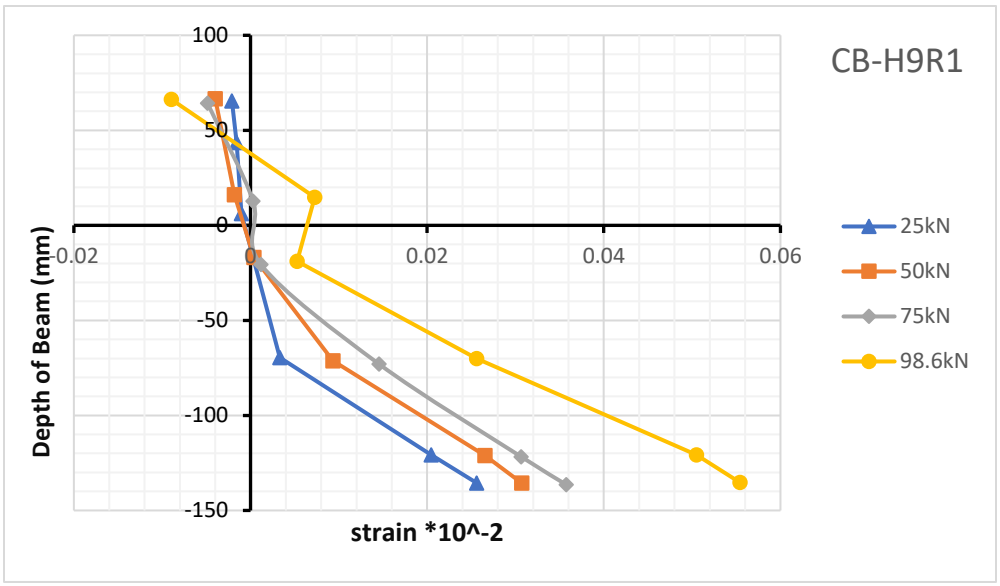

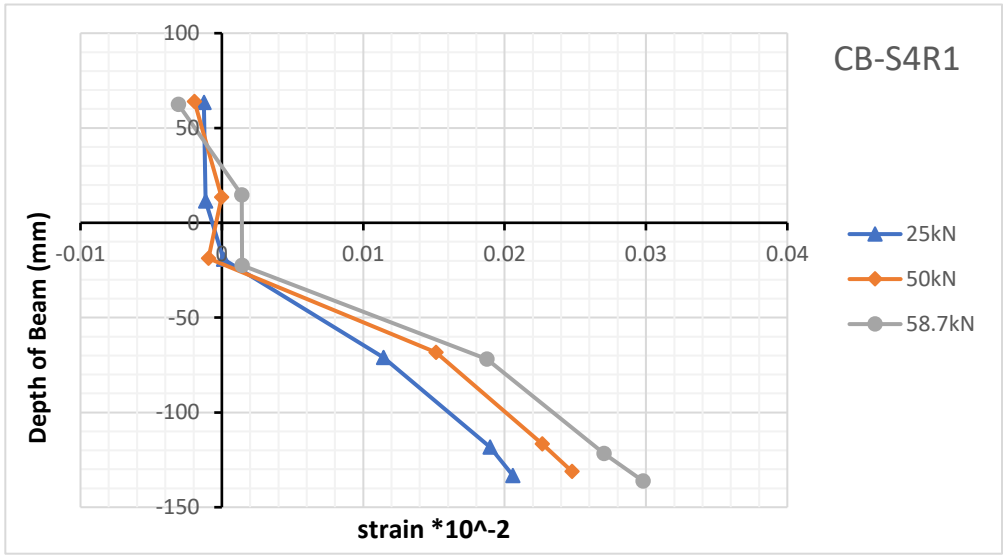

Figure 4-32: Strain Distribution at Mid-Span of Beam.

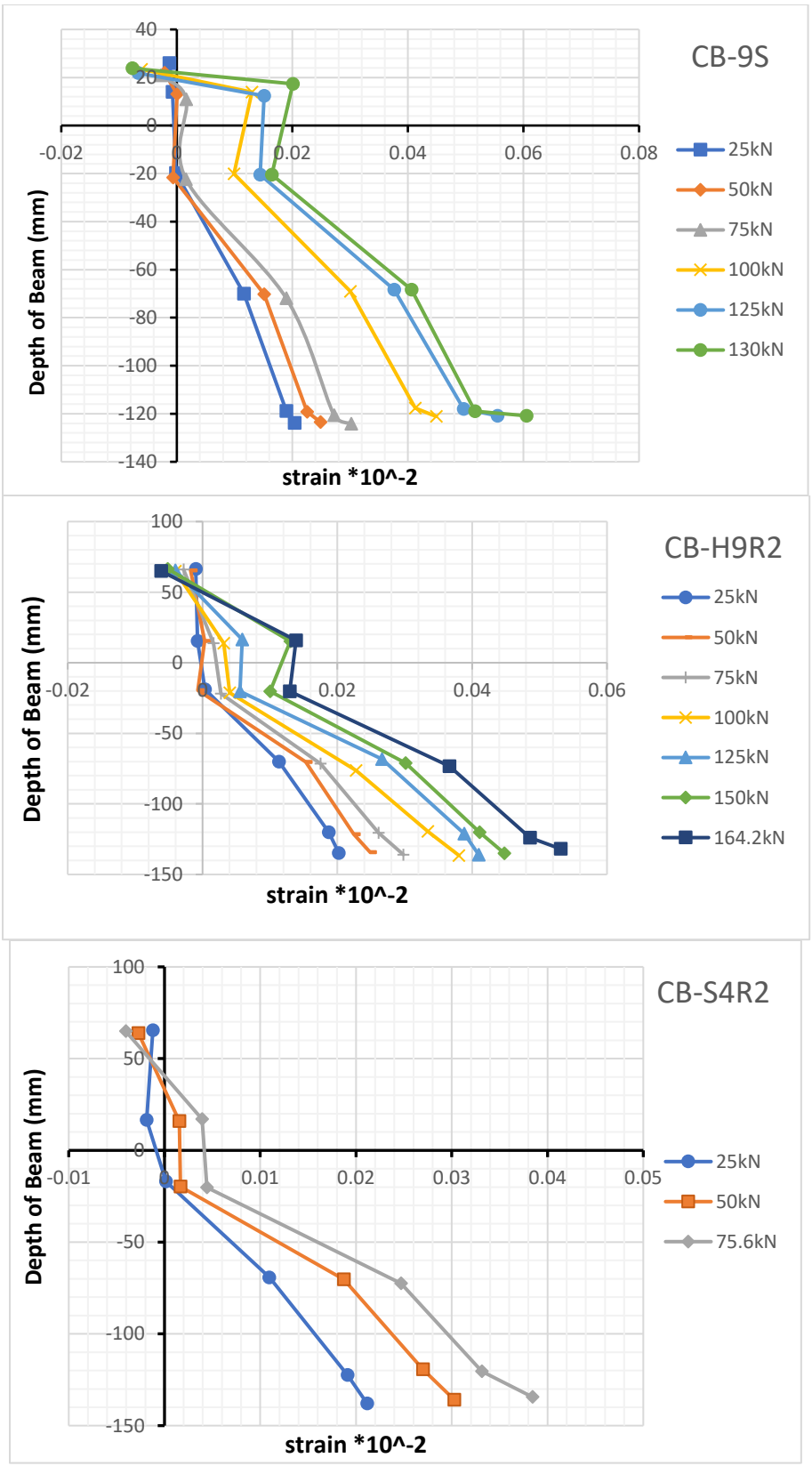

Figure 4-33: Strain Distribution at Mid-Span of Beam.

4.7 Summary of Experimental Results

The experimental results of the study offer crucial insights into the performance of composite castellated beams under diverse loading conditions and design parameters:

1. Load-Deflection Behavior: Different beam configurations exhibited varying load-deflection characteristics, highlighting responses to applied loads.
2. Shear Connector Influence: Models with more shear connectors showed enhanced load-carrying capacity and deflection behavior, underscoring their importance in structural performance.
3. Opening Shape Effect: Hexagonal openings generally outperformed circular and square ones, impacting structural response.
4. Stiffeners and Vertical Plates: Their presence improved load-carrying capacity and structural efficiency by resisting deformation and carrying loads.
5. Shear Connector Optimization: Optimizing shear connector number and distribution is crucial, especially under repeated load conditions.
6. Slip Characteristics: Slip, representing relative displacement between concrete slab and steel beam, significantly affects flexural stiffness and structural evaluation. In conclusion, these results reveal the intricate influence of design parameters on composite castellated beam performance, offering valuable guidance for their practical design and evaluation to optimize structural efficiency under various loading scenarios.

Chapter Five: Finite Elements Analysis

Chapter Five: Finite Elements Analysis

5.1 Introduction

This chapter compares three-dimensional nonlinear finite element (FE) analysis results with experimental observations. The comparison aims to evaluate the suitability of element types, material properties, convergence patterns, and material parameters for representing composite castellated beam models. Parametric analysis further explores the influence of opening shape, stud shear distribution, and strengthening. The study uses ABAQUS/Explicit to develop models for composite castellated steel beams and compare their behavior with empirical findings. This validation process involves comparing experimental data with numerical analysis results, focusing on ultimate load, load-deflection relationship, and load-slip correlation.

5.2 Finite Element Modeling

The finite element modeling of the composite castellated beam used the same physical properties, loading conditions, and boundary constraints as the experimental study. The beam had the same shape and length. The modeling process consisted of eight distinct components, each contributing to representing the fifteen composite castellated beams. These components encompassed the steel beam, concrete slab, headed stud, longitudinal rebar, transverse rebar, top-bearing plate, bottom-support plate, and vertical stiffener plates. Each component was meticulously delineated individually and subsequently integrated to construct the comprehensive specimen model.

5.2.1 Geometry

The study analyzes fifteen composite castellated beams with two-point loads using 3D nonlinear finite element analysis. The beams have similar span details and concrete slab dimensions. The steel beams are affixed to the

concrete slab using the stud technique. The composite member consists of a steel castellated beam and reinforced concrete slab connected by 9 or 4 shear connectors.

Table 5-1: Finite Element Types for Composite Castellated Beam Model

No	Part	Types of Elements
1	Steel Beam	C3D8R: An 8-node linear brick, reduced integration.
2	Concrete Slab	C3D8R: An 8-node linear brick, reduced integration.
3	Headed Stud	C3D8R: An 8-node linear brick, reduced integration.
4	Rebar Longitudinal	T3D2: A 2-node linear 3-D truss.
5	Rebar Transverse	T3D2: A 2-node linear 3-D truss.
6	Top-Bearing plate	R3D4: A 4-node 3-D bilinear rigid quadrilateral.
7	Bottom-Support plate	R3D4: A 4-node 3-D bilinear rigid quadrilateral.
8	Vertical stiffener plate	C3D8R: An 8-node linear brick, reduced integration.

During the process of finite element analysis, all beams that were subjected to experimental testing were characterized by having identical diameters. The finite element mesh depicted in Figure 5-1 was employed to simulate the behavior of the composite castellated beam CB-H9R2.

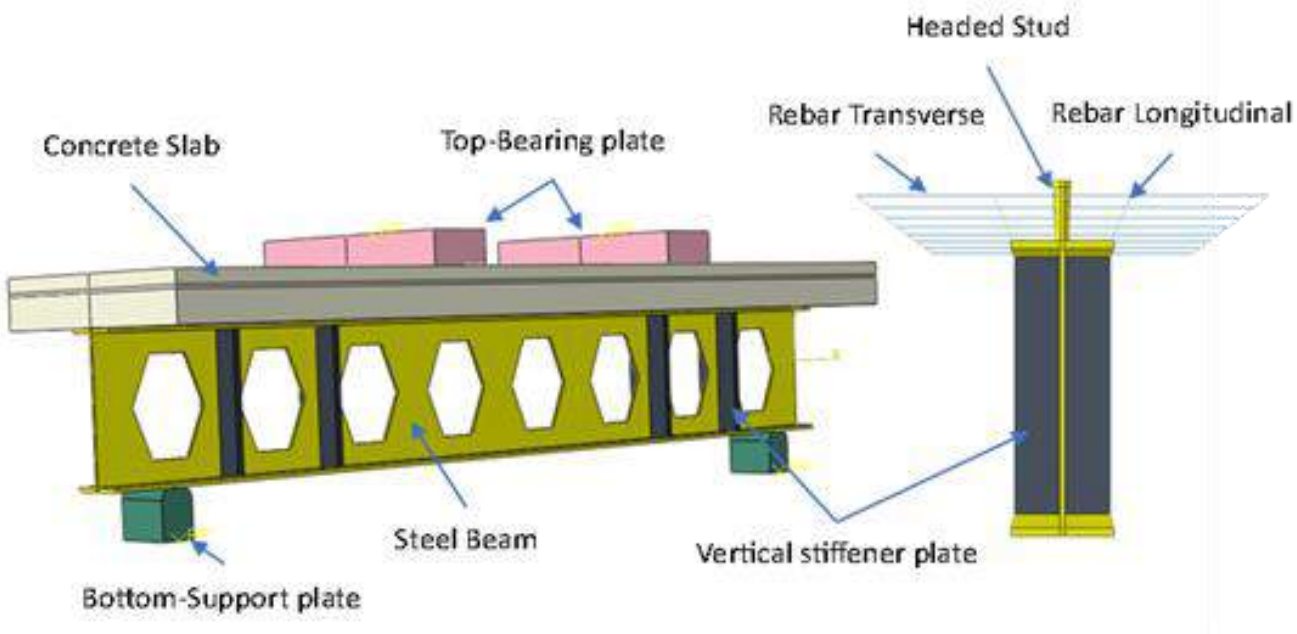

Figure 5-1: Geometry of the Numerical Model.

5.2.2 Convergence Study

Selecting a suitable mesh size is of utmost importance in finite element modeling. A thorough initial analysis was conducted, considering several mesh densities, to determine the ideal density that could achieve the needed level of accuracy. The achievement of successful convergence of outcomes occurs when the beam is appropriately divided into a sufficient number of distinct elements. This phenomenon becomes apparent in cases where reducing the mesh size has only a modest impact on the ensuing data. To achieve this objective, a convergence analysis was undertaken as an essential element of the ongoing finite element analysis (FEA) to determine the most suitable mesh size. The present investigation entailed deliberately choosing discrete element dimensions for the CB-9S model, namely 45, 35, 25, and 15 mm, as visually illustrated in Figure 5.4.

Moreover, a noticeable improvement in the precision of deflection measurements may be shown when comparing the obtained values with the experimental data for the control beam, as presented in Table 5-2. As a result, a mesh size of 25 mm was chosen for all the beams that underwent testing. Figure 5.1 presents a graphical representation illustrating the fluctuations in load-mid-span deflection associated with various mesh sizes.

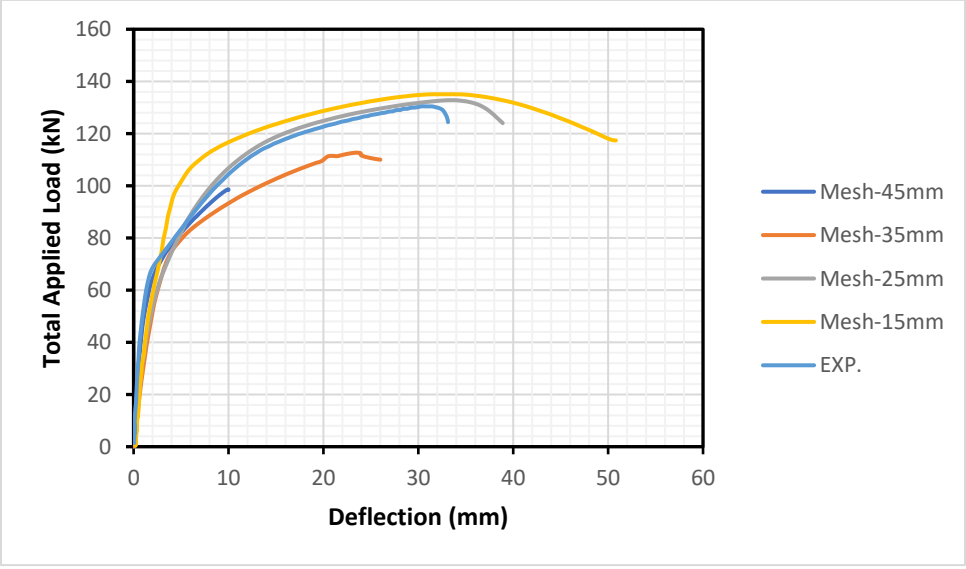

Figure 5-2: Mesh Size Effect on Mid-Span Load-Deflection Curve.

Table 5-2: Effect of Mesh Size on Ultimate Load And Deflection.

Mesh Size (mm)	Name	Ultimate load (kN)	Maximum Deflection (mm)
15	EXP.	130.4	33.1
	FEA.	135.1	50.81
25	EXP.	130.4	33.1
	FEA.	132.8	38.9
35	EXP.	130.4	33.1
	FEA.	112.7	26
45	EXP.	130.4	33.1
	FEA.	98.65	10.1

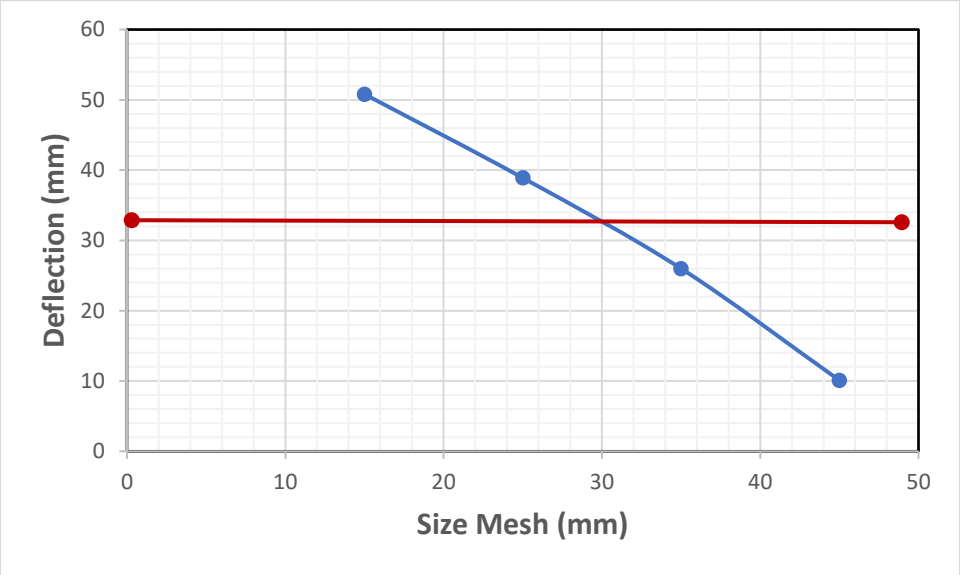

Figure 5-3: Effect of Mesh Size on Ultimate Load and Deflection.

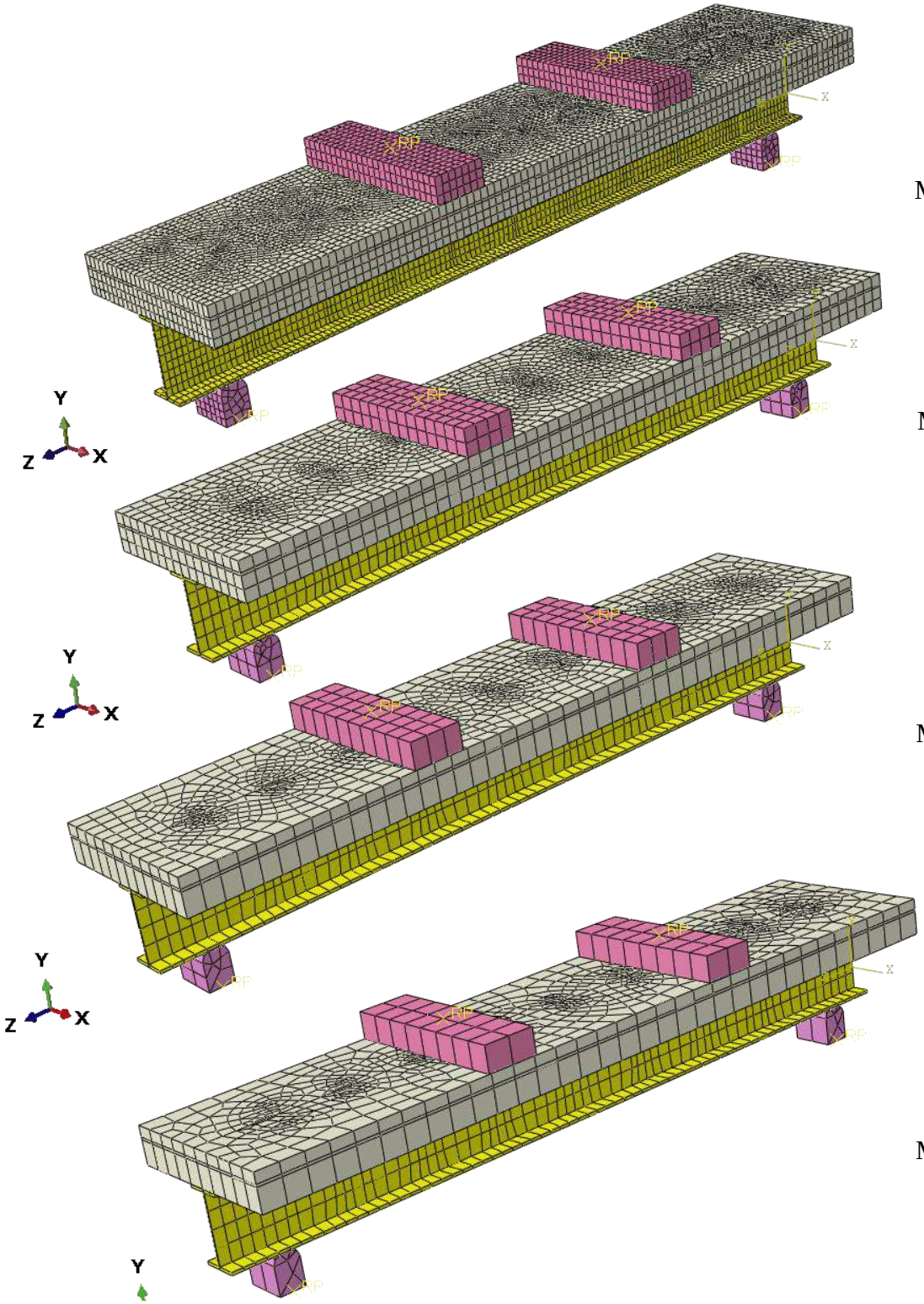

Figure 5-4: Finite Element Mesh Density.

5.2.3 Interaction

Following the assembly process, several components are brought together, such as the concrete slab, steel beam, steel reinforcement, shear connectors, and steel bearing plates. Establishing their relationships is facilitated by utilizing several constraint types aligned with experimental observations to construct a cohesive composite system.

Table 5-3: Finite Element Interactions for Composite Castellated Beam Model.

No	Part	Type of interaction	Master	Slave
1	Steel Beam and Concrete Slab	Surface to surface	Steel	Concrete
2	Concrete Slab and rebar	Embedded region	Rebar	Concrete
3	Headed Stud and Steel Beam	Tie	Steel	Stud
4	Steel Beam and Bottom-Support plate	Surface to surface	Support	Steel
5	Concrete Slab and Headed Stud	Tie	Stud	Concrete
6	Top-bearing plate and Concrete Slab	Surface to surface	Plate	Concrete
7	Vertical stiffener plate and steel beam	Tie	Stiffener	Steel

The composite castellated beam system uses surface-to-surface connections between the steel beam and concrete slab, accurately capturing interfacial behavior and load transfer dynamics. The interaction between the concrete slab and longitudinal and transverse rebar components uses an embedded region approach, allowing for detailed representation of interlocking behavior and load transfer mechanisms. The interaction between shear connectors and the steel beam's top flange is characterized by a "tie" interaction, emulating a mechanical bond for precise load transfer and structural behavior. The interaction between the steel beam's bottom flange and the bottom support plate is achieved through a "surface-to-surface" connection, effectively transmitting forces and displacements. The interaction between the concrete slab and headed stud is represented using a "tie" interaction, capturing cohesive behavior within the composite castellated beam structure. Mechanical constraints formulations, including the "penalty contact method" and "finite sliding" formulation, accommodate unrestricted motion between the steel sheet and concrete surfaces following slip failure.

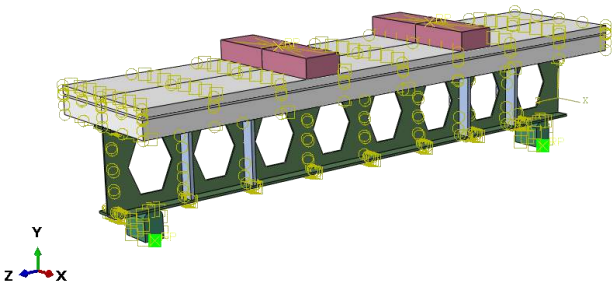

Figure 5-5: Interactions for Composite Castellated Beam Model.

5.2.4 Loading and Boundary Conditions

The loads were applied to each tested beam at two points in the experimental work. Two steel plates have performed these loads with dimensions of 100×50×350 mm located at the top face to transform the loads into the tested beam. Displacements at the boundaries were used to constrain all reinforced concrete specimens' models to get the appropriate solution. All models were constrained in the z-direction and y-direction (Uz=Uy=Ux=0) at the hinge support while constrained in the y-direction and x-direction (Uy=Ux=0) at the roller support, as illustrated in Figures 5-7.

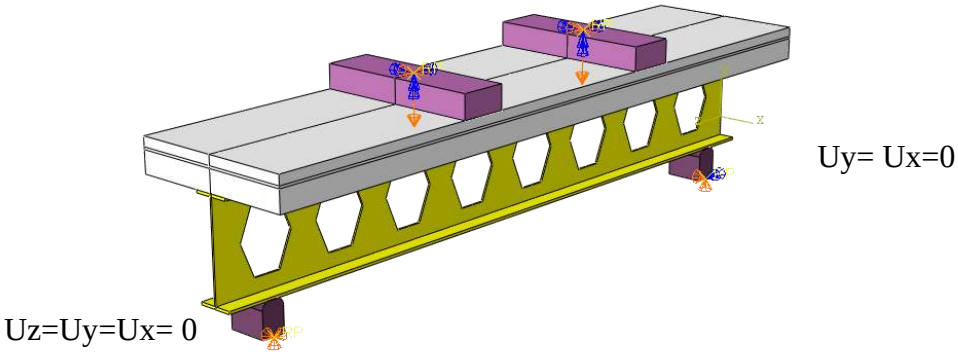

Figure 5-7: Boundary Conditions That Used in Test of Models.

5.3 Numerical Results

This study compared the ultimate load values and deflections found through finite-element analysis to those found through experimental tests. This comparative analysis was executed to validate the accuracy of the numerical model.

Table 5-4: Comparison of the Ultimate Load and Ultimate Deflection for Composite Castellated Beams.

Sample	Ultimate load Pu (kN)			Ultimate deflection (mm)		
	Exp.	Num.	Num. / Exp.	Exp.	Num.	Num. / Exp.
CB-9S	130.4	140.8	1.08	33.13	29.9	0.90
CB-H4S	101.3	104	1.03	32.9	31.45	0.96
CB-S9S	92.5	100.9	1.09	14.6	15.5	1.06
CB-H9R1	98.6	99.7	1.01	24.9	25	1.00
CB-C9R1	80.6	80.7	1.00	24	25	1.04
CB-S9R1	67.34	70.95	1.05	16.9	15	0.89
CB-H4R1	89	96.2	1.08	26.8	24.2	0.90
CB-C4R1	69.4	79.1	1.14	29.2	20	0.68
CB-S4R1	58.7	61.3	1.04	16.1	15	0.93
CB-H9R2	164.2	172.2	1.05	47.44	45.8	0.97
CB-C9R2	121.3	132.8	1.09	38.6	35	0.91
CB-S9R2	109.4	110.4	1.01	25.3	25	0.99
CB-H4R2	138.6	146.8	1.06	28.2	29.8	1.06
CB-C4R2	102.4	108.2	1.06	49.1	47.12	0.96
CB-S4R2	69.2	75.6	1.09	14.6	15.5	1.06

5.4 Comparison Between Experimental and Finite Element Results

The finite element analysis results from ABAQUS software were compared with experimental beams' ultimate load, ultimate deflection, load-deflection curve, and failure pattern for various samples.

5.4.1 Group one

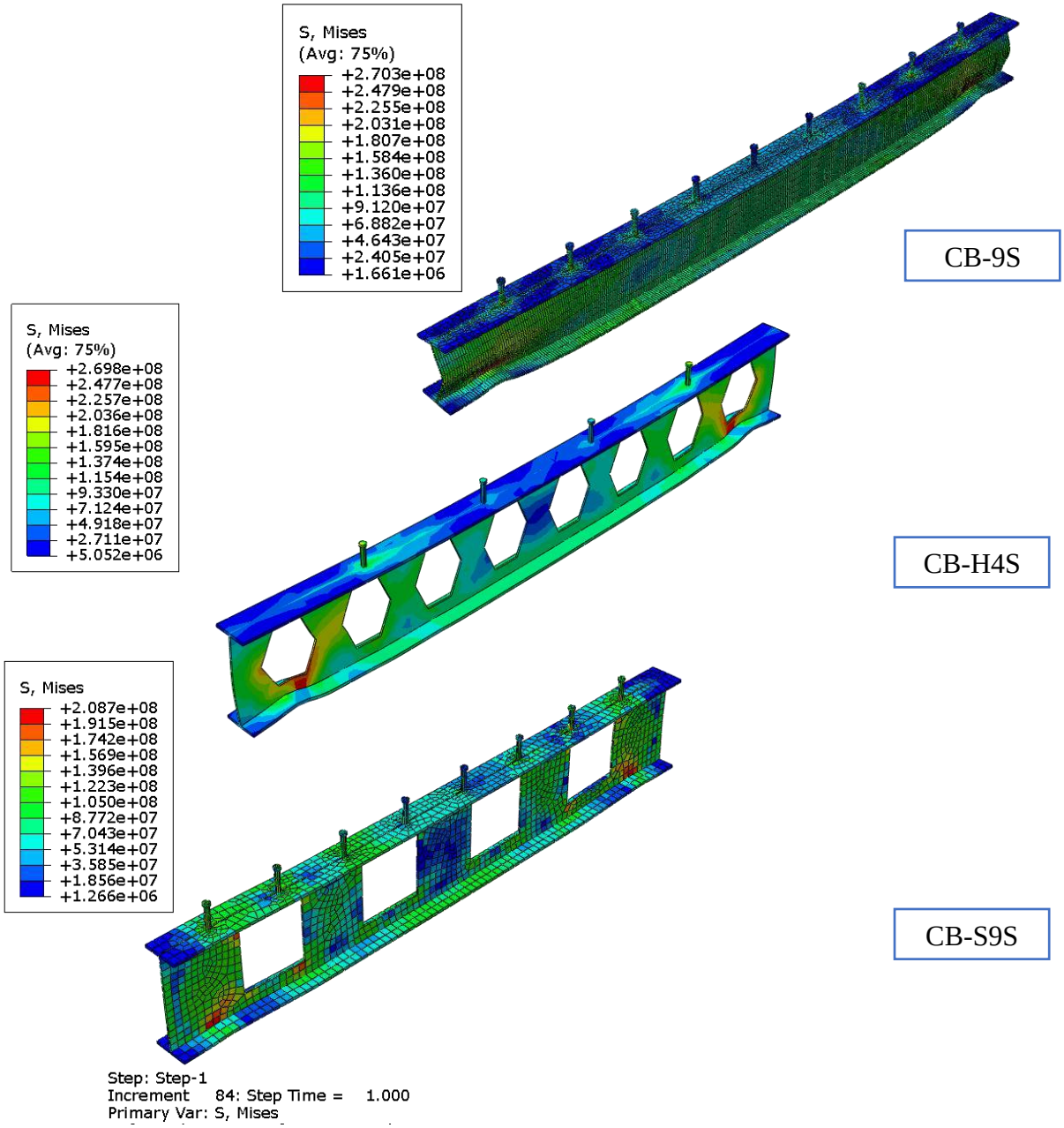

Figure 5-8 : Distribution of von Mises Stresses for Group one.

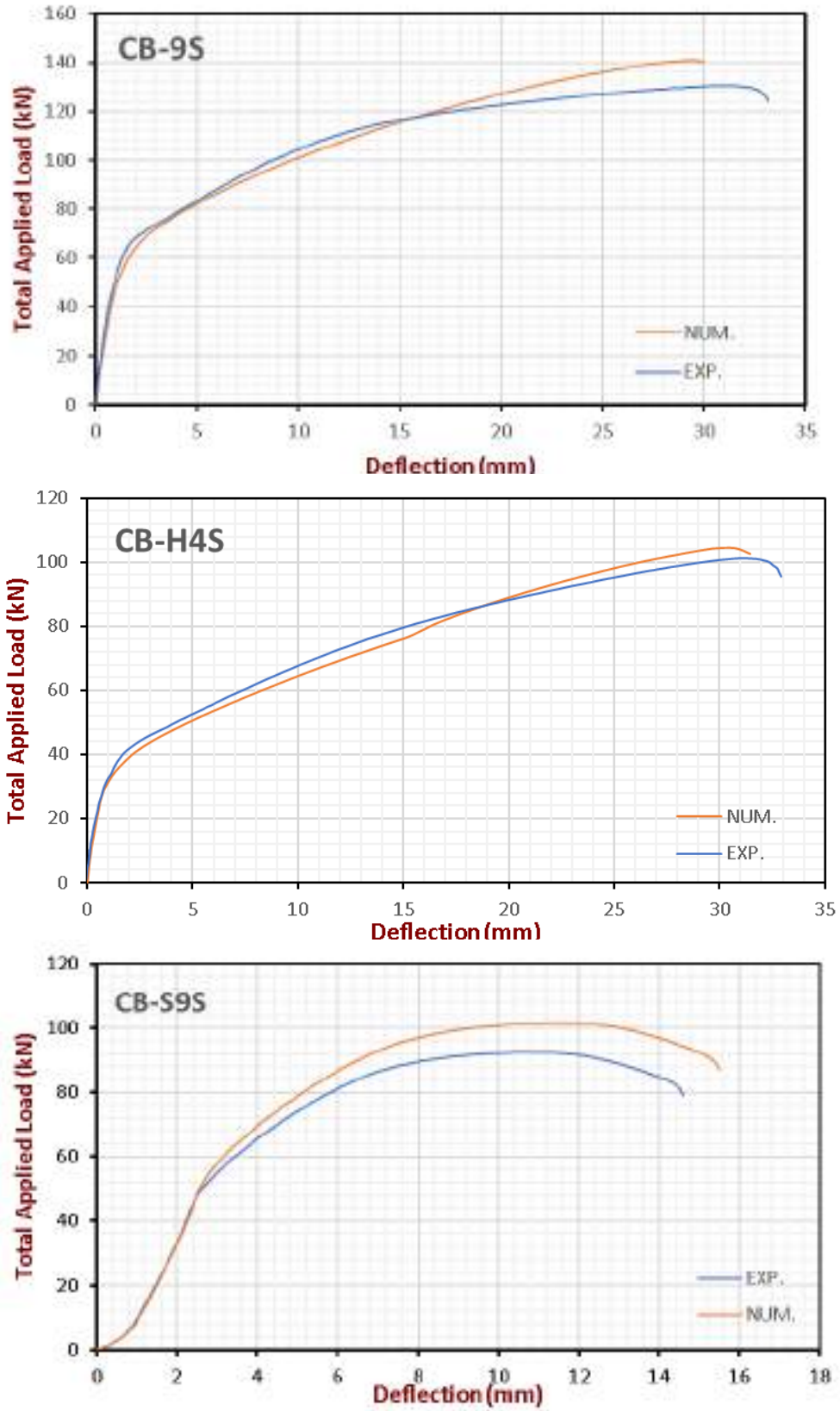

Figure 5-9 : Comparison between Experimental and Numerical Load-Deflection Curve for Group one

5.4.2 Group Two

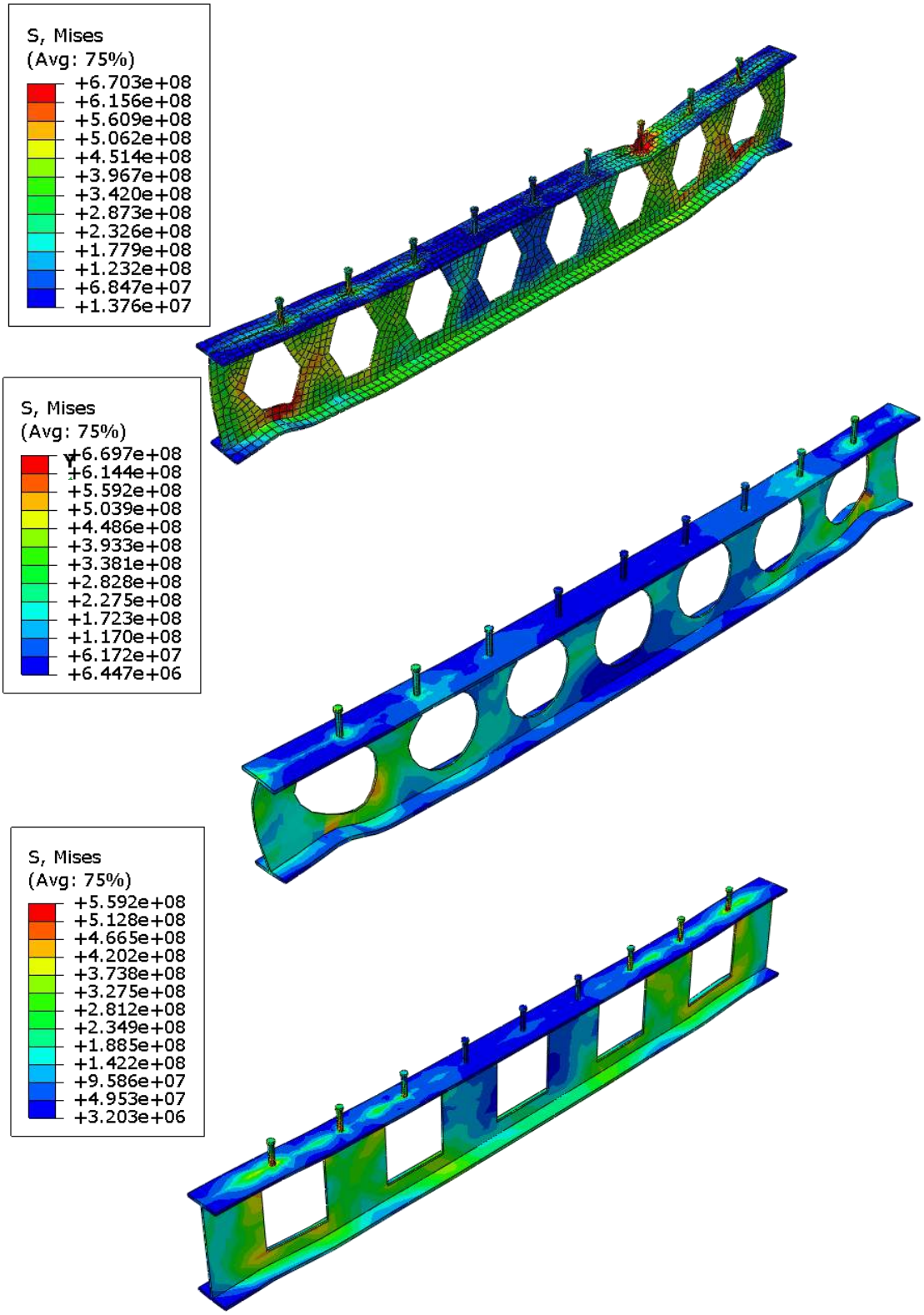

Figure 5-10: Distribution of von Mises Stresses for Group Two.

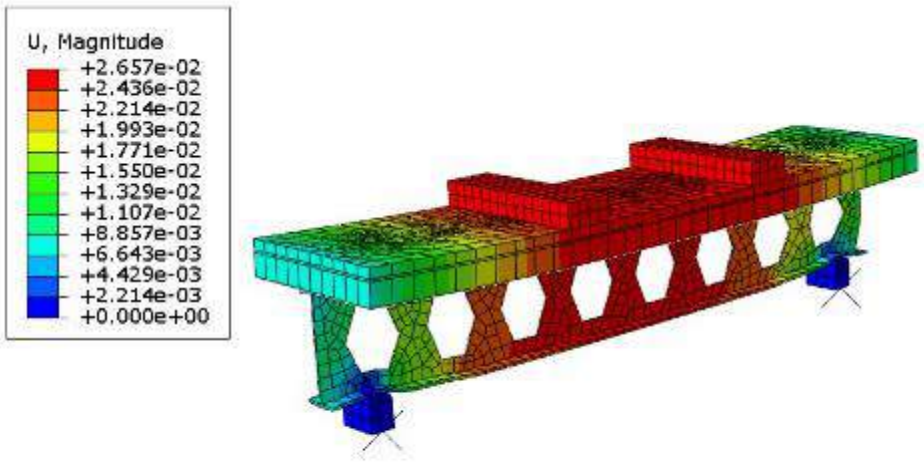

Figure 5-11: Deflection Shape of model CB-H9R1.

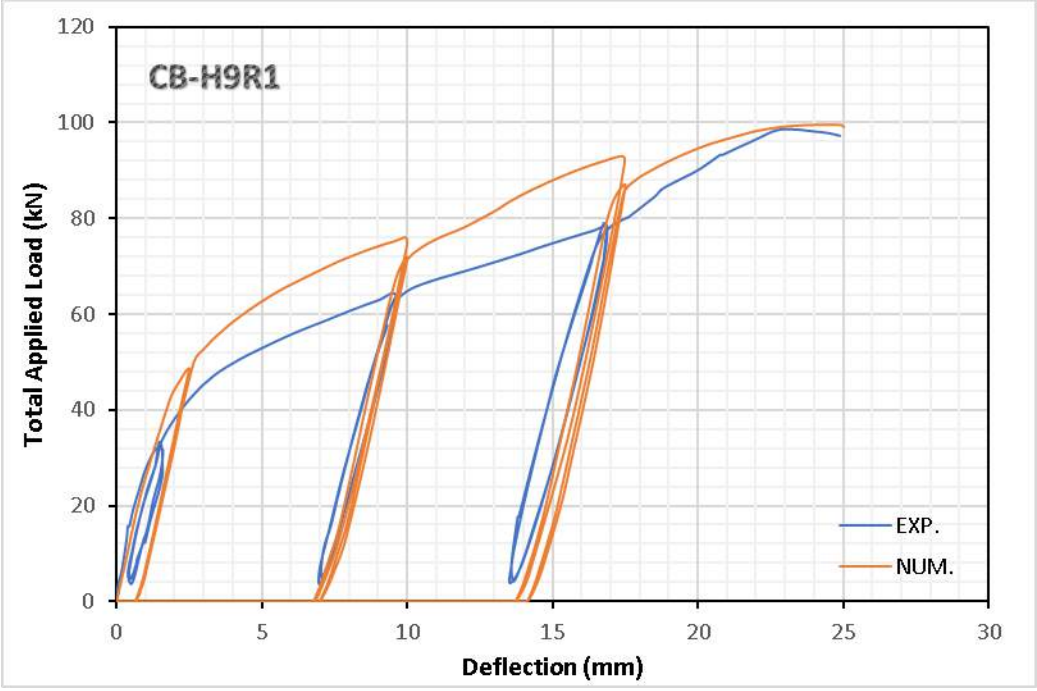

Figure 5-12: Comparison between Experimental and Numerical Load-Deflection Curve for (CB-H9R1) Specimen

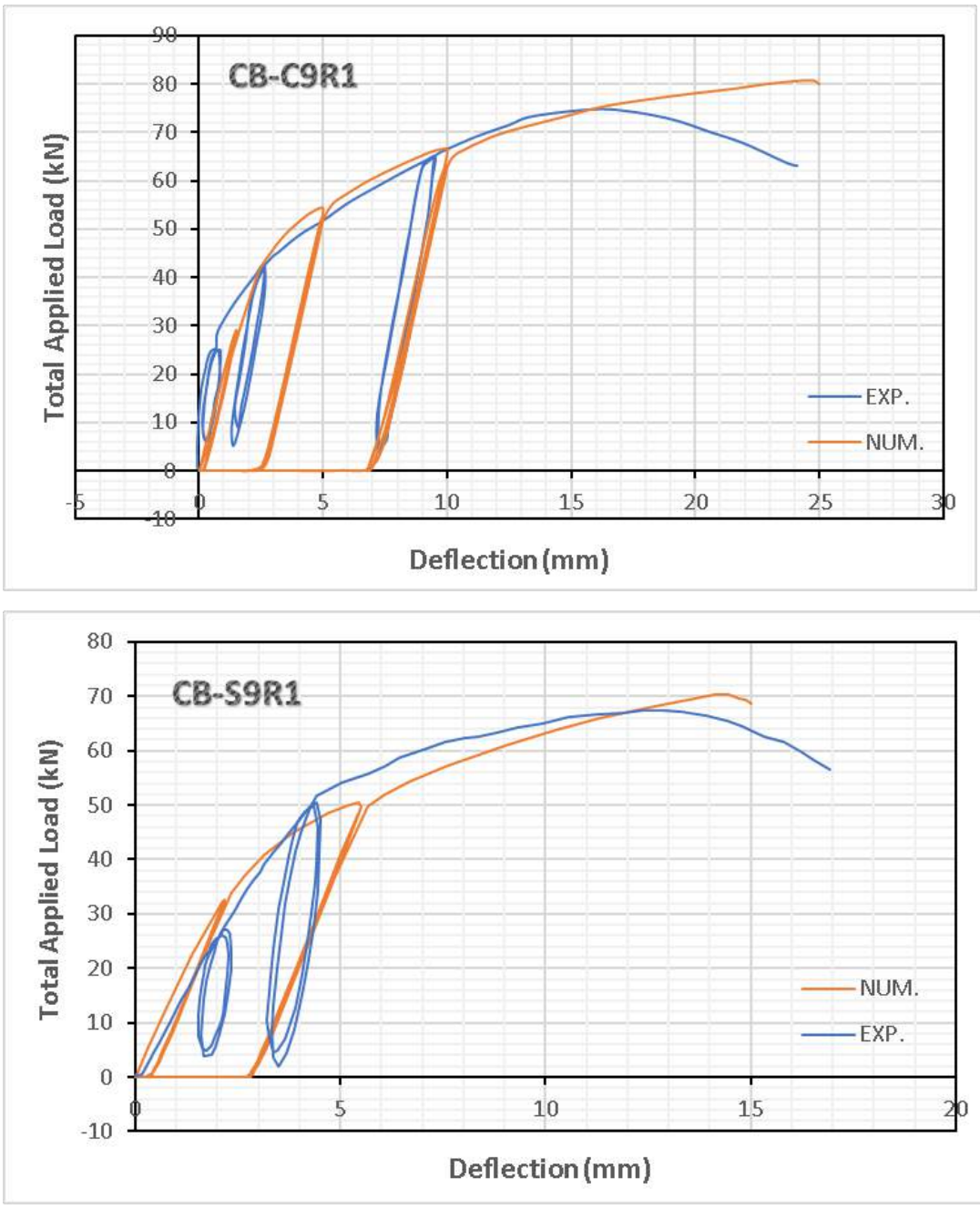

Figure 5-13: Comparison between Experimental and Numerical Load-Deflection Curve for (CB-S9R1) Specimen

5.4.3 Group Three

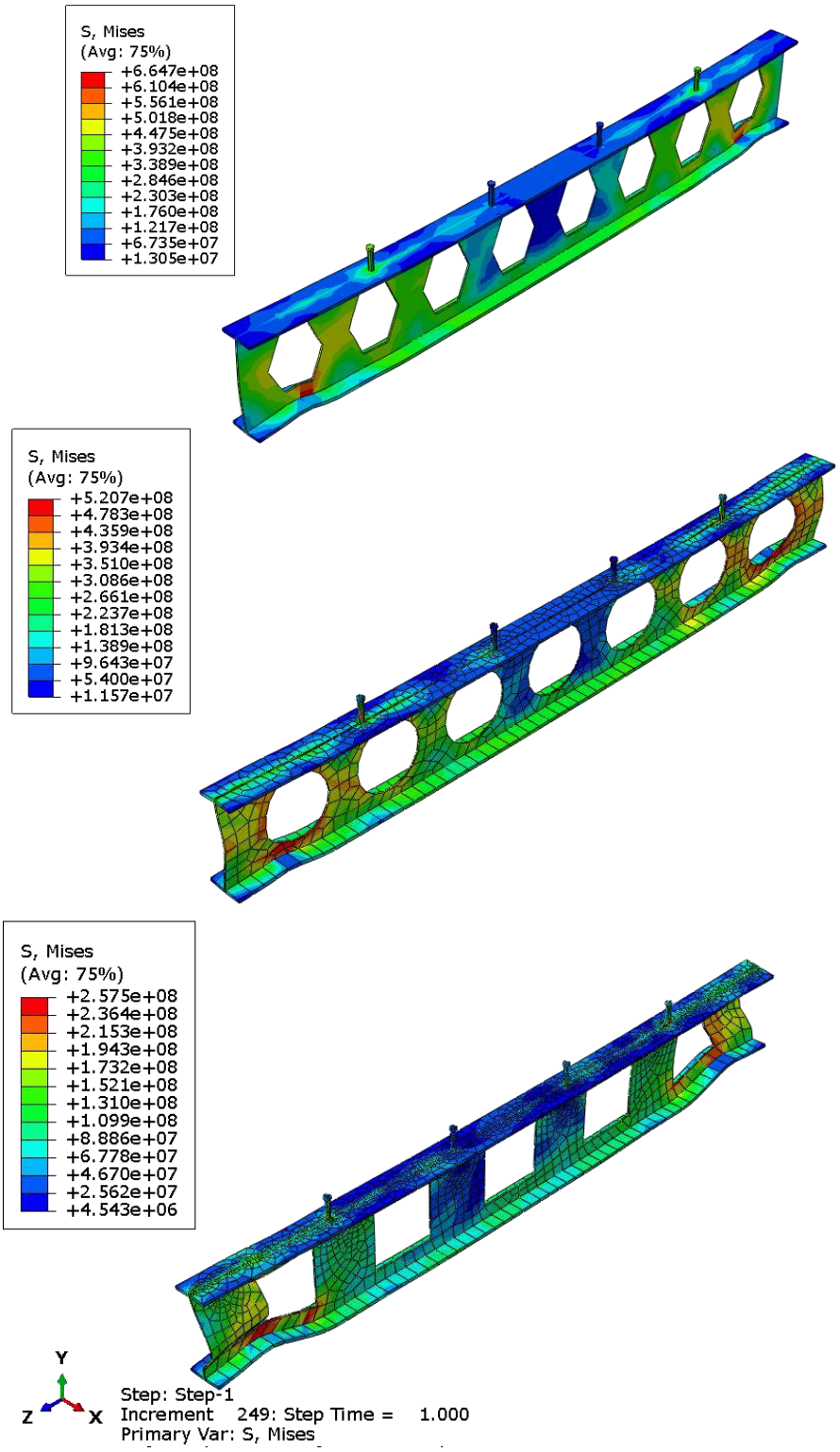

Figure 5-14: Distribution of von Mises Stresses for (CB-H4R1) Specimen

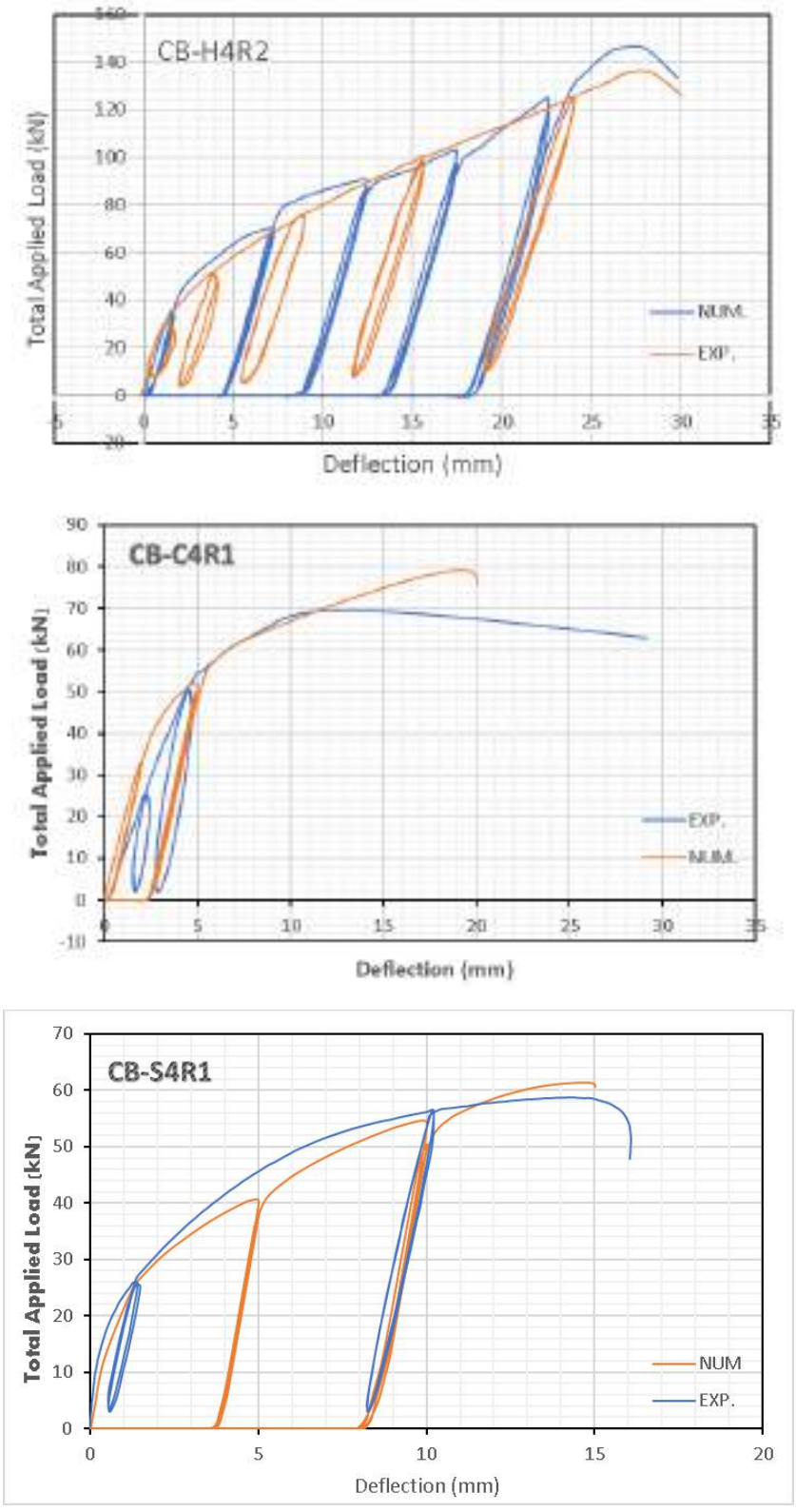

Figure 5-15: Comparison between Experimental and Numerical Load-Deflection Curve for (Group Three) .

5.4.4 Group Four

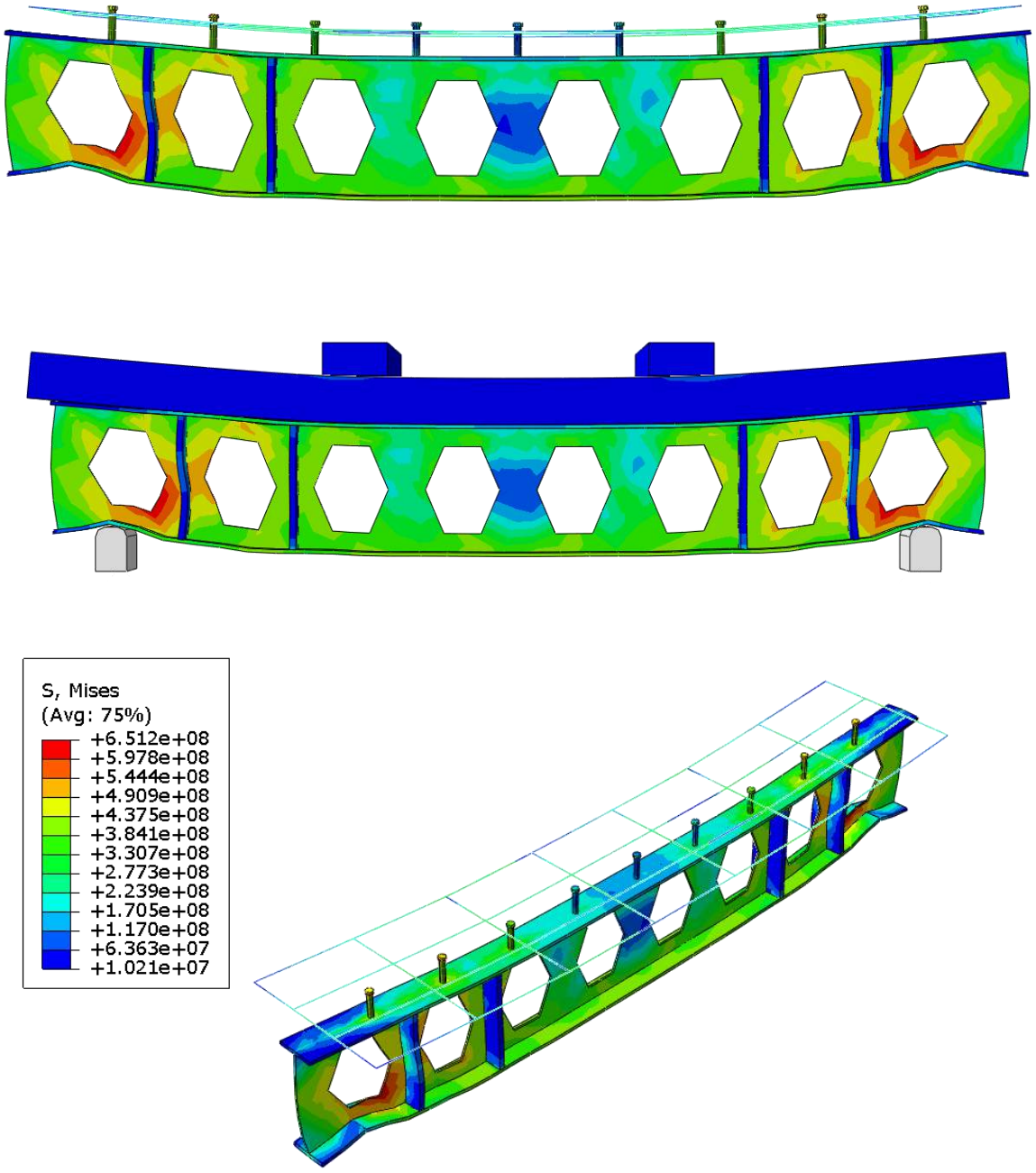

Figure 5-16: Distribution of von Mises Stresses for (CB-H9R2) Specimen

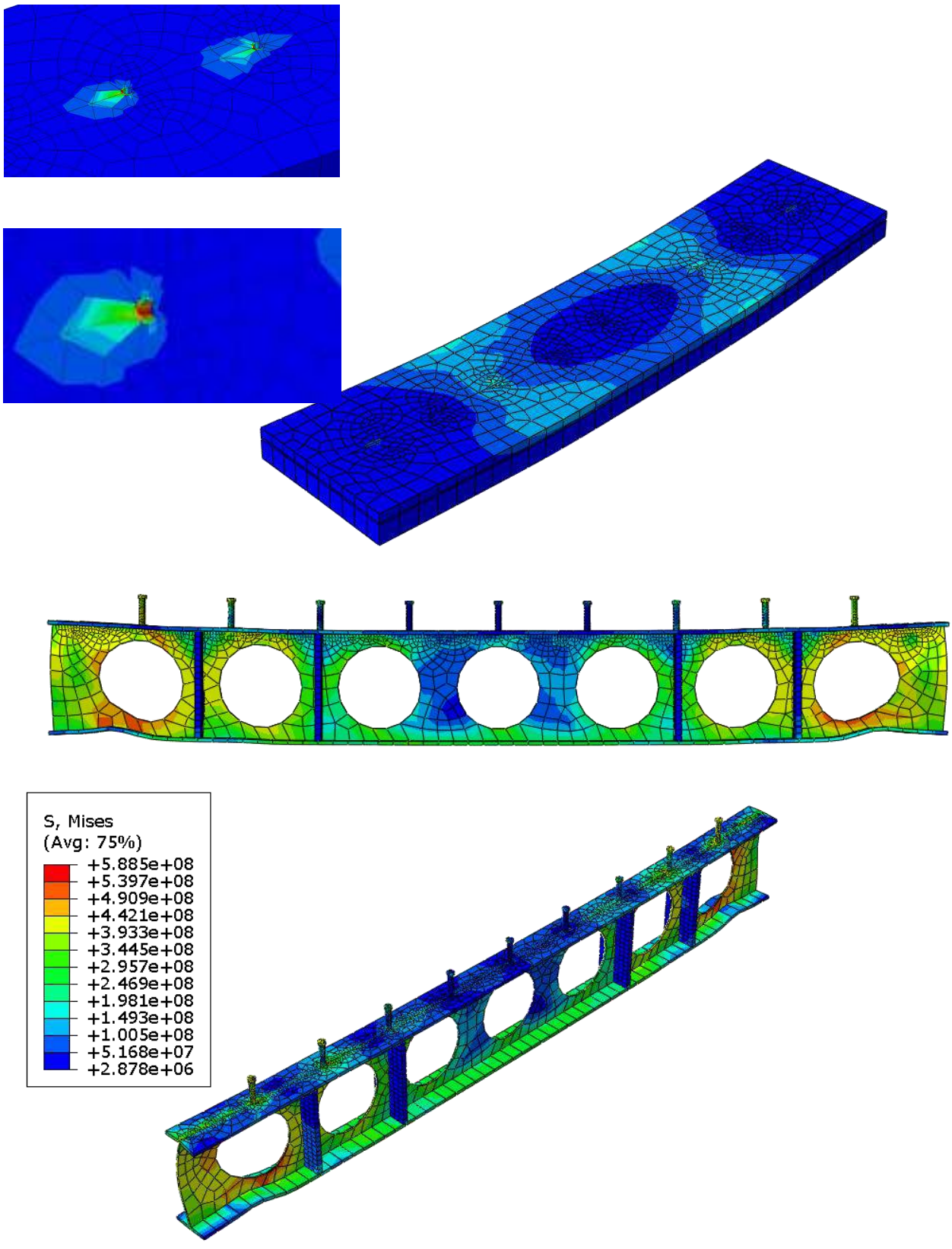

Figure 5-17: Distribution of von Mises Stresses for (CB-C9R2) Specimen.

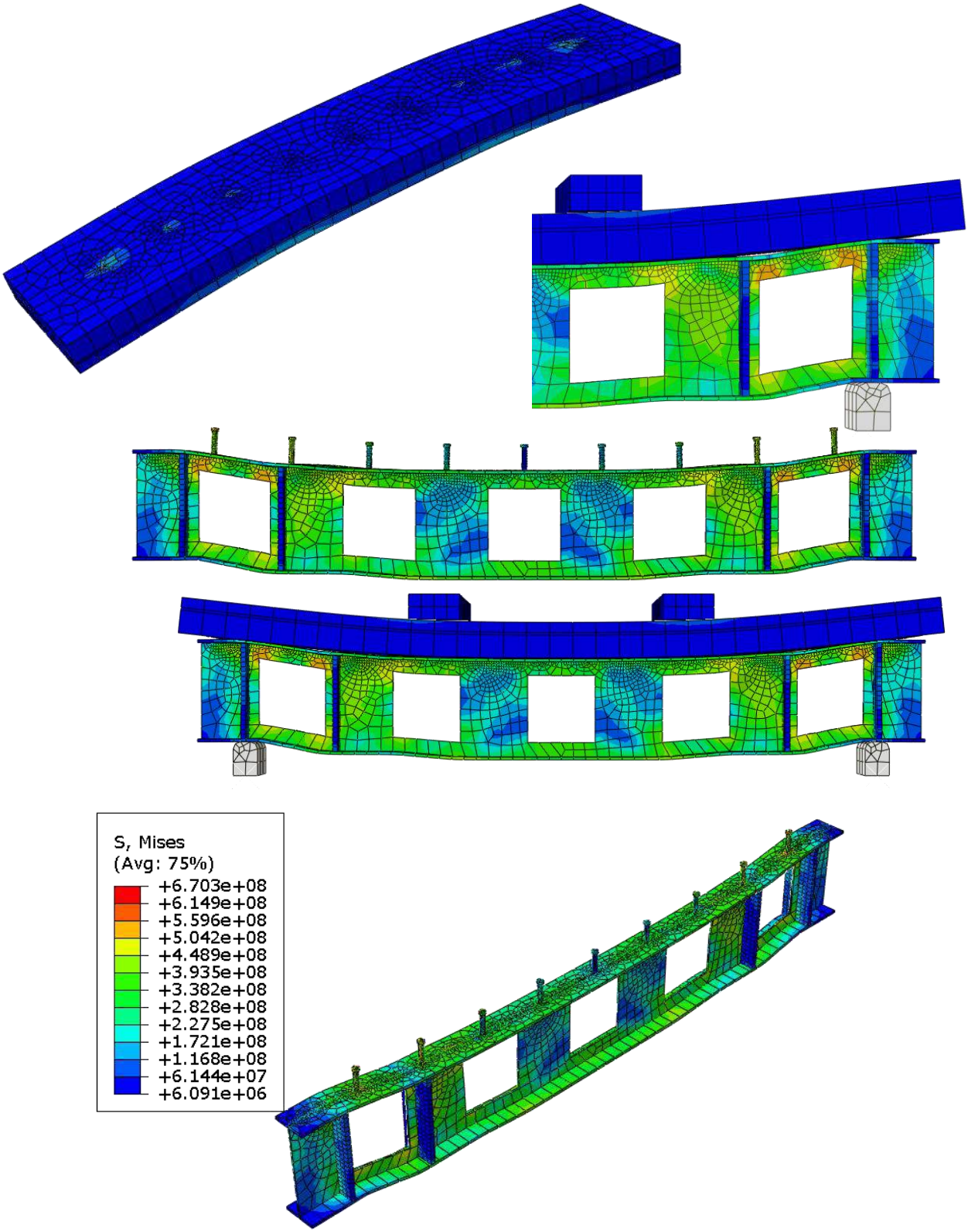

Figure 5-18: Distribution of von Mises Stresses for (CB-S9R2) Specimen.

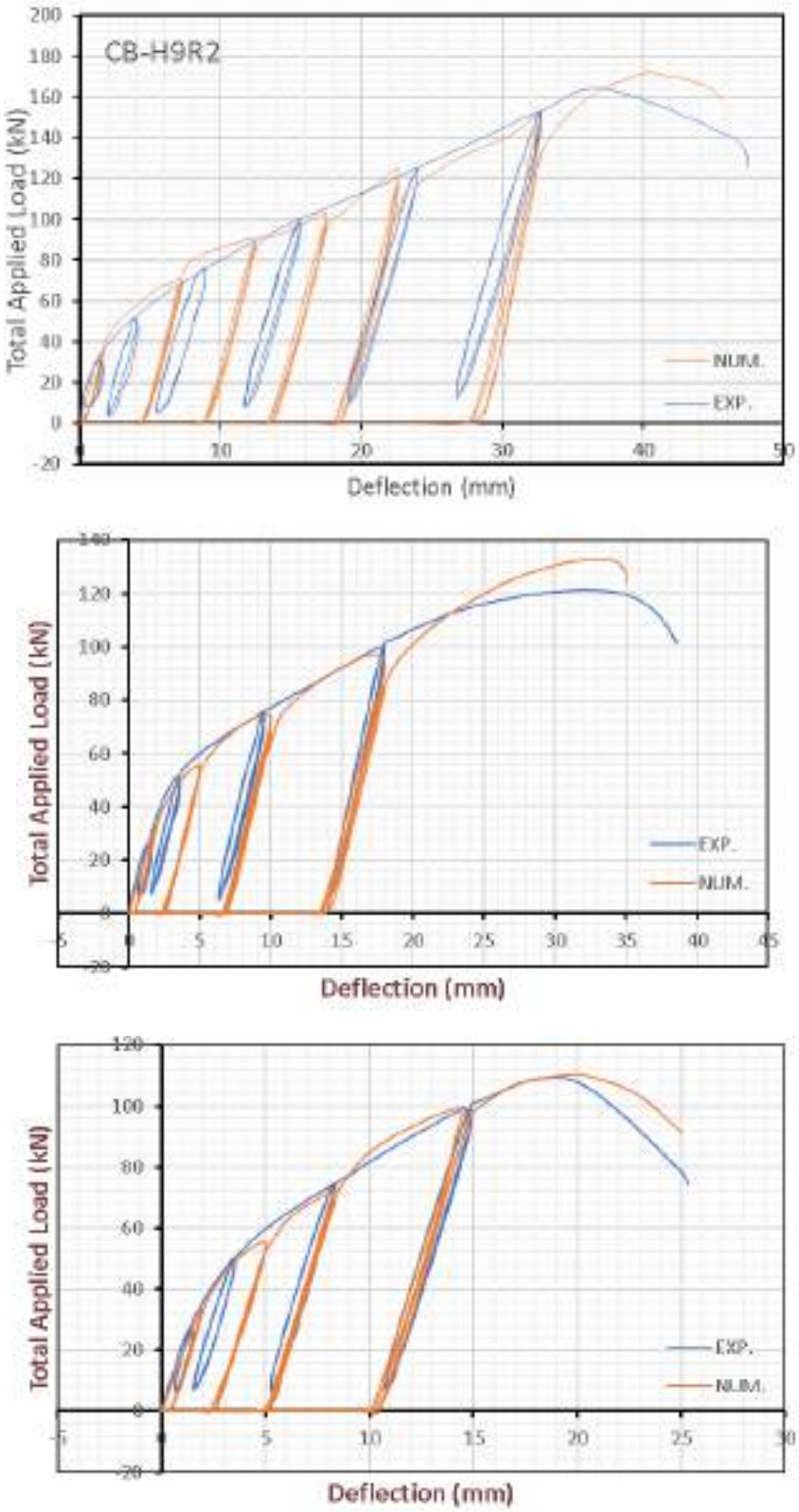

Figure 5-19: Comparison between Experimental and Numerical Load-Deflection Curve for (Group Four).

5.4.5 Group Five

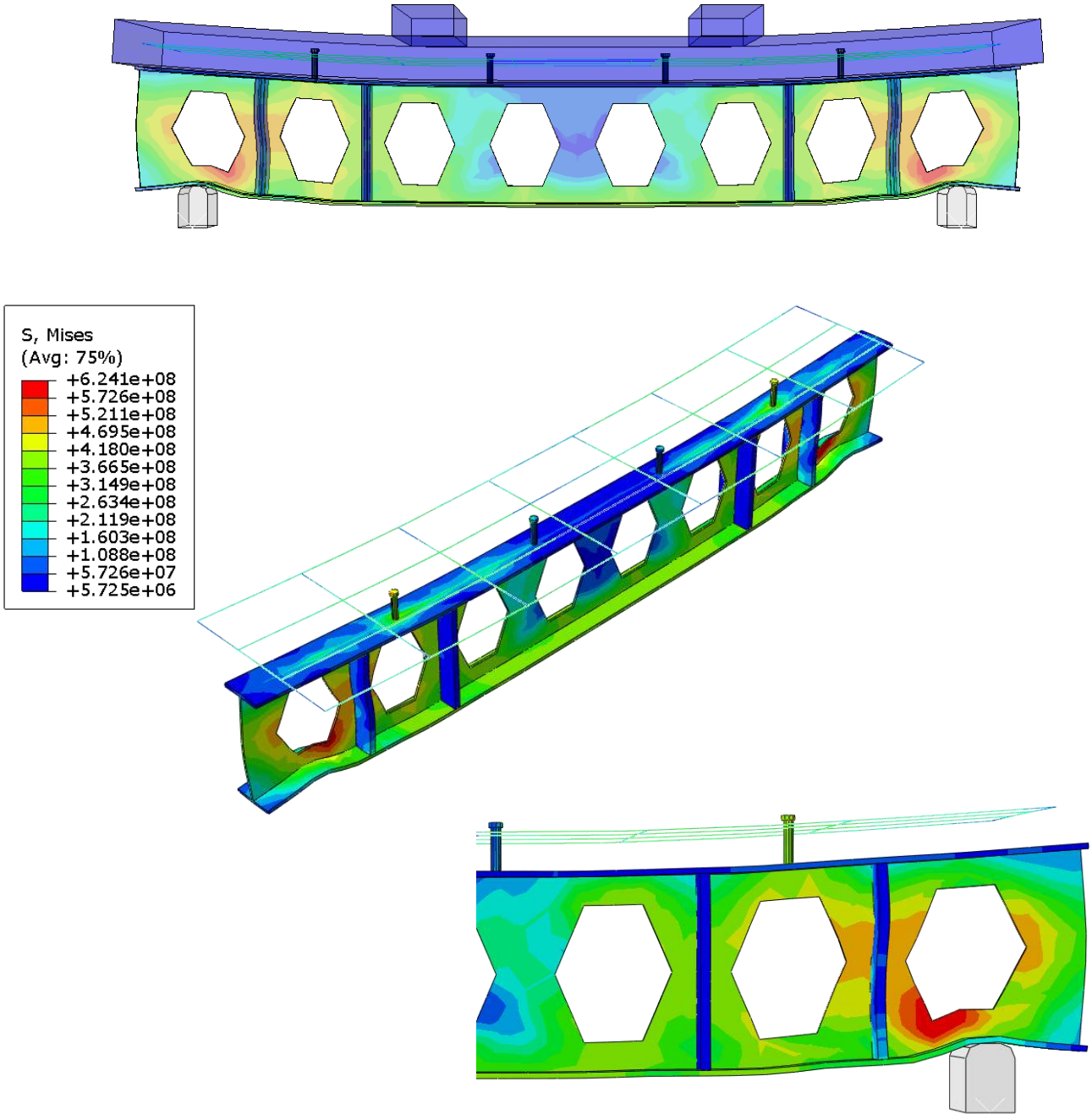

Figure 5-20: Distribution of von Mises Stresses for (CB-H4R2) Specimen

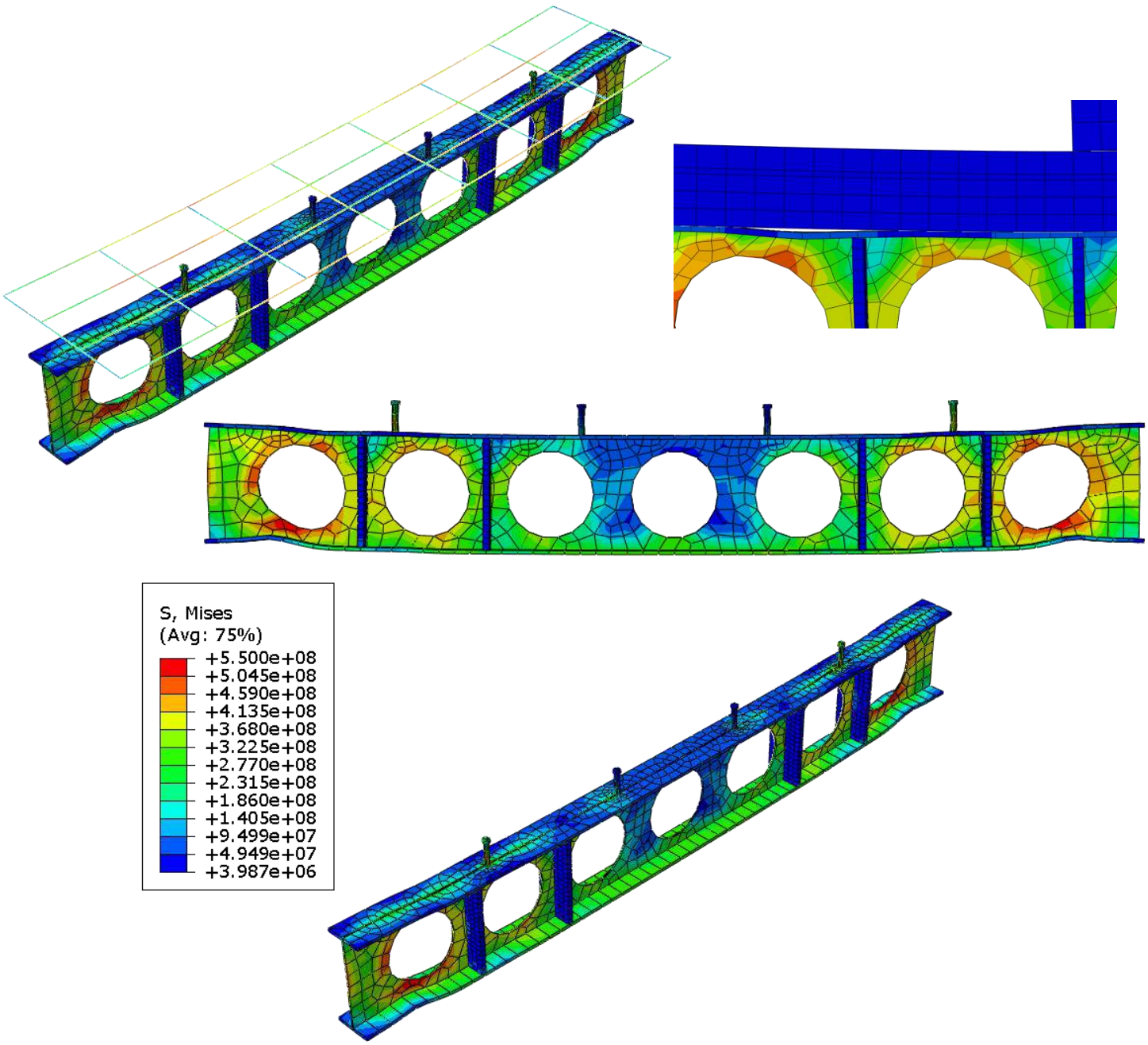

Figure 5-21: Distribution of von Mises Stresses for (CB-C4R2) Specimen.

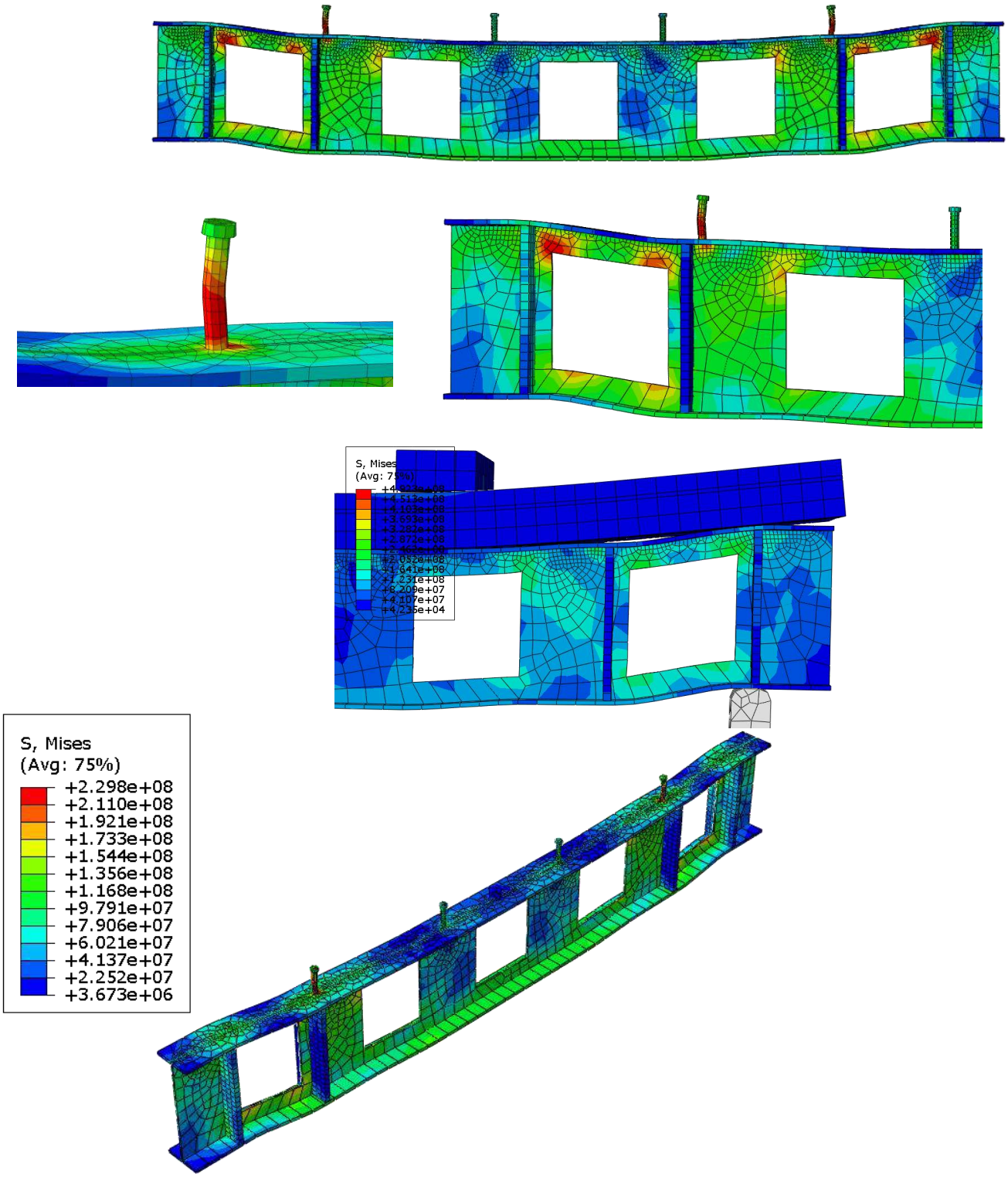

Figure 5-22: Distribution of von Mises Stresses for (CB-S4R2) Specimen.

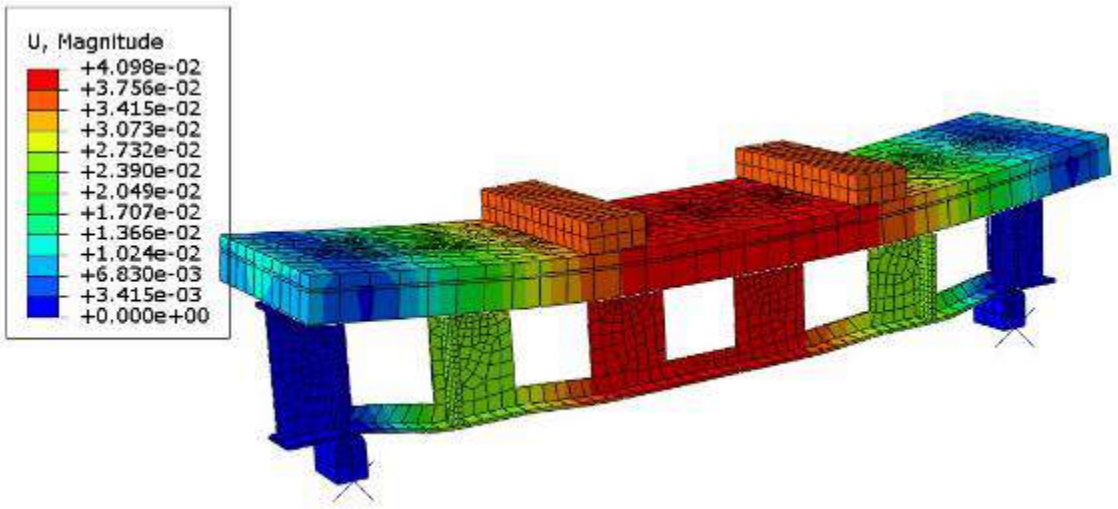

Figure 5-23:Deflection Shape of model CB-S4R2.

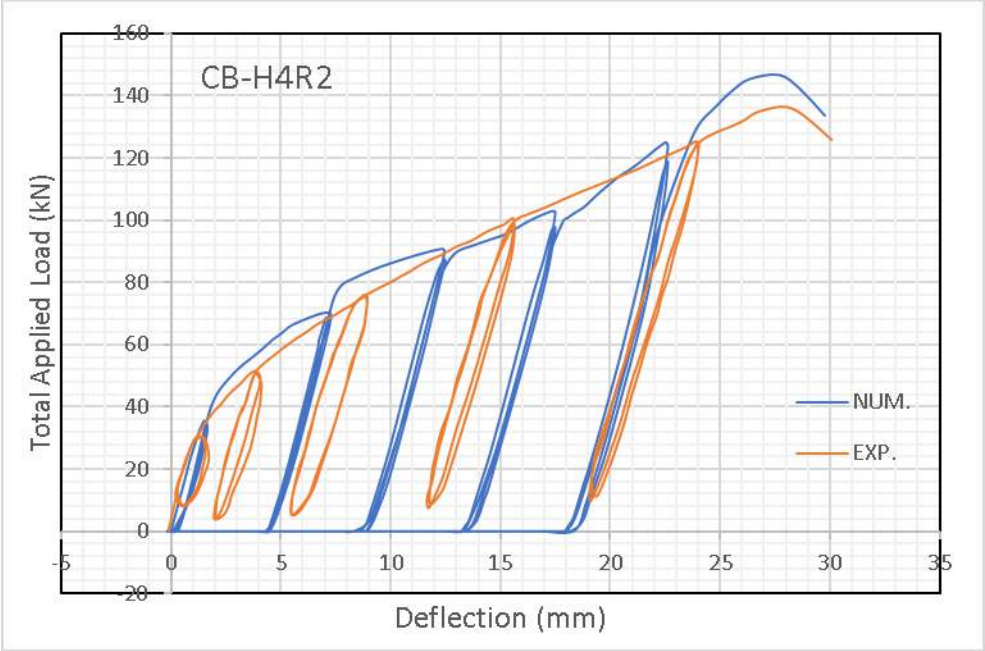

Figure 5-24: Comparison between Experimental and Numerical Load-Deflection Curve for (CB-H4R2) Specimen

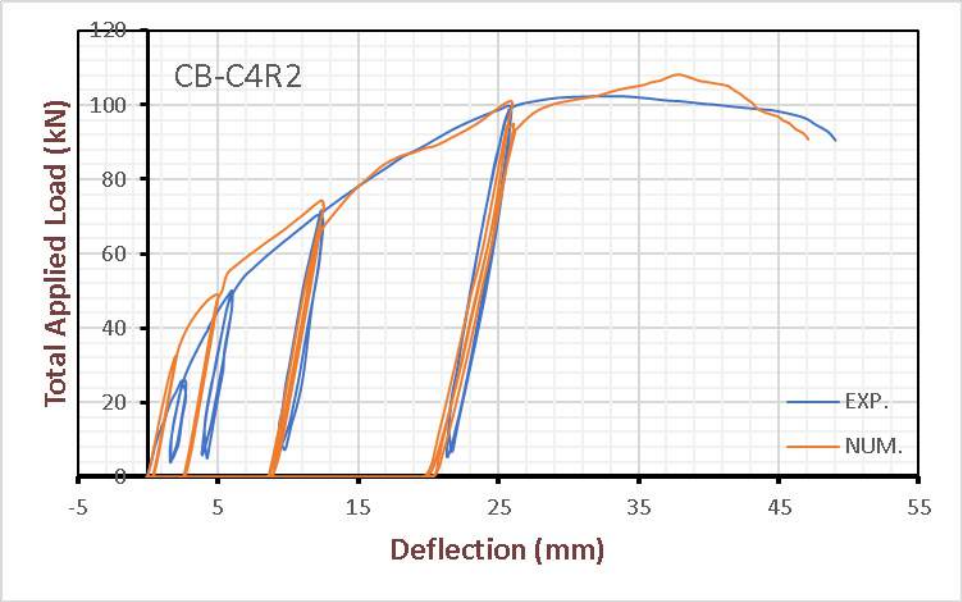

Figure 5-25: Comparison between Experimental and Numerical Load-Deflection Curve for (CB-C4R2) Specimen.

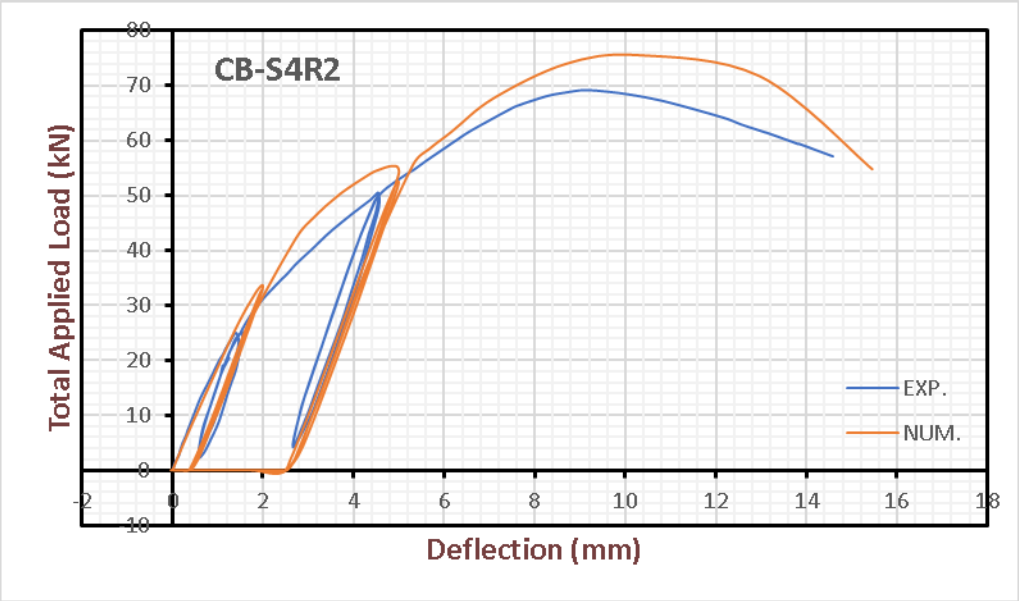

Figure 5-26: Comparison between Experimental and Numerical Load-Deflection Curve for (CB-S4R2) Specimen

5.5 Load-Slip Relationship

The numerical analysis successfully incorporates an interface model to simulate slip, which refers to the displacement between the concrete slab and steel beam. The shape of slip encountered by the finite element beam in response to the vertical load is visually presented in Figure (5-39). A total of ten composite beams were constructed by combining steel beams and concrete slabs, which were connected using shear connectors to facilitate their mutual interaction. When a load is applied to a composite beam, the bending moment generates opposing forces that result in a horizontal slide between the concrete and steel components of the composite section. The flexural rigidity of the composite section was lowered due to the horizontal movement, also known as relative slip.

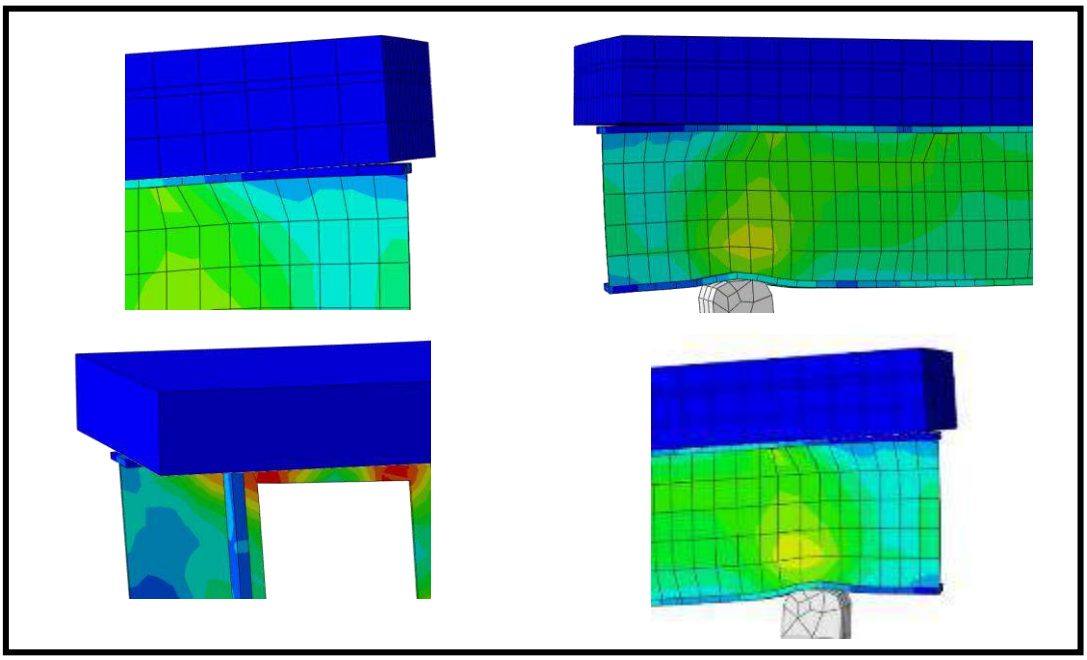

Figure 5-27: Slip Shape of The Finite Element Beam at Ultimate Load.

Table 5-5:Comparison between experimental and numerical slip at ultimate load.

BEAM	EXP. SLIP	F.E.M SLIP	F.E.M / EXP.
CB-C9R1	7.28	7.53	1.03
CB-S9R1	3.42	3.63	1.06
CB-C4R1	5.53	5.41	0.98
CB-S4R1	2.83	2.60	0.92
CB-C9R2	9.65	10.09	1.05
CB-S9R2	5.49	5.13	0.93
CB-C4R2	2.20	2.56	1.16
CB-S4R2	1.46	2.15	1.47
CB-9S	2.85	3.00	1.05
CB-S9S	2.19	2.19	1.00

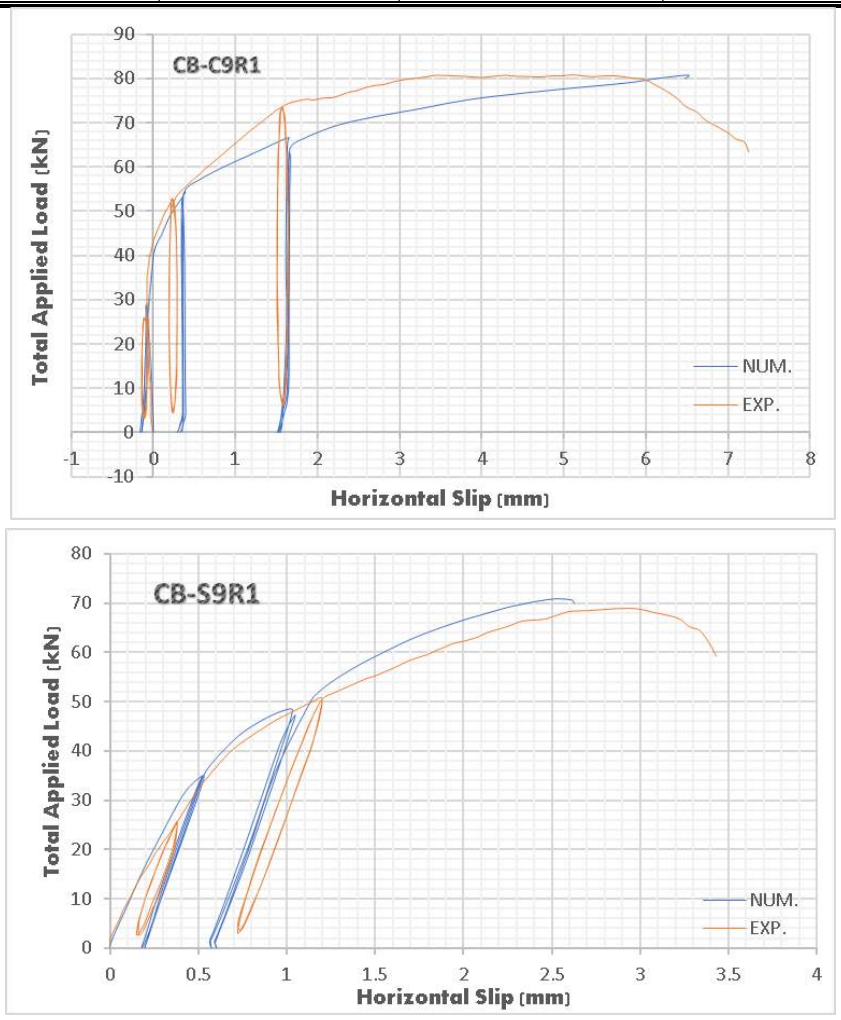

Figure 5-28:Comparison between Experimental and Numerical Slip at Ultimate Load

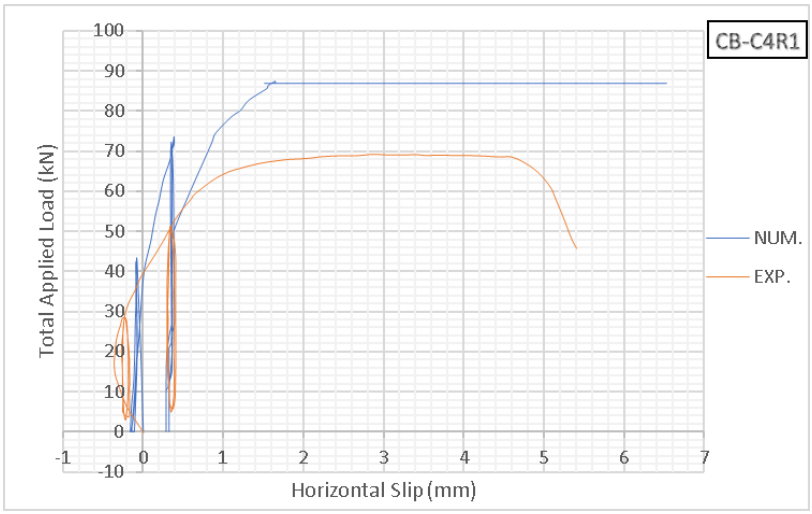

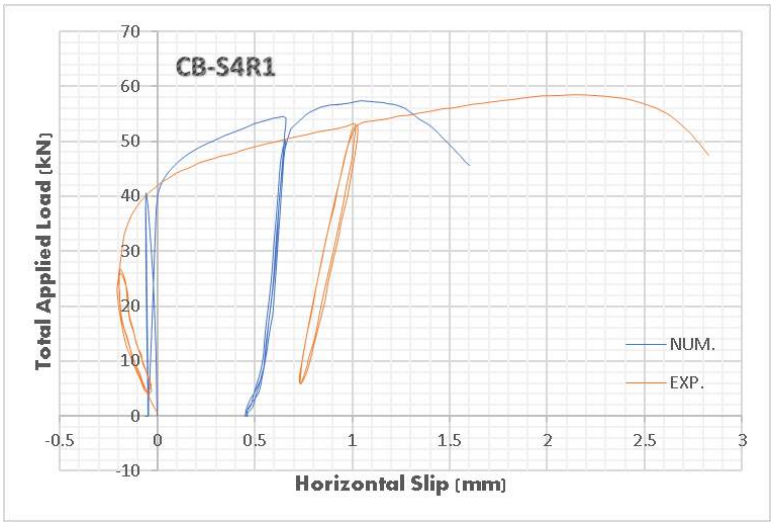

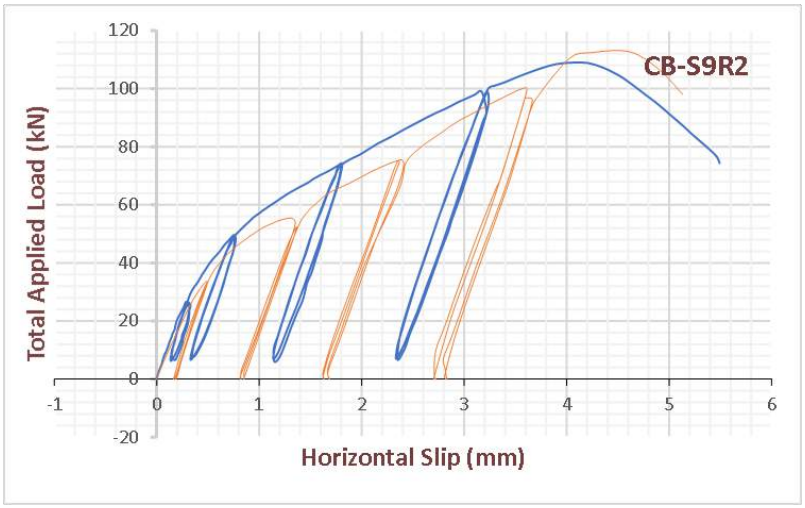

Figure 5-29:Comparison between Experimental and Numerical Slip at Ultimate Load

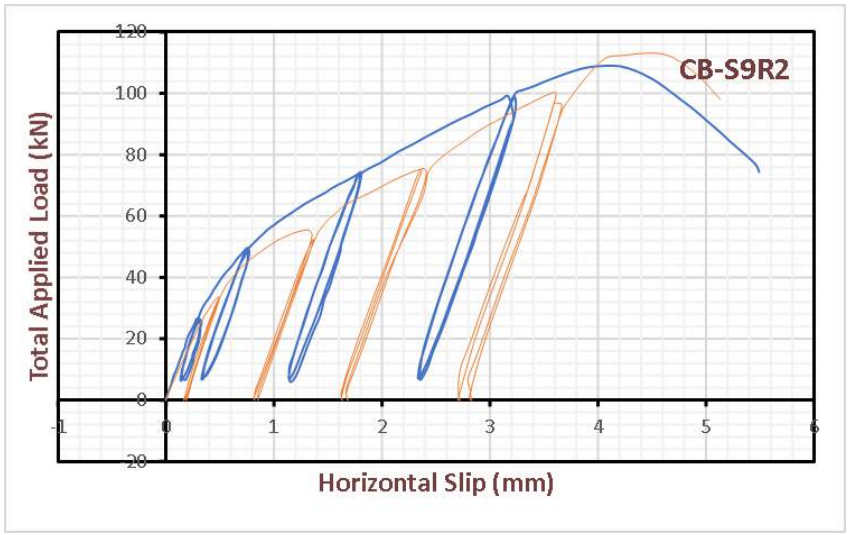

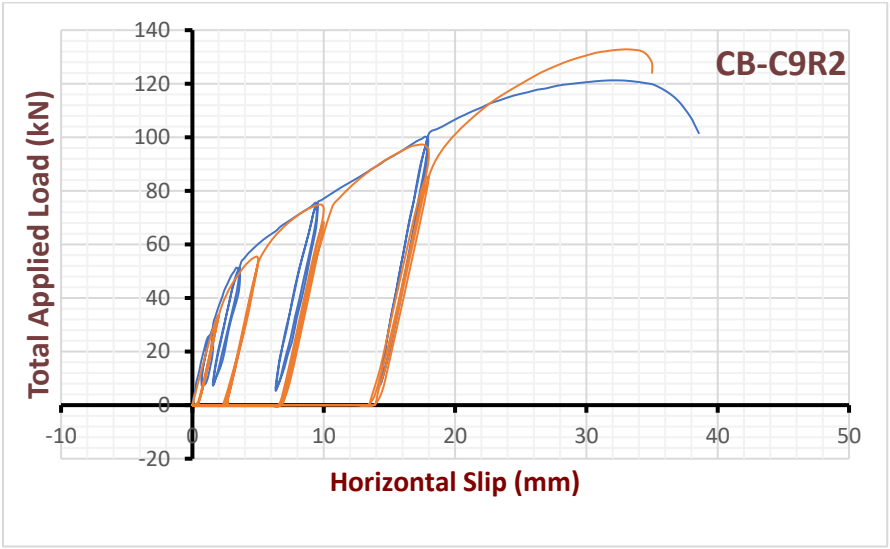

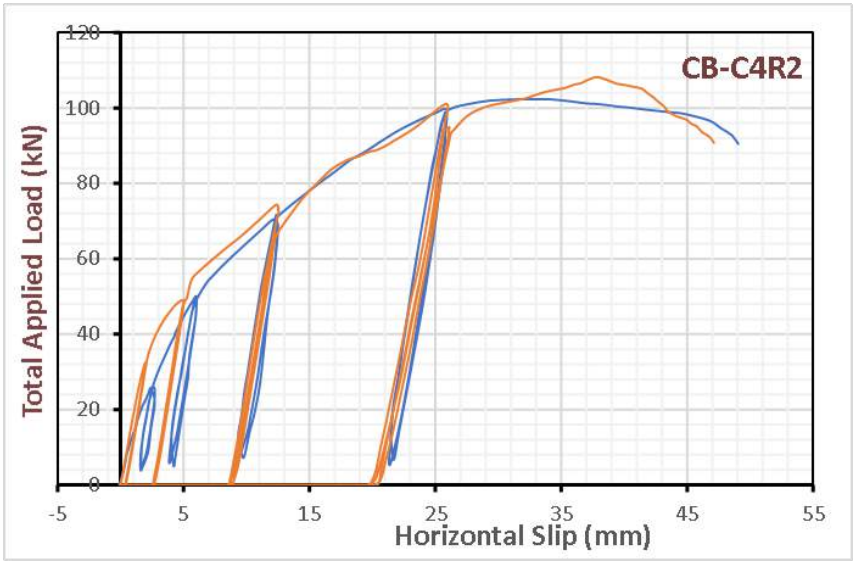

Figure 5-30:Comparison between Experimental and Numerical Slip at Ultimate Load

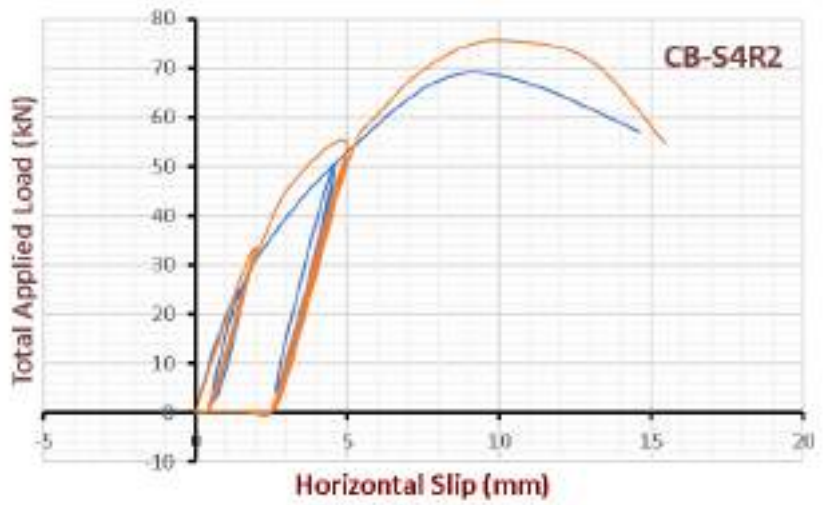

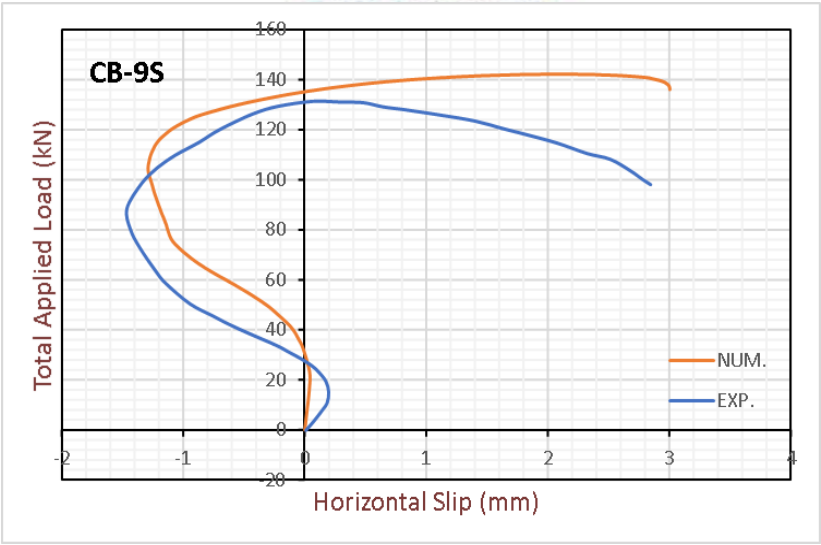

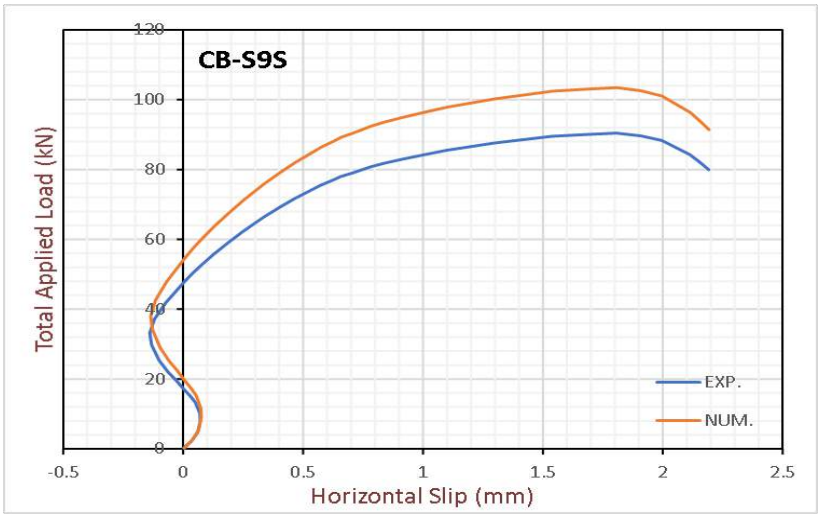

Figure 5-31:Comparison between Experimental and Numerical Slip at Ultimate Load

5.6 Validation of Numerical Analysis

The study validated numerical analysis using experimental data for composite beams, focusing on load-deflection relationships and interface slip. The results agreed with the experimental data, indicating the model's accuracy. The study also presented numerical failure modes and load-strain distribution profiles, providing a deeper understanding of composite beam behavior and improving structure design. Comparing load-displacement curves and failure modes is a common method for structural analysis validation, with the results aligning well with the experimental curves. This approach ensures the accuracy of the results.

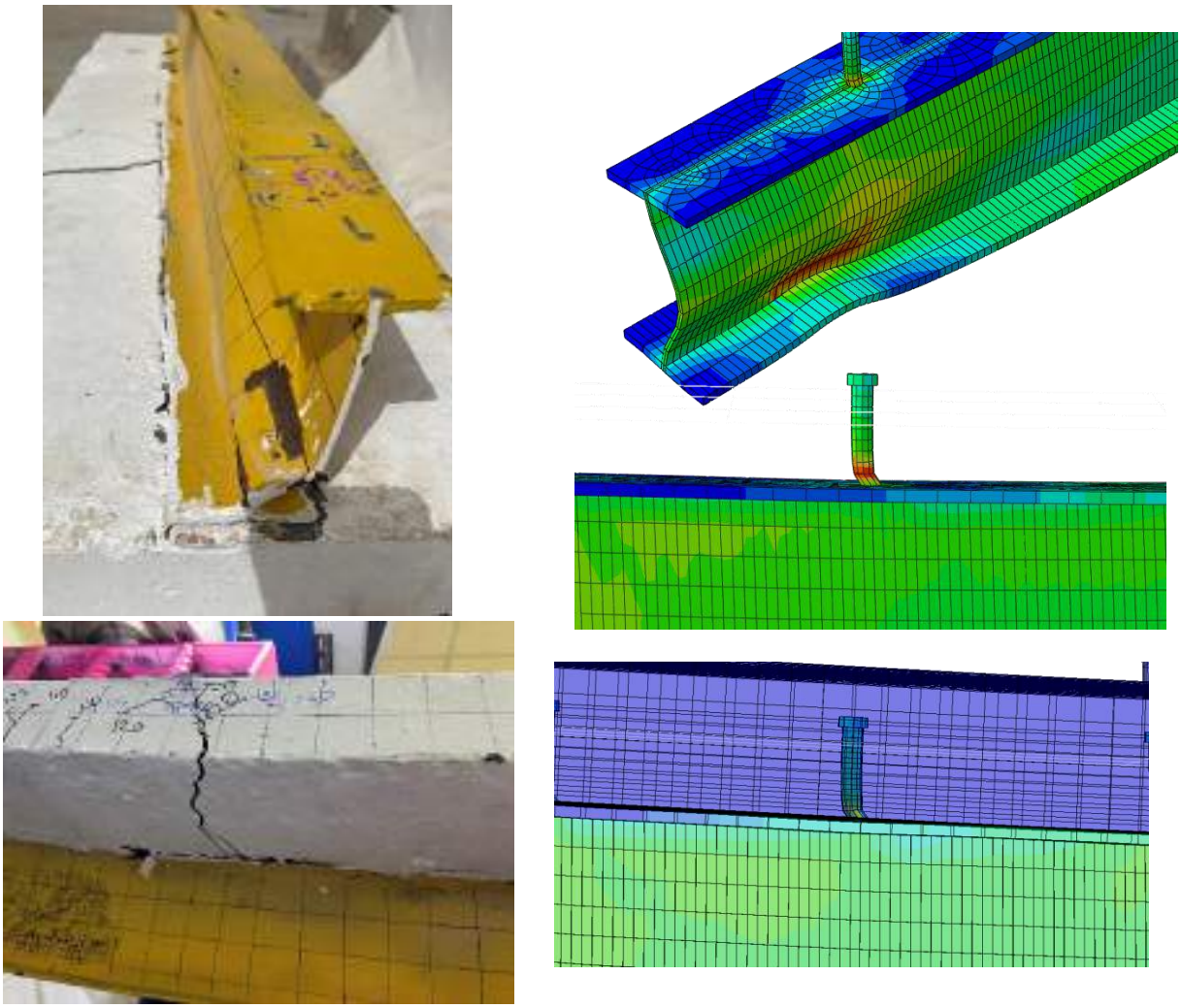

Figure 5-32:Comparison of the Experimental and Finite Element Analysis Failure modes (CB-9S).

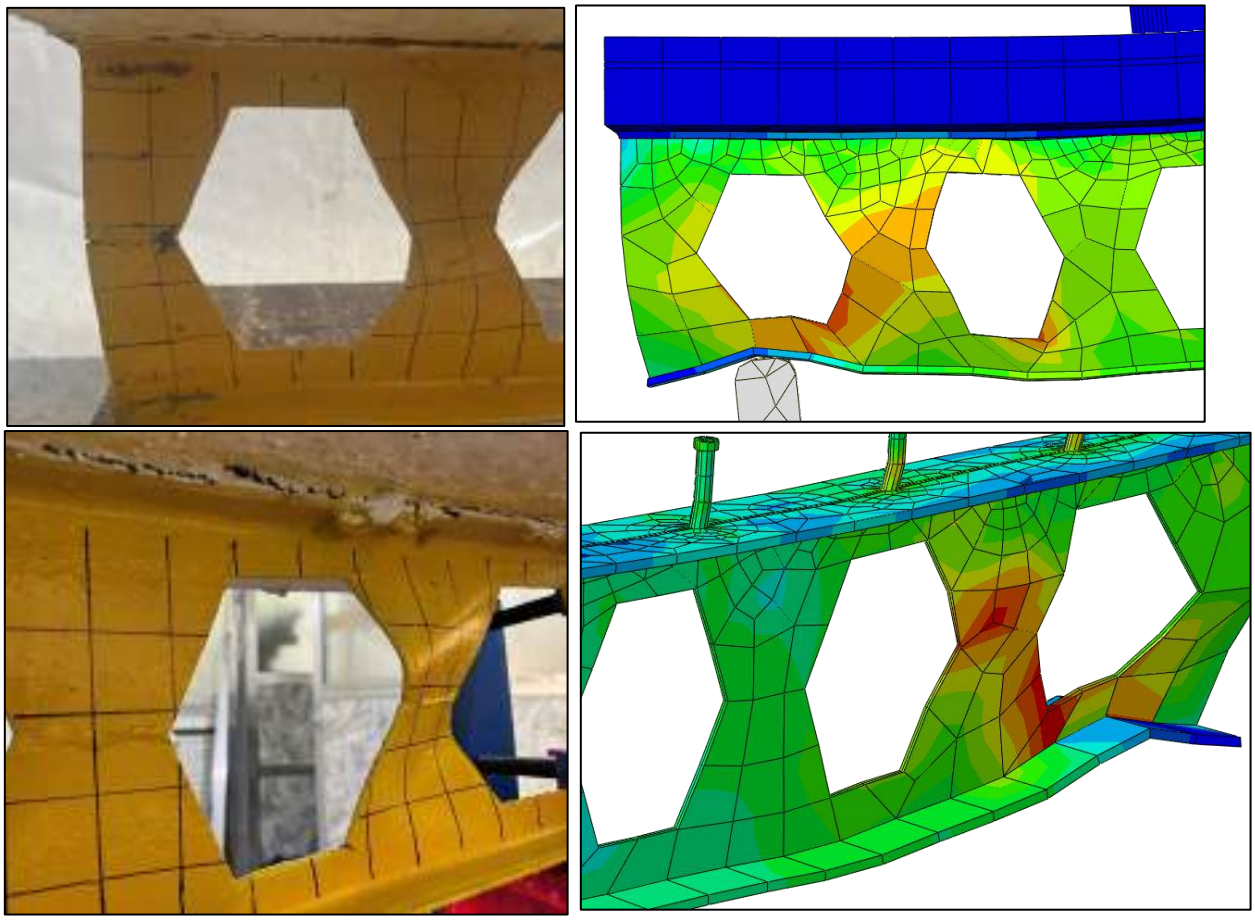

Figure 5-33:Comparison of the Experimental and Finite Element Analysis Failure modes. (CB-H9R1)

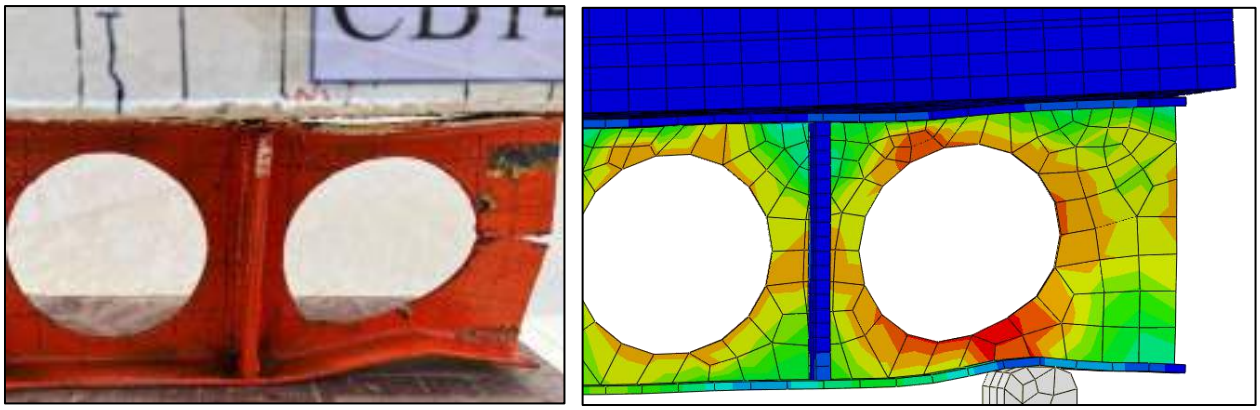

Figure 5-34:Comparison of the Experimental and Finite Element Analysis Failure modes. (CB-C4R1)

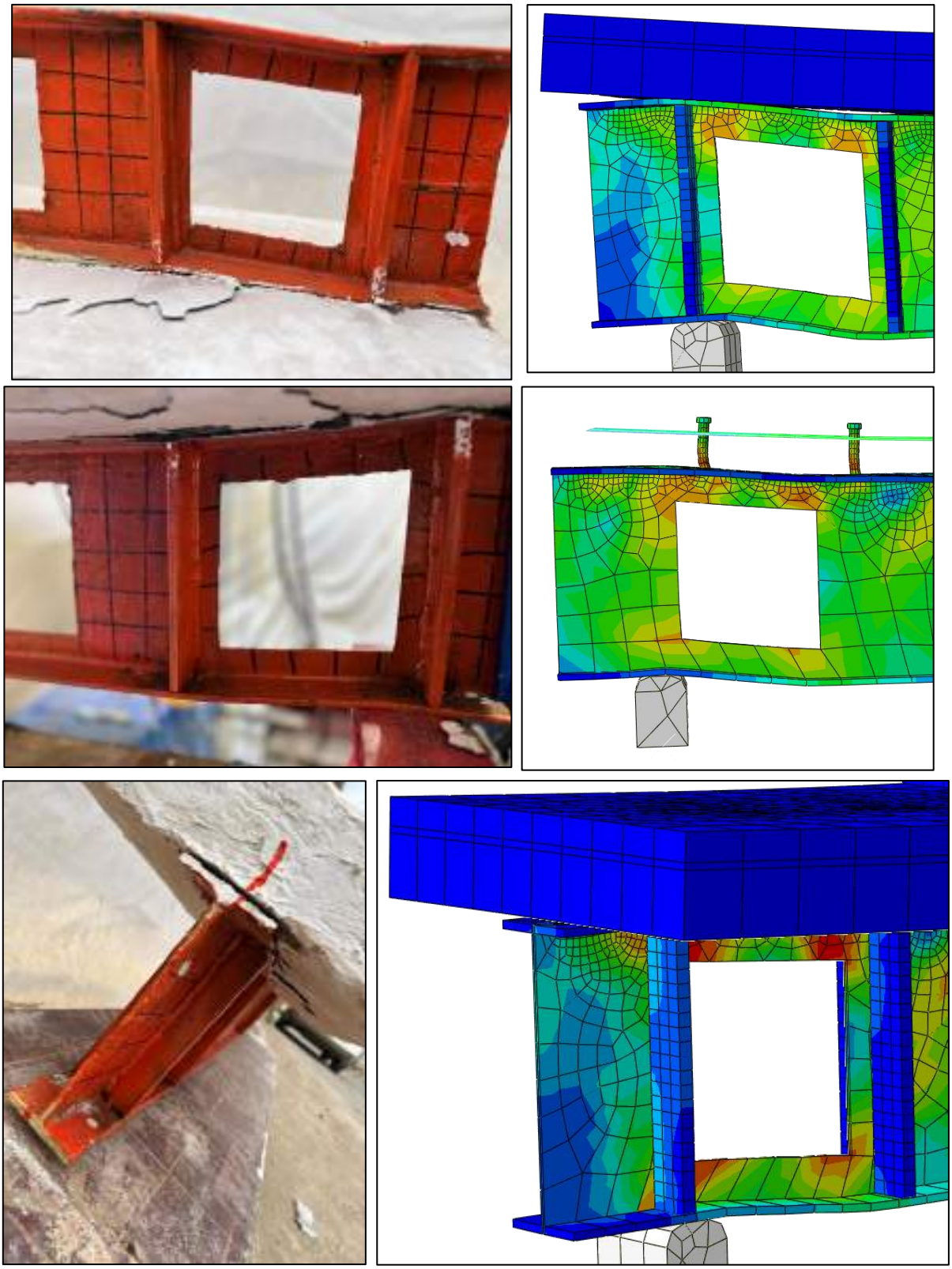

Figure 5-35:Comparison of the Experimental and Finite Element Analysis Failure modes. (CB-S4R2)

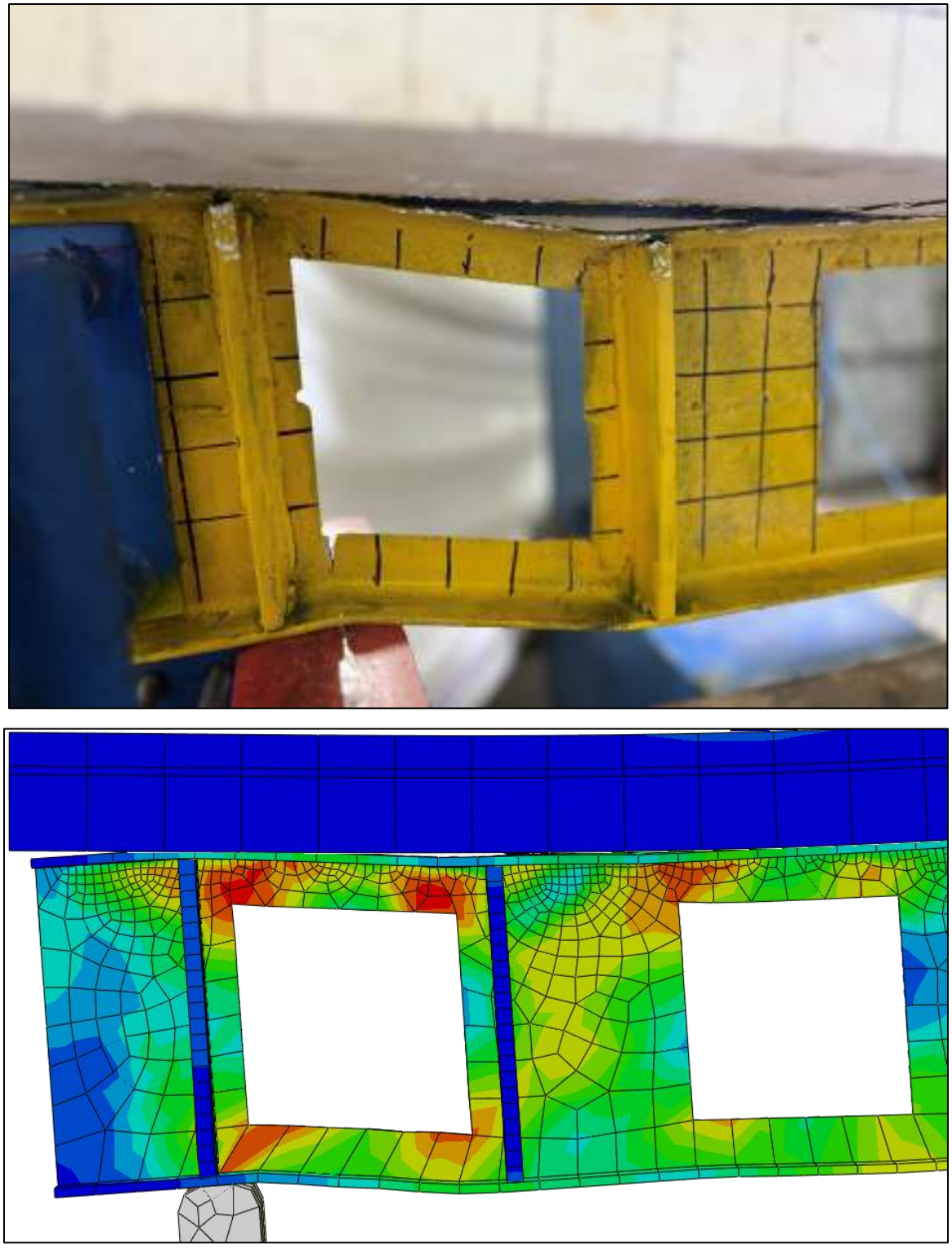

Figure 5-36:Comparison of the Experimental and Finite Element Analysis Failure modes. (CB-S9R2)

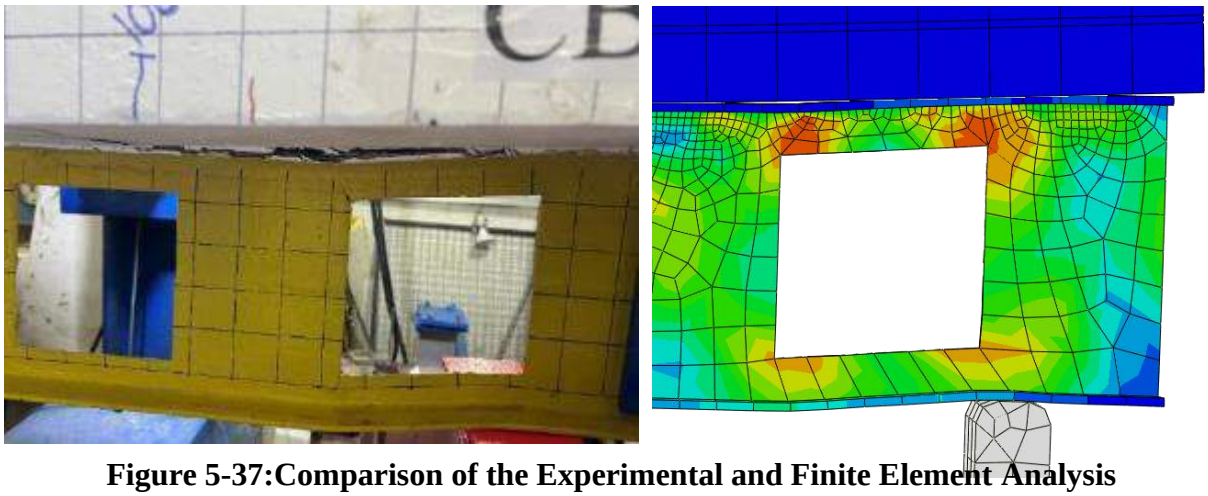

Figure 5-37:Comparison of the Experimental and Finite Element Analysis Failure modes. (CB-S9R1)

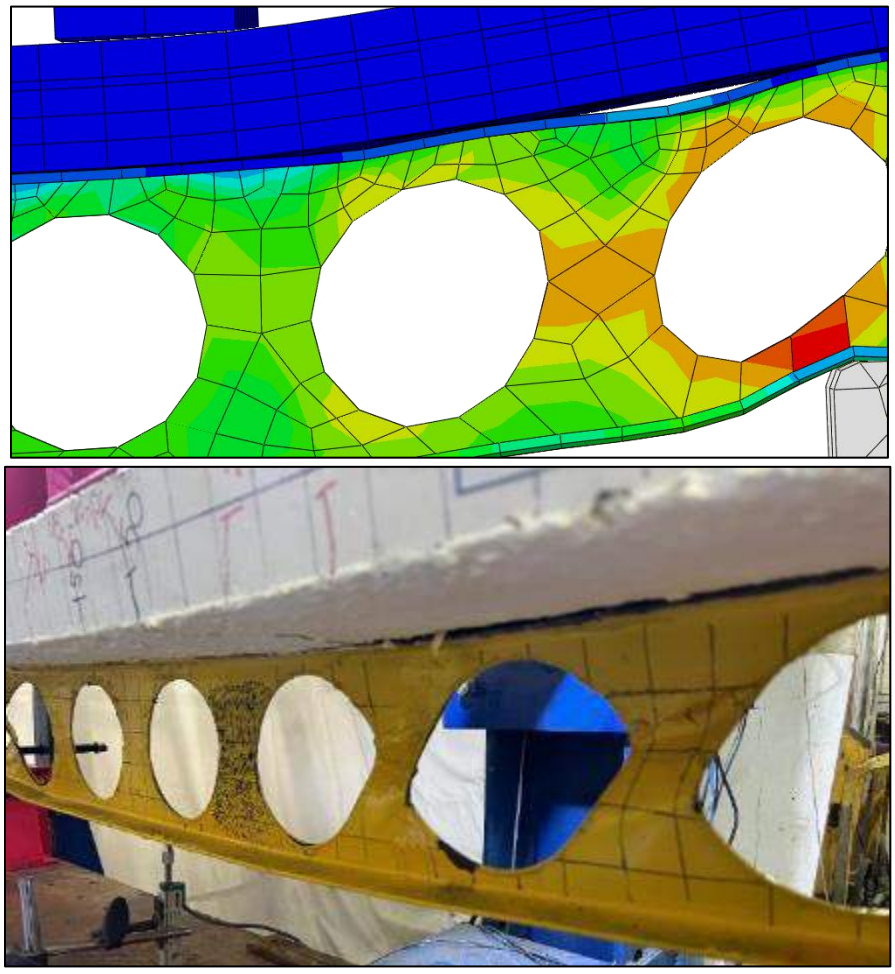

Figure 5-38:Comparison of the Experimental and Finite Element Analysis Failure modes. (CB-C9R1)

5.7 Parametric Study

The main purpose of the parametric study is to investigate the effect of some parameters, such as geometric changes in structure, and to investigate some parameters that are not studied in laboratory tests for actual members, which would have an important influence on the structural behavior, and to cover research objectives with much more detailed information. The parameters studied in this research are as follows:

5.7.1 Number of rows for stud connectors

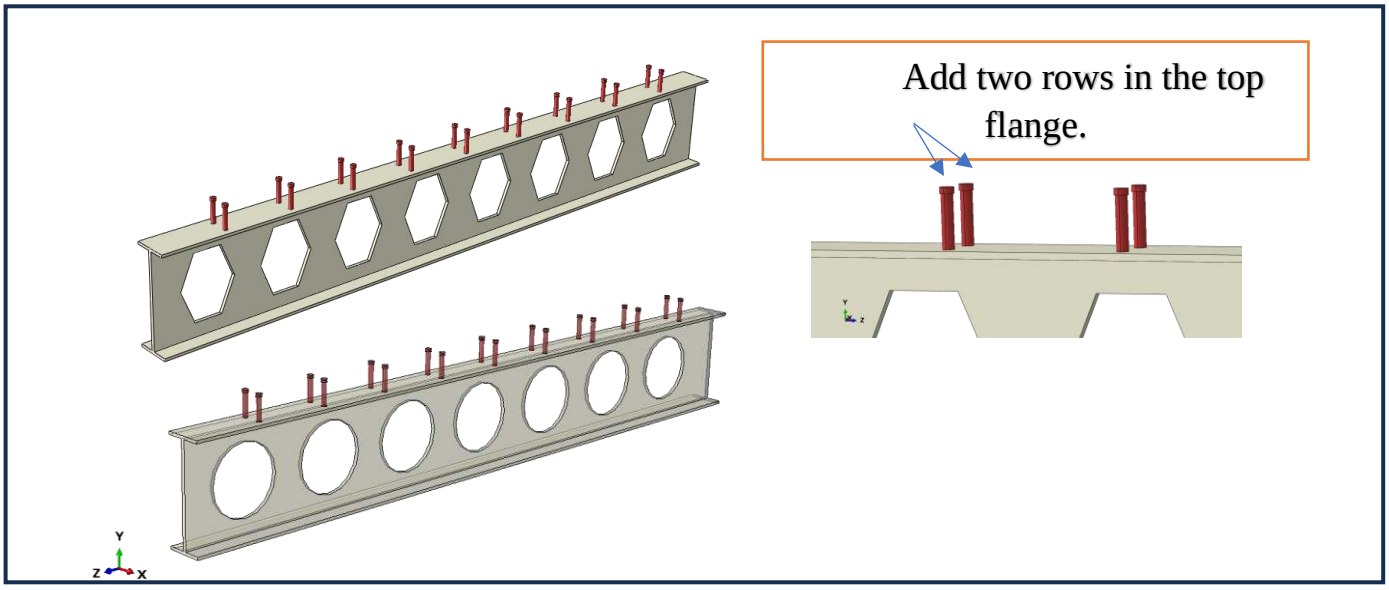

Table 5-6:The Effect of number rows on the Ultimate load

Beams	One Row	Two Row
	Ultimate Load (kN)	
CB-H9R1	99.6528	199.306
CB-C9R1	80.7255	137.64

Increasing the number of rows for stud connectors significantly enhances the ultimate load-bearing capacity of the castellated beams. The results demonstrate a clear correlation between the number of stud connector rows and structural strength.

- For CB-H9R1, the ultimate load more than doubles when transitioning from one row to two rows.
- CB-C9R1 also experiences substantial increases in ultimate load, highlighting the positive impact of additional stud connector rows.

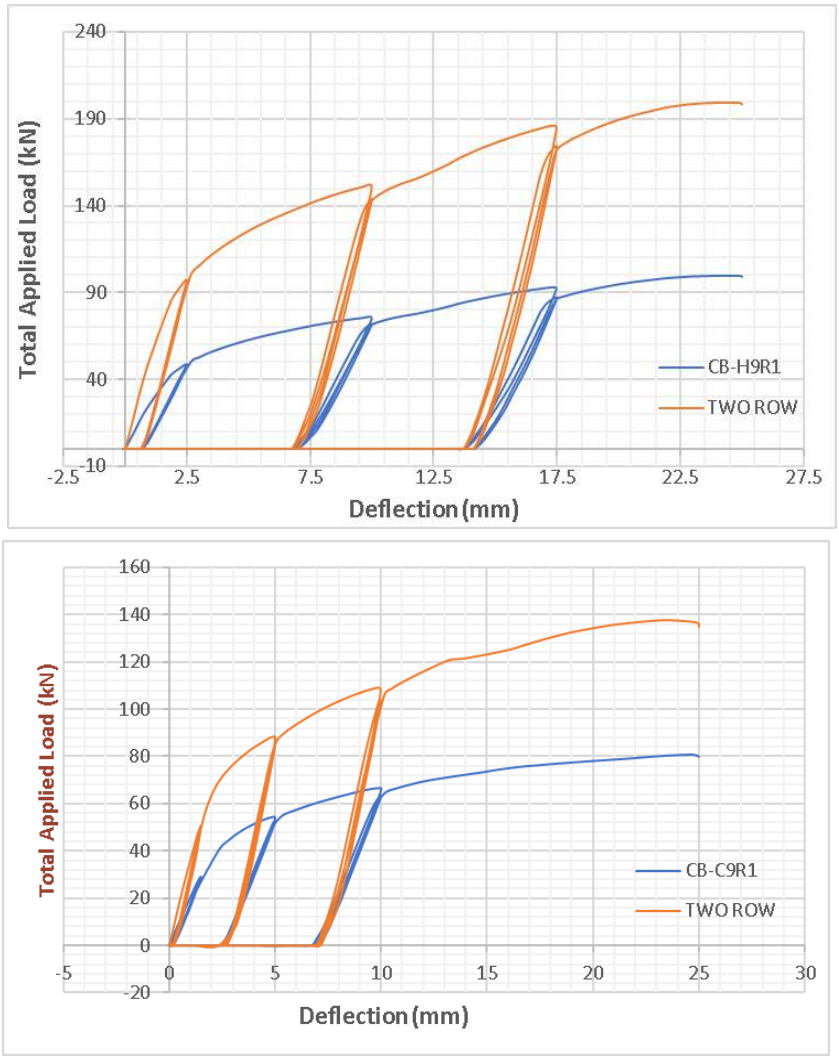

Figure 5-39: Compare the Results for The Number of Rows Between Stud Shears.

5.7.2 The stiffeners in the I-steel section.

a. stiffeners in the transverse direction; Type I

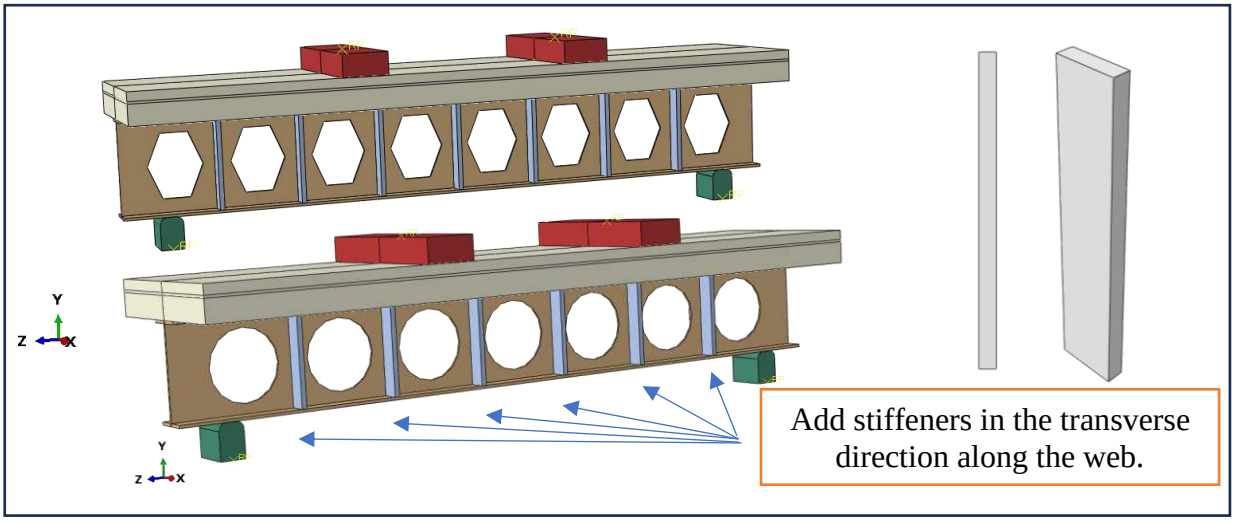

b. stiffeners along the edge of openings; Type II

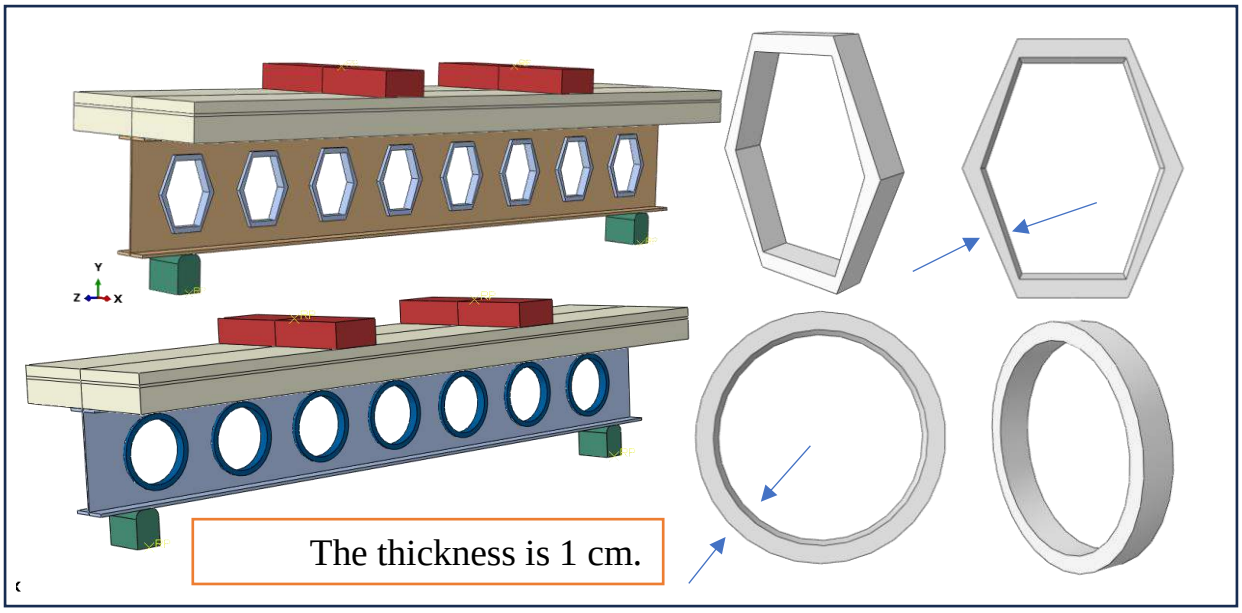

Table 5-7:The Effect of stiffeners on the Ultimate load

	CB-H9R2	*CB-C9R2*
	Ultimate Load (kN)	
Beams in Study	172.190	121.264
Type I	324.115	199.306
Type II	243.414	153.542

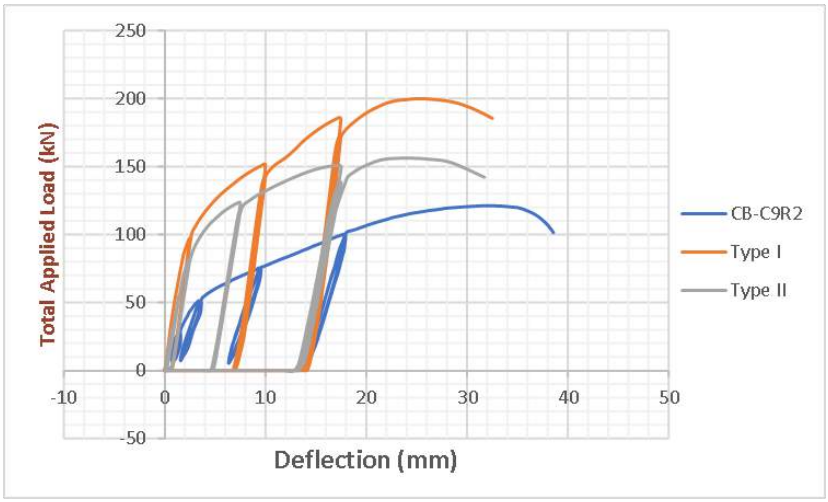

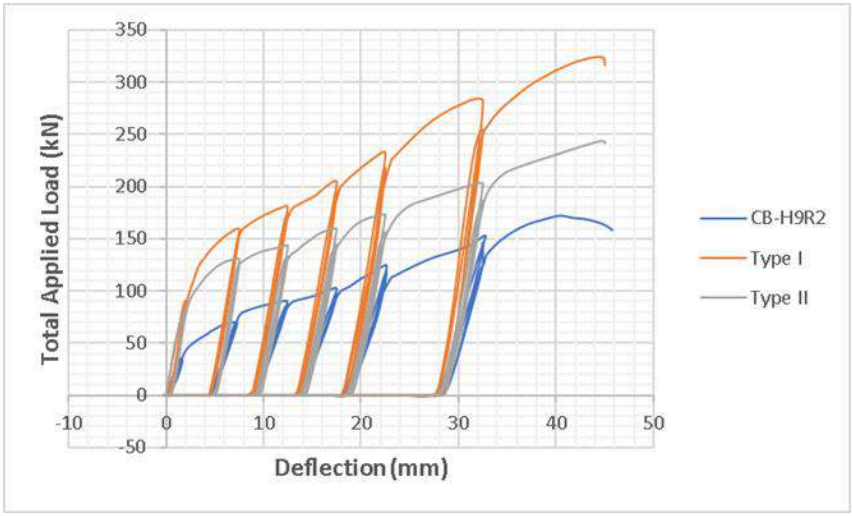

Figure 5-40:Compare the Results for The Stiffeners in The I-Steel Section.

The study reveals that the presence of stiffeners in the I-steel section significantly impacts the ultimate load-bearing capacity of castellated beams. Type I stiffeners result in higher ultimate loads for both CB-H9R2 and CB-C9R2, indicating the importance of the stiffener configuration. Type I stiffeners appear to be more effective in enhancing the structural strength of the castellated beams. The choice between Type I and Type II stiffeners should consider factors such as ease of fabrication, cost implications, and specific design requirements. The study concludes that the choice between one or two rows of stud connectors and the type of stiffeners should be made based on the specific requirements of the project.

5.8 Summary

- Model Validation and Accuracy: The study utilized ABAQUS/Explicit for finite element analysis and demonstrated a strong correlation between numerical predictions and experimental results. This suggests that the numerical model is valid and accurately represents the behavior of composite castellated beams under various conditions.
- Mesh Size Optimization: A convergence study determined that a mesh size of 25 mm strikes a balance between computational efficiency and result accuracy. This optimized mesh size was used consistently across all beams in the analysis.
- Load-Deflection Consistency: The load-deflection curves obtained through finite element analysis closely matched the experimental data. This consistency indicates that the numerical model effectively captures the structural response of the composite beams.
- Ultimate Load Prediction: The comparison between experimental and numerical ultimate loads revealed a high level of agreement, with variations remaining within a reasonable threshold of 7%. This suggests that the finite element model is reliable for predicting the ultimate load capacity of the composite castellated beams.
- The employed interaction modeling techniques, such as tie constraints and surface-to-surface connections, proved effective in simulating the complex relationships between different composite structure components.
- The numerical analysis incorporated an interface model to simulate slip between the concrete slab and steel beam. The comparison of experimental and numerical slip at ultimate load demonstrated reasonable agreement, confirming the model's ability to simulate this important aspect of behavior.

Chapter Six: Conclusion and Recommendation

Chapter Six: Conclusion and Recommendation

6.1 Summary

This chapter explains the conclusions from the experimental investigations and finite element analysis performed on the composite castellated beams. Furthermore, this study also provides suggestions for future research endeavors in this academic domain.

6.2 Conclusions from Experimental Work

1. Hexagonal beams consistently outperformed circular and square beams regarding ultimate load capacity, offering strength up to 28.26% and 100.43 % higher, respectively.
2. The percentage difference in ultimate load between shapes varied depending on the presence of stiffeners and shear connector spacing.
3. Circular beams generally exhibited intermediate performance, while square beams were the least effective in ultimate load.
4. The choice of opening shape significantly impacts the load-carrying capacity of composite castellated beams, with hexagonal shapes emerging as the most efficient design choice.
5. Decreasing the spacing between shear connectors (increasing their number) generally increases the ultimate load capacity. The magnitude of this effect varied across different beam configurations, ranging from 7.91% to 58.09%.
6. The most significant effect was observed in square beams with stiffeners, where decreasing spacing led to a 58.09% increase in ultimate load.
7. Stiffeners significantly enhanced the ultimate load capacity of all beam types, with increases ranging from 17.89% to 66.53%. The benefits of

stiffeners were particularly pronounced for hexagonal and square beams, leading to substantial strength improvements.

8. The effect of stiffeners was often amplified in beams with closer shear connector spacing.
9. The use of stiffeners offers a valuable strategy for enhancing the load-carrying capacity of composite castellated beams, especially for hexagonal and square shapes.
10. The study found that composite castellated beams with hexagonal apertures performed higher after strengthening, with a relative enhancement of around 66.5% and 55.7%, respectively. However, models with circular and square apertures showed varying levels of improvement.
11. Various elements, including the degree of castellation, loading conditions, and the presence of web stiffeners, influence the type of failure mode.
12. The empirical findings have additionally demonstrated that using web stiffeners can effectively prevent the potential occurrence of web buckling. Including web stiffeners in castellated beams resulted in a notable average enhancement of 31.2% in the web buckling load.
13. Analysis of Slip Characteristics: Slip, which is the movement between the steel beam and the concrete slab, had a big effect on the flexural stiffness of the composite castellated beams.
14. The first cracks are formed at about 42.59% – 89.10% of the ultimate load level of the testing beams. This percentage is changed by varying the cases in the present study.
15. The reduction in shear connectors had a minor impact on maximum deflection but a significant effect on ultimate load, indicating a decrease in ultimate load.

6.3 Conclusions from Finite Element Analysis

1. Beams such as CB-H9R1, CB-C9R1, and CB-S9R1 exhibited a high level of concordance between numerical simulations and experimental data. Numerical values displayed minor discrepancies, ranging from 0.89 to 1.14, compared to the experimental data.

2. Similar concurrence was observed in beams H4R2, C4R2, and S4R2, with numerical values ranging from 0.96 to 1.09.

3. Modest variations were seen in slip percentages among different beams, ranging from -3.32% to 8.85%.

4. Accuracy in Predicting Ultimate Load: The model's predictive capabilities exhibited a commendable level of accuracy, with an average precision of 95.2%, in determining the ultimate load of castellated beams.

5. The proposed numerical model can adequately predict the structural response of castellated beams when subjected to various loading scenarios.

6.4 Recommendations for Further Research

- Dynamic Loading Analysis: Studying behavior under seismic for real-world insights.
- Material Optimization: Exploring alternative materials or combinations to enhance structural properties.
- Effect of Temperature: Examining temperature variations' impact on material properties.
- Explore the influence of maintaining equal area on the dimensions and configurations of different opening shapes. Investigate the effects of shape parameters, such as aspect ratio and perimeter length, on structural behavior under varying loading conditions.

References

[1] J. P. Boyer, “Boyer, J.P. ‘Castellated Beams - New Developments,’” *Eng. Journal, Am. Inst. Steel Constr.*, vol. Vol. 1, pp. 104-108., 1964, [Online]. Available: https://www.aisc.org/Castellated-Beams-New-Developments

[2] S. Nadine, “Development Stages of Structurally Optimised Concrete Girders: Design Concepts, Material Strategies and Experimental Investigation.” pp. 1403-1411., 2023. doi: 10.1007/978-3-031-32519-9_142.

[3] M. K. Abbas, “Experimental and Finite Element Analysis of Composite Castellated Steel Beams Self-Compacting Concrete Decks.” pp. 212-p3, 2011.

[4] Z. M. R. Abdul Rasoul, “Ultimate Strength Capacity and the Bond-Slip Behavior of Composite Ultra- High Performance Concrete-Steel Beams,” no. 1436, 2015.

[5] A. Rodera, “Design of Composite Beams Using Light Steel Sections,” no. 12, pp. 50–52, 2004.

[6] A. C. I. C. 363, *“High-Strength Concrete (ACI 363R),.”* ACI Symp. Publ. doi: 10.14359/14461.

[7] P. Panedpojaman, “Buckling analysis for web post of cellular beams,” 2012. [Online]. Available: https://api.semanticscholar.org/CorpusID:189859593

[8] R. G. Redwood, *Design of Composite Beams With Web Openings.*, no. April. 1986. doi: 10.1002/1528-2716(200004/06)2:2<157::aid-pse23>3.0.co;2-a.

[9] T. P. Bradley, “Stability of Castellated Beams During Erection,” *Stab. Castellated Beams Dur. Erection*, no. Knowles, pp. 1–15, 2003, [Online]. Available: http://scholar.lib.vt.edu/theses/available/etd-02032003-104656/

[10] H. Showkati, T. Ghanbari Ghazijahani, A. Noori, and T. Zirakian, “Experiments on elastically braced castellated beams,” *J. Constr. Steel Res.*, vol. 77, pp. 163–172, 2012.

[11] K. KUCHTA and M. Maślak, “Failure Modes Determining the Resistance and the Stability of Steel Cellular Beams,” *J. Civ. Eng. Environ. Archit.*, vol. XXXII, no. 4/2015, pp. 263–280, 2015, doi: 10.7862/rb.2015.194.

[12] A. S. de Carvalho, C. H. Martins, A. Rossi, V. M. de Oliveira, and S. G. Morkhade, “Moment gradient factor for steel I-beams with sinusoidal web openings,” *J. Constr. Steel Res.*, vol. 202, no. January, 2023, doi: 10.1016/j.jcsr.2023.107775.

[13] M. A. Ihssan, “Reinforced Concrete Beams with Steel Fibers Subjected to Static Cyclic Loads.” M.Sc., University of Technology, Baghdad,.

[14] A. Kaveh and F. Shokohi, “Application of Grey Wolf Optimizer in design of castellated beams,” *Asian J. Civ. Eng.*, vol. 17, no. 5, pp. 683–700, 2016.

[15] A. Z. dan D. Yusri, “**済無**No Title No Title No Title,” *J. Ilmu Pendidik.*, vol. 7, no. 2, pp. 809–820, 2020.

[16] “Jackson, R., ‘Vibration and Flexural Strength Characteristics of Composite Castellated Beams,’ M.Sc. Thesis, the Faculty of the Virginia Polytechnic Institute and State University, February 2002.”

[17] “Demirdjian, S., ‘Stability of Castellated Beam Webs,’ M.Sc. Thesis, Department of Civil Engineering and Applied Mechanics, McGill University Montreal, Canada, March 1999.”

[18] “Castellated {Beam}: History, {Applications}, and {Advantages}.”

[19] “Boyer, J. P., ‘Castellated Beams – New Developments,’ AISC Engineering Journal, paper presented at the AISC National Engineering Conference, Omaha, Nebr., May 1964, pp. 104-108.”

[20] D. Sandy, H. R. Limbong, D. Runtulalo, and H. Rante, “Experimental Study on Castellated Beams with Hexagonal Variation Using Monotonic Loading,” *Int. J. Eng. Sci. Appl.*, vol. 1, no. November, pp. 67–76, 2014.

[21] M. Junus, P. Herman, T. Jonie, and D. Rudy, “Behavior of castellated beam column due to cyclic loads,” *ARPN J. Eng. Appl. Sci.*, vol. 10, no. 6, pp. 2307–2311, 2015.

[22] A. S. Shaikh and P. B. Autade, “Structural Analysis and Design of Castellated Beam in Fixed Action,” *Int. J. Innov. Res. Adv. Eng.*, vol. 3, no. 08, pp. 92–97, 2016.
[23] P. Wang, K. Guo, M. Liu, and L. Zhang, “Shear buckling strengths of web-posts in a castellated steel beam with hexagonal web openings,” *J. Constr. Steel Res.*, vol. 121, pp. 173–184, 2016, doi: 10.1016/j.jcsr.2016.02.012.
[24] L. Budi, Sukamta, and W. Partono, “Optimization Analysis of Size and Distance of Hexagonal Hole in Castellated Steel Beams,” *Procedia Eng.*, vol. 171, pp. 1092–1099, 2017, doi: 10.1016/j.proeng.2017.01.465.
[25] . M. A. A.-M., “Experimental study of Castellated Steel Beams,” *Iraqi J. Civ. Eng.*, vol. 11, no. 3, pp. 68–78, 2017, doi: 10.37650/ijce.2017.172895.
[26] O. W. Blodgett, *Blodgett, O. W., “Design of Welded Structures”, The James F. Lincoin Arc Welding Foundation. Cleveland, Ohio, 1968*.
[27] P. R. Knowles, *Design of Castellated Beams: For Use with BS 5950 and BS 449*. [Croydon, London] SE - 54 pages : illustrations ; 30 cm: Constrado [Croydon, London], 1986. doi: LK - https://worldcat.org/title/51356519.
[28] A. J. Mehetre and R. S. Talikoti, “Castellated Steel Beams A Torsional Analysis,” *Int. J. Eng. Adv. Technol.*, vol. 9, no. 5, pp. 536–540, 2020, doi: 10.35940/ijeat.e9606.069520.
[29] K. A. Cashell, M. Malaska, M. Khan, M. Alanen, and K. Mela, “Experimental and numerical analysis of stainless steel cellular beams in fire,” *Fire Saf. J.*, vol. 121, 2021, doi: 10.1016/j.firesaf.2021.103277.
[30] R. E.S.Ismail, A. S. Fahmy, and N. M. Tawfik, “Ultimate Behavior of Composite Castellated Beams under Vertical Loads,” *Int. J. Comput. Appl.*, vol. 108, no. 5, pp. 40–46, 2014, doi: 10.5120/18911-0214.
[31] A. H. A. Al-Zuhairi, A. I. Mansi, A. H. A. Al-Zuhairi, and A. I. Mansi, “Behavior of Composite Concrete-Castellated Steel Beams in Flexure,” no. July, pp. 6–11, 2017, [Online]. Available: https://www.researchgate.net/publication/318307768
[32] P. Pandilatha and R. S. Surumi, “Comparitive study on flexural behaviour of steel concrete composite beam using welded and bolted shear connector,” *Int. J. Civ. Eng. Technol.*, vol. 8, no. 5, pp. 1016–1024, 2017.
[33] N. K. Oukaili and S. S. Abdullah, “Behavior of composite concrete-castellated steel beams under combined flexure and torsion,” *Proc. 6th Asia-Pacific Conf. FRP Struct. APFIS 2017*, no. July, 2017.
[34] S. Yahya Al-Darzi, “Effect of Repeated Loads on Steel-Concrete Composite Beams with High Strength Reinforced Concrete المثنى للهندسة والتكنولوجيا . *Suhaib.D. / Muthanna J*,” مجلة /*.Eng. Technol.*, vol. 47, no. 5, pp. 47–56, 2017, doi: 10.52113/3/eng
[35] L. K. Al-Hadithy and M. S. Jaafar, “Performance of Composite Steel-Concrete Beams with Stud Shear Connectors under Periodical Loadings,” *Al-Nahrain J. Eng. Sci.*, vol. 20, no. 2, pp. 341–352, 2017.
[36] S. Q. Abdulridha, H. H. Muteb, and S. S. Abdulqader, “Experimental investigation of structural behavior of composite steel concrete beams subjected to impact loads,” *Int. J. Civ. Eng. Technol.*, vol. 9, no. 7, pp. 633–641, 2018.
[37] M. Sukanya, C. Balakrishnan, and K. Devanathan, “Experimental investigation of composite deck slab with castellated beam,” *Int. J. Adv. Res. Eng. Technol.*, vol. 10, no. 5, pp. 55–64, 2019, doi: 10.34218/IJARET.10.5.2019.006.
[38] A. Rossi, R. S. Nicoletti, A. S. C. de Souza, and C. H. Martins, “Numerical assessment of lateral distortional buckling in steel-concrete composite beams,” *J. Constr. Steel Res.*, vol. 172, p. 106192, 2020, doi: 10.1016/j.jcsr.2020.106192.
[39] F. P. V. Ferreira, K. D. Tsavdaridis, C. H. Martins, and S. De Nardin, “Buckling and post-buckling analyses of composite cellular beams,” *Compos. Struct.*, vol. 262, no. January, p. 113616, 2021, doi: 10.1016/j.compstruct.2021.113616.
[40] F. P. V. Ferreira, C. H. Martins, and S. De Nardin, *Sensitivity Analysis of Composite*

Cellular Beams to Constitutive Material Models and Concrete Fracture, vol. 21, no. 1. 2021. doi: 10.1142/S0219455421500085.
[41] H. W. Al-Thabhawee, "Experimental investigation of composite steel-concrete beams using symmetrical and asymmetrical castellated beams," *Curved Layer. Struct.*, vol. 9, no. 1, pp. 227–235, 2022, doi: 10.1515/cls-2022-0019.
[42] Z. H. Dakhela and S. D. Mohammed, "Response of composite steel-concrete cellular beams of different concrete deck types under harmonic loads," *J. Mech. Behav. Mater.*, vol. 31, no. 1, pp. 127–134, 2022, doi: 10.1515/jmbm-2022-0014.
[43] Y. M. Alharthi *et al.*, "Flexural Behavior and Capacity of Composite Concrete-Steel Beams Using Various Shear Connectors," *Arab. J. Sci. Eng.*, vol. 48, no. 4, pp. 5587–5601, 2023, doi: 10.1007/s13369-022-07485-y.
[44] H. M. E. D. Afefy, A. M. Atta, and S. E. D. F. Taher, "Behavior of Strengthened Composite Castellated Beams Pre-stressed with External Bars: Experimental Study," *Arab. J. Sci. Eng.*, vol. 37, no. 6, pp. 1521–1534, 2012, doi: 10.1007/s13369-012-0278-2.
[45] S. A. Patil and P. D. Kumbhar, "Comparative Study of Transverse Stiffeners and Stiffeners along the Opening Edge used for Castellated Beam," *Int. J. Innov. Res. Sci. Eng. Technol.*, vol. 5, no. 5, pp. 8516–8522, 2016, doi: 10.15680/IJIRSET.2016.0505236.
[46] H. W. A. Al-Thabhawee and M. A.-A. Al-Kannoon, "Improving Behavior of Castellated Beam by Adding Spacer Plat and Steel Rings," *J. Univ. Babylon Eng. Sci.*, vol. 26, no. 4, pp. 331–344, 2018, doi: 10.29196/jub.v26i4.810.
[47] K. N, D. S. R, and D. J. K, "Experimental analysis and Study on Shear Performances of Castellated Beam Chassis under Three Cases of Stiffener," *J. Eng. Res.*, pp. 1–43, 2021, doi: 10.36909/jer.11907.
[48] M. A. Ameer, "Experimental study of the behaviour and failure modes of tapered castellated steel beams," *Open Eng.*, vol. 12, no. 1, pp. 245–253, 2022, doi: 10.1515/eng-2022-0028.
[49] M. K. Abbas and H. W. Al-Thabhawee, "Experimental study of composite concrete cellular steel beams," *IOP Conf. Ser. Earth Environ. Sci.*, vol. 961, no. 1, 2022, doi: 10.1088/1755-1315/961/1/012095.
[50] "AISC American Institute of Steel Construction,"" Manual of Steel Construction "', New York, 2005."
[51] No.5, "Iraqi Specifications for Portland Cement," *Ministry of Planning - Central Organization For Standardization And Control Quality*. 1984.
[52] "Iraqi Specifications No. (45), 1984 for Aggregates of Natural Resources used for Concrete and Construction." [Online]. Available: https://www.scribd.com/document/395467049/Iraqi-Standard-Materials-Specification-Construction-Works
[53] F. O. F. Application and T. Data, "MasterRoc ® MS 610".
[54] ASTM C1240-15, "C1240 Standard Specification for Silica Fume Used in Cementitious Mixtures," *Annu. B. ASTM Stand.*, pp. 1–7, 2020, doi: 10.1520/C1240-15.2.
[55] M. O. F. Action and T. Applications, "MasterGlenium ® 54".
[56] "Iraqi Specification No.1703/1992." [Online]. Available: https://www.scribd.com/document/395467049/Iraqi-Standard-Materials-Specification-Construction-Works
[57] B. S. I. Standards, "Testing concrete — compressive strength of concrete cubes," *Br. Stand. Inst.*, no. 1, pp. 1–10, 1983.
[58] ASTM C39/C39M, "Standard Test Method for Compressive Strength of Cylindrical Concrete Specimens 1 This standard is for EDUCATIONAL USE ONLY .," *Annu. B. ASTM Stand.*, no. C, pp. 1–7, 2010, doi: 10.1520/C0039.
[59] ASTM C469-11, "Standard Test Method for Splitting Tensile Strength of Cylindrical Concrete Specimens," *ASTM Stand. B.*, vol. i, pp. 545-545–3, 2008, doi: 10.1520/C0496.
[60] C. C. Test, T. Drilled, and C. Concrete, "Standard Test Method for Flexural Strength of

Concrete (Using Simple Beam with Third-Point Loading) 1," *Hand*, vol. C78-02, no. C, pp. 1–4, 2010, doi: 10.1520/C0293.

[61] H. G. Russell Chairman Arthur R Anderson Jack O Banning Irwin G Cantor *et al.*, "ACI 363R-92 State-of-the-Art Report on High-Strength Concrete Reported by ACI Committee 363," vol. 92, no. Reapproved, 2010.

[62] ASTM A615/A615M, "Standard Specification for Deformed and Plain Carbon-Steel Bars for Concrete Reinforcement," *ASTM Int.*, no. March, pp. 1–8, 2015, doi: 10.1520/A0615.

[63] ASTM-C511-13, "Standard Specification for Mixing Rooms , Moist Cabinets , Moist Rooms , and Water," *ASTM Stand. Guid.*, pp. 23–25, 2015, doi: 10.1520/C0511-13.2.

[64] "GOM Correlate is now ZEISS INSPECT Correlate." [Online]. Available: https://www.gom.com/en/products/metrology-software/gom-correlate-pro

[65] "BS 5950: Part 1 : 1990 UDC 693.814: 669.14.018.29 British Standard Structural use of steelwork in building Part 1."

[66] N. C. Street and N. W. Suite, *@ Seismicisolation @ Seismicisolation @ Seismicisolation @ Seismicisolation*. 2010.

[67] F. Haji Aboutalebi and A. Banihashemi, "Numerical estimation and practical validation of Hooputra's ductile damage parameters," *Int. J. Adv. Manuf. Technol.*, vol. 75, no. 9–12, pp. 1701–1710, 2014, doi: 10.1007/s00170-014-6275-8.

[68] M. Fallahi, S. S. Roudsari, T. M. Abu-Lebdeh, and F. I. T. Petrescu, "Invistigating the effects of frp bars on the seismic behavior of reinforced concrete coupling beams," *Indep. J. Manag. Prod.*, vol. 10, no. 8, p. 1819, 2019, doi: 10.14807/ijmp.v10i8.1058.

[69] I. M. Metwally, "Three-dimensional nonlinear finite element analysis of concrete deep beam reinforced with GFRP bars," *HBRC J.*, vol. 13, no. 1, pp. 25–38, 2017, doi: 10.1016/j.hbrcj.2015.02.006.

[70] A. S. M. Mendis, S. Al-Deen, and M. Ashraf, "Flexural shear behaviour of reinforced Crumbed Rubber Concrete beam," *Constr. Build. Mater.*, vol. 166, pp. 779–791, 2018, doi: 10.1016/j.conbuildmat.2018.01.150.

APPENDIX-A

Design Examples of The Tested Beams

Here, both CB-H9R and CB-S9R were chosen as an example to determine the shear and flexure nominal strength theoretically according to the limitations of a composite section of AASHTO [OBJ] and AISC-2005 [OBJ] using the LRFD method. The elected beams' cross-section and parameters are explained in **Figure (A-1)**.

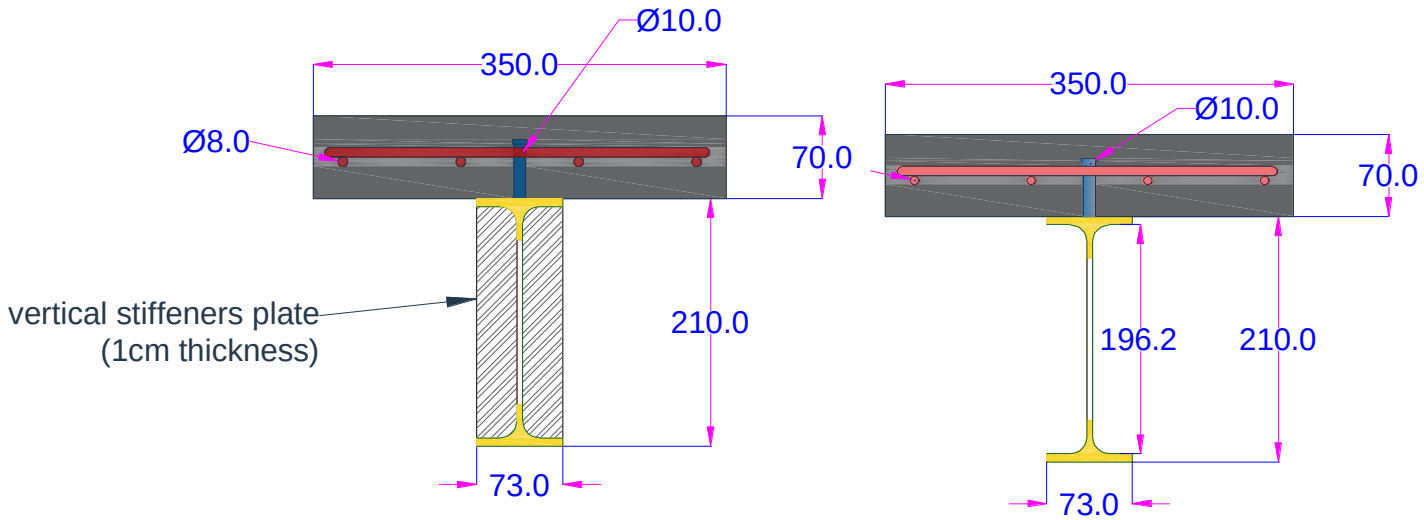

Figure (A-1): Typical Cross-Section of the CB-S9R and CB-H9R.

Design Steps

- Span length

According to Effective Length (BS 5950-1:1990),[65] the effective length (span) of a supported beam is defined as the smaller of the following two values:
The effective span of the beam can be calculated as follows:
Step 1:
Effective length of the beam = Clear span + 1/2 support width× 2
Effective length of the beam = 1200 mm + 50 + 50mm
The effective length of the beam = 1300 mm
Step 2:
Effective length of the beam = Clear span of the beam + effective depth
Effective length of the beam = 1200 mm + 210 mm= 1410 mm

Therefore, the effective span of the beam is the smaller of the two values calculated above, which is 1300 mm.

2- Calculating the effective slab width of the composite beams.

In the composite section, the width of the slab is controlled by the limitations of effective flange width as follows:

- AISC (I3.1a) (16-83), “the effective width of the concrete slab is the sum of the effective widths for each side of the beam centerline, each of which shall not exceed:”[50]

(1) 1/8 of the beam span, c. to c. of supports;
(2) 1/2 the distance to the centerline of the adjacent beam; or
(3) The distance to the edge of the slab.

- AASHTO[66]

, " The total width of slab effective as a T-girder flange shall not exceed:"
(1) 1/4 span length of the rafter.
(2) 6 times slab thickness.
(3) Clear distance between webs.
Thus, the slab width $bc = beff. = 1500 \ / 4 = 375\ mm$, but 350 mm used.

Using standard I-steel section with the following properties:

Root Depth (mm)	**d**	**140**
Flange Width (mm)	bf	73
Flange Thickness (mm)	tf	6.9
Web Thickness (mm)	tw	4.7
Yielding Stress (MPa)	Fy	327
Ultimate Strength (MPa)	Fu	446
Modulus of Elasticity (GPa)	Es	200

By applying the formulas for geometry criteria, other castellated section properties will appear as follows:

Depth (mm)	D	210
Opening Depth (mm)	ho	140
Tee Depth (mm)	hp	35
Sectional Area at opening (mm^2)	As	1277.2
Moment of Inertia at opening (mm^4)	Ix	12.28×10^6

Slab thickness is considered 70 mm, and compressive strength of concrete is taken as 65MPa for the cylinder.

Calculation of Ultimate Load

a- Elastic Stage

The modulus of elasticity and modular ratio are:

$E_C=3320\sqrt{F_c}+6900$ (ACI-363R-23)

E_C = 32616.6 MPa

$n=\frac{Es}{Ec}=\frac{200000}{32616.6}=6.1\cong 6$

Depth to the elastic neutral axis (y):

$y=\frac{0.5tc+n\times r\times(0.5D+tc)}{1+n\times r}=68.29\ mm$

Where r: area ratio $r=\frac{As}{(beff\times tc)}=\frac{1277.2}{350\times 70}=0.052$

$Icom.=I_x+\frac{A_s(D+tc)^2}{4\times(1+n\times r)}+\frac{beff\times tc^3}{12\times n}=32.28\times 10^6\ mm^4$

Section modulus for the steel and concrete:

$Sxs=\frac{Icom.}{(D+tc-y)}=152.472\times 10^3\ mm^3$

$Sxc=n\times\frac{Icom.}{y}=2836.1\times 10^3\ \ mm^3$

Calculating maximum elastic moment:

$M=fc'\times Sxc=170.168\ kN.m$

$M=Fy\times Sxs=41.9\ kN.m\ (control)$

The total applied load (Pn) for the beam loaded by two concentrated loads (Pn/2) applied at the third point of the span;

$Pn=6M/L=167.71\ kN$

b- Plastic Stage

Tensile Yielding of the Steel Section

$F_{s\ max}=A_s\times F_y=460.2\ kN$

Concrete Crushing

$F_{c\ max}=0.85fc'\ beff\ tc=1249.5\ kN$

$F_{c\ max}>F_{s\ max}$ the slab is adequate, then

$a=\frac{\text{Fs max}}{0.85\ fc\ beff}=25.7\ mm$

The arm of opposite forces (e) is equal to:

$e=0.5D+tc-0.5a=162.2mm$

Calculating maximum plastic moment:

$Mn=Fs\ max\times e=74.62\ kN\rightarrow\therefore Pn=6Mn/L=298\ kN$

6. Ultimate Vertical Shear

Vs = 0.6Fy × 2$hptw$ = 54.025 kN
Vc = 0.17$\sqrt{fc'}$ × $bc\ tc$ = 22.85 kN
$Vn = Vs + Vc$ = 76.87 $kN \rightarrow \therefore Pn$ = 2 × 76.87 = 153.75 $(control)$
7. Stud Shear Connectors
The shear resistance (Qn) of a stud is lesser than:
Resistance of Concrete; Qn = 0.5$Asc\sqrt{fc'\ Ec}$ = 58kN
Resistance of Stud; Qn = Asc×Fu = 79kN
Where Asc= cross-sectional area of stud=0.078
Fu= ultimate tensile strength of stud.
In the present study, the diameter of the stud is (10 mm), and the ultimate tensile strength is assumed (1010 MPa), thus Qn = 58 kN
Calculating the upper required number of shear connectors:
Longitudinal shear force;
V' = min ($Fs\ max$,) = 417.6 kN
$\therefore No.\ of\ Studs$ = 2 × $\frac{V}{Qn} \cong$ 15

- Calculating the lower required number of shear connectors:

Longitudinal shear flow; q =$\frac{Q \times V}{I}$= 299.14 N/mm
$No.\ of\ Studs$ = 2 ×$\frac{L/2}{Qn/q} \cong$ 4

- Calculating Degree of Composite Action:

$D.\ C.\ A$ = $\frac{Provided\ connectors}{No.of\ connectors\ for\ full\ composite\ action}$
$D.\ C.\ A$ =$\frac{4}{15} = 26.67\% \geq 25\%$ [50]
Geometry Provisions for Shear Connectors
(1) H/D ≥ 4 [50][66]
(2) Longitudinal spacing (c. to c.) ≤ 600mm (24")[66] , ≥ 6D[50][66]
(3) Transverse spacing (c. to c.) ≥ 4D[50][66]
(4) Clear distance between the edge of the top flange and the edge of the nearest shear connector shall not be less than 25mm (1.0")[50][66]
(5) Cover ≥ 50mm (2") and Penetration ≥ 50mm (2")[66]
(6) D ≤ 2.5 flange thickness (unless located over the web) [50]
(7) Maximum spacing ≤ 8 slab thickness [50] ≤ 36" [50]

APPENDIX-B

MATERIAL DATASHEETS

B.1 Datasheet of silica fume provided by the manufacturer

BASF
We create chemistry

MasterRoc® MS 610

Densified silica fume for cast and sprayed concrete

DESCRIPTION

MasterRoc MS 610 is a high quality silica fume powder for high performance concretes. It changes the porous structure of the concrete making it denser and more resistant to any type of external influence.

FIELDS OF APPLICATION

- Wet-mix sprayed concrete applications
- Pre-cast concrete
- Cast in-situ concrete
- High strength concrete
- Underwater concrete
- Concrete with low cement content
- Annulus grouting (TBM)

FEATURES AND BENEFITS

- Wet-mix sprayed concrete applications
- Pre-cast concrete
- Cast in-situ concrete
- High strength concrete
- Underwater concrete
- Concrete with low cement content
- Annulus grouting (TBM)

PACKAGING

MasterRoc MS 610 is supplied in 20 kg plastic bags and big bags.

TECHNICAL DATA*

Form	Powder
Color	Grey
Density	0.55 - 0.7 kg/l
Chloride content	<0.1%

COMBINATION

The use of superplasticizers is recommended for any silica fume concrete. For frost resistance, an additional air-entraining agent must be added.

MIXING

MasterRoc MS 610 is added to the concrete during batching. Minimum mixing time is 90 seconds. The recommended dosage is 5 to 15% of the cement weight.

STORAGE

If stored dry and in tightly closed original bags, **MasterRoc MS 610** has a shelf life of at least 12 months.

MASTER® BUILDERS SOLUTIONS

BASF
We create chemistry

MasterRoc® MS 610

SAFETY PRECAUTIONS

Avoid contact with eyes and prolonged contact with skin. If contact occurs, wash thoroughly with water and seek medical advice.

For further information refer to the product Material Safety Data Sheet.

* Properties listed are based on laboratory controlled tests.

® = Registered trademark of the BASF Group in many countries.

BASF_CC-UAE/Roc_MS610/v1/10_13

STATEMENT OF RESPONSIBILITY	The technical information and application advice given in this BASF publication are based on the present state of our best scientific and practical knowledge. As the information herein is of a general nature, no assumption can be made as to a product's suitability for a particular use or application and no warranty as to its accuracy, reliability or completeness either expressed or implied is given other than those required by law. The user is responsible for checking the suitability of products for their intended use.
NOTE	Field service where provided does not constitute supervisory responsibility. Suggestions made by BASF either orally or in writing may be followed, modified or rejected by the owner, engineer or contractor since they, and not BASF, are responsible for carrying out procedures appropriate to a specific application.

BASF Construction Chemicals UAE LLC
P.O. Box 37127, Dubai, UAE
Tel. +971 4 8090800, Fax. +971 4 8851002
www.master-builders-solutions.basf.ae

Disclaimer: the LRQA mark relates to certified management system and not to the product mentioned on this datasheet

MASTER® BUILDERS SOLUTIONS

B.2 Datasheet of superplasticizer provided by the manufacturer

MASTER® BUILDERS SOLUTIONS

MasterGlenium® 54

A high performance concrete superplasticiser based on modified polycarboxylic ether

DESCRIPTION

MasterGlenium 54 has been developed for applications primarily in precast but also readymix concrete industries where the highest durability and performance is required.

MECHANISM OF ACTION

MasterGlenium 54 is differentiated from conventional superplasticisers, such as those based on sulphonated melamine or naphthalene formaldehyde condensate as it is based on a unique carboxylic ether polymer with long lateral chains. This greatly improves cement dispersion. At the start of the mixing process the same electrostatic dispersion occurs but the presence of the lateral chains, linked to the polymer backbone, generate a steric hindrance which stabilises the cement particles capacity to separate and disperse.

This mechanism provides flowable concrete with greatly reduced water demand and enhanced early strength.

TYPICAL APPLICATIONS

The excellent dispersion properties of **MasterGlenium 54** make it the ideal admixture for precast or ready-mix where low water cement ratios are required. This property allows the production of very high early and high ultimate strength concrete with minimal voids and therefore optimum density. Due to the strength development characteristics the elimination or reduction of steam curing in precast works may be considered as an economical option.

- high workability without segregation or bleeding
- less vibration required
- can be placed and compacted in congested reinforcement
- reduced labour requirement
- improved surface finish

MasterGlenium 54 may be used in combination with **MasterMatrix** for producing Smart Dynamic Concrete (SDC). The technology produces advanced self compacting concrete, without the aid of vibration. For economic, ecological and ergonomic ready-mix / precast concrete production.

MasterGlenium 54 can be used to produce very high early strength floor screeds. For screed mix designs consult Master Builders Solutions Technical Services.

PACKAGING

MasterGlenium 54 is available in 208 litre drums and in bulk tanks upon request.

STANDARDS

ASTM C-494 Type F& G
BS EN 934-2

TYPICAL PROPERTIES*

Form	Whitish to straw coloured liquid
Relative density	1.07
pH	5-8

APPLICATION GUIDELINES

MasterGlenium 54 is a ready to use admixture that is added to the concrete at the time of batching.

The maximum effect is achieved when the **MasterGlenium 54** is added after the addition of 70% of the water. **MasterGlenium 54** must not be added to the dry materials.

Thorough mixing is essential and a minimum mixing cycle, after the addition of the **MasterGlenium 54**, of 60 seconds for forced action mixers is recommended.

A brand of MBCC GROUP

MASTER® BUILDERS SOLUTIONS

MasterGlenium® 54

DOSAGE

The normal dosage for **MasterGlenium 54** is between 0.50 and 1.75 litres per 100kg of cement (cementitious material). Dosages outside this range are permissible subject to trial mixes.

COMPATIBILITY

MasterGlenium 54 is not compatible with **MasterRheobuild** superplasticizers.
MasterGlenium 54 is suitable for mixes containing all types of Portland cement and cementious materials as follows:

- microsilica
- fly ash (PFA)
- ground granulated blast furnace slag GGBS

EFFECT ON HARDENED CONCRETE

- increased early and ultimate compressive strengths
- increased flexural strength
- better resistance to carbonation
- lower permeability
- better resistance to aggressive atmospheric conditions
- reduced shrinkage and creep
- increased durability

STORAGE AND SHELF LIFE

MasterGlenium 54 should be stored above 5°C In closed containers or storage tanks to protect from evaporation and extreme temperatures.
The shelf life is 12 months when stored as above.

The occurrence of a surface layer with **MasterGlenium 54** is normal and will have no effect on the performance of the product.

HEALTH AND SAFETY

MasterGlenium 54 contains no hazardous substances requiring labelling. For further information refer to the Material Safety Data Sheet.

QUALITY AND CARE

All products originating from Master Builders Solutions Dubai, UAE facility are manufactured under a management system independently certified to conform to the requirements of the quality, environmental and occupational health & safety standards ISO 9001 and ISO 14001.

* Properties listed are based on laboratory controlled tests.

® = Registered trademark of the MBCC Group in many countries.

MBS_CC-UAE/GI_54_09_07/v2/03_16

STATEMENT OF RESPONSIBILITY The technical information and application advice given in this Master Builders Solutions publication are based on the present state of our best scientific and practical knowledge. As the information herein is of a general nature, no assumption can be made as to a product's suitability for a particular use or application and no warranty as to its accuracy, reliability or completeness either expressed or implied is given other than those required by law. The user is responsible for checking the suitability of products for their intended use.

NOTE Field service where provided does not constitute supervisory responsibility. Suggestions made by Master Builders Solutions either orally or in writing may be followed, modified or rejected by the owner, engineer or contractor since they, and not Master Builders Solutions, are responsible for carrying out procedures appropriate to a specific application.

Master Builders Solutions Construction Chemicals LLC
P.O. Box 37127, Dubai, UAE
Tel: +971 4 8090800
www.master-builders-solutions.com/en-ae

Disclaimer: the TÜV mark relates to certified management system and not to the product mentioned on this datasheet

TÜV SÜD ISO 9001 TÜV SÜD ISO 14001

A brand of MBCC GROUP

APPINDEX-C

6.4.1 Material Properties

The present study utilized finite element models that encompassed several characteristics, as outlined in Table (5-3). In Appendix C, the material characteristics for concrete and steel reinforcement were modeled, and the input data consisted of the modulus of elasticity and Poisson's ratio.

Table 6-1: Material Model Behavior for Steel Section and Stiffeners.

No	Part	Type	Shape
1	Steel Beam	Deformation 3D	Solid-Extrusion
2	Concrete Slab	Deformation 3D	Solid-Extrusion
3	Headed Stud	Deformation 3D	Solid-Revolution
4	Rebar Longitudinal	Deformation 3D	Wire-Planer
5	Rebar Transverse	Deformation 3D	Wire-Planer
6	Top-Bearing plate	Deformation 3D	Solid-Extrusion
7	Bottom-Support plate	Discrete rigid 3D	Solid-Extrusion
8	Vertical stiffener plate	Deformation 3D	Solid-Extrusion

C. 1 Ingredients used in ABAQUS Program

Table C-1: Parameters for Elements Used in F.E. Model for Beam.[67]

Steel Beam		
Steel parameter	Definition	Value
fy	Yield stress (N/mm^2)	486.67
E_s	Modulus of elasticity(N/mm^2)	200000
υ	Poisson's ratio	0.3
Headed Stud (Shear stud connector)		
mass density = 7850		
modules of elasticity	Poisson ratio	
200000	0.3	
Shear stud parameter	Definition	Value
$\emptyset_{st}$	Diameter(mm)	10
L_{st}	Overall Length(mm)	50
N_r	Number of rows	1
Concrete		
mass density = 2000		
modules of elasticity	Poisson ratio	
210000	0.2	
Concrete Damaged Plasticity		

dilation angle	eccentricity	fb0/fc0	K	viscosity parameter
40	0.1	1.1	0.66	0.001

Concrete parameter	Definition	Value
$f'c$	Compressive strength (N/mm^2)	60
f_r	Modulus of rupture (N/mm^2)	6.3
υ	Poisson ratio	0.3
E_c	Young's Modulus (N/mm^2)	200000

Reinforcing steel	
mass density = 7800	
modules of elasticity	Poisson ratio
210000	0.3
yield stress	plastic strain
460	0
608	0.02

Rigid	
mass density = 7850	
modules of elasticity	Poisson ratio
210000	0.3

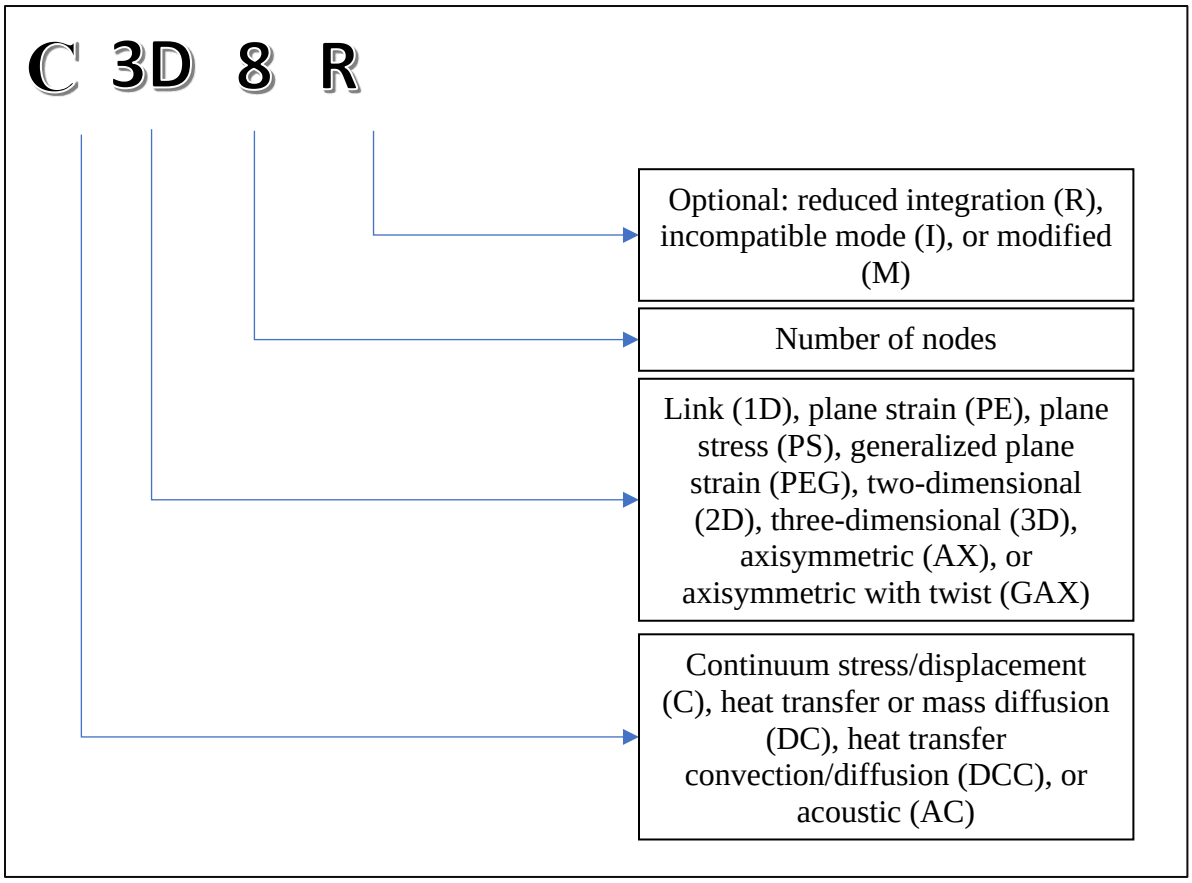

Figure C-6-1:Elements types in ABAQUS.

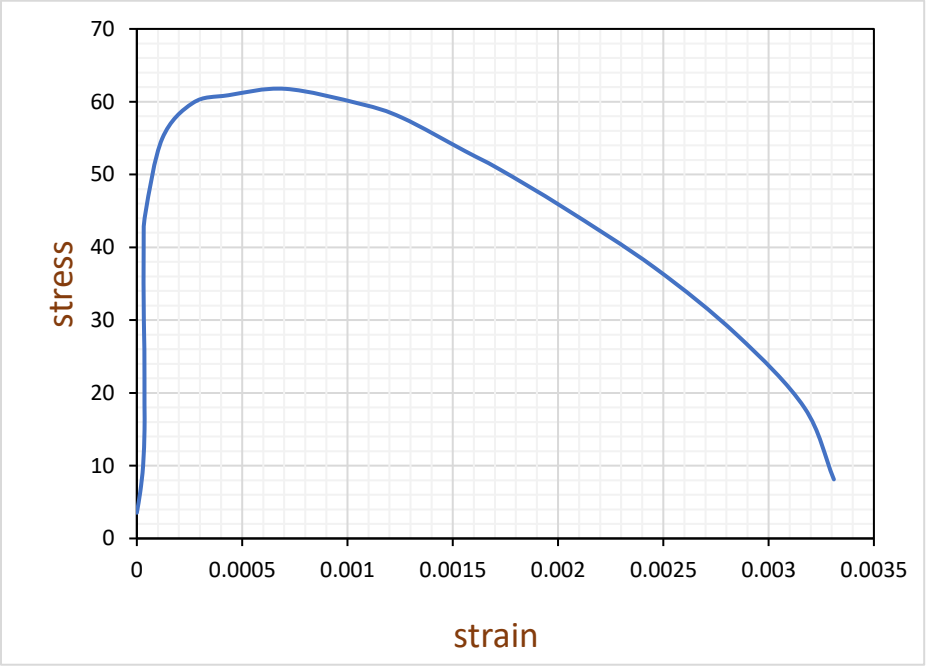

Figure C-2: Compressive Stress-Strain Behavior.

C.2 3D Solid Elements

In the realm of Finite Element Analysis (FEA), the choice of a suitable element type is crucial for accurately modeling the behavior of materials and structures. When simulating concrete components, a three-dimensional solid element is often recommended due to its ability to more faithfully represent the geometry and local stress distribution of the structure.[68]

The ABAQUS element package provides a comprehensive set of options, including various three-dimensional solid elements to cater to diverse simulation needs. Among the elements available in the package are the 4-node linear tetrahedron, 6-node linear triangular prism, 8-node linear brick, 10-node quadratic tetrahedron, 15-node quadratic triangular prism, and 20-node quadratic brick elements. Each of these elements offers unique advantages and is tailored for different scenarios, allowing engineers to choose the most suitable element for their specific concrete modeling requirements.[69]

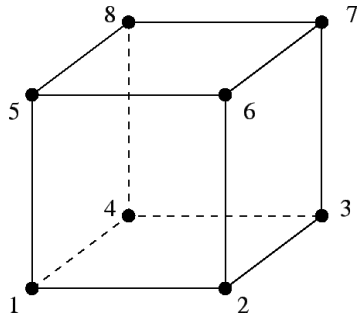

Figure C-3 : 8-node brick element.[69][68]

C.3 Truss Element

Using a linear 3D two-node truss element (T3D2) to simulate reinforcing steel bars in reinforced concrete beams is a common approach in finite element analysis (FEA). Truss elements are well-suited for modeling axial forces and are particularly useful when the primary mode of deformation in a structure is axial elongation or compression.[70]

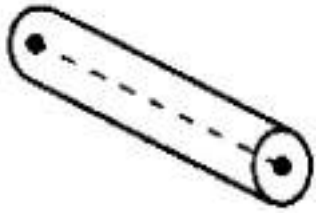

Figure C-5: General view of the Truss element (T3D2), ABAQUS.[68]

C.4 Rigid elements

In the three-dimensional quadrilateral (R3D4), In finite element analysis software packages, rigid elements are used to connect nodes and enforce specific geometric relationships without introducing deformations. These elements are commonly employed to model rigid bodies or to simulate the effects of constraints.

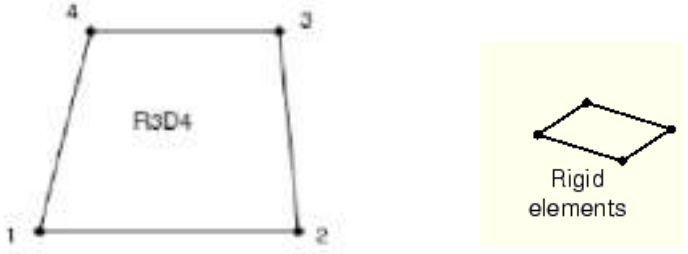

Figure C-6: R3D4 rigid element in ABAQUS.[69]

الخلاصة

تركزت هذه الدراسة على إجراء تحليلات تجريبية وعددية لفحص أداء الجسور الخلوية المركبة تحت التحميل المتكرر. وتهتم بدراسة عدة معاملات منها أشكال الفتحات (السداسية والدائرية والمربعة) والتباعد بين المسامير القصية (150 مم و300 مم) مع وجود أو غياب الدعامات (التقوية). تضمنت المرحلة التجريبية اختبارات على الخصائص الميكانيكية والكيميائية للمواد. تعرضت العوارض لتحميلات متكررة و الساكن . ونتيجةً لنسبة الزيادة ، زاد ارتفاع العارضة بنسبة 50% (في منطقة الويب). وفي المرحلة التجريبية، تم تصنيع خمسة عشر مقطعًا مركبًا، ثلاثة منها عينة مرجعية. تم إنشاء الاتصال بين لوح السطح الخرساني والجسر الفولاذي (الحديدي) باستخدام المسامير الفولاذية ذات الرأس الملحومة على الحواف العلوية. يبلغ طول لوح السطح 1500 مم وعرضه 350 مم وسمكه 70 مم. العنصر الهيكلي المستخدم هو عارضة IPE 140 بطول 1500 مم. قسمت العوارض إلى خمس مجموعات بناءً على عوامل متغيرة، وكل مجموعة تضم ثلاثة جسور . كشفت الدراسة أن بعض العوامل تؤثر بشكل كبير على سلامة العوارض. فالتباعد المتناقص لمسامير القص ادى إلى زيادة في قدرة التحمل وانخفاض الانحرافات. كما أن تصميم الفتحة يؤثر بدرجة كبيرة على الأداء، حيث تتفوق التكوينات السداسية عادةً على الدائرية والمربعة بنسب تتراوح بين 28.26% و100.43% في جميع المجموعات، مما يؤكد التفوق الهيكلي للفتحات السداسية. علاوة على ذلك، تؤثر المسافة بين مسامير القص بشكل كبير على الحد الأقصى لقدرات التحميل، مما يؤدي إلى اختلافات تتراوح من 7.91% إلى 58.09%. ومن هنا تأتي أهمية تقييم تباعد وصلات القص بدقة في تصميم الجسور الخلوية المركبة. أخيرًا، تظهر طرق التقوية فاعليتها، مما يؤدي إلى زيادات متباينة في الحمولة القصوى تتراوح بين 17.89٪ و66.53٪. كما تقارن الدراسة المحاكاة الرقمية بالنتائج التجريبية باستخدام برنامج ABAQUS/Explicit. يشمل التحليل معاملات منها تكوين الفتحة وتوزيع مسامير القص و التقوية . تظهر النتائج أن معدل توافق الجسور ضمن نطاق مقبول. يؤكد تحليل العناصر المحدودة هذه النتائج، ويوضح مستوى عالٍ من الدقة يبلغ حوالي 93.67٪ في التنبؤ بالحمل النهائي وشكل المنحني (الحمل و الازاحة). توفر هذه الدراسة رؤى قيمة في تصميم الجسور الخلوية المركبة، وتؤكد على الحاجة إلى تحسين معاملات التصميم لتعزيز الكفاءة الهيكلية.

جمهورية العراق

وزارة التعليم العالي و البحث العلمي

جامعة كربلاء

كلية الهندسة

قسم الهندسة المدنية

التصرف الإنشائي للجسور المركبة الخلوية المعرضة للاحمال الساكنة و تكرارية

رسالة مقدمة الى مجلس كلية الهندسة / جامعة كربلاء وهي جزء من متطلبات نيل درجة الماجستير في علوم الهندسة المدنية

المؤلف:

نورالهدى كاظم حسين الموسوي

باشراف :

أ.م.د بهاء حسين العباس

أ.م.د علي غانم عباس الخفاجي

رمضان - 1445

نيسان - 2024